

NOTE TO USERS

Page(s) missing in number only; text follows. Page(s) were scanned as received.

xiv, 10, 98, 108, 148, 186, 204

This reproduction is the best copy available.

UMI[®]

MODEL-BASED CONTROL OF METAL POWDER BALL MILLING

Alexandre Rail

Mechanical Engineering
McGill University, Montreal

December, 2005

A thesis submitted to McGill University in partial fulfillment of the
requirements of the degree of Ph.D. of Engineering

© Alexandre Rail, 2005



Library and
Archives Canada

Bibliothèque et
Archives Canada

Published Heritage
Branch

Direction du
Patrimoine de l'édition

395 Wellington Street
Ottawa ON K1A 0N4
Canada

395, rue Wellington
Ottawa ON K1A 0N4
Canada

Your file Votre référence

ISBN: 978-0-494-25235-2

Our file Notre référence

ISBN: 978-0-494-25235-2

NOTICE:

The author has granted a non-exclusive license allowing Library and Archives Canada to reproduce, publish, archive, preserve, conserve, communicate to the public by telecommunication or on the Internet, loan, distribute and sell theses worldwide, for commercial or non-commercial purposes, in microform, paper, electronic and/or any other formats.

The author retains copyright ownership and moral rights in this thesis. Neither the thesis nor substantial extracts from it may be printed or otherwise reproduced without the author's permission.

AVIS:

L'auteur a accordé une licence non exclusive permettant à la Bibliothèque et Archives Canada de reproduire, publier, archiver, sauvegarder, conserver, transmettre au public par télécommunication ou par l'Internet, prêter, distribuer et vendre des thèses partout dans le monde, à des fins commerciales ou autres, sur support microforme, papier, électronique et/ou autres formats.

L'auteur conserve la propriété du droit d'auteur et des droits moraux qui protègent cette thèse. Ni la thèse ni des extraits substantiels de celle-ci ne doivent être imprimés ou autrement reproduits sans son autorisation.

In compliance with the Canadian Privacy Act some supporting forms may have been removed from this thesis.

Conformément à la loi canadienne sur la protection de la vie privée, quelques formulaires secondaires ont été enlevés de cette thèse.

While these forms may be included in the document page count, their removal does not represent any loss of content from the thesis.

Bien que ces formulaires aient inclus dans la pagination, il n'y aura aucun contenu manquant.


Canada

ABSTRACT

Model-Based Control of Metal Powder Ball Milling

Alexandre Rail

At Domfer Metal Powders, the ball milling operation is critical since it determines many characteristics of the final product, such as density, green strength, compressibility and dimensional change. Highly variable input material properties and operational procedures accompanied by poor product feedback frequency generate large variations in powder properties. The goal of the research is to develop a model-based control system for the ball milling process of metal powder. The following research objectives are aimed at reducing process variations while maximizing throughput: include ball mill physics into design and computer models, develop control strategies and computer architectures for real-time control, and develop process monitoring and fault diagnosis techniques.

Ball mill size reduction theory is presented as a basis for process characterization. Next, process physics are described along with the measurability and controllability of the variables. Then, plant trials are performed to define system behavior and performance specifications of variables and sensors. After that, a sampler for metal powder is developed to automate the entire sieve analysis process.

A new ball mill model is created for open-circuit dry ball milling of metal powders. The process model is a combination of rules, equations and heuristics and is implemented using an agent based architecture that can deal with multiple data streams and a network of related sub-models of different sizes and operating time scales.

The model architecture is integrated using a programmable logic controller. Control and monitoring algorithms are developed in low-level PC language. A performance plant trial validated the control system and demonstrated that ball milling product specifications, namely size distribution and apparent density, are achievable and maintainable at a 99.7%

confidence interval. This new technology will endow Domfer with a serious lead in metal powder manufacturing.

Key words: model-based control, ball milling, metal powder.

RÉSUMÉ

Contrôle modélisé pour le broyage de grenailles de fonte

Alexandre Rail

L'opération de broyage de grenailles de fonte s'effectue à l'aide de broyeur à boulets chez Domfer Poudres Métalliques. Cette étape du procédé s'avère très critique puisqu'elle détermine les caractéristiques des produits finis, tels que la densité apparente, la force à vert, la compressibilité et le changement dimensionnel. Les variations de propriétés de la grenaille de fonte et de procédures opérationnelles, ainsi que la faible fréquence en rétroaction des propriétés du produit broyé, induisent de grandes variations des propriétés de la poudre. L'objectif de la recherche est de créer un nouveau système de contrôle modélisé de broyeur à boulets réduisant les variations de procédé et incluant les éléments suivants : développement de techniques d'intégration de phénomènes physiques dans des modèles mécaniques et informatiques, conception d'un module de surveillance stable et robuste, création d'une nouvelle stratégie de contrôle, et finalement, développement d'une architecture informatique pour un contrôle multi-variables en temps réel.

Premièrement, la théorie sur la réduction de la taille des particules à l'aide de broyeur à boulets est présentée afin de caractériser le procédé de broyage. La dynamique du procédé est ensuite décrite en parallèle avec le mesurage et le contrôle des variables. De plus, des essais en usine sont effectués afin de définir le comportement du système et les spécifications de performance des variables et senseurs. Enfin, un échantillonneur de poudres métalliques est conçu afin d'automatiser l'analyse granulométrique et fournir une rétroaction plus fréquente.

Un nouveau modèle est créé pour le broyage à sec en circuit ouvert de grenailles de fonte à l'aide de broyeur à boulets. Ce modèle est composé de règles, d'équations et d'heuristiques et est intégré en utilisant une architecture à base d'agents pouvant traiter de multiples flux de données et un réseau de sous-modèles inter reliés de différentes tailles et échelles de temps d'exploitation.

L'architecture du modèle est implantée en utilisant un automate programmable. Des algorithmes de contrôle et de surveillance sont développés en niveau bas de logique. Un essai de performance en usine a validé le système de contrôle et démontré que les spécifications des produits de l'opération de broyage, à savoir, la distribution granulométrique et la densité apparente, peuvent être obtenues et maintenues à un intervalle de confiance de 99.7%. Cette nouvelle technologie permettra à Domfer de fabriquer des poudres métalliques de très haute qualité.

Mots clés : contrôle modélisé, broyeur à boulets, poudre métallique.

TABLE OF CONTENTS

	Page
Abstract.....	i
Résumé.....	iii
Table of contents.....	v
List of tables.....	ix
List of figures.....	xi
Acknowledgements.....	xv
Chapter	
1.0 Introduction.....	1
1.1 Domfer metal powder manufacturing process.....	1
1.2 Problem description.....	4
1.3 Research objectives and proposed approach.....	6
2.0 Size reduction theory: ball milling.....	11
2.1 Definitions and formulation of problems.....	12
2.2 Laws of grinding.....	17
2.3 Powder characterization.....	23
2.4 Performance trends.....	32
2.4.1 Mill speed.....	33
2.4.2 Ball size.....	33
2.4.3 Ball and powder charge.....	34
2.4.4 Feed size distribution.....	34
2.5 Charge motion.....	36
2.6 Media Wear.....	39
2.7 Conclusion.....	42
3.0 Ball milling process characterization.....	43
3.1 Process physics.....	43
3.2 Measurability and controllability of the variables.....	48
3.2.1 Input material properties.....	48
3.2.2 Powder feed rate.....	49
3.2.3 Grinding balls.....	55
3.2.4 Liners.....	58
3.2.5 Ball and powder charges.....	64
3.2.6 Residence time.....	66
3.2.7 Powerdraw.....	67
3.2.8 Rotational speed.....	70
3.2.9 Air flow rate.....	72
3.2.10 Outlet trunnion pressure.....	76
3.2.11 Product rate.....	77
3.2.12 Product properties.....	78

3.3 Performance specifications of variables and sensors.....	83
3.3.1 Effect of feed rate and air flow rate changes	84
on product properties	
3.3.2 Validation of size distribution function.....	94
3.3.3 Suction air flow monitoring.....	96
3.4 Conclusion.....	97
4.0 Product size feedback.....	99
4.1 Automatic sampler design.....	99
4.2 Particle sizing.....	103
4.3 Conclusion.....	107
5.0 Process model development.....	109
5.1 Process modelling background.....	109
5.2 Control strategy.....	113
5.3 Agent based architecture.....	119
5.4 Ball mill model.....	122
5.4.1 Model statements.....	122
5.4.2 Control model.....	124
5.4.3 Data model.....	126
5.4.4 Process sub-models.....	127
5.4.4.1 Liner wear.....	127
5.4.4.2 Ball feed rate.....	129
5.4.4.3 Powder charge.....	130
5.4.4.4 Residence time.....	132
5.4.4.5 Product rate.....	132
5.4.4.6 Powder feed rate.....	133
5.4.4.7 Air flow rate.....	135
5.4.5 Diagnostic system and error recovery.....	137
5.4.5.1 Size distribution function.....	138
5.4.5.2 Product apparent density.....	138
5.4.5.3 Outlet trunnion pressure.....	139
5.4.5.4 Loading and emptying phases.....	140
5.4.5.5 Powerdraw, feed rate and air flow rate ranges.....	141
5.4.5.6 Powerdraw vs feed rate.....	142
5.4.5.7 Product size verification.....	143
5.4.5.8 Equipment.....	144
5.5 Conclusion.....	147
6.0 Control and monitoring.....	149
6.1 Background.....	149
6.2 Control algorithms.....	154
6.3 Monitoring algorithms.....	161
6.4 Controller hardware.....	168
6.5 Conclusion.....	174

7.0 Results and discussion.....	175
7.1 Validation of the control system.....	175
7.2 Future development.....	182
7.3 Conclusion.....	185
8.0 Contribution to knowledge and benefits to industry.....	187
8.1 Contribution to knowledge.....	187
8.2 Benefits to industry.....	189
9.0 Conclusion.....	191
References.....	197
Appendix 1 Domfer ball mill 408 technical drawings and specifications.....	205
Appendix 2 MPIF apparent density and sieve analysis standard test methods.....	231
Appendix 3 Results of plant trials.....	239
Appendix 4 Automatic sampler detailed drawings and component specifications.	253
Appendix 5 Ladder diagram instructions.....	285
Appendix 6 Controller hardware specifications.....	291

This page and others at the end of sections and chapters are purposely left blank to assist pagination for double-sided copies of the thesis.

LIST OF TABLES

TABLE	Page
1.1. Domfer specifications vs average production results..... from Dec 02 to July 03	7
1.2. Domfer specifications compared to specific research objectives.....	8
2.1. The International Standard Sieve Series.....	14
2.2. Particle size distribution data.....	26
2.3. Standard deviations on a cumulative size distribution.....	31
3.1. List of variables.....	45
3.2. Domfer ball mills dimensions.....	47
3.3. Product density and size with respect to residence time.....	66
3.4. Powerdraws for ball mill 408 products.....	69
3.5. Typical MP2 ground shot sieve analysis and apparent density results....	80
3.6. Ball mill 408 produced grade parameters.....	82
3.7. Powder charge, product response time and powder charge sensitivity.... results for the feed rate tests	90
3.8. Feed rate test m1 cumulative distribution results.....	94
5.1. Allowable powerdraw, feed rate and air flow rate ranges.....	141
7.1. MP2 and MP3 final product properties.....	183
7.2. MP2 and MP1 dimensional change comparison.....	185

LIST OF FIGURES

FIGURE	Page
1.1 Domfer steel powder manufacturing process.....	2
1.2 Domfer ball mill BM-108.....	5
2.1. Illustration of a tumbling ball mill at rest.....	11
2.2. Cumulative distribution data for powder size.....	13
2.3. Feed particles fragmentation.....	15
2.4. Experimental size distribution for dry grinding.....	18
2.5. Primary progeny fragment distribution.....	21
2.6. Illustration of mass balance action in fully mixed batch grinding.....	23
2.7. SEM micrographs of diverse shapes and sizes of metal powders.....	24
2.8. Histogram plot of the screening data.....	27
2.9. Cumulative particle size distribution.....	27
2.10. Comparison of the common types of particle size distributions.....	28
2.11. Comparison of particle size distribution plotted on several bases.....	30
2.12. Log-normal size distribution plot using standard deviation points.....	31
2.13. Mill breakage rate function.....	32
2.14. Typical ball charge motion profile.....	36
2.15. Charge motion simulation with different speeds and lifter characteristics..	38
2.16. Outlet view of Domfer ball mill 408.....	39
2.17. Different liner profiles.....	40
2.18. Ball charge forces acting on mill liner.....	40
2.19. Wave liner profile wear simulation.....	41
2.20. Mill power consumption over liner usable life.....	41
3.1. Ball mill 408 grinding circuit at Domfer.....	44
3.2. Automated weighing system for metal powders.....	50
3.3. Negative unity feedback feed rate control block diagram.....	53
3.4. Ball size distribution.....	56
3.5. Ball bed height.....	57
3.6. Used and new Domfer BM-408 liners.....	59

3.7. Charge motion comparison for used and new liners.....	60
3.8. Cross sectional view of a new liner compared to a used liner.....	60
3.9. 3-D drawing of BM-408 inside volume with new and used liners.....	61
3.10. Negative unity feedback air flow rate control block diagram.....	74
3.11. Ball mill 408 suction circuit.....	79
3.12. Ground shot SEM micrograph.....	81
3.13. Feed rate trial # m1 results.....	84
3.14. Feed rate trial # m2 results.....	86
3.15. Feed rate trial # m3 results.....	88
3.16. Air flow rate trial # Q1 results.....	91
3.17. Air flow rate trial # Q2 results.....	92
3.18. Feed rate test m1 cumulative distribution results on log-normal paper.....	95
3.19. Outlet trunnion pressure trials # dp1 and dp2 results.....	96
4.1. Automatic sampler design.....	101
4.2. Sampler location.....	102
4.3. Fully automated sieve analyzer.....	106
5.1. Simple residence time distribution.....	115
5.2. Agent based architecture.....	120
5.3. PI controllers for feed rate and air flow rate output control parameters.....	125
5.4. Powerdraw versus powder charge.....	131
5.5. Product size derivative with respect to time.....	143
5.6. Ball mill model.....	146
6.1. Basic ladder diagram.....	150
6.2. Programmable logic controller cycle.....	152
6.3. PLC architecture diagram.....	153
6.4. Feed rate and air flow rate control algorithm.....	154
6.5. Powder feed rate sub-model control algorithm.....	158
6.6. Air flow rate sub-model control algorithm.....	159
6.7. Ball feed rate control algorithm.....	160
6.8. <i>S100</i> monitoring algorithm.....	161
6.9. Product apparent density monitoring algorithm.....	162

6.10. Outlet trunnion pressure monitoring algorithm.....	164
6.11. Loading phase monitoring algorithm.....	165
6.12. Programmable logic controller configuration.....	172
6.13. Ball mill 408 human machine interface page.....	173
7.1. Ball mill 408 product property results.....	176
7.2. Air flow rate variations with respect to <i>S200</i>	178
7.3. Feed rate variations with respect to mill powerdraw.....	180

ACKNOWLEDGEMENTS

We constantly seek to stretch the boundaries of knowledge, capability and technology. Do we create these new ideas? Or do we just accomplish dreams, visions and aspirations of previous generations? In trying for the apparently impossible, we travel in the unknown and think of the opportunities beyond the limits of our minds. In so doing, we will confirm the truth of what Oliver Wendell Holmes said:

‘A mind once stretched by a new idea never regains its original dimension.’

Thus, I would like to express my gratitude to the following persons who contributed to the realization of this thesis.

‘Dans un premier temps, je veux remercier mes parents, Carole et Valère, pour l’immense soutien donné tout au long de mes études. L’écoute et les encouragements ont grandement facilité la réussite de ce projet. Leur exemple et les valeurs transmises ont fait de moi une personne cherchant constamment à se surpasser. Je leur voue un respect inconditionnel.’

Mr. Kenneth Stodola, President at Domfer Metal Powders, for his tremendous experience and wisdom in manufacturing. It was an honor for me to work with Mr. Stodola in the elaboration of solutions in research and development.

Mr. Michel Lessard, Plant Manager at Domfer Metal Powders, who provided me with the opportunity to create and complete this project. I thank him for his trust in my abilities, and his knowledge in industrial project development and implementation.

Mr. Luc Lachapelle, Chief Engineer at Domfer Metal Powders, for his support in the characterization of the ball milling process.

Prof. Vince Thomson, McGill University, for his supervision and guidance in model-based control design.

Prof. Peter Radziszewski, McGill University, for his scientific approach and good advice in the literature review and ball mill automation.

Mr. Gaetan Hénault, System Integrator, for his philosophy and the creation of control strategies with proper controller hardware architectures.

Mr. Patrick Tanguay, for his technical support in the mechanical design of the automatic sampler.

Mr. Luc Martel, for his help in graphics design.

Ball mill operators, Jean Poirier, Michel Matewsky and, Jude Chartrand, lab manager Jean-Louis Charlebois and R&D foreman Jacques Côté, for their experience and understanding of the metal powder ball milling process that contributed to the creation of adaptive and representative rule-based sub-models.

My true friends, Matthieu, Serge, Jean-Phillipe, Luc, Dominick, Stéphane, Richard, Pierre-Yves, Christine and Lysanne, who refreshed my spirit with good discussions, sport activities and nice evenings.

Last and foremost, I'm most grateful to my Brandice, who always kept my creativity level to a maximum...

1.0 INTRODUCTION

1.1 Domfer metal powder manufacturing process

The last four decades have been a period of high development and growth for the powder metallurgy (P/M) industry. From 1960 to 1980, the consumption of iron powder increased ten times. P/M has become a proven method for parts production and is now considered to be a good alternative in the manufacture of many components. The current market split for P/M products is 70% automotive, 15% appliances, 12% business machines and 3% farm and garden equipment [1]. Areas of rapid growth include aerospace applications, advanced composites, electronic components, magnetic materials and metalworking tools.

The powder metallurgy process generally consists of four basic steps: metal powder manufacturing, mixing, compacting and sintering. Optional secondary processing often follows to obtain special characteristics or greater precision, such as, repressing, coining, sizing, P/M forging, impregnation, infiltration, and finishing. The attributes of powder metallurgy products are very dependent on the characteristics of the metal powders used. Chemistry and purity, particle size distribution, particle shape and surface texture are important properties and characteristics of the metal particles.

The Domfer process provides powder metallurgy grade steel powder. The process was developed at Iberville, Quebec in 1952. A high-carbon iron melt is water atomized into granular 'shot', which is then ball milled to powder size. Because of its high carbon content, the shot is very brittle and can be easily ground to the required size. Then, the ground shot is mixed with ground mill scale (iron oxide). The carbon from the shot and oxygen from the mill scale are chemically combined in a belt furnace at sintering temperatures. Carbon monoxide (CO) gas forms, thus leaving a pure iron cake. Finally, the cake is disintegrated and refined to powder size. A flowchart of Domfer powder process is shown in figure 1.1.

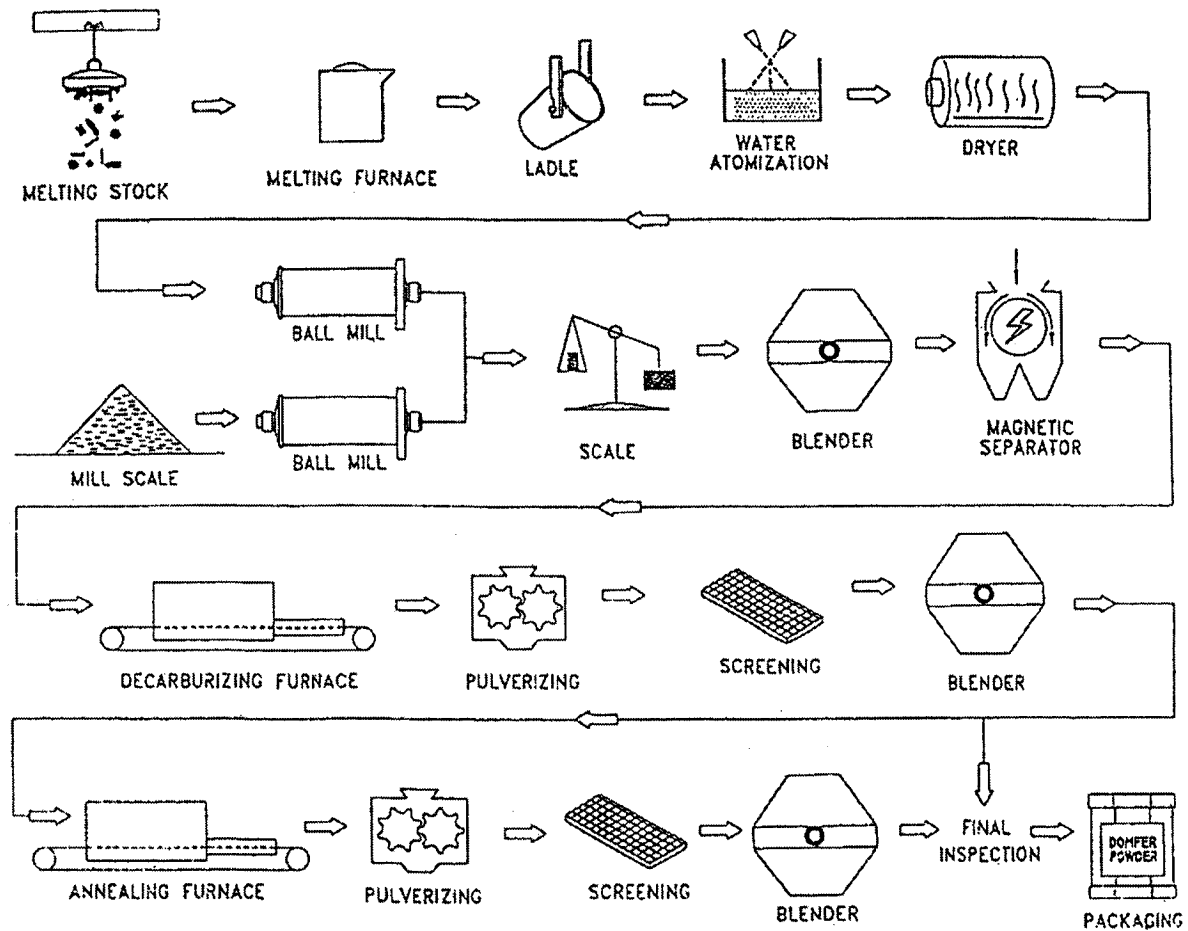


Figure 1.1: Domfer steel powder manufacturing process

High-quality selected steel scrap is melted in a 12.7 metric ton coreless induction furnace with the addition of low-sulfur carbon to produce a melt with approximately 3.5% carbon. Nickel and molybdenum can be added to the furnace for low-alloy steel powders. Nearly 30% of the furnace charge is tapped into a ladle. The molten metal is then poured through a tundish that has bottom openings for controlling the size of the stream. The molten metal is atomized by high-pressure jets of water to a granular material of size varying approximately from 0.03 to 0.12 in (0.8 to 3.2 mm). The grains are dewatered in a cyclone and dried in a gas-fired dryer.

Because of its high carbon content, the shot is very brittle and can be easily ground in an air-swept ball mill to the required powder size. Similarly, mill scale, which is a by-

product of hot rolling and wire drawing, is ground to powder using a ball mill. The ground shot and mill scale are blended to achieve a desired carbon-to-oxygen ratio that will decarburize and deoxidize in the belt furnace, leaving mostly pure iron. The amount of mill scale required to achieve the desired ratio is generally 20% of total weight.

For selected grades, the mixed powder is purified by using a magnetic separator and transported onto a steel belt that passes through an electrically heated furnace that uses glowing bars. The high temperature causes a reaction to occur between the high-carbon iron and mill scale. The carbon monoxide gas generated by the reaction provides a reducing atmosphere and a furnace seal. The resulting pure iron sinters to form a cake that is cooled to near room temperature before leaving the electrical furnace. Afterwards, the cake is reduced to powder size by a lump breaker and disc mill, and screened to obtain the desired size. A double-cone blender is utilized to blend the powder to the required specifications.

Carbon and oxygen levels are reduced to the specified values in the first stage processing. The resulting powder is adequate for manufacturing welding rods, lancing, cutting, scarfing and for friction applications.

A pure and soft powder is required for powder metallurgy parts in order to reduce die wear and lower the pressing force required to obtain the desired density. The powder from the first stage is blended and fed to a second belt furnace. This will produce a very soft cake that can be reduced to powder size without work hardening. Decarburizing and annealing can be conducted in a one pass operation for selected P/M grade powders by modifying the furnace conditions.

The annealing (second stage process) will reduce the concentration of carbon and oxygen to respectively 0.01% and 0.35%. The powder produced is very soft with good compressibility. The powder can be pre-mixed according to customer specifications and blended with lubricant, graphite and copper.

1.0 INTRODUCTION

The quality assurance of Domfer is provided by multi-step testing between the stages to permit a wide range of powder qualities. The essential properties controlled are carbon, oxygen and sulphur content. Screen analysis, apparent density and flow characteristics are also performed. For powder metallurgy part applications, sample bars are pressed and sintered to control or test compressibility, green strength (strength of the pressed powder immediately after compacting), dimensional change during sintering and strength and hardness of the sintered bar. The final metal powder serves for many different applications such as electrodes for arc welding, friction (brake pads), car industry (valve guides, seats and gears) and gardening.

1.2 Problem description

Ball milling is a process in which brittle shot is ground to the required powder size. Coarse material is fed into a big rotating cylinder filled with steel balls (Figure 1.2). As the cylinder rotates, the lifters inside the structure create a cascading effect of steel balls. The multiple impacts made by the balls produce the grinding effect and reduce the coarse powder. Once the particles are reduced to the desired size, they are swept along by the air flow generated by a downstream blower. The powder is recuperated by a combination dropout and cyclone separator.

The ball milling operation is critical since it determines many characteristics of the final products (density, dimensional change, green strength, compressibility, etc.). Based on the size distribution and density results, the operator adjusts the following ball mill parameters: feed rate, air flow rate and level of balls.

The quality of the powder coming out of the ball milling operation is based on operator experience and expertise since he has to simultaneously adjust all the variables for a desired size distribution and density. It is very hard to establish an operational procedure since many adjustment combinations are possible to achieve the desired results. Highly variable input material properties constantly change the milling dynamics and consequently the product. Also, samples are taken only every 3-4 hours out of the receiving impact bin. Therefore, inertial problems are created since the effect of the

changes in parameter adjustments are seen only after few hours. Hence, process control becomes a necessity in order to meet the quality specifications.

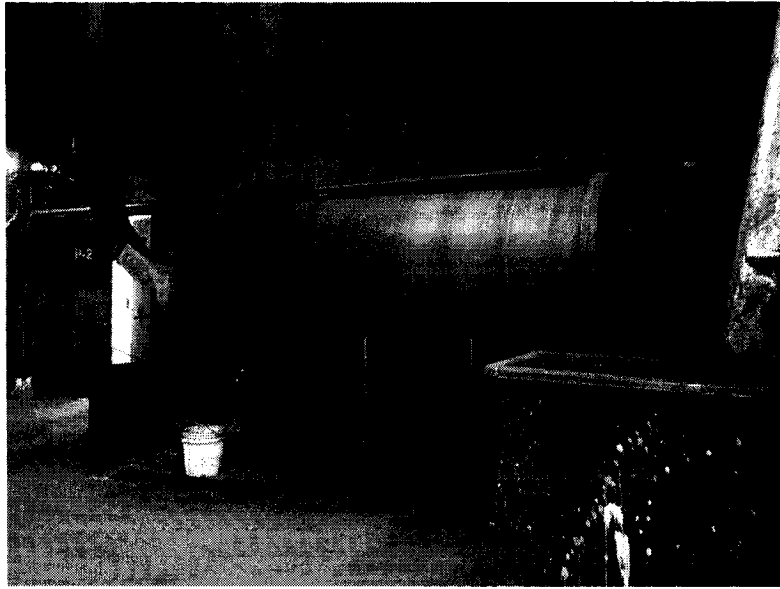


Figure 1.2: Domfer ball mill BM-108

The models and control systems already developed [2-12] are for closed-circuit (coarse particle recirculation) wet ball milling. Moreover, references [6-9] describe mining industry grinding circuits consisting of primary open-circuit SAG mills followed by closed-circuit ball mills. Reference [13] outlines modeling and control of closed-circuit cement mills.

Model-based control has never been used in open-circuit dry ball milling of metal powders.

The highly non-linear and oscillatory behavior of many particulate processes implies the need to implement non-linear model-based feedback controllers in order to ensure a stable and efficient operation [14]. In addition to being highly non-linear and dimensionally infinite, the population balance models of most particulate processes are uncertain. At this stage, there is no general framework for the synthesis of practically implementable non-linear feedback controllers for particulate processes that allow

attaining desired particle size distributions in the presence of significant model uncertainty [14].

As a result, the ball milling operation generates large variations in powder properties. These variations are reflected on all the downstream operations and, therefore, on the final product properties.

Advances in the development of testing tools and process know-how in the field of mixing, compacting and sintering in powder metallurgy have enabled Domfer's customers to test the powders more rigorously. Model-based control built on the integration of process know-how and simulation tools can address these ever increasing control requirements [15]. The priority is now on reducing the final powder variations in particle size which, in turn, will reduce end product variations.

1.3 Research objectives and proposed approach

Goal:

The goal of the research is to develop model-based control for the ball milling process of metal powder.

Objectives:

1. Develop techniques to include process physics into design and computer models.
2. Develop process monitoring and fault diagnosis techniques.
3. Develop control strategies for model-based control.
4. Develop computer architectures for real-time model-based control.

The proposed research will focus on optimizing the ball milling process of metal powders. The research objectives are aimed at reducing product size variations while maximizing throughput. However, the following aspects of ball milling will also be improved: powder quality, energy cost, personnel cost, and operating cost.

This will provide Domfer, a Canadian company, with a serious advantage worldwide with respect to product quality and competitiveness.

Specific Objectives

The comparison in table 1.1 shows the apparent density (A.D.) and size distribution (-200mesh (-75 μ m)) results from December 2002 to July 2003 with respect to required ball milling product specifications. Product size distribution is often defined by a single point measurement, such as the percentage passing a 200mesh (75 μ m) sieve.

Table 1.1: Domfer specifications vs average production results from Dec 02 to July 03

Grade	Specifications: $\mu \pm 3\sigma$		Results: $\mu \pm 3\sigma$	
	A.D. (g/cc)	-200 mesh (%)	A.D. (g/cc)	-200 mesh (%)
MP3	3.10 ± 0.30	70 ± 6	3.09 ± 0.33	70.1 ± 11.4
MP1	3.20 ± 0.30	62 ± 4	3.09 ± 0.36	62.4 ± 11.7
MP4	3.50 ± 0.30	53 ± 6	3.30 ± 0.33	52.5 ± 11.4
MP2	3.50 ± 0.30	48 ± 6	3.38 ± 0.30	49.8 ± 15.3

We can see that the ball milling operation generates large variations in the powder properties, i.e., lack of accuracy for density and no precision for size distribution. These variations are reflected in all downstream operations and, therefore, in the final product properties. Rejected final product lots were directly related to the ball milling process:

<u>Year</u>	<u>Rejected lots</u>
2001	28
2002	55
2003	59

Dimensional change problems (too much growth of sintered parts) forced the modification of ball mill specifications. After compaction, the sintering process provides solid state diffusion and bonding between the powder particles. The driving force of the reaction is to minimize free surfaces. A finer product having greater free surface reduction potential will react faster, expand less or even tend to shrink.

Table 1.2 shows the new Domfer ball milling product specifications compared to the specific research objectives, i.e., they are identical.

Table 1.2: Domfer specifications compared to specific research objectives

Grade	Specifications: $\mu \pm 3\sigma$		Specific Objectives: $\mu \pm 3\sigma$	
	A.D. (g/cc)	-200mesh (%)	A.D. (g/cc)	-200mesh (%)
MP3	3.10 ± 0.20	74 ± 4	3.10 ± 0.20	74 ± 4
MP1	3.10 ± 0.20	67 ± 4	3.10 ± 0.20	67 ± 4
MP4	3.50 ± 0.20	57 ± 4	3.50 ± 0.20	57 ± 4
MP2	3.50 ± 0.20	53 ± 4	3.50 ± 0.20	53 ± 4

Research objectives are aimed at achieving Domfer ball milling specifications at a 99.7% confidence interval ($\pm 3\sigma$), providing enhanced downstream equipment controllability and reducing by 50% the number of rejected final product lots.

Characterization of the model:

The feedback control system will be composed of a ball mill whose output variables are regulated by a controller through variation of the ball mill input parameters based on the difference between desired and measured product properties. The controller design will be model-based.

In order to develop a process model describing the physics of the ball mill, the following steps are performed:

1. Research existing process models or components for models from published material and interviews with experts.
2. Define control structure and strategy.
3. Develop rules based on the knowledge of most experienced operators.
4. Develop equations to relate dependent variables and allow inference measurement.
5. Create process models and sub-models.
6. Include a control architecture that integrates the models and achieves the desired response time for a robust real-time process control.

Thus, the process model is a combination of rules, equations and heuristics. It deals with all the variables of the ball mill described previously and applies the various rules and relations as appropriate. The outputs of the process model are given to the control system for action.

Research Work Plan

The research plan has been broken down into 6 main activities:

1. Review the literature on advanced process dynamics and control, size reduction theory, ball mill models, and other existing grinding models.
2. Characterize and analyze the ball milling process: process physics, measurability, observability and controllability of the variables affecting the powder, performance specifications of the variables and sensors.
3. Create a new sampler and integrate an automatic size analyzer.
4. Develop a process model of the ball milling process.
5. Design monitoring and control: control algorithms, monitoring algorithms and controller hardware.
6. Verify and validate the proposed model-based control system.

Chapter 1 has introduced the context of the need for better process control. Next, size reduction theory is presented in chapter 2. A description of the ball milling process follows in chapter 3. Then, product size feedback provided by automatic sampler design and particle sizing is explained in chapter 4. Process model development is detailed in chapter 5: control strategy, architecture and ball mill model. Subsequently, process control and monitoring, such as created algorithms and controller hardware architecture, are described in chapter 6. A discussion is presented in chapter 7 on system performance and future development. Chapter 8 outlines personal contributions to knowledge. Finally, chapter 9 concludes the thesis, followed by references and appendices.

2.0 SIZE REDUCTION THEORY: BALL MILLING

Size reduction theory is reviewed to develop model-based control for the ball milling process. The definitions, laws, formulation of problems, performance trends and dynamics from the theory help to understand the process and allow the characterization of the required variables to define the control structure and strategy, and create the ball mill model.

Size reduction by mechanical grinding is a very important operation in the metallurgical, mineral, power and chemical industries. The quantity of brittle materials such as ores, rocks, cement products, coal and metal powder ground annually in the United States is at least 1 Gt (one giga ton) with large associated energy consumption [16]. Single plants handling 10 Mt (million tons) or more per year are quite common. The ball milling operation has a theoretical basis which has evolved in the last three decades. This theoretical basis is similar to the theory of chemical reactor design and uses many common concepts and terminology. In designing a reactor, a primary task is to size the reactor for a desired output rate with a desired quality of product, using heat transfer coefficients, rate constants, mass and thermal balances, etc. Sufficient energy is needed to accomplish the desired reactions and the design must minimize undesired reactions. The system must be controllable and stable in order to meet a range of product specifications. A specific quantity of output must be produced in the most efficient way, with a minimum of capital expenditure, energy, maintenance and labor costs. Consider the most widely used type of mill, the tumbling ball mill, shown in figure 2.1.

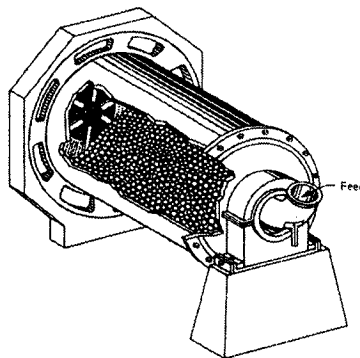


Figure 2.1: Illustration of a tumbling ball mill at rest [17]

2.0 SIZE REDUCTION THEORY: BALL MILLING

Similar to reactor design, ball milling can be considered as a continuous reactor where energy input is converted to mechanical breakage action; the reaction being accomplished is size reduction. Coarse powder is fed into the mill, passes through while receiving breakage actions caused by the tumbling balls, and leaves as product with a finer size distribution. The capital expenditure per unit of mill capacity has to be minimized with precise and stable product properties, which involves good mill conditions such as rotational speed, ball load and sizes, and liners. The conditions for minimum energy per ton of product are not necessarily at maximum capacity. The mill should operate with as efficient a grinding action as possible, i.e., high specific mill capacity and low specific energy consumption, subject to constraints of maintenance costs, wear, and contamination. Like many reactor systems, the use of grinding combined with recycling is advantageous. The material coming out of a mill passes through a size classifier, which splits the product in two streams, one containing coarser (oversize) particles and the other finer particles. The oversize particles are recycled back into the mill feed. The process of selective size separation is called classification and is performed using either continuous screen, spiral classifiers, cyclones or air separators. A complete design of the ball milling operation involves the feeders, classifiers, dust collectors, blowers, etc. Optimal design involves making a desired product with minimum capital investment, power and maintenance costs, and a maximum of reliability and controllability.

2.1 Definitions and formulation of problems

The reactant in the mill is the feed, which has a complete distribution of sizes. This size distribution can be represented by a continuous curve $P(x)$, representing the cumulative weight fraction below size x . It is convenient to use log-log scales for this plot, as shown in figure 2.2. The simplest and most reliable method for size analysis is sieving, and size frequently refers to sieve size (Table 2.1). The weight fraction, w , also represented in figure 2.2, describes the size distribution. It is convenient to use size intervals in geometric progression corresponding to standard sieve progression. It is customary to number the largest size as 1, 2 for the next smaller and n for the smallest material. Considering any general size interval, the i th size interval, the weight fraction of material in the i th interval is w_i . It is not easy to extend size distribution to very small sizes, below

400 mesh (38 μm) due to the experimental difficulty to measure small sizes and operate such small screens. The sink interval, w_n , is receiving material from breakage of all larger sizes but material cannot be broken out of the interval.

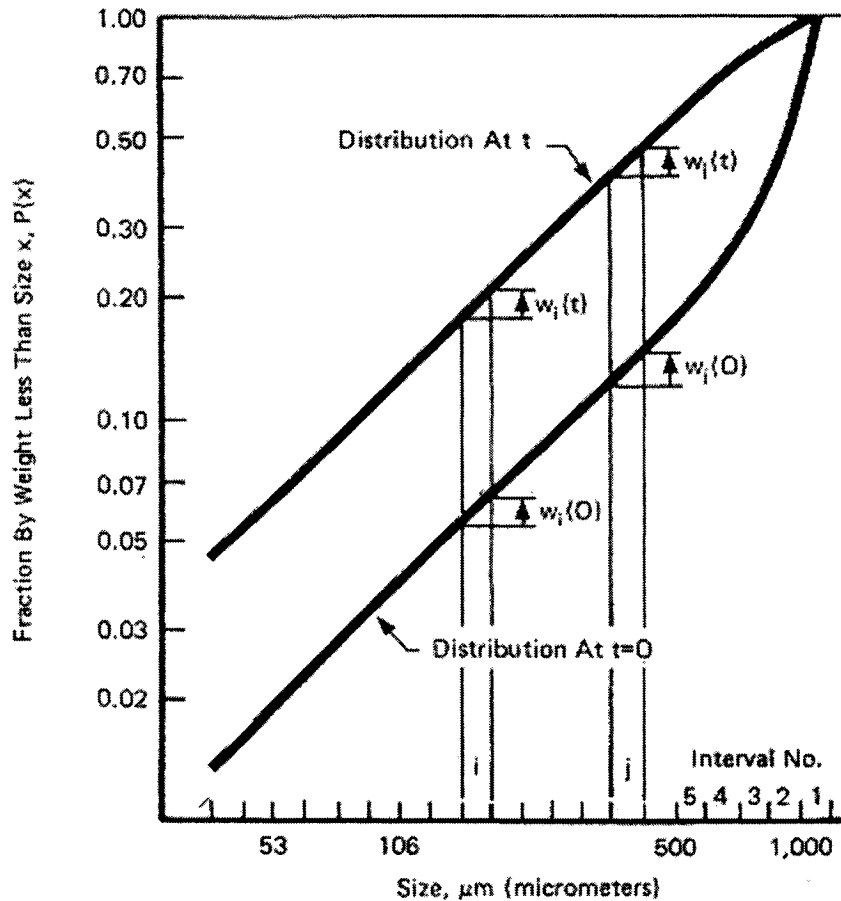


Figure 2.2: Cumulative distribution data for powder size [17]

The product from the ball mill is the distribution of the material coming out. Again, this is never a single size and a curve or set of numbers is used to characterize the size distribution. In order to define a grinding system, the desired product must be clearly specified. But, it is not generally possible to describe the complete size distribution and the product is usually defined by: (1) a single point, e.g., 80%-by-weight passes 200 mesh (75 μm), (2) two points, e.g., 50% less than 400 mesh (38 μm) and no more than 5% greater than 60 mesh (250 μm), (3) an equivalent specific surface area of the distribution.

Table 2.1: The International Standard Sieve Series

Standard	US Sieve Designation	Standard	US Sieve Designation
125 mm	5 in	850 μm	No.20
106 mm	4.24 in	710 μm	No.25
100 mm	4 in	600 μm	No.30
90 mm	3 1/2 in	500 μm	No.35
75 mm	3 in	425 μm	No.40
63 mm	2 1/2 in	355 μm	No.45
53 mm	2.12 in	300 μm	No.50
50 mm	2 in	250 μm	No.60
45 mm	1 3/4 in	212 μm	No.70
37.5 mm	1 1/2 in	180 μm	No.80
31.5 mm	1 1/4 in	150 μm	No.100
26.5 mm	1.06 in	125 μm	No.120
25.0 mm	1 in	106 μm	No.140
22.4 mm	7/8 in	90 μm	No.170
19.0 mm	3/4 in	75 μm	No.200
16.0 mm	5/8 in	63 μm	No.230
13.2 mm	0.530 in	53 μm	No.270
12.5 mm	1/2 in	45 μm	No.325
11.2 mm	7/16 in	38 μm	No.400
9.5 mm	3/8 in		
8.0 mm	5/16 in		
6.7 mm	0.265 in		
6.3 mm	1/4 in		
5.6 mm	No.3 1/2		
4.75 mm	No.4		
4.00 mm	No.5		
3.35 mm	No.6		
2.80 mm	No.7		
2.36 mm	No.8		
2.00 mm	No.10		
1.70 mm	No.12		
1.40 mm	No.14		
1.18 mm	No.16		
1.00 mm	No.18		

The product specifications are a function of the process following the milling. For example, the +100mesh/-200mesh (+150 μm /-75 μm) size distribution ratio is critical for apparent density and dimensional change during sintering in the Domfer process. There is no general agreement on what should constitute the minimum adequate characterization of the product size distribution from a milling circuit. The pertinent question is whether one or two points on a size distribution can be sufficient to pre-determine a negligibly narrow band of size distributions [18].

From common-sense reasoning, we can say that the rates at which particles break in a grinding device depend on the size of the particle. A ball mill operates on a whole set of feed sizes and produces a whole set of final sizes. The capacity in tons per hour is meaningless without defining the feed and product size distributions. Obviously, more breakage actions are required to grind coarser feed to a desired product size; the energy per ton is higher and mill output lower. The fragmentation of a fixed size of particle produces a complete range of product size, as illustrated in figure 2.3. The product can be defined as the fraction of material broken from a fixed size that falls into smaller size intervals. The detailed understanding of the ball mill requires a knowledge of the primary progeny fragment distributions or the primary breakage distribution function [16].

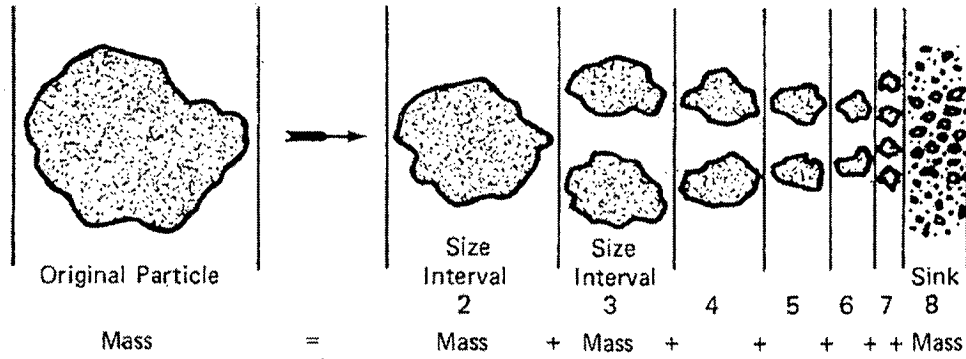


Figure 2.3: Feed particles fragmentation [17]

To define breakage in a ball mill, consider a mill volume V containing a mass of powder M_p . At a size interval i , the fraction of M_p of size i is w_i ; therefore, the mass of size i is $w_i M_p$. The specific rate of breakage, S_i , is the mass of size i broken per unit time per mass of size i present. Thus,

$$\text{rate of breakage of size } i = S_i w_i M_p \quad (\text{kg/sec}) \quad (2.1)$$

A widely used term is mill capacity (tons per hour), defined as the rate of production of a desired product from a specified feed. Another fundamental concept is the residence time, also called retention time. If the feed rate is decreased, the material spends more time in the mill, receives more breakage actions and is hence ground finer. However, some material may leave the mill almost immediately, while some may hold up for a longer

2.0 SIZE REDUCTION THEORY: BALL MILLING

period of time, leading to the concept of residence time distribution. Many residence time models have been developed [20], such as two parameters models, where the mean residence time is one parameter and the other characteristic parameter can be the number of sections, the relative size of sections, the dimensionless mixing factor, etc. These models provide approximations of the complete feed size distribution grinding time. In many cases, the mean residence time τ is defined by M_p/\dot{m} , \dot{m} being the feed rate (kg/hr). M_p is often called the hold-up in the mill.

The Domfer process utilizes a dry open-circuit ball milling operation. Under those conditions, i.e., no classification of recycle, material already fine enough still passes naturally along the mill and is ground finer at the same time as coarse material is being produce below the control size. Incorporating a classifier and closing the circuit permits running the mill at higher mass flow rates and shorter residence times. The higher flow rate removes material faster, the fines are separated in the classifier and the coarser particles returned to the mill inlet. The overall effect is that the particle size distribution being acted on in the mill is pushed toward the coarser side and less fines are present.

There are two types of ball milling inefficiency [17]. The first type is called indirect inefficiency, where energy is wasted in over-grinding material even if the breakage is efficient. The second type, direct inefficiency, occurs when the mill conditions are providing poor breakage actions, for example, under-filling the mill so that the energy of tumbling balls is utilized in steel-to-steel contact without particle breakage, overfilling the mill so that the ball-powder-ball action is cushioned by excessive powder, or too high slurry density in wet grinding that absorbs impact without giving breakage.

Two important mill conditions will now be defined. The first one is the critical speed N_c : rotational speed at which balls just start to centrifuge on the mill walls and not tumble. By balancing gravity force and centrifugal force on a ball at the top of the mill we get the well known equation:

$$N_c(RPM) = \frac{42.2}{\sqrt{D-d}} \quad (D, d \text{ in m}) \quad (2.2)$$

where D is the internal mill diameter and d the maximum ball diameter.

The tumbling action will depend on the fraction of the critical speed at which the mill runs; thus, the ball mill angular speed is normally specified by ϕ_c , the fraction of critical speed. The above equation has been accepted widely and is described in many papers and books, but it does not determine precisely the optimal grinding efficiency. This is because the repulsive force of collision among the balls and the frictional force between the ball and the inner wall of the mill are greater than the impact force generated by the falling of the ball; so, the critical speed equation becomes [21]:

$$N_c = \frac{(23 \text{ to } 38)}{\sqrt{D}} \quad (2.3)$$

In most ball mills, the optimum grinding will be seen at $\phi_c \approx 0.75$.

The second important mill condition is clearly the mill volume filled with balls. However, it is very difficult to determine in production the weight of balls and therefore not possible to determine their volume. The mill must be emptied from its powder content and then stopped. It is then possible to measure the height from the ball bed to the center line of the ball mill rotating axis. This enables the estimation of the fractional ball filling, J , which is expressed as the fraction of the mill filled by balls at rest. In order to convert from bed volume to mass of balls present, it is necessary to know the bulk density of the ball bed. The bed porosity varies slightly depending on the ball size distribution, but it is conventional to define a constant bed porosity for calculations.

2.2 Laws of grinding

There have been several scientific attempts to develop fundamental laws of grinding or to explain empirical relations on a scientific basis. A number of empirical laws linking energy requirements to size reduction have been proposed, but their lack of any fundamental foundation severely limits their range of applicability. Figure 2.4 shows typical results obtained by batch grinding a brittle material in a ball mill, where the size distribution is getting finer and finer for longer periods of time. Obviously, this data allows the calculation of the capacity (kg/hr) to grind from one size distribution in this set of curves to another. If the mill power is known, the specific energy (kWh/kg) also

follows. A mathematical representation of the data would be very useful for interpolation and extrapolation of the results. This section will describe some mathematical models, which forms the empirical relations in ball mill design.

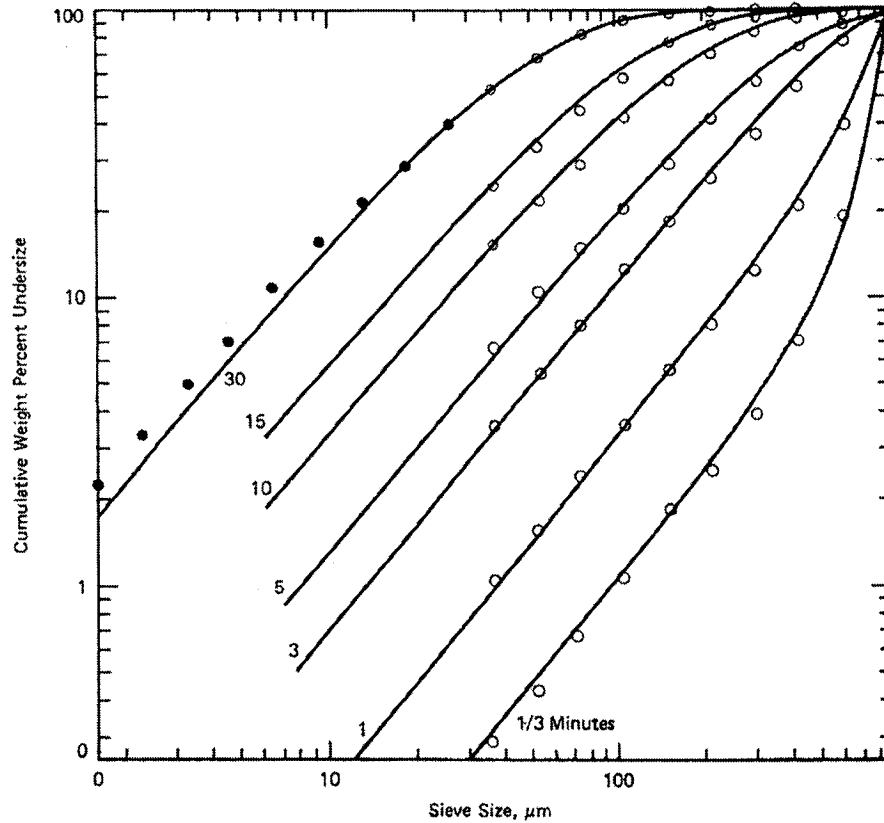


Figure 2.4: Experimental size distribution for dry grinding [17]

Rittinger's Law [22] states that the energy required for breakage is related to the fresh surface produced in a unit amount of mass:

$$\text{specific energy} = \gamma (\text{new surface area} - \text{old surface area}) \quad (2.4)$$

where γ is the mean surface energy per unit area. This law is appealing since it represents a logical physicochemical law. Since the mill energy is the design or control parameter, it is necessary to find a relation between energy input to the mill and the surface energy. In a series of classic experiments, Rose [23] by careful energy balance in the mill, found that the surface energy is a very small portion of the energy input to the mill. He discovered that most of the energy to the mill is consumed through heat loss, sound or energy of phase transformation.

The fraction of input energy converted to surface energy in a fracture process greatly depends on flaw structure of the feed material and method of stress application.

In practice, the Bond's Law [24] of batch grinding is often utilized:

$$E = \varphi \left(\frac{10}{x_p^{1/2}} - \frac{10}{x_f^{1/2}} \right) \quad (2.5)$$

where E is the specific grinding energy (kWh/t), x_p the 80% passing size of products (μm), x_f the 80% passing size of feed (μm), and φ a constant describing the efficiency of grinding. Harder materials will have a high value of φ compared to weaker or more brittle ones.

Also, the shaft power, P (kW), can be calculated by:

$$P = QE \quad (2.6)$$

where Q is the mill capacity (t/hr).

The Bond relation can be converted to shaft mill power P (kW) as a function of mill dimensions [17]:

$$P = 7.33 J \phi_c (1 - 0.937 J) \left[1 - \frac{0.1}{2^{9-10\phi_c}} \right] (\rho_{b,true} L D^{2.3}) \quad (2.7)$$

where D is the internal diameter (m), L the mill length (m), $\rho_{b,true}$ the true density of the grinding media (t/m^3), ϕ_c the fraction of critical speed and J the fraction of the mill filled by balls at rest. Hence, knowing P and the specifications of J , ϕ_c , and $\rho_{b,true}$, the values of D and L necessary for this power can be evaluated.

In any fracture process, a minimum strain must be applied to the particles to initiate propagation of fracture cracks. The presence of pre-existing cracks or flaws, the hardness, the geometry and rate of stress application will dictate whether fracture initiates at low or high energy strain. In a tumbling mill, the energy is used to raise the balls against the force of gravity, and when the balls fall their potential energy is converted to kinetic energy. The balls strike the particles, converting their kinetic energy to strain energy in

2.0 SIZE REDUCTION THEORY: BALL MILLING

the particles. If the impact force is sufficient, the particle is stressed to fracture point and breaks via branch fractures propagation, producing many fragments. Every fragment will convert the remainder of stored strain energy to heat after the fracture process. The fraction of mill energy converted to heat is very high. It follows that the utilization of energy in a mill is very inefficient. In industrial ball milling machines, a rapid massive straining of particles is taking place, followed by explosive fracture to a variety of fragments, releasing energy primarily as heat, sound and endothermic phase change or residual stresses in the fragments.

Grinding is a mechanical process where efficiency is dictated by the mechanics of stressing particles to the failure point at high rates. So the total efficiency involves efficient conversion of input energy to mechanical action, efficient transfer of mechanical action to the particles and achieving failure stress of the particles. If a ball mill is running with a too low powder loading, the impacts will be of steel ball on steel ball and the mechanical action will not be transfer to the particles. Similarly, if the mill is overfilled, the particles will not break, except by slow abrasion, and grinding will be inefficient.

It is convenient to describe the size distribution of the powder in the mill as shown in figure 2.2. It would appear reasonable that the rate of disappearance of size i might fit a first-order law [25]:

Rate of disappearance of size i due to breakage $\propto w_i(t)M_p$

or

$$-\frac{d[w_i(t)M_p]}{dt} \propto w_i(t)M_p \quad (2.8)$$

For batch grinding, since the total mass M_p is constant, equation 2.8 becomes,

$$\frac{dw_i(t)}{dt} = -S_i w_i(t) \quad (2.9)$$

where S_i is the proportionality constant and is called the specific rate of breakage. Then if S_i is independent of time and other sized particles,

$$w_i(t) = w_i(0) \exp(-S_i t) \quad (2.10)$$

To describe more precisely the influence of the variables in the grinding process, a more detailed description is needed: the size-mass rate balance. The analysis is performed using the concepts of specific rates of breakage and primary progeny fragment distributions. For the particulate process, it has become popular to refer to population balance. In fact, the word balance can be misleading since the major objective of most particle processes is to change the particle population and functional properties of the system. The particle population at the end of the process is different than at the beginning; otherwise, the process has achieved little. The word balance is used because the change in population is usually written as some form of the continuity equation [26].

Primary breakage is defined by: particles break and the fragments produced are mixed back in with the mass of powder in the mill. Figure 2.5 shows a typical distribution of fragments just before they are reselected for further breakage. If the material of size 1 is broken, the weight fraction of the products in the size i is $b_{i,1}$. The set of numbers $b_{i,1}$, for i ranging from 2 to n , describes the distribution of fragments produced from size 1. Generally, the numbers $b_{i,j}$ describe the breakage of all sizes, that is, $b_{i,1}$ for $n \geq i \geq 2$ plus $b_{i,2}$ for $n \geq i \geq 3$, etc.

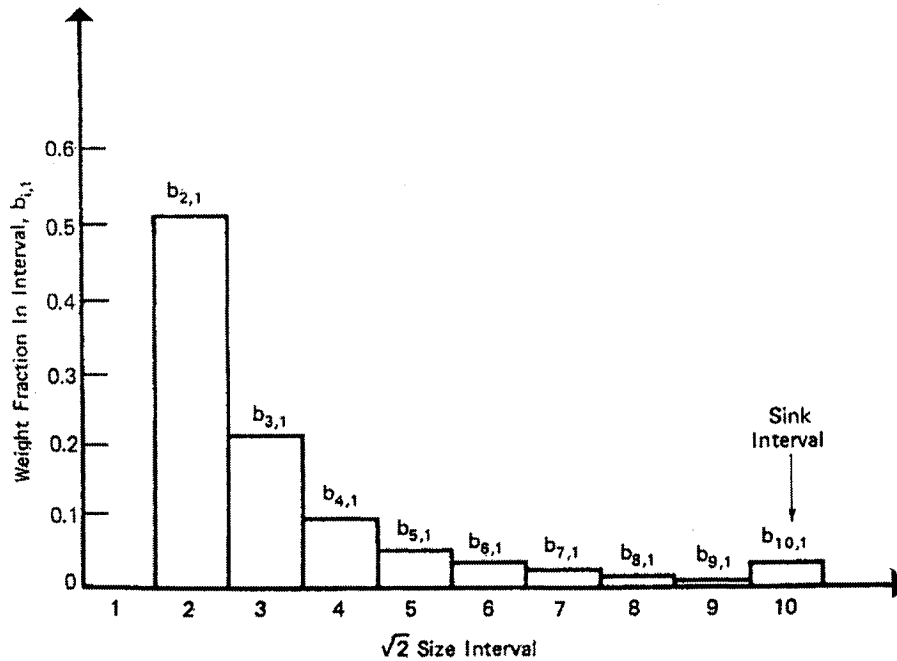


Figure 2.5: Primary progeny fragment distribution [17]

2.0 SIZE REDUCTION THEORY: BALL MILLING

The rates of production of finer materials are described as:

$$\begin{aligned} &\text{Rate of production of size } i \text{ from breakage of larger size } j \\ &= (\text{fraction to } i \text{ from } j)(\text{rate of breakage of size } j) \\ &= b_{ij}S_jw_j(t)M_p \end{aligned}$$

where b_{ij} is the weight fraction of products from j to i , S_j the specific rate of breakage (time^{-1}) of size j , w_j the fraction of material of size j , and M_p the holding mass.

A complete size-mass balance or population balance of the batch grinding system is described below, where the concept of first-order breakage leads to simpler solutions [27]. The following statements are involved:

1. The rate of disappearance of size j material by breakage to smaller sizes = $S_jw_j(t)M_p$.
2. The rate of appearance of size i material produced by fracture of size j material = $b_{ij}S_jw_j(t)M_p$.
3. The rate of disappearance of size i material by breakage to smaller sizes = $S_iw_i(t)M_p$.
4. The net rate of production of size i material equals the sum rate of appearance from breakage of all larger sizes minus the rate of its disappearance by breakage.

The final balance is:

$$\frac{d[w_i(t)M_p]}{dt} = -S_iw_i(t)M_p + \sum_{j=1, i>j}^{i-1} b_{ij}S_jw_j(t)M_p, \quad n \geq i \geq j \geq 1 \quad (2.11)$$

An illustration of the mass balance action is shown in figure 2.6. We can see that size interval 2 is receiving material from size 1, size interval 3 is receiving material from sizes 1 and 2, etc, and the finest sink interval is receiving material from all larger sizes.

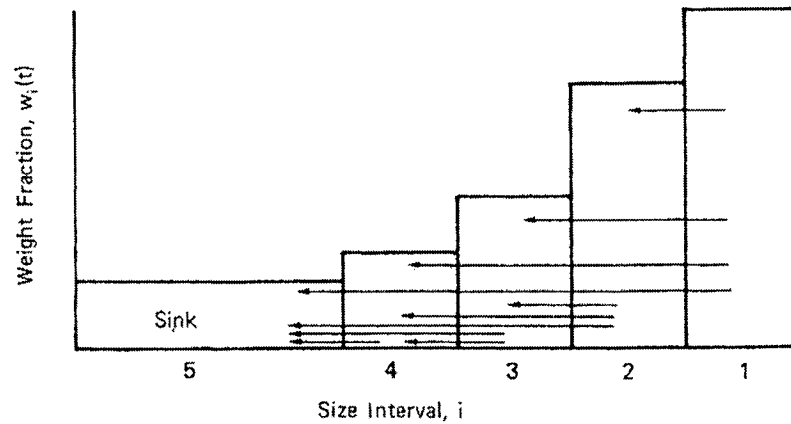


Figure 2.6: Illustration of mass balance action in fully mixed batch grinding [17]

There are several assumptions in this above formulation: grinding is a first-order process, the b values are constant with time, no regrowth of particles by cold welding, fracture properties of a given size j in the products of breakage are the same as size j material in the raw feed and the material being broken is homogeneous from the breakage point of view, i.e. it is not a mix of stronger and weaker components nor does it develop such a mix as it breaks. However, as described by Spring, Larsen and Mular [28], the size-mass rate balance equation gets complicated very quickly when the following aspects are considered: breakage functions, residence time distributions for all sizes of particles, selection functions, effect of missing screen sizes, effect of not knowing the average residence time and the effect of operating variables.

2.3 Powder characterization

To understand the ball milling process, we must understand the nature of the material that is reduced: metal powder. Generally, the particles are larger than smoke (0.01 to 1 μm) and smaller than sand (0.1 to 3 mm). Many metal powders have a size similar to the diameter of a human hair (25 to 200 μm). The scanning electron microscope (SEM) is one of the best tools available for observing the discrete characteristics of metal powders. An array of SEM micrographs for several powders is shown in figure 2.7. Variations in shape from flake to spherical and in particle size from the submicron to 1 mm illustrate the wide range of possible characteristics.

2.0 SIZE REDUCTION THEORY: BALL MILLING

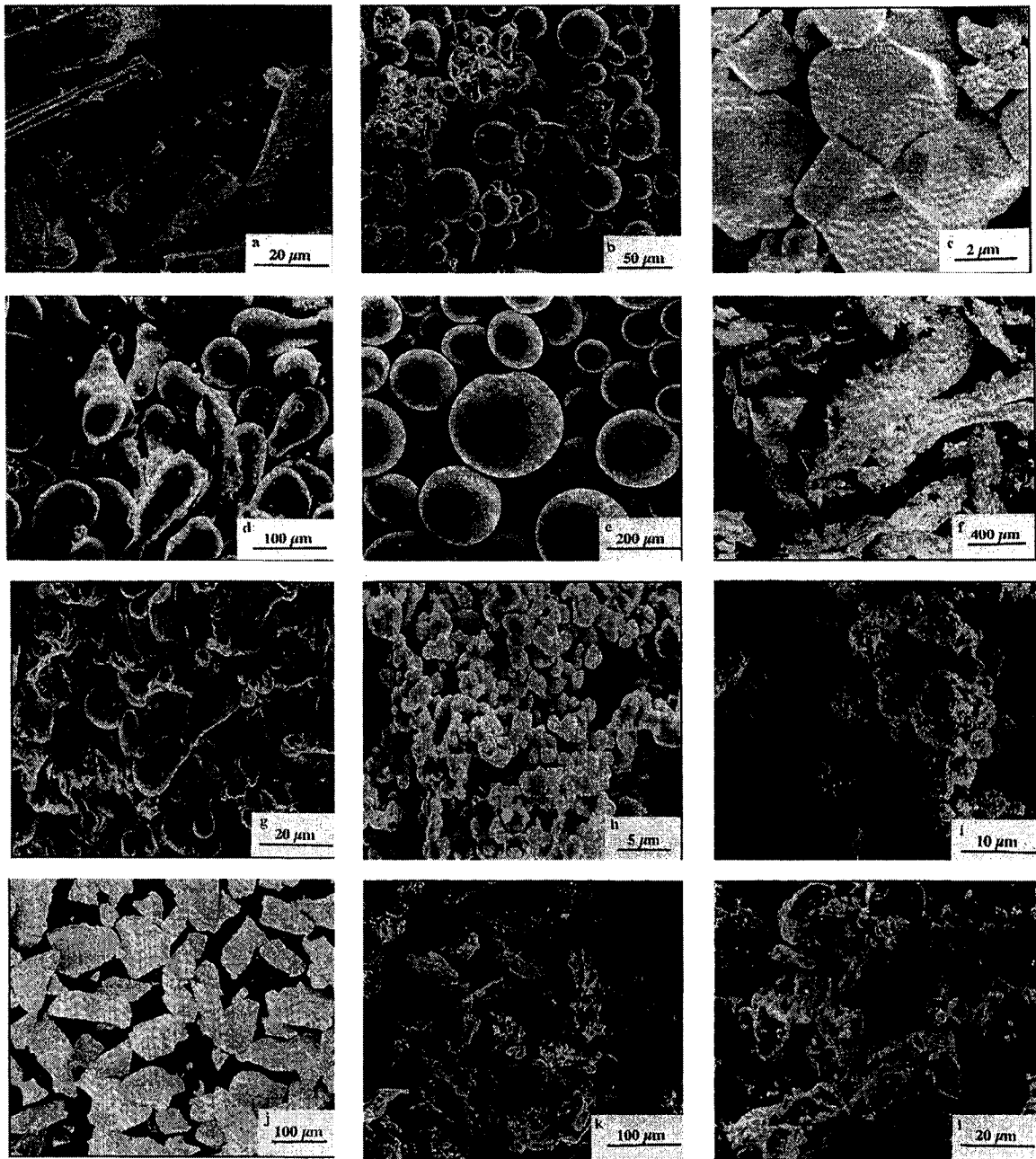


Figure 2.7: SEM micrographs of diverse shapes and sizes of metal powders [29]

Figure 2.7 illustrates a variety of materials, fabrication methods and particle shapes: a) tellurium, milled, acicular, b) iron alloy, argon atomized, spherical with agglomerated fines, c) tungsten, gas reduced, polygonal aggregates, d) tin, air atomized, rounded and ligamental, e) iron alloy, centrifugally atomized, spherical, f) tin, splat quenched, flake, **g) Domfer process**, stainless steel, water atomized, rounded and irregular, h) palladium, electrolytic, sponge, i) nickel, carbonyl decomposition, porous and cubic, j) iron-based metallic glass, crushed ribbon, angular plates, k) titanium, sodium reduced and milled, irregular, l) niobium hydride, milled, angular.

Beyond particle appearance, quantitative data is required to fully characterize metal powders: particle size and distribution, particle shape and its variation with particle size, surface area, internal particle structure, composition, homogeneity and contamination. To fully specify the nature of a powder, it is necessary to qualitatively describe how it is fabricated. Dimensioning a particle is quite difficult because of the shape. Widely differing size determination techniques are possible depending on the size parameter used and the shape. Usually, a simplifying assumption for the shape is necessary to reduce the size information to a single parameter.

Collecting a representative sample of powder is critical for proper process control. A typical production lot may be several tons in size but many modern analytical instruments require sample sizes of a gram or less. Frequent sampling provides more representative results. Sampling errors can be avoided using some simple rules [29]:

1. Powder samples should be taken from a moving stream, not from stagnant lots.
2. Sample quality is highest when it is a blend of several small specimens taken from a moving powder stream.
3. If static sampling procedure is necessary, then many small samples taken from random locations avoid bias.

Particle size is the determination of the dimensions of a particle. Particle sizing analysis can be achieved by any of several instruments which usually do not give equivalent determinations because of differences in the measured parameters. Particle size is probably one of the most important characteristics to the powder metallurgist. Size data are useful when presented within the context of the assumed particle shape and measurement basis. Screening is a common technique for rapidly analyzing particle size. A square grid of evenly spaced wires creates a mesh. The number of wires per unit length determines the mesh size. For example, 200 mesh implies 200 wires per inch, or 127 μm between wire centers. For that mesh, the wire are 52 μm in diameter, the remaining opening size being 75 μm . The screening technique is usually applied to particles larger than 38 μm due to screens manufacturing limitations. Although screening is the most widely used size analysis technique, it is not without its problems. Screens have from 3 to

2.0 SIZE REDUCTION THEORY: BALL MILLING

7% permissible variation in the average opening size as a manufacturing tolerance. Moreover, individual openings can be up to 50% larger than the prescribed mesh size. This produces a soft cut rather than a sharp division. With the smaller screen openings, a common problem is overloading, which blocks the mesh openings, thereby inhibiting powder from reaching the limiting screen size. Hence, the size distribution results are skewed toward the coarser particle sizes. Also, defects in screens will allow oversized particles to pass. Too long of a screening duration may result in the particles breaking into finer pieces and too short of a screening duration will give insufficient time for fines to pass all the way through the screen stack. Because of these difficulties, it is important to use standardized test methodologies, which are described in detail in section 3.2.12.

An analysis of the distribution can be made once size data are collected. The distribution is given as a histogram or frequency plot showing the amount of powder in each size increment. For example, consider the sieving data in table 2.2, which give the weight of material retained on each screen after sieving. First, the weight retained is converted into incremental percentages by dividing each increment by the total sample weight. The histogram for these data is created by plotting the incremental percentages versus the screen opening size as shown in figure 2.8, where the mode is the peak particle size. For this plot, the particle size is converted to a log scale to make increment widths equal.

Table 2.2: Particle size distribution data [29]

Mesh Size	opening μm	weight retained, g	interval percent	cumulative percent
70	212	0.0	0.0	0.0
80	180	1.1	0.9	0.9
100	150	3.0	2.5	3.3
120	125	8.7	7.1	10.4
140	106	13.2	10.8	21.2
170	90	16.5	13.5	34.7
200	75	20.8	17.0	51.7
230	63	18.0	14.7	66.4
270	53	16.9	13.8	80.2
325	45	13.6	11.1	91.3
400	38	10.8	8.8	100.0
500	25	0.0	0.0	100.0

total weight = 122.6g

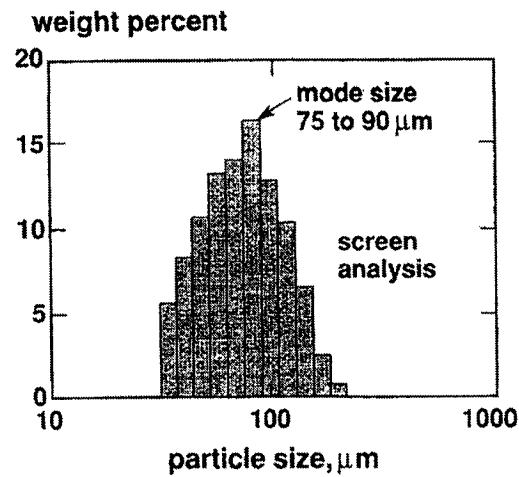


Figure 2.8: Histogram plot of the screening data [29]

In most instances, metal powders are found to exhibit a bell shaped curve (Gaussian or normal distribution) when plotted on a log scale of sizes, termed log-normal [29]. Adding the interval percentages and plotting the result versus the lower incremental particle size will generate a cumulative particle size distribution. Using the data in table 2.2, the cumulative distribution is plotted in figure 2.9.

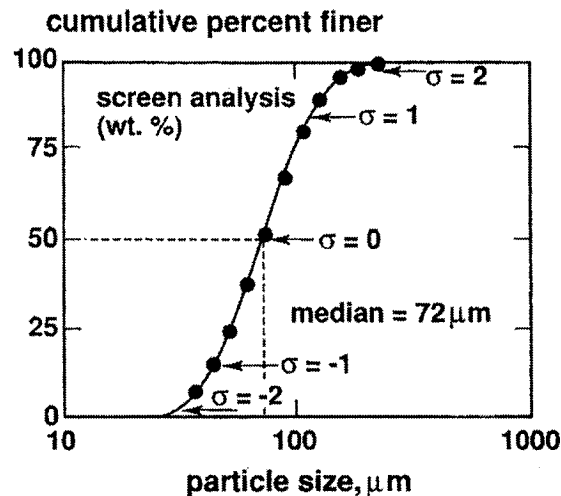


Figure 2.9: Cumulative particle size distribution [29]

On the cumulative distribution, the median size corresponds to the 50% value. The mode particle size corresponds to the most frequent size, which is the highest peak on the histogram distribution. The standard deviation of sizes ($\pm 1\sigma$) correspond to the particle sizes at 84.13% and 15.87%.

From the histogram data, the arithmetic mean size D_{am} is calculated as follows:

$$D_{am} = \frac{1}{N} \sum y_i D_i \quad (2.12)$$

where D_i is the midpoint size of each interval, y_i is the frequency of occurrence in the size interval, and N is the total number of occurrences (sum of y_i over all size intervals).

Frequently seen shapes of particle size distribution encountered in P/M are shown in figure 2.10.

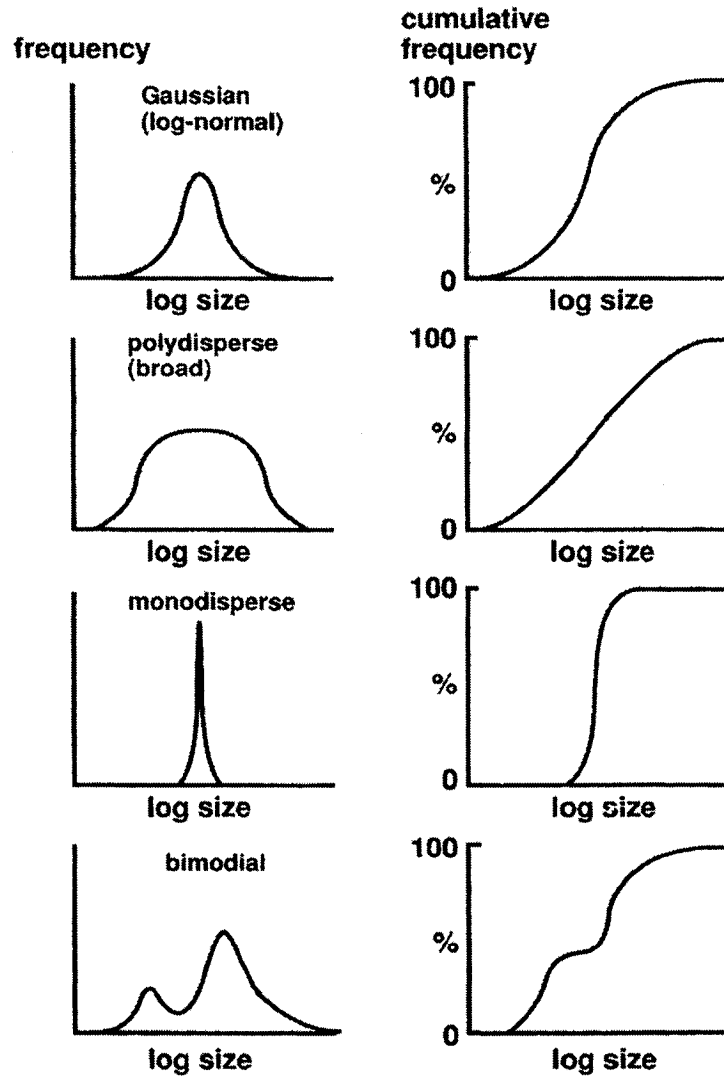


Figure 2.10: Comparison of the common types of particle size distributions [29]

Figure 2.10 shows the nature of both the frequency and cumulative plots, including broad and narrow distributions as well as a bimodal distribution. Normal powder fabrication practices cannot form a single sized powder (monodisperse). The typical product is polydisperse with a wide range of sizes. Very special efforts are needed to achieve a monodisperse product. Thus, a mean size or median and the dispersion in particle size are necessary to describe the powder. The dispersion is the standard deviation. In P/M, the particle size distribution information is very often presented into three points designated D_{90} , D_{50} , D_{10} , corresponding to particle sizes at the 90, 50, and 10% points on the cumulative distribution.

Most powders in their natural unscreened state follow the log-normal form. A log-normal size distribution gives a bell curve when frequency is plotted on a linear scale versus the log of the particle size. A modified form of the Gaussian probability function can describe mathematically the distribution.

Let $P(x)$ be the probability of a particle size $x = \ln(\text{size})$,

$$P(x) = \frac{1}{\sqrt{2\pi}\sigma_x} \exp\left[-\frac{(x-U)^2}{2\sigma_x^2}\right] \quad (2.13)$$

where $U = \ln(D_{am})$ and σ_x is the standard deviation of the distribution on a logarithmic scale,

$$\sigma_x = \ln\left(\frac{D_{84}}{D_{50}}\right) = \ln\left(\frac{D_{50}}{D_{16}}\right) \quad (2.14)$$

where D_{84} , D_{50} , D_{16} , correspond to particle sizes at the 84, 50, and 16% points on the cumulative distribution.

A schematic comparison of a particle size distribution plotted on several bases is given in figure 2.11.

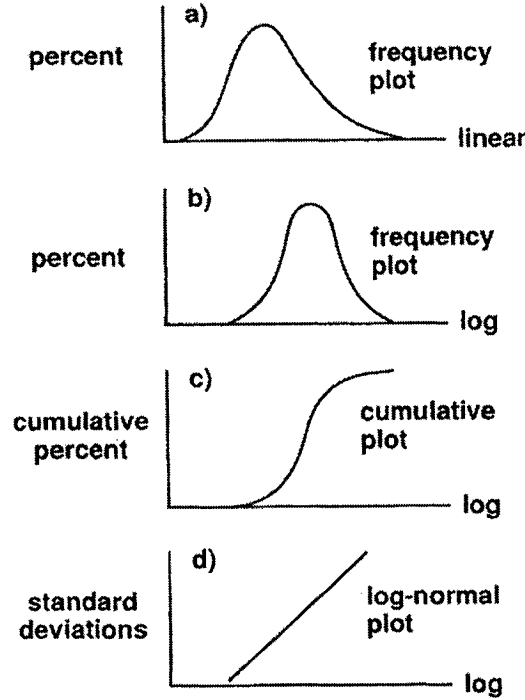


Figure 2.11: Comparison of particle size distribution plotted on several bases [29]

We see that the linear scale gives a skewed particle size distribution while the log scale shows the expected bell curve. The cumulative particle size distribution $F(x)$ can be expressed in terms of the integral of $P(x)$ from 0 to x ,

$$F(x) = \int_0^x P(x) dx \quad (2.15)$$

which is usually given on a percentage basis.

Consider a plot using standard deviations instead of percentages. The standard deviations correspond to specific percentage points. The standard deviations and corresponding cumulative percentage points are listed in table 2.3. The log-normal particle size distribution is created by replotting the percentage points from a cumulative distribution in terms of deviations, as shown in the bottom of figure 2.11. Many powders exhibit straight line behavior on the log-normal plot. Hence, the particle size distribution can be

reduced to just two parameters, the slope and intercept or slope and mean size. Generally, the log-normal distribution is the most useful when dealing with metal powders [29].

Table 2.3: Standard deviations on a cumulative size distribution

<u>Standard deviations</u>	<u>Cumulative percentage</u>
-2.0	2.28
-1.5	6.68
-1.0	15.87
-0.5	31.85
0.0	50.00
0.5	69.15
1.0	84.13
1.5	93.32
2.0	97.72

In figure 2.12, the particle data of table 2.3 is plotted on a cumulative log-normal basis. The standard deviation points have been used, giving a straight line for the distribution. The fundamental attraction of the log-normal distribution is that screening analysis results can be easily compared. If the slope and intercept of a distribution are known, then the distribution of a coarser or finer powder can be estimated by a translation.

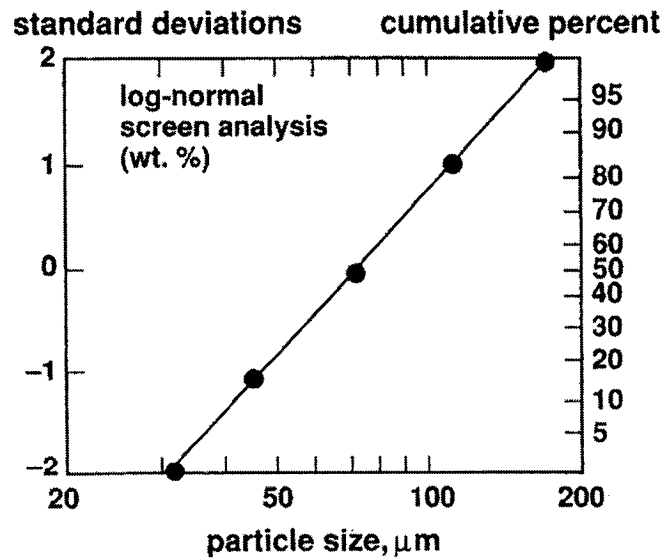


Figure 2.12: Log-normal size distribution plot using standard deviation points [29]

2.4 Performance trends

Performance trends contribute to characterize the process and define the important variables for the analysis. Insight from the trends facilitate the development of rules and equations for the process model.

The mode of operation of a tumbling ball mill is as follows. First, a massive impact will give complete disintegration of a particle (fracture), then a strong blow can chip off a corner (chipping), and finally rubbing will give wear of surfaces (abrasion). When a parent particle breaks, if there is no fragment in the progeny that can be readily identified as the remnant of the parent particle, we speak of impact breakage. Chipping and abrasion will lead to production of fine material and their combined effects is referred to as attrition. In any ball mill operating in normal conditions, all these size reduction mechanisms are at work. The rates of breakage are the net effect of the sum of these mechanisms. The collisions with other balls as a ball tumbles down is the major method of transferring stress to the particles. The power required to turn the mill passes through a maximum as rotational speed increases, corresponding to a maximum in lifting rate and mean height of lift. Thus, the maximum breakage rates are obtained approximately at the rotational speed of maximum power draw, close to 75% of critical speed, depending on the type of lifters and ball load.

The breakage rate is related to particle size and takes the form shown in figure 2.13. The shape of the breakage rate distribution is mainly governed by the charge particle size distribution and the frequency at which the charge is turned over [30]. It will hence depend on mill speed, ball size, ball and powder charge, and feed size distribution.

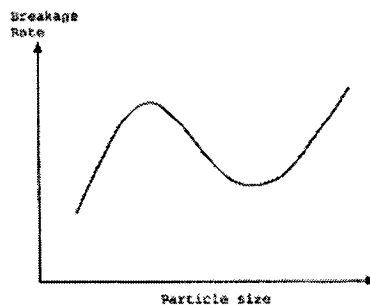


Figure 2.13: Mill breakage rate function [30]

2.4.1 Mill speed

As the mill speed increases, the rate of breakage of coarser particles increases while the rate of breakage of finer particles decreases. The local maximum on the curve of figure 2.13 is the effective limit for impact breakage. Below this size, attrition breakage is predominant and associated with the cascading motion of the grinding media. So, at low speeds the attrition breakage action is enhanced, giving rise to a finer product size. At the coarse end of the size distribution, impact and abrasion breakage occur and are related to the cataracting motion of the grinding media.

The higher mill speeds produce higher breakage rates of coarser sizes, which in operational terms give rise to higher productivity. Attrition breakage at lower speed and impact breakage at the higher speed is a reflection of the changes in mill charge motion. It can be concluded that higher mill speeds provide higher mill throughput with a coarser mill product. But as the centrifugal forces increase with speed, a point will be reached where the breakage rates of the coarser particles are expected to decrease.

2.4.2 Ball size

The breakage rates of coarser sizes is increased with the use of larger ball size. This is explained by the additional kinetic energy provided for breakage. However, the number of larger balls in a given volume is less than that with smaller diameter balls. Charging with large diameter balls results in a high kinetic energy, but less frequent breakage impacts. The net result is that as the particle size decreases, the effect of increased kinetic energy provided by larger balls becomes less pronounced and overshadowed by the effect of a lesser number of balls. The breakage rate is dominated by the size distribution of the ball charge. Increasing the number of smaller size balls will correspondingly increase the surface area and therefore enhance breakage rates of finer sizes.

2.4.3 Ball and powder charge

The effect of adding balls to the mill increases the breakage rates over most of the size range, which in practice results in an increased mill throughput. However, as the powder size is made finer, the effect will eventually reverse and the breakage rate will reduce. Higher ball charge is detrimental to finer grinding performance of the mill.

At lower powder filling, much of the energy of the tumbling balls is taken up in steel-to-steel contact giving low values of rates of breakage and overgrinding of the fines. On the other hand, at high powder charge, the powder cushions the breakage action which has the effect of reducing the grinding efficiency. The operators are able to detect this phenomenon by listening to the high-intensity acoustic vibration signal produced by mechanical grinding. The strength of the acoustic noise decreases greatly when the balls are cushioned with the grinding media. Yigen Zeng and Eric Forssberg describe the monitoring of grinding parameters by sound signal measurements [31].

Breakage rate as a function of powder filling at specific ball load is explained as follows. A low quantity of powder obviously gives a small rate of breakage. As the amount increases, the collision spaces between the balls are filled and higher rates of breakage are obtained. When all the effective spaces where collisions between tumbling balls occur are filled with powder, the rates of breakage reach a maximum. Further addition of powder increases the hold-up without increasing productivity because the collision zones are already saturated and further powder just accumulates in the mill. A plateau of constant breakage rates is obtained. Eventually, overfilling leads to the reduction of effective collisions by powder cushioning. The ball-powder bed expands to give poor powder-ball-powder nipping collisions, and the breakage rates decrease.

2.4.4 Feed size distribution

Any change in the feed material size distribution will directly affect the grinding media size distribution and hence the breakage rates [5]. However, the effect of feed size is a lot stronger on fully autogeneous mills where the grinding media is provided exclusively by the feed product. In ball mills, the grinding media charge is less affected by the feed and

the breakage rates are relatively insensitive to feed size distribution. In autogeneous mills, coarser feed particles cause an increase in the breakage rates in the coarser size fractions. In the case of ball mills, the trend is for the coarse breakage rates to decrease as the feed size increases. The coarser feed contributes less as grinding media and is instead a burden which needs to be ground. This is reflected in the performance of ball mills, where a decrease in feed size results in an increase in throughput.

The effect of increasing rotational speed, ball charge and size is to increase the degree of coarse breakage, often associated with a reduction in the degree of fine particle breakage. The grinding efficiency, which is defined by the production of surface area per unit of grinding energy, decreases as grinding proceeds to fine sizes for dry grinding [32]. The decrease of efficiency is caused by the finer particles being very difficult to break. However, at long grinding times, the specific rates of breakage decrease as fine material accumulates in the mill causing non-first-order breakage, i.e., the slowing down of breakage rates of all sizes present.

2.5 Charge motion

In ball milling, the internal dynamics are fundamental for product properties and productivity. An optimized and stable charge motion will greatly reduce process variations and enhance throughput. Stabilizing the mill dynamics greatly simplifies the model-based control approach.

A typical charge motion profile (Figure 2.14) has four zones characterized by the type of action produced [33]:

1. Flight zone: balls in flight follow a parabolic path under the action of gravity.
2. Crushing zone: balls in flight re-enter the charge and crush particles at high energies.
3. Grinding zone: ball layers slide over one another grinding the material trapped between them.
4. Tumbling zone: balls roll over one another, breaking material in low energy breakage.

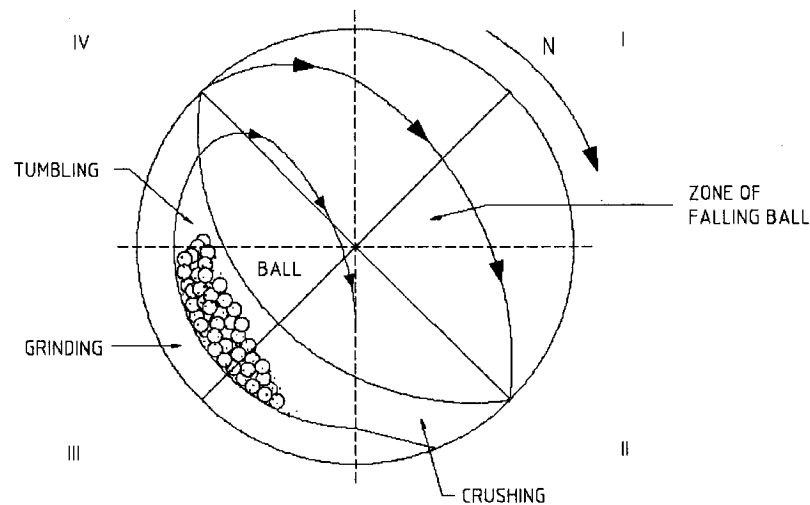


Figure 2.14: Typical ball charge motion profile [33]

At relatively lower rotational speeds (approx. up to 60% N_c), balls ascend from the bottom of the load, called toe position, to the shoulder position where they fall from the mill shell and cascade down along the free surface back to the toe position. At higher rotational speeds, balls ascend with the lifters to a higher shoulder position, cataract and land at the toe position or on the descending liners.

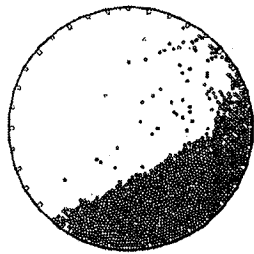
The mill charge is a system of interdependent and interactive elements all working together. Basically, the elements of this system are the balls, the liners (lifters), the mill shell and the powder. The interactions between these elements occur cyclically and are described using the four quadrants of a circle as shown in figure 2.14 [34].

1. In the first quadrant, only one type of interaction needs to be described: ball flight using flight trajectory relationships under gravity.
2. The second quadrant has two relationships describing the charge profile in this region: slurry pool effect on ball trajectories and foot or toe stability.
3. Quadrant three represents the heart of the charge. Many characteristics can be defined: characteristic media size, slippage between ball layers, and ball trajectory and speed.
4. Finally, in the fourth quadrant, lifter and ball lift effect for balls along the mill liner and the mill charge are defined.

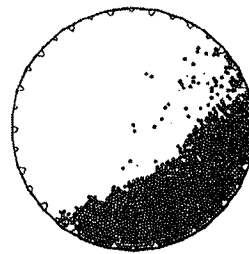
It should be noted that the behavior of the outermost layer is very different from that of the inner layers. The balls in the outermost layer are subjected to the strong lifting action of the lifters. Balls in inner layers experience lifting action only from balls in their outer adjacent layers, which is much weaker than that from the lifters. So, the outermost balls are lifted higher than the inner balls. The lifting height of balls in the outermost layer is only a function of the speed of rotation. On the other hand, the lifting height of balls in inner layers is related not only to the speed of rotation, but to dynamic pressure inside the mill and coefficient of friction as well [35].

The Mishra/Rajamani discrete element method (DEM) models are used to determine the motion behavior for a 12m SAG mill running at 30% charge volume, 65/75/85% critical speed using Hi-Lo lifters and 60 degree Hi-Lo lifters, as shown in figure 2.15 [36, 37]. The DEM approach cannot, at this time, describe completely the charge motion. Future development should mostly include: an accurate slippage model with rheological phenomena, explicit integration of lifter profiles in the charge simulation, and liner wear models. However, the DEM approach is sufficient for a better understanding of the charge motion.

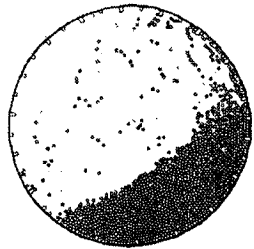
By looking at figure 2.15, we can clearly see the effect of mill speed on charge motion. As rotational speed increases, the mill charge is projected higher, hitting the unprotected wall. Under such conditions, lifter wear greatly increases due to surface fatigue, fracture and cratering. At 85% critical speed, the charge starts to centrifuge on the mill walls and not tumble. The rectangular Hi-Lo lifters and 60 deg Hi-Lo lifter face comparison is utilized to understand the wear effect of the liners. The 60 deg Hi-Lo lifter representing a worn rectangular Hi-Lo lifter that needs more speed for the same charge motion or lifting efficiency. An optimum charge motion is like the simulation in figure 2.15 with 75% critical speed and 60 deg Hi-Lo lifter face, where we can see a good combination of cataracting, cascading, tumbling and sliding of the balls that provides optimum grinding (fracture, chipping, abrasion) without projecting the charge against the unprotected wall.



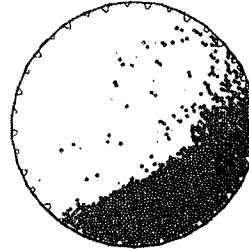
65% crit. speed, Rectangular Hi-Lo lifters



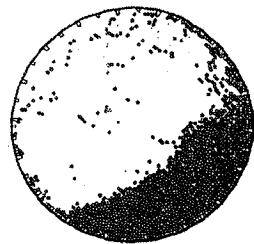
65% crit. speed, 60 deg Hi-Lo lifter face



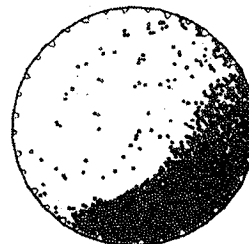
75% crit. speed, Rectangular Hi-Lo lifters



75% crit. speed, 60 deg Hi-Lo lifter face



85% crit. speed, Rectangular Hi-Lo lifters



85% crit. speed, 60 deg Hi-Lo lifter face

Figure 2.15: Charge motion simulation with different speeds and lifter characteristics [33]

2.6 Media wear

The grinding processes used in the mineral processing industry are associated with metal wear which world-wide represents an annual consumption estimated over 600 000 tons of steel [38]. The ball mill is a system composed of interactive and interrelated elements working together to grind a given input. Integrating media wear to model development maximizes system performance and endows adaptive control with respect to changes in grinding dynamics. Figure 2.16 shows the outlet interior view of Domfer ball mill 408 with new liners at outlet and used ones at entry.

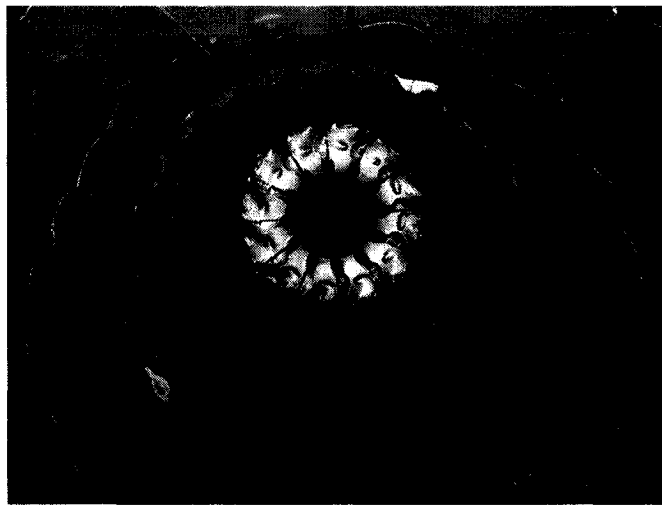


Figure 2.16: Outlet view of Domfer ball mill 408

Lifters and/or liners are always fitted onto mill shells not only to protect, but more importantly to enhance the grinding efficiency by producing a fraction of cataracting load for high energy impact breakage and a velocity gradient within the cascading region for abrasion/attrition breakage [39]. Grinding performance in a ball mill is determined primarily on how energy is distributed into the four grinding zones of the ball charge profile. The form of the charge profile, and consequently the importance of each comminution zone, is directly dependent on the friction force existing between the ball charge and the mill wall [40]. Typical ball mill liner types [41], as shown in figure 2.17, affect the friction force between the ball charge and the mill wall, consequently affecting grinding performance. An optimal liner can be utilized for a given grinding context; however, with time, wear will modify the initial liner profile and subsequently charge

motion. Wear of the liners has the effect of decreasing the lifting efficiency. Therefore, the angular speed should be increased to compensate the lifting loss and maintain optimum charge motion.

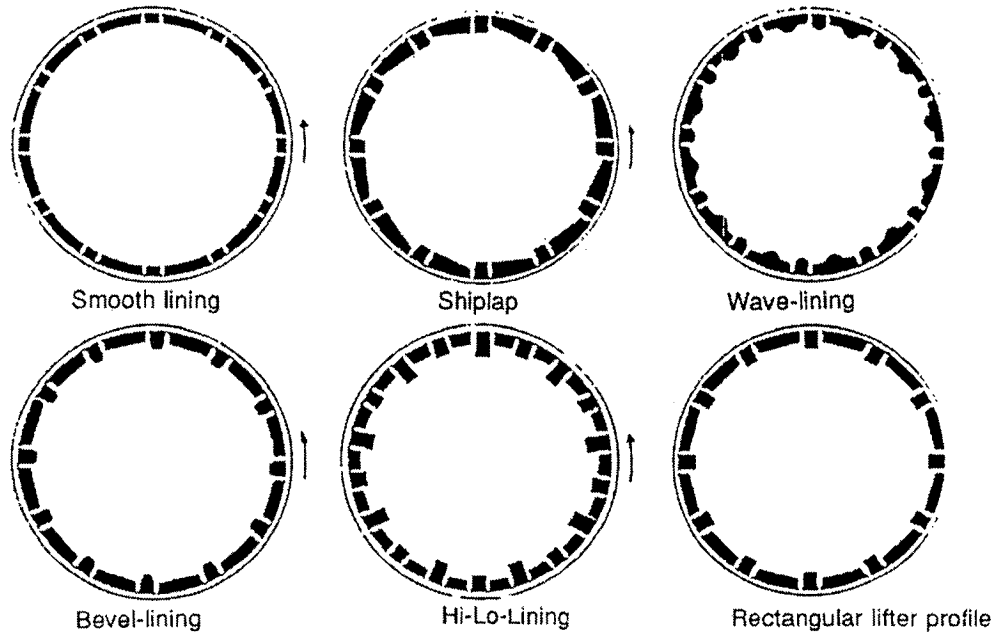


Figure 2.17: Different liner profiles [41]

During mill operation, the ball charge exerts a force field composed of gravitational and centrifugal components on the mill liner (Figure 2.18) [42-44].

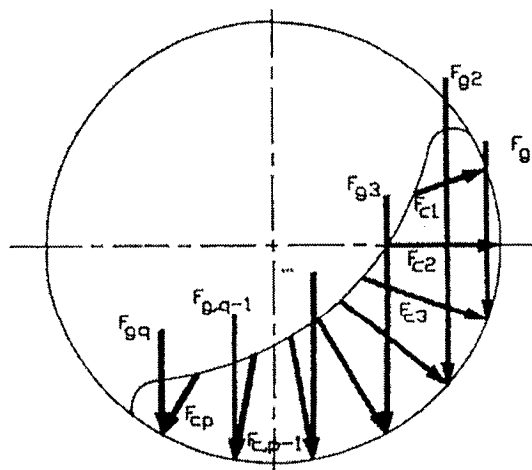


Figure 2.18: Ball charge forces acting on mill liner [44]

Raziszewski and Tarasiewicz developed an algorithm for liner profile wear simulation [42-44]. Figure 2.19 illustrates wave liner profile wear simulation.

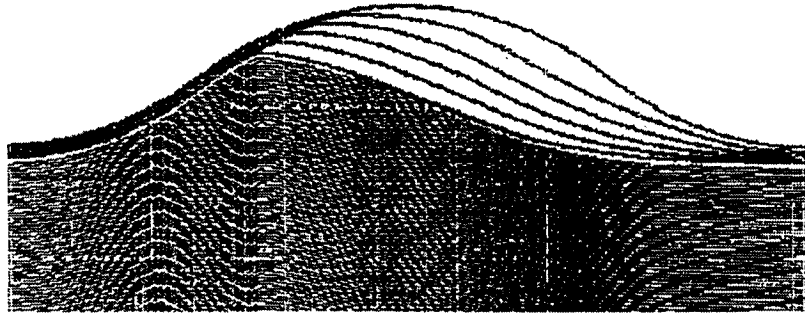


Figure 2.19: Wave liner profile wear simulation [44]

The mill energy consumption decreases with liner wear as shown in figure 2.20 [40]. This illustrates the possibility of optimizing ball mill performance as a function of predetermined effect of wear by increasing ball and powder charge with respect to liner wear in order to keep mill power constant. The increased gravitational and centrifugal forces will offset the effect of worn flattened shape liners. This is discussed in detail in section 3.2.4 and 3.2.7.

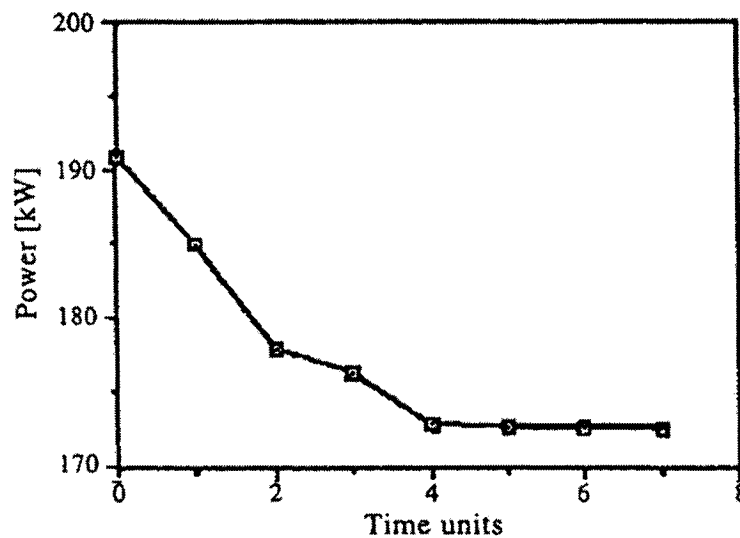


Figure 2.20: Mill power consumption over liner usable life [40]

The fraction of the input power that will be consumed in friction will increase with a decrease of the lifter height. This will result in less energy being consumed in high-energy impact breakage. Consequently, the overall rate of size reduction within the mill will decrease, although the product may become finer [45].

A variation in the friction factors, caused by the possible change in the rheological characteristics of a given charge, can increase or decrease the amount of slippage between ball layers and thus increase or decrease liner wear. The simulation presented in figure 2.19 assumes that the ball mill is not run empty or that operating conditions do not send the mill balls crashing directly into the liners. Under such conditions, the added wear mechanisms (surface fatigue, fracture, cratering) will increase wear speed significantly. Moreover, for high L/D ratio ball mills, as we go along the longitudinal axis of the ball mill, from inlet to outlet, liner wear decreases for the following reasons:

1. Amount of unground material decreases, which decreases material apparent density. This reduces gravitational and centrifugal forces on the liner.
2. Towards the discharge end, the material becomes finer and less abrasive and the proportion in suspension being swept away increases.
3. The grinding burden seen by the liners decreases significantly approaching the discharge end.
4. The softer and finer bed increases powder cushioning.

2.7 Conclusion

In this chapter, definitions, laws and formulations of problems were presented as a base for ball milling process characterization that follows in chapter 3. Powder characterization was described for product properties measurability and controllability, also outlined in chapter 3, and automated sampler design in chapter 4. Performance trends, charge motion and media wear provide guidelines to create the rules and equations for process model development found in chapter 5, which is used for ball mill control and monitoring in chapter 6.

3.0 BALL MILLING PROCESS CHARACTERIZATION

The ball milling process at Domfer is used for size reduction of granular shot to powder. This process is unique since it is performed in dry conditions and in an open circuit, i.e., no recirculation of the coarse product. The operation is critical since it determines many characteristics of the final product (density, compressibility, green strength, dimensional change, etc.). In this chapter, the measurability and controllability of the variables are described along with detailed process physics. Then, plant trials are performed to define overall system behavior and performance specifications of variables and sensors. The characterization emphasizes the variables used to develop the process model. For control, process modelling allows the estimation of process dynamics based on first principles. Thus, a highly adaptive control system can be developed and implemented if a sound understanding of the process physics is available [15].

3.1 Process physics

Coarse brittle cast iron shot from a selected raw material tank is fed into a big rotating cylinder filled with steel balls. As the cylinder rotates, the lifters inside the structure create a tumbling effect of steel balls. The energy is used to raise the balls against the force of gravity, and when the balls fall, their potential energy is converted to kinetic energy. The balls strike the particles, converting their kinetic energy to strain energy in the particles. If the impact force is sufficient, the particle is stressed to fracture point and breaks via branch fracture propagation, producing many fragments. A massive impact will fracture a particle, then a strong blow can chip off a corner, and finally rubbing will give wear of surfaces. Every fragment will convert the remainder of stored strain energy to heat after the fracture process. Once the particles reach the desired size, they are swept along by the air flow generated by a downstream blower equipped with a damper. The powder is recuperated in the impact receiving tank by a combination dropout and cyclone separator. The extremely fine powder is recuperated using a dust collector system.

3.0 BALL MILLING PROCESS CHARACTERIZATION

Figure 3.1 shows the grinding circuit of ball mill 408 at Domfer. The grinding process is composed of the following equipment, each having the specific task described above: raw material feeding tanks (R-406), raw material feeder (C-407, E-405), steel balls feeder (ADB-408), ball mill (M-408), receiving tank (R-413), cyclone separator (S-414), dust collector (D-415), damper, blower (V-416), muffler and filter. Technical drawings and specifications are presented in Appendix 1.

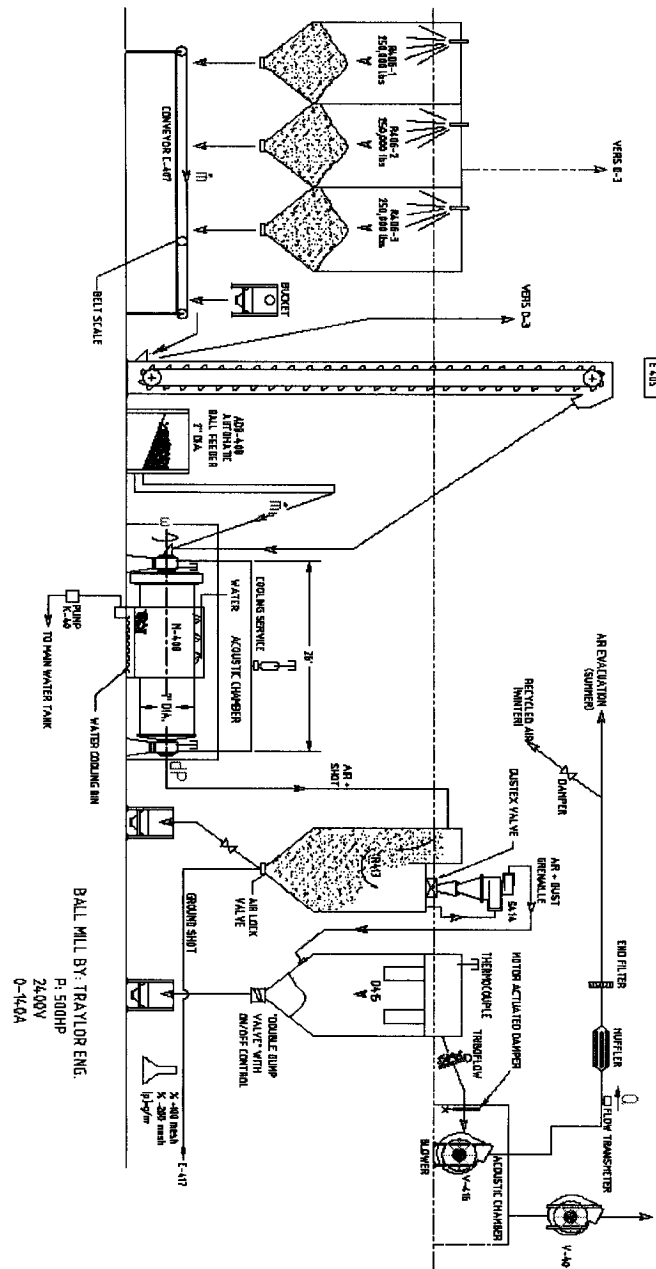


Figure 3.1: Ball mill 408 grinding circuit at Domfer

Below, you will find a list of all the variables of the ball milling operation (Table 3.1). The variables are not necessarily independent among themselves and are presented for model-based control.

Table 3.1: List of variables

Variable	Symbol	Units
Input material size distribution	%+20mesh, S20	%
Input material apparent density	A.D., ρ_i	g/cm
Powder feed rate	\dot{m}	lb/hr (kg/hr)
Desired powder feed rate	$\dot{m}_{\text{set point}}$	lb/hr (kg/hr)
Ball feed rate	\dot{m}_b	lb/hr (kg/hr)
Total ball usage	B	lb (kg)
Ball bulk density	ρ_b	g/cm ³
Ball feed rate to compensate ball and liner wear	$\dot{m}_{b(408)*}$	lb/hr (kg/hr)
Ball true density	$\rho_{b,true}$	g/cm ³
M-408 ball usage	$M_{ub(408)}$	lb (kg)
Bed porosity	J_{bed}	—
M-408 run time	T_{408}	hr
Ball bed height	H	in (m)
Ball bed height offset	ΔH	in (m)
Maximum ball diameter	d	in (m)
Liner wear	W_L	in ³ /hr (cm ³ /hr)
Liner wear with respect to balls	$W_{L(ball)}$	in ³ /hr (cm ³ /hr)
Wear volume with respect to balls	$\Delta V_{L(ball)}$	ft ³ (m ³)
Inlet wear volume with respect to balls	$\Delta V_{Lin(ball)}$	ft ³ (m ³)
Outlet wear volume with respect to balls	$\Delta V_{Lout(ball)}$	ft ³ (m ³)
Ball volume offset	ΔV_b	ft ³ (m ³)
Ball feed rate correction factor	$\Delta \dot{m}_b$	lb/hr (kg/hr)
Campaign run time	T_{camp}	hr
Mill volume	V	ft ³ (m ³)
Total wear volume	ΔV_L	ft ³ (m ³)
Inlet wear volume	ΔV_{Lin}	ft ³ (m ³)
Outlet wear volume	ΔV_{Lout}	ft ³ (m ³)
Liner life	T_L	hr
Inlet liner life	T_{Lin}	hr
Outlet liner life	T_{Lout}	hr
Ball feed rate to compensate liner wear	$\dot{m}_{b(408)**}$	lb/hr (kg/hr)

3.0 BALL MILLING PROCESS CHARACTERIZATION

Variable	Symbol	Units
Total charge	M	lb (kg)
Ball charge	M_b	lb (kg)
Powder charge	M_p	lb (kg)
Ball charge with new liners	$M_{b(new)}$	lb (kg)
Ball charge with used liners	$M_{b(used)}$	lb (kg)
Ball volume with new liners	$V_{b(new)}$	ft ³ (m ³)
Ball volume with used liners	$V_{b(used)}$	ft ³ (m ³)
Minimum ball feed rate	$\dot{m}_{b\min}$	lb/hr (kg/hr)
Maximum ball feed rate	$\dot{m}_{b\max}$	lb/hr (kg/hr)
Ball charge variation	dM_b	lb (kg)
Ball feed rate variation	$d\dot{m}_b$	lb/hr (kg/hr)
Minimum total charge	M_{\min}	lb (kg)
Maximum total charge	M_{\max}	lb (kg)
Mean residence time	τ	hr
Mill powerdraw	P	kW
Lumped mill powerdraw parameter	k	
Total charge powerdraw	P_{charge}	kW
Empty mill powerdraw	$P_{no\ load}$	kW
Mill powerdraw attributable to balls	P_b	kW
Mill powerdraw attributable to powder	P_p	kW
Fraction of the mill filled by balls at rest	J	—
Fraction of critical speed	ϕ_c	—
Ball mill internal diameter	D	ft (m)
Ball mill length	L	ft (m)
Rotational speed	ω	RPM (rad/sec)
Critical speed	N_c	RPM (rad/sec)
Air flow rate	Q	ACFM (m ³ /sec)
Desired air flow rate	$Q_{set\ point}$	ACFM (m ³ /sec)
Outlet trunnion pressure	dP_o	inH ₂ O (N/m ²)
Product rate	\dot{m}_o	lb/hr (kg/hr)
Dust rate	\dot{m}_{D415}	lb/hr (kg/hr)
Product % retained by a 100 mesh sieve	+100mesh, $S100$	%
Product % passing a 200 mesh sieve	-200mesh, $S200$	%
Product apparent density	A.D., ρ_o	g/cm ³

Variable	Symbol	Units
Powder charge sensitivity	$M_{p(min)}$	lb (kg)
Product response time	T_R	min
Feed rate step change	$\Delta \dot{m}$	lb/hr (kg/hr)
Air flow rate sensitivity	ΔQ_{min}	ACFM (m ³ /sec)

A combination of SI and English units are utilized for the process variables because of historical usage. These units correspond to Domfer Metal Powders plant personnel knowledge base and North American industrial standards. Where English measurement units are used, the SI equivalent is presented in parentheses. The required English to SI conversions are presented below:

1 lb = 0.454 kg
 1 in = 0.0254 m
 1 ft = 0.3048 m
 1 in³ = 16.387 cm³
 1 ft³ = 0.0283 m³
 1 RPM = 0.105 rad/sec
 1 ACFM = 0.000472 m³/sec
 1 inH₂O = 248.84 N/m²
 20 mesh = 850 μm
 100 mesh = 150 μm
 200 mesh = 75 μm

There are 4 ball mills at Domfer: ball mill 108, 208, 308 and 408. The dimensions of each ball mill is shown in table 3.2.

Table 3.2: Domfer ball mills dimensions

<u>Ball mill</u>	<u>Diameter</u>	<u>Length(ft)</u>
108	4ft (1.22m)	10ft (3.05m)
208	5ft (1.52m)	16ft (4.88m)
308	5ft (1.52m)	16ft (4.88m)
408	7ft (2.13m)	26ft (7.92m)

The analysis is performed on the largest mill, ball mill 408, which produces 60% of total ground shot.

3.2 Measurability and controllability of the variables

The overall performance of a model-based controller is directly related to the measurability and controllability of its system key variables. A precise measurement and robust control of the parameters provides the foundation for multivariable controller design. The most important parameters of the ball milling process will now be presented.

3.2.1 Input material properties

A steel melt is water atomized to granular shot, which constitutes the input material of the ball milling operation. During the atomization process, three major properties are measured: chemical composition, density and size distribution. First, for chemical analysis, a sample taken in the melt just before the tundish is cooled and shaped as a puck for testing on a spectrometer. Based on the calculated chemical composition of the atomized shot (94-95% iron, 3.3-4.5% carbon, sulfur, manganese, silica, nickel, phosphorus, molybdenum, copper, chromium, aluminum), adjustments are made on the induction furnace raw materials to achieve the desired chemical content. Carbon and silica are known to increase the hardness of the shot particles, which become more brittle and which in turn increase ball mill productivity.

Second, a density measurement is performed in the following matter: 10 minutes after the atomization has started, a sample is taken underneath the hydro-cyclone using a 200ml capacity sampling device. The sample is dried and carefully poured in an Erlenmeyer flask of known mass and volume. Then, the flask is weighed and apparent density calculated.

Third, one point measurement is taken for determining the size distribution of atomized shot. The Erlenmeyer flask content is emptied onto a 20 mesh (850 μm) screen with a pan that vibrates for 5 minutes. The amount of material over 20 mesh (850 μm) is weighed on a digital scale. Based on the result, the water jets atomizing pressure is adjusted to achieve the desired size. The residence time of the particles inside the mill is greatly influenced by the size of the input shot: coarser grades require more mechanical breaking action for proper size reduction. In turn, this affects the shape of the ground shot; a small

residence time produces a more spherical shape and longer residence time giving rise to more irregular and flatter particles. The latter is a very important geometrical aspect providing excellent green strength properties in the finished product. In the case of ball mills, coarse breakage rates decrease as the feed size increases. A coarser feed contributes less as grinding media and is instead a burden which needs to be ground. This is reflected in the performance, where a decrease in feed size results in an increase in throughput.

The granular atomized shot is stored in 250 000 lb (113500 kg) capacity feeding tanks, ready to be fed to the mill. However, segregation inside the tanks must be taken into consideration. Structural vibrations cause fine particles to go to the bottom of the tank, while coarser particles stay on top. This produces a variation in input shot size distribution as the tank is emptying, from a fine size distribution to a coarser one. Moreover, at the end of a campaign, very fine material is fed to the mill because of the dust deposit on the material surface inside the emptying tank.

3.2.2 Powder feed rate

Feed rate is a very important parameter since it dictates productivity, residence time and powder charge. Increasing feed rate generates coarser and denser ground shot whereas a reduced feed rate generates finer and less dense shot. A higher feed rate increases powder charge and reduces residence time, allowing the spherical atomized shot to receive less breaking action, keeping more of its original shape and reaching the exit faster to be swept away by the air flow. On the other hand, a lower feed rate reduces powder charge and increases the ball/powder ratio. The particles receive more breakage action and are subject to higher residence times. The increased number of impacts produces more irregularly shaped product with low density and finer size distribution.

For ball mill 408, the feed rate is regulated via a single idler belt scale mounted on the feed conveyor. In operation, the vertical force, representing the actual belt load, is sensed by load cells to provide the weight signal. A shaft mounted speed sensor provides a signal for belt speed. An integrator processes the weight and speed signals, providing accurate

3.0 BALL MILLING PROCESS CHARACTERIZATION

indication of mass flow rate. Using PID control, feed conveyor speed is varied to achieve the desired mass flow rate.

A new automated weighing system for metal powders was created by Rail [46] and installed at Domfer on ball mills 108, 208 and 308 (Figure 3.2).

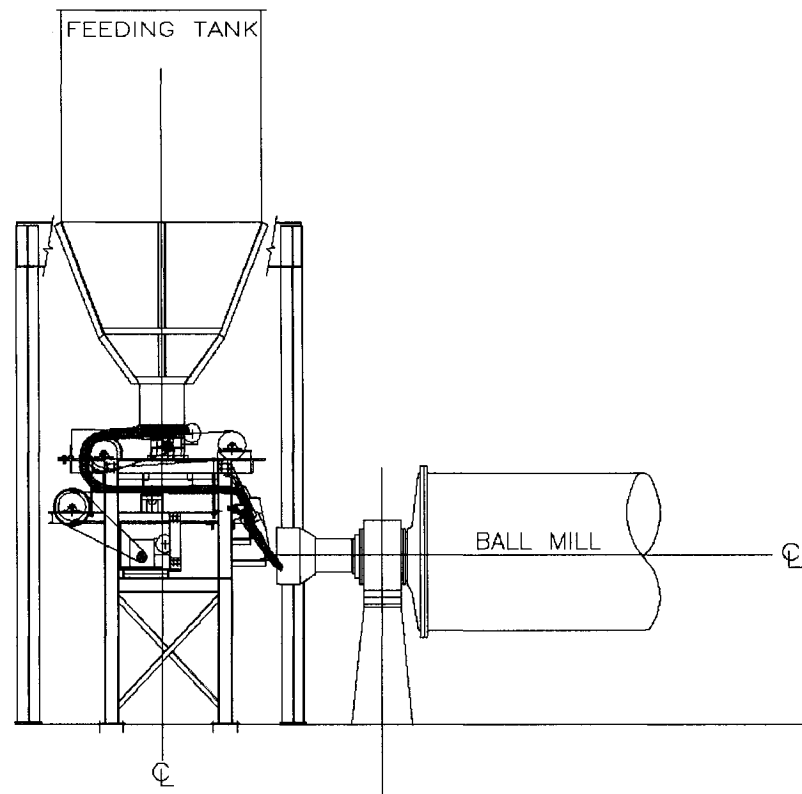


Figure 3.2: Automated weighing system for metal powders [46]

It consists of two conveyors assembled one on top of the other. The top conveyor carries the powder from the feeding tank to the bottom conveyor via a chute located between the two. The top conveyor, which is fixed to the ground by its structure, is utilized for canceling the effect of the constantly varying pressure head generated by the powder level in the tank. Also, the disturbance in the flow that exits the hopper is carried by the first conveyor and is greatly reduced by using a specially designed chute that brings the powder to the next (bottom) conveyor. The bottom conveyor, which is suspended using 4 load cells, receives a constant and regular flow of powder from the chute and drops it into the ball mill through another chute. The signal generated by the load cells and the known

constant speed of the bottom conveyor provide, through an algorithm, the mass flow rate of powder that is fed to the ball mill. This is treated by the programmable logic controller (PLC) that compares the actual mass flow rate of powder with the desired flow. A PID function within the PLC controls a variable frequency drive, which in turn varies the speed of the AC motor of the top conveyor, which regulates the flow of powder. A desired mass flow rate of material fed to the ball mill is therefore achieved.

First, the PID operation will be briefly explained in order to understand the selection of PID parameters chosen for the system. The PID control contains three control operations that generate an output amount that is sent to the drive to attain the desired value: proportional operation, derivative operation and integral operation.

The proportional operation is an operation in which a proportional band is established with respect to the set value. Within that band the control output amount is established in proportion to the deviation. If the actual value is smaller than the proportional band, the output amount will be 100%. If the actual value is greater than the proportional band, the output amount will be 0%. But, if the actual value is within the proportional band, the output amount is set proportional to the deviation and will gradually decrease until the set value and actual value match (deviation of 0). When the deviation is 0, the output amount will take the previous value. With proportional operation an offset occurs (residual deviation). Making the proportional band smaller reduces the offset, but if the proportional band is too small, a hunting (large oscillations around the set point) phenomenon occurs.

Integral operation can be combined with proportional operation to reduce the offset according to the time that has passed. The strength of the integral operation is related to the integral time, which is the time required for the integral output amount to reach the same level as the proportional output amount with respect to the step deviation. A short integral time brings a stronger correction. If the integral time is too short, the result is a much too strong correction that causes hunting.

Since proportional operation and integral operation are corrected with respect to the control results, there is a response delay. The derivative operation compensates by decreasing the response time of the system. In response to a sudden disturbance, the derivative delivers a large operational correction that rapidly restores the original state. The output amount is proportional to the slope of the deviation. The strength of the derivative is related to the derivative time, which is the time required for the output amount of the derivative to reach the output amount of the proportional operation with respect to the step deviation. A stronger correction by the derivative can be implemented by increasing the derivative time.

The PID operation combines proportional operation to provide smooth control without hunting, integral operation to automatically correct any offset and derivative operation to increase the response time of the system.

Listed below are some relationships between PID parameters and desired control status:

1. No overshooting and long settling time desired: enlarge the proportional band.
2. Overshooting and short settling time desired: reduce the proportional band.
3. When there is broad hunting, or when the operation is tied up between overshooting and undershooting: decrease integral operation or enlarge proportional band.
4. If hunting occurs in a short period, the control system response is too quick: decrease the derivative operation.

For the weighing system, a wide proportional band is selected since the speed of the system is very slow and many disturbances can occur. The system smoothly corrects the disturbances caused by chunks of powder falling on or off the bottom conveyor and by shocks caused by someone accidentally hitting the system. Motor variations are not too brusque and the disturbance probably stops before the proportional band has had time to significantly change the speed to correct the deviation. The system is, therefore, very stable. Using a proportional band that is too narrow increases the response time, but generates some hunting. Since the response time is not a major issue, a wide proportional band produces a very robust and stable system that can easily accommodate disturbances.

To reduce the offset caused by the wide proportional band, a relatively weak integral action is chosen. No derivative is used since it delivers a large operation output in response to a sudden disturbance in order to restore the original status. For this type of conveyor arrangement, the powder irregularities cause hunting in a short period.

The weighing system has a proportional integral controller (PI controller) with a wide proportional band and small integral time. The controller is robust with moderate response time, which corresponds well to the expected control capabilities:

Mass flow rate range: 0-12000 lb/hr (0-5443 kg/hr)

Standard deviation: 20 lb/hr (9.1 kg/hr)

Precision: 1%

Settling time: 3 min to a 1000 lb/hr (453.6 kg/hr) step change

Let us now theoretically demonstrate the effectiveness of the PI controller developed using a heuristic approach. A negative unity feedback control system in the Laplace domain is considered. The block diagram is shown in figure 3.3.

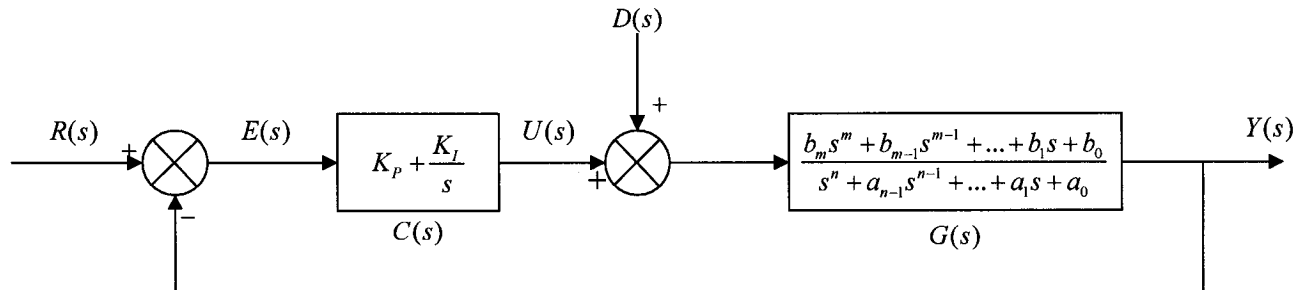


Figure 3.3: Negative unity feedback feed rate control block diagram

3.0 BALL MILLING PROCESS CHARACTERIZATION

where,

$G(s)$ = Automatic feeder (plant) transfer function with an n th-order characteristic equation

$C(s)$ = PI controller

$R(s) = \mathcal{L}\{ \dot{m}_{\text{set point}}(t) \}$

$Y(s) = \mathcal{L}\{ \dot{m}(t) \}$

$E(s) = R(s) - Y(s)$, error of the system

$D(s)$ = System disturbances

$U(s)$ = Controller output

First, the application of the final value theorem to the error of the system gives the following steady-state error formula:

$$\begin{aligned}
 e_{ss} &= \lim_{t \rightarrow \infty} e(t) = \lim_{s \rightarrow 0} s E(s) = \lim_{s \rightarrow 0} s \frac{1}{1 + C(s)G(s)} R(s) \\
 &= \lim_{s \rightarrow 0} s R(s) \frac{1}{1 + \left(K_p + \frac{K_I}{s} \right) \left(\frac{b_m s^m + b_{m-1} s^{m-1} + \dots + b_1 s + b_0}{s^n + a_{n-1} s^{n-1} + \dots + a_1 s + a_0} \right)} \\
 &= \lim_{s \rightarrow 0} s^2 R(s) \frac{a_0}{K_I b_0}
 \end{aligned} \tag{3.1}$$

The equation shows that the system is type 1 with respect to reference tracking, i.e., the control system perfectly tracks ($e_{ss}=0$) a desired step powder feed rate input ($R(s)=1/s$). This corresponds well with the design requirements.

Then, the steady-state error to a disturbance input is:

$$y_{ss} = \lim_{t \rightarrow \infty} y(t) = \lim_{s \rightarrow 0} s Y(s)_{\text{due to } D} \tag{3.2}$$

where the output equation $Y(s)$ is:

$$Y(s) = \frac{G(s)}{1 + C(s)G(s)} D(s) + \frac{C(s)G(s)}{1 + C(s)G(s)} R(s) \tag{3.3}$$

But $Y(s)_{\text{due to } D}$ is $Y(s)$ with $R(s)=0$. Therefore, the steady-state error equation becomes:

$$\begin{aligned}
 y_{ss} &= \lim_{s \rightarrow 0} s \frac{G(s)}{1 + C(s)G(s)} D(s) \\
 &= \lim_{s \rightarrow 0} s D(s) \frac{\left(\frac{b_m s^m + b_{m-1} s^{m-1} + \dots + b_1 s + b_0}{s^n + a_{n-1} s^{n-1} + \dots + a_1 s + a_0} \right)}{1 + \left(K_p + \frac{K_I}{s} \right) \left(\frac{b_m s^m + b_{m-1} s^{m-1} + \dots + b_1 s + b_0}{s^n + a_{n-1} s^{n-1} + \dots + a_1 s + a_0} \right)} \\
 &= \lim_{s \rightarrow 0} s^2 D(s) \frac{1}{K_I}
 \end{aligned} \tag{3.4}$$

This is a system type 1 with respect to disturbance rejection, i.e., the control system rejects ($y_{ss}=0$) step disturbances ($D(s)=1/s$). This correspond well with actual system disturbances caused by feed surges. The designed PI controller provides robust powder feed rate control.

3.2.3 Grinding balls

The Domfer steel balls have the following specifications:

Shape:	Spherical
Diameter:	2 in (5.08 cm)
Weight:	535 g
Hardness:	63 HRc, constant from surface to center
Chemistry:	1% C, 0.6% Mn, 0.35% Cr, 0.18% Ni

The relatively small ball size increases the surface area and enhances breakage rates of finer sizes. The constant hardness favors a more uniform ball wear, from initial 2 in (5.08cm) spherical shape to powder size. Once the balls reach powder size, they are swept along with the powder by the air flow. A picture of the size distribution of the grinding balls is presented in figure 3.4.

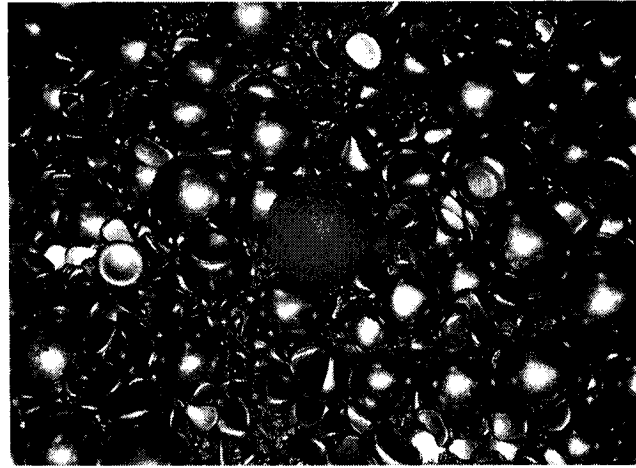


Figure 3.4: Ball size distribution

The balls are fed continuously to compensate ball and liner wear for constant ball level control.

An automated volumetric feeder, consisting of a receiving hopper, adjustable bottom sliding gate and bucket elevator is used to feed the mill with new steel balls. A known volume of balls is brought to the bucket elevator, raised at regular intervals and fed to the mill by gravity using a steel pipe.

The automated feeder provides the following control capabilities:

Mass flow rate range: 0-400 lb/hr (0-181.4 kg/hr)

Standard deviation: 1 lb/hr (0.454 kg/hr)

Precision: 15%

Due to the lack of precision of the feeding system, the ball bed height H is measured ($\pm 1/2$ in (± 1.27 cm)) after each campaign through the inlet. According to ball mill operators, a height of 10 in (25.4cm) between the ball bed and the output conduit provides good grinding performance (Figure 3.5).

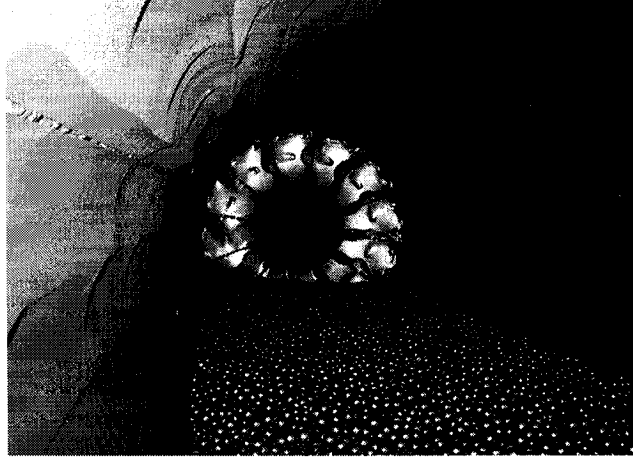


Figure 3.5: Ball bed height

At each liner change, the grinding balls are emptied in containers with known volume. The average ball bulk density can be calculated by weighing each container and dividing by the total volume:

$$\text{Ball bulk density, } \rho_b = 4.77 \text{ g/cm}^3$$

Knowing the ball true density, $\rho_{b,true} = 7.81 \text{ g/cm}^3$, the bed porosity can be calculated:

$$J_{bed} = \frac{\rho_{b,true} - \rho_b}{\rho_{b,true}} = \frac{7.81 \frac{\text{g}}{\text{cm}^3} - 4.77 \frac{\text{g}}{\text{cm}^3}}{7.81 \frac{\text{g}}{\text{cm}^3}} = 0.39 \quad (3.5)$$

The most practical way to implement continuous feeding with constant ball bed height control is to evaluate ball wear based on annual consumption, productivity and run times of the four ball mills at Domfer.

First, consider the run times and average productivity of the ball mills and total ball usage for the year 2003:

BM-108: 4500 hr at 2000 lb/hr (907.2 kg/hr), mill scale

BM-208: 3700 hr at 1350 lb/hr (612.3 kg/hr)

BM-308: 6500 hr at 1550 lb/hr (703.1 kg/hr)

BM-408: 6000 hr at 4100 lb/hr (1859.7 kg/hr)

Total ball usage, B = 83444 lb (37849.6 kg)

3.0 BALL MILLING PROCESS CHARACTERIZATION

According to annual ball consumption per mill, the Domfer process displays a ball wear that is proportional to average productivity. Therefore, the continuous ball feed rate to compensate for ball and liner wear on ball mill 408 is:

$$\begin{aligned}\dot{m}_{b(408)*} &= \frac{M_{ub(408)}}{T_{408}} \\ &= \frac{\left(\frac{\dot{m}_{(408)}}{\varepsilon \dot{m}_{(108)} + \dot{m}_{(208)} + \dot{m}_{(308)} + \dot{m}_{(408)}} \right) B}{T_{408}} \\ &= \frac{\left(\frac{4100 \text{ lb/hr}}{0.25(2000 \text{ lb/hr}) + 1350 \text{ lb/hr} + 1550 \text{ lb/hr} + 4100 \text{ lb/hr}} \right) (83444 \text{ lb})}{6000 \text{ hr}} \\ &= 7.6 \text{ lb/hr} \quad (3.45 \text{ kg/hr})\end{aligned}\tag{3.6}$$

where, $M_{ub(408)}$ and T_{408} are BM-408 ball usage and run time respectively.

A correcting factor ε is required since mill scale is ground on ball mill 108 with different grinding dynamics and powder and ball charges. Annual ball consumption data shows a ball wear on BM-108 that is four times lower than that of ball wear on BM-208, 308 and 408.

Therefore, new balls fed at a rate of 7.6 lb/hr are required to palliate ball and liner wear on ball mill 408.

3.2.4 Liners

The Domfer ball mill 408 liners have the following specifications:

Shape:	Wave
Hardness:	635 BHN
Alloy:	NI-HARD 11
Chemistry:	3.21% C, 4.43% Ni, 0.69% Mn, 2.27% Cr, 0.07% Mo 0.59% Si, 0.18% Cu, 0.03% P, 0.09% S
Density:	0.28 lb/in ³ (7.75 g/cm ³)

Complete liner dimensions of feed end, discharge end and inside shell are shown in Appendix 1.

The Ni-Hard liners for Domfer mills are sand-casted then annealed for stress relief. A uniform hardness is seen across the thickness because of its relatively small size (4in (10.2cm) thick maximum). Also, molybdenum is used in the recipe to homogenize the hardness.

Liner life at the inlet side is shorter compared to the discharge end. This is demonstrated by plant data, where the inlet and outlet liners are changed every 6500 hr and 9000 hr respectively. Product results show an average apparent density for input atomized shot that is 25% higher than output ground shot. As we go along the longitudinal axis of the ball mill, from inlet to outlet, the amount of unground shot decreases, which in turn decreases the apparent density of the material. This has the effect of reducing the gravitational and centrifugal force acting on the liner. Also, towards the discharge end, the shot becomes finer and the proportion of material being swept away increases. Consequently, the grinding burden seen by the liners decreases significantly as the discharge end is approached. Figure 3.6 shows a new liner in the center with used liners on each side. By looking at the figure, one can understand that a worn liner will provide a less efficient friction force on ball and powder charge, which in turn greatly affects charge motion. Moreover, we can see that figure 3.6 corresponds well with the wave liner profile wear simulation illustrated previously in figure 2.19.



Figure 3.6: Used and new Domfer BM-408 liners

When the liners are worn out, only half of the set is changed, either at the feed or discharge end. The reason for this is that changing a complete set generates severe changes in charge motion. This is represented in figure 3.7 using the charge motion

simulation of figure 2.15 with two different speeds and lifter characteristics: the 60 deg Hi-Lo lifter face at 65% critical speed (used liners) and the rectangular Hi-Lo lifters at 85% critical speed (new liners).

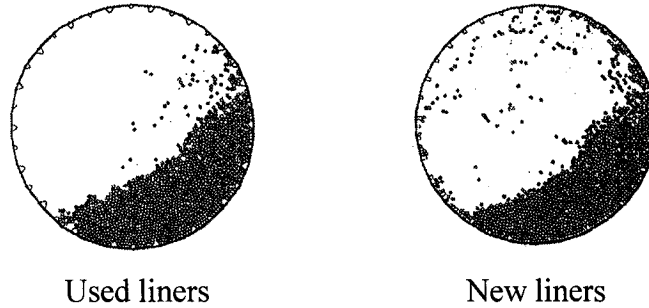


Figure 3.7: Charge motion comparison for used and new liners

The fluid drive cannot provide sufficient rotational speed reduction to compensate for the increased friction factor. An under-designed heat exchanger was installed with the fluid drive causing oil overheating problems at high percentage slip (reduced speeds). Moreover, inlet liners have a shorter life than outlet liners:

$$T_{Lin} = 6500 \text{ hr}$$

$$T_{Lout} = 9000 \text{ hr}$$

Domfer decided to keep rotational speed constant at $77\%N_c$ and change only one-half of the set at a time, minimizing the overall effect on charge motion and maximizing the outlet liner life.

In order to incorporate liner wear in ball charge control, the inside grinding volume augmentation as a function of liner wear must be calculated. Multi-point measurement of worn out liners was performed to create a 3-D model of the mill with used liners. Figure 3.8 shows a cross sectional view of a new liner compared to a used liner.

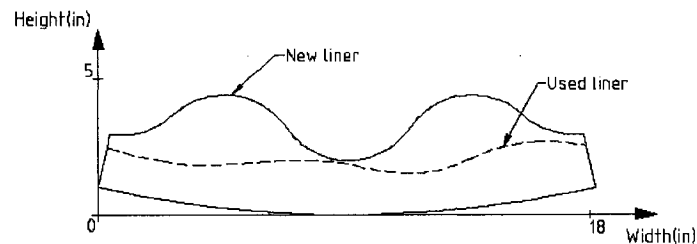


Figure 3.8: Cross sectional view of a new liner compared to a used liner

Figure 3.9 illustrates BM-408 inside volume and ball volume at rest with new and used liners.

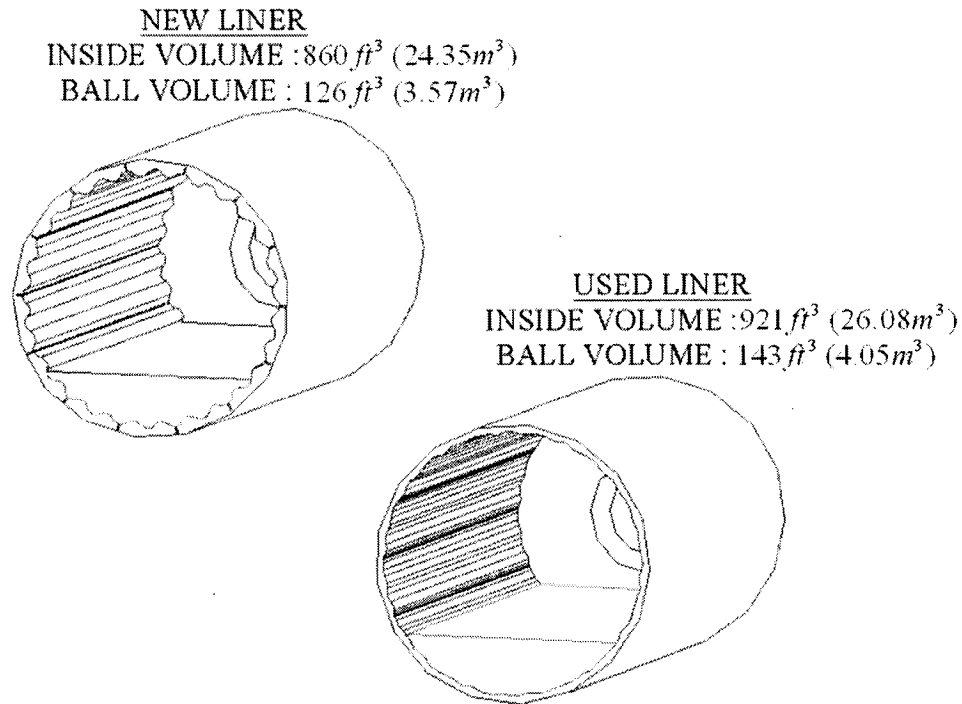


Figure 3.9: 3-D drawing of BM-408 inside volume with new and used liners

Constant liner wear W_L for overall liner life is assumed for the following reasons:

1. The effect of liner wear on charge motion, consequently grinding dynamics, is negligible for a single grade production run with a maximum campaign duration of 1 week.
2. Liner hardness is constant across thickness because of its relatively small size and molybdenum content.
3. The aggressive shape of new liners projects the ball charge against the unprotected wall to create surface fatigue, fracture and cratering. On the other hand, the used liners, which provide less kinetic energy to the balls, are subject to higher sliding friction with increased gravitational and centrifugal forces (greater ball and powder charges).

3.0 BALL MILLING PROCESS CHARACTERIZATION

From figure 3.9, the total wear volume ΔV_L is:

$$\Delta V_L = 921 \text{ ft}^3 - 860 \text{ ft}^3 = 61 \text{ ft}^3 \quad (1.73 \text{ m}^3) \quad (3.7)$$

Then, liner wear W_L is calculated using:

$$\begin{aligned} W_L &= \frac{\Delta V_{Lin}}{T_{Lin}} + \frac{\Delta V_{Lout}}{T_{Lout}} \\ &= \frac{\Delta V_L / 2}{T_{Lin}} + \frac{\Delta V_L / 2}{T_{Lout}} \quad \text{where: } \Delta V_{Lin} + \Delta V_{Lout} = \Delta V_L \\ &= \frac{30.5 \text{ ft}^3}{6500 \text{ hr}} + \frac{30.5 \text{ ft}^3}{9000 \text{ hr}} \quad \Delta V_{Lin} = \Delta V_{Lout} @ T_L \\ &= 13.96 \frac{\text{in}^3}{\text{hr}} \quad (228.76 \frac{\text{cm}^3}{\text{hr}}) \\ &= 13.96 \frac{\text{in}^3}{\text{hr}} \times 0.28 \frac{\text{lb}}{\text{in}^3} = 3.9 \frac{\text{lb}}{\text{hr}} \quad (1.77 \frac{\text{kg}}{\text{hr}}) \end{aligned} \quad (3.8)$$

where ΔV_{Lin} and ΔV_{Lout} , T_{Lin} and T_{Lout} are wear volume and liner life for the inlet and outlet respectively.

From figure 3.9, the wear volume with respect to the balls at rest is:

$$\Delta V_{L(ball)} = 143 \text{ ft}^3 - 126 \text{ ft}^3 = 17 \text{ ft}^3 \quad (0.48 \text{ m}^3) \quad (3.9)$$

Similarly, liner wear with respect to the balls at rest $W_{L(ball)}$ is calculated:

$$\begin{aligned} W_{L(ball)} &= \frac{\Delta V_{Lin(ball)}}{T_{Lin}} + \frac{\Delta V_{Lout(ball)}}{T_{Lout}} \\ &= \frac{\Delta V_{L(ball)} / 2}{T_{Lin}} + \frac{\Delta V_{L(ball)} / 2}{T_{Lout}} \quad \text{where: } \Delta V_{Lin(ball)} + \Delta V_{Lout(ball)} = \Delta V_{L(ball)} \\ &= \frac{8.5 \text{ ft}^3}{6500 \text{ hr}} + \frac{8.5 \text{ ft}^3}{9000 \text{ hr}} \quad \Delta V_{Lin(ball)} = \Delta V_{Lout(ball)} @ T_L \\ &= 3.89 \frac{\text{in}^3}{\text{hr}} \quad (63.75 \frac{\text{cm}^3}{\text{hr}}) \end{aligned} \quad (3.10)$$

where $\Delta V_{Lin(ball)}$ and $\Delta V_{Lout(ball)}$ are wear volume with respect to balls at rest for the inlet and outlet respectively.

The ball feed rate required to maintain a constant ball bed height inside BM-408 despite liner wear is:

$$\begin{aligned}
 \dot{m}_{b(408)**} &= W_{L(ball)} \times \rho_b \\
 &= 3.89 \frac{\text{in}^3}{\text{hr}} \times 0.172 \frac{\text{lb}}{\text{in}^3} \\
 &= 0.67 \frac{\text{lb}}{\text{hr}} \quad (0.30 \frac{\text{kg}}{\text{hr}})
 \end{aligned} \tag{3.11}$$

The ball feed rate required to compensate for liner wear is included in the previously calculated ball feed rate of equation 3.6. Therefore, the continuous ball feed rate for ball bed height control with respect to ball wear and liner wear is 6.93lb/hr (3.14kg/hr) and 0.67lb/hr (0.30kg/hr) respectively.

After each campaign, ball bed height H is verified to confirm and fine tune the calculated nominal value of equation 3.6. The desired bed height is 10in (25.4cm) below the output conduit. A ball feed rate correction factor $\Delta \dot{m}_b$ is calculated using the measured ball bed height H , the 3-D model of figure 3.9 and the following two equations:

$$H - 10\text{in} = \Delta H \tag{3.12}$$

From the 3-D model, the ball volume offset is determined:

$$\Delta H \rightarrow \Delta V_b$$

\therefore

$$\Delta \dot{m}_b = \rho_b \frac{\Delta V_b}{T_{camp}} \tag{3.13}$$

where ΔV_b is ball volume offset and T_{camp} the campaign run time.

Therefore, the ball feed rate \dot{m}_b is:

$$\dot{m}_b = \dot{m}_{b(408)*} + \Delta \dot{m}_b \tag{3.14}$$

3.2.5 Ball and powder charges

The breakage rates of most of the sizes are greatly affected by ball-powder ratio. At low powder filling, much of the energy of the tumbling balls is spent in steel-to-steel contact, providing low breakage rates and over-grinding of the fines. However, at high powder charge, the powder cushions the breakage action, reducing the grinding efficiency. When all the effective spaces where collisions between tumbling balls are taking place get filled with powder, the rates of breakage reach a maximum [47].

Based on the 3-D model of figure 3.9 and the ball bulk density, ball charge with new and used liners can be calculated:

$$\begin{aligned} M_{b(new \rightarrow used)} &= (V_{b(new)} \rightarrow V_{b(used)}) \times \rho_b \\ &= (126 \rightarrow 143 \text{ ft}^3) \times 297.90 \frac{\text{lb}}{\text{ft}^3} \\ &= 37535 \rightarrow 42600 \text{ lb} \quad (17025.6 \rightarrow 19323.0 \text{ kg}) \end{aligned} \quad (3.15)$$

The actual ball charge increases with liner wear. The ball feed rate $\dot{m}_{b(408)}$, calculated previously is averaged since we can expect the ball feed rate to increase with ball charge according to the following equation:

$$\dot{m}_b = \dot{m}_{b \min} + \frac{d\dot{m}_b}{dM_b} M_b \quad (3.16)$$

where,

$$\begin{aligned} dM_b &= M_{b(used)} - M_{b(new)} \\ &= \dot{m}_{b(408)} \times T_{408} \\ &= 0.67 \frac{\text{lb}}{\text{hr}} \times 6000 \text{ hr} = 4020 \text{ lb} \quad (1823.4 \text{ kg}) \end{aligned} \quad (3.17)$$

and,

$$d\dot{m}_b = \dot{m}_{b \max} - \dot{m}_{b \min} \quad (3.18)$$

$\dot{m}_{b \min}$ and $\dot{m}_{b \max}$ are minimum and maximum continuous ball feed rates.

Since,

$$\frac{dM_b}{M_b} \approx 10\%$$

let,

$$\frac{d\dot{m}_b}{\dot{m}_b} \approx 10\%$$

The precision of the automatic ball feeder is 15 %. Moreover, the maximum duration of a campaign is 1 week, so we can reasonably assume that $d\dot{m}_b$ with respect to liner wear or increased grinding volume is negligible per product produced. Therefore, the average continuous ball feed rate can be utilized with the correction factor $\Delta\dot{m}_b$ calculated after each campaign using equation 3.13.

To determine powder charge (hold-up), previous tests were performed where the ground shot was emptied in buckets and weighted. For the grades produced on BM-408, the powder charges were:

$$M_{p(3)} = 9000 \text{ lb} \quad (4082.3 \text{ kg})$$

$$M_{p(1)} = 10000 \text{ lb} \quad (4535.9 \text{ kg})$$

$$M_{p(4)} = 12000 \text{ lb} \quad (5443.1 \text{ kg})$$

$$M_{p(2)} = 12500 \text{ lb} \quad (5669.9 \text{ kg})$$

The total charge is expressed as:

$$M = M_b + M_p \quad (3.19)$$

with minimum and maximum values of:

$$\begin{aligned} M_{\min} &= M_{b(\text{new})} + M_{p(3)} & M_{\max} &= M_{b(\text{used})} + M_{p(2)} \\ &= 37535 \text{ lb} + 9000 \text{ lb} & &= 42600 \text{ lb} + 12500 \text{ lb} \\ &= 46535 \text{ lb} \quad (21107.9 \text{ kg}) & &= 55100 \text{ lb} \quad (24992.9 \text{ kg}) \end{aligned} \quad (3.20)$$

In practice, the total charge is estimated by the operators using motor power reading on the HMI. This is explained in detail in section 3.2.7.

3.2.6 Mean residence time

Residence time is a fundamental concept of the ball milling process that dictates the number of impacts providing disintegration and attrition of the particles and that significantly influences product shape. If the feed rate is decreased, the material spends more time in the mill, receives more breakage actions and is hence ground finer. In many cases, the mean residence time τ is defined as:

$$\tau = \frac{M_p}{\dot{m}} \quad (3.21)$$

Also, air flow rate influences mean residence time by affecting powder charge: a stronger flow emptying the mill faster and vice versa.

Some material may leave the mill almost immediately, while some may hold up for longer period of time. Residence time distributions are very complex and require more experimentation to correlate with plant results when considering particles of different sizes and longitudinal position inside mills with high L/D ratio.

Based on powder charge and typical feed rate for each grade, the mean residence time per grade produced can be calculated:

$$\begin{aligned} \tau_{MP2} &= \frac{M_{p(2)}}{\dot{m}_{MP2}} = \frac{12500 lb}{6000 \frac{lb}{hr}} = 2.08 hr \\ \tau_{MP4} &= \frac{M_{p(4)}}{\dot{m}_{MP4}} = \frac{12000 lb}{5500 \frac{lb}{hr}} = 2.18 hr \\ \tau_{MP1} &= \frac{M_{p(1)}}{\dot{m}_{MP1}} = \frac{10000 lb}{4000 \frac{lb}{hr}} = 2.50 hr \\ \tau_{MP3} &= \frac{M_{p(3)}}{\dot{m}_{MP3}} = \frac{9000 lb}{3500 \frac{lb}{hr}} = 2.57 hr \end{aligned}$$

A comparison between residence time, density and size for each product is shown in table 3.3.

Table 3.3: Product density and size with respect to residence time

	τ (hr)	ρ (g/cc)	$S_{200}(\%)$ (%minus 75 μ m)
MP 2	2.08	3.4	48
MP 4	2.18	3.3	53
MP 1	2.50	3.1	62
MP 3	2.57	3.0	70

At higher residence time, the particles are subject to more breakage action. This produces a more irregularly shaped product with lower density and finer size.

3.2.7 Powerdraw

The motor providing rotational speed to the 7ft DIA by 26ft long (2.13m by 7.92m) ball mill 408 has the following specifications:

500 HP (372.85 kW)
 2300V - 3 ϕ - 60 Hz
 1775 RPM FL speed (186.38 rad/sec)
 113 A FL current
 83% efficiency

A watt transducer connected to the motor electrical line provides power readings for total charge monitoring by the operators. Two current transformers connected to phase A and C along with two voltage transformers connected between phases A-B and phases B-C provide input signals to the transducer that will convert the signals to power. The transducer generates a 4-20 mA output that is read by an analog input card on the PLC. Using the following equation, the motor power is calculated:

$$P = E_{LL} \times I \times \sqrt{3} \times FP \times \eta \quad (3.22)$$

where: E_{LL} = line to line voltage (V)

I = current (A)

FP = power factor (0.95)

η = motor efficiency (0.83)

The power factor is influenced by the overall plant electrical network behavior and motor load. However, it is usually stable and averages 0.95.

The watt transducer provides powerdraw readings with the following specifications:

Powerdraw range: 150 – 275 kW

Standard deviation: 1.2 kW

Precision: 2%

Mill performance is greatly influenced by total load and ball load. Direct measurement of charge is difficult. Hence, inferential measurement is a very attractive option. The use of a powerdraw model can be used to estimate the total and ball charge. The mill inventories are key process variables and obtaining a measurement of these variables provides a means for their control [10]. Measurement options for these process variables are direct and indirect methods. Immediate inference of the process variable of interest involves design of a hardware sensor. However, direct measurement of the mill charges is problematic for various reasons, such as rotational motion of the mill and destructive tumbling action of the charge. Recent developments have been made in the direct measurement of the total charge by the use of conductivity probes located within the mill lining [48]. On the other hand, indirect measurement involves design of a software sensor that allows inference of the process variable of interest through the measurement of one or more alternative process variables. Advances have also been made in indirect measurement of the mill contents using powerdraw and mill weight models as soft sensor measurement models [49].

The powerdraw model developed by the Julius Kruttschnitt Mineral Research Centre [50], is written as:

$$P = P_{no\ load} + kP_{charge} = P_{no\ load} + k(P_b + P_p) \quad (3.23)$$

where, P is the mill powerdraw (kW), $P_{no\ load}$ is the no-load power of the mill (empty mill power draw) (kW), P_{charge} is the mill powerdraw attributable to the entire content of the mill (kW), P_b is the mill powerdraw attributable to balls, P_p is the mill powerdraw attributable to powder, and k is a lumped mill powerdraw parameter that accounts for heat losses caused by internal friction, energy of attrition/abrasion breakage, rotation of the grinding media, inaccuracies in assumptions, ambient conditions, gear drive system friction, motion measurements and liner wear.

For Domfer ball milling process with ideal conditions, we can assume that,

$$k = 1$$

Otherwise, with increased heat losses, gear drive system friction and detrimental grinding conditions, the mill powerdraw parameter becomes,

$$k > 1$$

By looking at figure 2.20, we can see that power decreases with liner wear. Also, by looking at figures 2.19 and 3.6, we understand that the flattened worn out liner shape has a lower friction factor, which reduces the charge rising height (increased slipping), consequently reducing the work needed per revolution. However, since the height of balls and the ball/powder ratio are kept constant, the total charge increases, which requires more power. Therefore, the increased gravitational and centrifugal forces more or less cancel the effect of the flattened shape, leaving the powerdraw constant with respect to liner wear.

Below are specific BM-408 powerdraws providing good grinding performance and product quality:

Table 3.4: Powerdraws for ball mill 408 products

	<u>P_b (kW)</u>	<u>P (kW)</u>
MP 3	178.5	195.2
MP 1	178.5	199.9
MP 4	178.5	214.2
MP 2	178.5	226.1

When ball mill conditions deteriorate, the powerdraw constant k value increases. This in turn increases the powerdraw required for best performance and product quality. This can be detected by a higher starting P_b at $P_p = 0$.

Consider the Bond relation to estimate the required shaft mill power as a function of ball mill 408 dimensions:

$$\begin{aligned}
 P &= 7.33 J \phi_c (1 - 0.937 J) \left[1 - \frac{0.1}{2^{9-10\phi_c}} \right] (\rho_{b,true} L D^{2.3}) \quad (3.24) \\
 &= 7.33(0.15)(0.77)(1 - 0.937(0.15)) \left[1 - \frac{0.1}{2^{9-10(0.77)}} \right] \left(7.81 \frac{t}{m^3} (7.92 m) (2.13 m)^{2.3} \right) \\
 &= 245.8 kW
 \end{aligned}$$

3.0 BALL MILLING PROCESS CHARACTERIZATION

Comparing with the powerdraws of table 3.4, the Bond relation approximates well the required shaft mill power.

3.2.8 Rotational speed

Another important ball mill parameter is angular speed since it directly affects charge motion. As the mill speed increases, the breakage rate of coarser particles increases while the breakage rate of finer particles reduces. At low speeds, the attrition breakage action is enhanced producing finer sizes. Attrition breakage at lower speed and impact breakage at higher speed is a reflection of the variations in charge motion. A higher mill speed provides higher throughput with coarser product. However, as the centrifugal forces increase with speed, a point is reached where the breakage rates of the coarser particles are expected to decrease.

The critical speed (rotational speed at which balls just start to centrifuge on the mill walls and not tumble) of BM-408 can be calculated using equation 2.2:

$$\begin{aligned} N_c &= \frac{42.2}{\sqrt{D-d}} \\ &= \frac{42.2}{\sqrt{2.1336\text{ m} - 0.0508\text{ m}}} \\ &= 29.24\text{ RPM} \quad (3.07\text{ rad/sec}) \end{aligned}$$

Below are the components providing rotational speed to ball mill cylinder shell. From top to bottom, the connecting sequence from motor to cylinder shell is shown with speeds and reducing ratios:

1. 500 HP (372.85 kW) motor at 1775 RPM (186.38 rad/sec)
2. Gyrol Fluid Drive: 3.7% to 10% slip
3. Falk parallel shaft speed reducer: 9.55 to 1
4. Pinion: 19 teeth
5. Main gear: 152 teeth

By varying the % slip of BM-408 fluid drive, the rotational speed range is:

$$\begin{aligned}\omega &= 1775 \text{ RPM} \times \frac{1}{9.55} \times \frac{19}{152} \times (0.9 \rightarrow 0.963) \\ &= 20.9 \rightarrow 22.4 \text{ RPM} \quad (2.19 \rightarrow 2.35 \text{ rad/sec})\end{aligned}\tag{3.25}$$

with an accuracy and repeatability within $\pm 1\%$ of maximum speed.

Expressed in terms of fraction of critical speed, the range is:

$$\begin{aligned}\phi_c &= \frac{20.9}{29.24} \rightarrow \frac{22.4}{29.24} N_c \\ &= 71\% \rightarrow 77\% N_c\end{aligned}\tag{3.26}$$

The fluid drive uses hydrodynamic principles to transmit power from a prime mover to a load. It is based on power transmission principles originally developed by Dr. Hermann Föttinger, of Hamburg, Germany in 1905 [51]. The characteristics of a pump and turbine are combined into a hydrokinetic device. Hydraulic oil is utilized to transmit power smoothly and without shock. Oil particles are accelerated in the impeller connected to the prime mover and power is transmitted as they strike the blades of the runner connected to the driven load. There is no mechanical connection between the input and output shafts. The amount of oil in the working circuit can be changed while the machine is operating, providing speed adjustments. The working oil, while in the rotating elements (impeller and runner), is thrown outward where it takes the form of a toroid (doughnut shape). Varying the quantity of oil in the toroid varies the output speed. A movable scoop tube controls the amount of oil in the toroid. The position of the scoop tube (amount of oil in the working circuit) is controlled manually on the BM-408 Gyrol fluid drive. However, using a Gyroltrol controller would enable automatic control of the device.

Using a Gyrol fluid drive to control BM-408 rotational speed has the following advantages:

- Stepless speed control over a wide range
- No-load starting allowing the use of economical starters and motors
- Can easily accelerate high-inertia load using low-cost induction drive motor
- Limits torque to protect the drive train or driven equipment

3.0 BALL MILLING PROCESS CHARACTERIZATION

- Eliminates high starting torques
- Transmits power at maximum efficiency (95% or more)
- Absorbs shock and torsional vibrations

The gear drive arrangement and Gyrol fluid drive specifications are shown in Appendix 1.

A circulating pump, driven from the input shaft, pumps oil from the housing reservoir through an external heat exchanger to remove excess heat, then returns it to the working elements. An under-designed heat exchanger was installed with the fluid drive causing oil overheating problems at higher percentage slip (reduced speeds). With the oil high temperature issue and the different liner lives ($T_{Lin} = 6500$ hr and $T_{Lout} = 9000$ hr), it was decided to keep the rotational speed constant at $77\%N_c$ (3.7% slip) and change one-half of the liner set at a time.

In ideal conditions, the control strategy is to start with a completely new set of liners at minimum rotational speed ($71\%N_c$), then increase the speed gradually as the lifting efficiency decreases (liner wear), up to $77\%N_c$ for a worn out set, to keep charge motion constant.

3.2.9 Air flow rate

The size distribution of the material coming out of the ball mill is dictated by the strength of the air flow. A stronger air flow rate provides higher air velocity to pull out coarser and more dense ground shot. On the other hand a smaller air flow rate sweeps finer product. Moreover, the air flow rate influences powder charge: a stronger flow emptying the mill faster (lower residence time) and vice versa.

The air flow rate inside ball mill 408 is generated using a centrifugal fan driven by a 100HP (74.57kW) motor. Fully developed air flow rate measurement is provided by a Diamond II+Annubar primary flow element installed on a straight portion of the output conduit of the blower. The flow element operates by sensing an impact pressure and a

reference pressure through multiple sensing ports connected to dual averaging plenums. The resultant difference is a differential pressure signal. Sensing ports are located on both up and downstream sides of the flow element. The number of ports is proportional to the pipe diameter. The Diamond II+ sensor is a multiple-tube, rigid structure that provides dual averaging chambers with a diamond-shaped cross section and bi-directional flow sensing. The flow element produces a dP signal proportional to the square of the flow rate in accordance with Bernoulli's theorem:

$$\int_1^2 \frac{dP}{\rho} + \frac{1}{2} \left(\frac{Q_2^2}{A_2^2} - \frac{Q_1^2}{A_1^2} \right) + g(Z_2 - Z_1) = 0 \quad (3.27)$$

The dP signal has two components: the high pressure and the low pressure. The high pressure is produced by the impact or stagnation of the moving fluid on the sensor. The velocity profile results in a corresponding stagnation pressure profile. Multiple sensing ports, located on the front of the tube, sense the impact pressure profile. As the fluid continues around the sensor, it generates a vortex shedding pattern and creates a low pressure profile, which is used as a pressure reference so the velocity can be determined independently of the pipe static pressure. The low pressure is sensed by ports, located downstream and opposite to the high pressure. The diamond shape of the tube establishes a fixed separation point of the fluid from the sensor. The fixed separation point reduces changes in the low or reference pressure, that causes a corresponding loss of accuracy in flow measurements. The dP signal is piped to a differential pressure transmitter that converts the pressure input to a flow signal using a square root function. The result is outputted to the PLC via a 4-20mA signal.

The actual flow signal is treated by the PLC and compared with the desired value. A PID function varies the angular opening of a butterfly type motorized damper, installed on the suction circuit, just before the inlet of the blower. The desired air flow rate is achieved by controlling flow restriction in the conduit.

The desired air flow rate (sweeping action) is obtained and maintained using PID control. For the air flow rate control system, a wide proportional band is selected since many

3.0 BALL MILLING PROCESS CHARACTERIZATION

disturbances can occur: turbulence, leaks and circuit resistance variations (dust collector cartridges, cyclone, impact tank discharge valve). Damper angular position variations are not too brusque and the disturbance probably stops before the proportional band has had time to significantly change the opening to correct the deviation. Since the response time is not a major issue, a wide proportional band produces a very robust and stable system that can accommodate disturbances. To reduce the offset caused by a wide proportional band, a relatively weak integral correction is chosen. No derivative is used since turbulence irregularities would generate hunting in a short period.

The air flow rate control system has a PI controller with a wide proportional band and weak integral action. The controller is robust with moderate response time, which corresponds well to the expected control capabilities:

Air flow rate range: 0–7000 ACFM (0–3.304 m³/sec)

Standard deviation: 35 ACFM (0.017 m³/sec)

Precision: 1%

Repeatability: ±0.1%

Settling time: 1.5min to a 500 ACFM (0.236 m³/sec) step change

As in section 3.2.2, let us theoretically demonstrate the effectiveness of the PI controller developed using a heuristic approach. A negative unity feedback control system in the Laplace domain is considered. The block diagram is shown in figure 3.10.

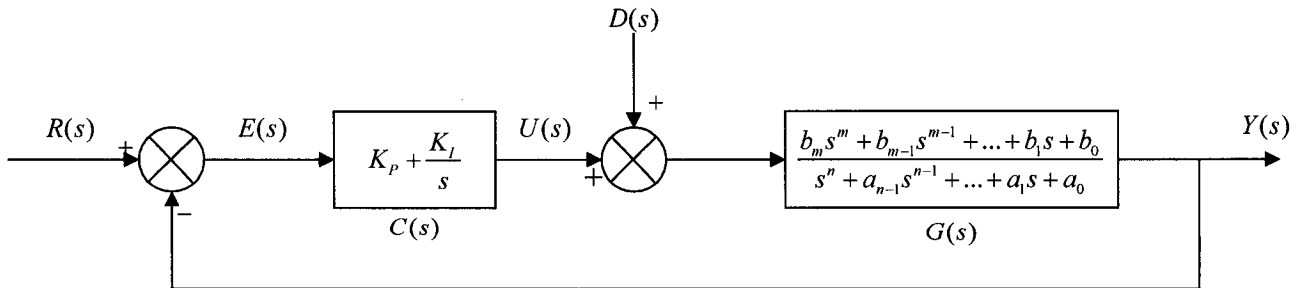


Figure 3.10: Negative unity feedback air flow rate control block diagram

where,

$G(s)$ = damper (plant) transfer function with an n th-order characteristic equation

$C(s)$ = PI controller

$R(s) = \mathcal{L}\{Q_{\text{set point}}(t)\}$

$Y(s) = \mathcal{L}\{Q(t)\}$

$E(s) = R(s) - Y(s)$, error of the system

$D(s)$ = System disturbances

$U(s)$ = Controller output

The application of the final value theorem to the error of the system gives the following steady-state error formula:

$$\begin{aligned}
 e_{ss} &= \lim_{t \rightarrow \infty} e(t) = \lim_{s \rightarrow 0} s E(s) = \lim_{s \rightarrow 0} s \frac{1}{1 + C(s)G(s)} R(s) \\
 &= \lim_{s \rightarrow 0} s R(s) \frac{1}{1 + \left(K_p + \frac{K_I}{s} \right) \left(\frac{b_m s^m + b_{m-1} s^{m-1} + \dots + b_1 s + b_0}{s^n + a_{n-1} s^{n-1} + \dots + a_1 s + a_0} \right)} \\
 &= \lim_{s \rightarrow 0} s^2 R(s) \frac{a_0}{K_I b_0}
 \end{aligned} \tag{3.28}$$

The equation shows that the system is type 1 with respect to reference tracking, i.e., the control system perfectly tracks ($e_{ss}=0$) a desired step air flow rate input ($R(s)=1/s$). This corresponds well with the design requirements.

Then, the steady-state error to a disturbance input is:

$$y_{ss} = \lim_{t \rightarrow \infty} y(t) = \lim_{s \rightarrow 0} s Y(s)_{\text{due to } D} \tag{3.29}$$

where the output equation $Y(s)$ is:

$$Y(s) = \frac{G(s)}{1 + C(s)G(s)} D(s) + \frac{C(s)G(s)}{1 + C(s)G(s)} R(s) \tag{3.30}$$

But $Y(s)_{\text{due to } D}$ is $Y(s)$ with $R(s)=0$. Therefore, the steady-state error equation becomes:

$$\begin{aligned}
 y_{ss} &= \lim_{s \rightarrow 0} s \frac{G(s)}{1 + C(s)G(s)} D(s) \\
 &= \lim_{s \rightarrow 0} s D(s) \frac{\left(\frac{b_m s^m + b_{m-1} s^{m-1} + \dots + b_1 s + b_0}{s^n + a_{n-1} s^{n-1} + \dots + a_1 s + a_0} \right)}{1 + \left(K_p + \frac{K_I}{s} \right) \left(\frac{b_m s^m + b_{m-1} s^{m-1} + \dots + b_1 s + b_0}{s^n + a_{n-1} s^{n-1} + \dots + a_1 s + a_0} \right)} \\
 &= \lim_{s \rightarrow 0} s^2 D(s) \frac{1}{K_I}
 \end{aligned} \tag{3.31}$$

This is a system type 1 with respect to disturbance rejection, i.e., the control system rejects ($v_{ss}=0$) step disturbances ($D(s)=1/s$). This corresponds well with actual system disturbances caused by turbulence, leaks and circuit resistance variations. The designed PI controller provides robust air flow rate control.

3.2.10 Outlet trunnion pressure

The size distribution of the material coming out of the ball mill is dictated by the air flow rate inside the mill cylindrical shell. However, air flow rate control actions are taken based on the flow transmitter installed after the blower. Any equipment between the transmitter and the mill may bias the strength of the suction air flow:

1. Cyclone: variable flow restriction, blockage
2. Cyclone air lock valve
3. Dust collector: cartridge cleanliness
4. Impact tank discharge valve
5. Suction circuit

Using a pressure transmitter connected on the suction circuit, just after the outlet trunnion, the effectiveness of the sweeping action is monitored. A vacuum pressure signal proportional to air flow rate is generated. For a specific air flow rate, the pressure signal can be too low for the following reasons: impact tank discharge valve leak, cyclone air lock valve leak, suction circuit leak and dust collector cartridges dirty. On the other hand, if one of the dust collector cartridges breaks, the resistance of the circuit drops drastically,

generating higher outlet trunnion pressure signals, related to a higher suction air flow. For size distribution control, a stable suction air flow inside the cylindrical shell is very important. A drop in outlet pressure is compensated by increasing the air flow rate.

The low pressure port of the pressure transmitter is connected to the conduit and the high pressure port is left open to atmospheric pressure. The transmitter provides vacuum pressure signals with the following specifications:

Output trunnion pressure range: 0-10.00 inH₂O (0-2488.40 N/m²)

Precision: 2%

Standard deviation: 0.04 inH₂O (9.95 N/m²)

3.2.11 Product rate

Capacity is meaningless without defining the feed and product size distribution. Obviously, more breakage actions are required to grind a coarser feed to a desired product size, the energy per ton being higher and mill output lower. For Domfer ball milling process, product rate is defined by:

$$\dot{m}_o = \dot{m} - \dot{m}_{D415} - \frac{dM_p}{dt} \quad (3.32)$$

where, \dot{m}_o is product rate, \dot{m} is feed rate, \dot{m}_{D415} is dust rate at dust collector D-415 and M_p is powder charge.

During loading phase,

$$\frac{dM_p}{dt} > 0$$

On the other hand, during emptying phase,

$$\frac{dM_p}{dt} < 0$$

When the ball mill has reached stable operating conditions (constant charge), we can assume that:

$$\frac{dM_p}{dt} = 0$$

3.0 BALL MILLING PROCESS CHARACTERIZATION

Therefore, equation 3.32 reduces to:

$$\dot{m}_o = \dot{m} - \dot{m}_{D415} \quad (3.33)$$

The rate of very fine product going to the dust collector is a function of the effectiveness of the air separator (cyclone, air lock valve). Any malfunction of the separator can be detected by a lower outlet trunnion pressure at specific air flow rate. By weighing the dust collector discharge bucket after each production run, it is found that dust rate is proportional to feed rate and averages to:

$$\dot{m}_{D415} = 0.02 \dot{m} \quad (3.34)$$

Therefore, the product rate equation 3.34 simplifies to:

$$\dot{m}_o = 0.98 \dot{m} \quad (3.35)$$

3.2.12 Product properties

The quality of the product generated by the ball milling operation is defined using two properties: apparent density and size distribution. The research objectives are aimed at reducing apparent density and size distribution variations, providing enhanced controllability of downstream operations and better final product characteristics: density, dimensional change, green strength, compressibility.

Knowing powder charge and outlet trunnion pressure, and based on size distribution and density results, powder feed rate and airflow are adjusted. The control strategy is discussed in detail in chapter 5.

A key factor in characterizing the ball mill discharge is to get a sample that is representative of the process. One can be equipped with top of the line particle analyzers, if the sample is not representative, process control becomes very complicated and ineffective. Sampling procedures are critical for output product properties stabilization.

On BM-408, the sample is taken inside the inclined pipe connecting the impact tank with the bucket elevator that feeds the ground shot tank. All the ground material passes

through this pipe. The air flow sweeps the reduced shot out of the mill through a ceramic square conduit that links the mill and the impact receiving tank. The air velocity reduces greatly in the impact tank which allows the product to deposit at the bottom and discharge in the inclined pipe. The suction circuit is presented in figure 3.11.

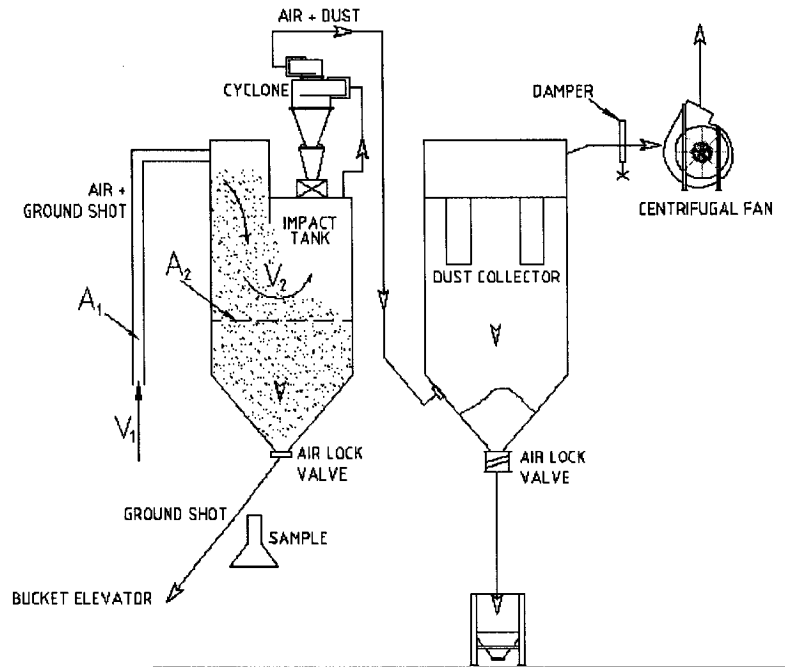


Figure 3.11: Ball mill 408 suction circuit

Looking at figure 3.11 and the continuity equation for steady flow with no storage of mass, and using average velocities, the air velocity drop inside the impact tank is approximated:

$$\begin{aligned}
 V_2 &= \frac{A_1}{A_2} V_1 \\
 &= \frac{167 \text{ in}^2}{9216 \text{ in}^2} V_1 \\
 &= 1.8\% V_1
 \end{aligned} \tag{3.36}$$

where A_1 , V_1 and A_2 , V_2 are the cross sectional area and air average velocity of the ceramic conduit and the impact tank respectively.

3.0 BALL MILLING PROCESS CHARACTERIZATION

As shown in equation 3.36 and figure 3.11, the first powder-air separation occurs in the impact tank followed by a second separation in the cyclone. The extremely fine product is recuperated in the dust collector. The inclined pipe below the impact tank is a good location to get a representative sample since product flow is continuous and stable.

Three samples of approximately 300g are scooped with a sampling device inside the inclined pipe at 20 second intervals. These samples are mixed to produce 2 reference test specimens: 100g specimen for the sieve analysis test and 90-120g specimen for the apparent density test. Sample quality is highest when it is a blend of several small specimens taken from a moving powder stream [29].

The tests are performed using the Metal Powder Industries Federation (MPIF) standards presented in Appendix 2:

MPIF standard 04: Determination of Apparent Density of Free-Flowing Metal Powders Using the Hall Apparatus

MPIF standard 05: Determination of Sieve Analysis of Metal Powders

Typical MP2 ground shot sieve analysis and apparent density results are presented in table 3.5.

Table 3.5: Typical MP2 ground shot sieve analysis and apparent density results

New U.S. Standard Series		
Particle Size (μm)	Mesh Designation No.	Percentage By Mass
>250	+ 60	trace
≤ 250 >180	-60 + 80	3.0%
≤ 180 >150	-80 + 100	6.9%
≤ 150 >106	-100 + 140	13.9%
≤ 106 >75	-140 + 200	23.1%
≤ 75 >45	-200 + 325	25.3%
≤ 45	-325	27.8%
Apparent density:	3.47 g/cm ³	

Human resource limitations at Domfer restrict samples to be taken and tested only every 3-4 hours. A two point measurement of product size is performed:

1. Percentage retained by a 100 mesh sieve: $S_{100}(\%)$, +100mesh(%) (+150 μm)
2. Percentage passing a 200 mesh sieve: $S_{200}(\%)$, -200mesh(%) (-75 μm)

Inertial problems are created since the effect of changes in parameter adjustments are seen only after a few hours. Using a fully automated sampler and sieve analyzer provides more frequent size distribution feedback, which in turn greatly enhances overall control system performance in order to meet quality specifications. A new automated sampler was created to work in conjunction with an automated sieve analyzer. This is described in detail in chapter 4.0.

Ground shot quality is defined by accurate, precise and stable size distribution, apparent density and shape. Figure 3.12 shows a scanning electron microscope (SEM) micrograph of ground shot. We can see the size distribution of the particles having a combination of spherical (from the atomization process) and irregular shapes (after ball milling process).

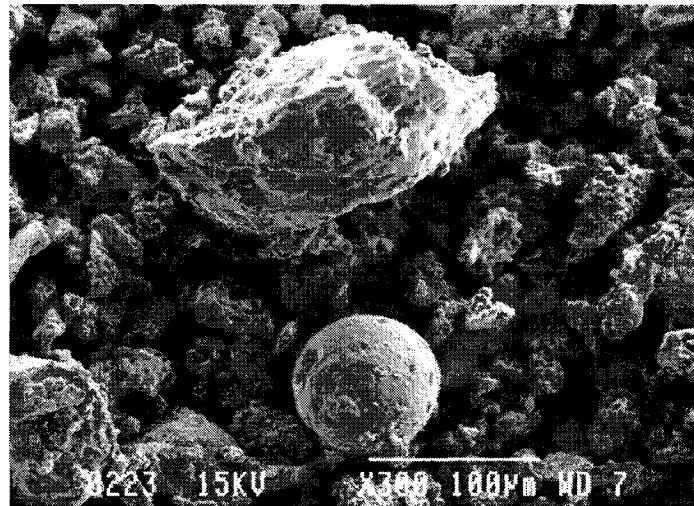


Figure 3.12: Ground shot SEM micrograph

3.0 BALL MILLING PROCESS CHARACTERIZATION

Product properties are influenced by the following previously described variables:

1. Input product properties
2. Powder feed rate
3. Grinding ball properties, size distribution and charge
4. Liner properties, wear and geometry
5. Ball and powder charge
6. Residence time
7. Powerdraw
8. Rotational speed
9. Air flow rate
10. Product rate

Important average parameters for the grades produced on ball mill 408 are summarized in table 3.6.

Table 3.6: Ball mill 408 produced grade parameters

Grade	+20mesh(%)	%C	-200mesh(%)	A.D.(g/cc)	\dot{m} (lb/hr)	Q(ACFM)	P(kW)	M_p (lb)	τ (hr)
3	50	3.3	70	3.0	3500	4500	195.2	9000	2.57
1	80	4.0	62	3.1	4000	5400	199.9	10000	2.5
4	15	3.3	53	3.3	5500	6500	214.2	12000	2.18
2	11	3.8	48	3.4	6000	6500	226.1	12500	2.08

Now, compare MP2 and MP3 ground shots using table 3.6. With a finer spherical input (+20mesh (850 μ m) = 11%), MP2 grade requires less breakage action to achieve the desired coarser output size (-200mesh (75 μ m) = 48%). A higher feed rate reduces residence time, allowing the spherical shot to be less deformed, which in turn enables better particle arrangement, and, consequently higher bulk density (A.D.). At low powder charge, like MP3 (M_p =9000lb (4082.3kg)), the steel-to-steel contact is more aggressive, which in turn reduces the product more (-200mesh (75 μ m) = 70%). On the other hand, at high powder charge (MP2, M_p =12500lb (5669.9kg)), the powder cushions the breakage action, conserving more initial particle sphericity. Also, a higher air flow rate (MP2, Q =6500ACFM (3.068m³/sec)) discharges a coarser and denser product.

In order to define system behavior with respect to parameter variations, 7 trials were performed on different product campaigns during normal operation. This is outlined in detail in section 3.3.

3.3 Performance specifications of variables and sensors

Plant trials were performed on ball mill 408 to define overall system behavior. The objectives were:

- Determine the effect of parameter variations on product size distribution and density.
- Validate the size distribution function.
- Provide fundamentals for automatic sampler design and process model development.

Three different series of tests with specific objectives were executed:

1. Determine the effect of feed rate on size distribution and density
2. Determine the effect of air flow rate on size distribution and density
3. Evaluate the actual suction air flow

Seven trials were executed on different product campaigns during normal mill operation. The parameters were varied and evaluated using the human machine interface. Samples were taken inside the inclined pipe located below the impact tank using the procedure described previously in section 3.2.12 to get 2 reference test specimens for sieve and apparent density analysis. The tests were performed using MPIF standard 04 and 05 with new U.S. Standard Series screens. Complete plant trial results are shown in Appendix 3.

The results are presented below on graphs showing size, density and charge variation with respect to specific parameter change. Cumulative +100mesh (+150 μ m) and -200mesh (-75 μ m) are used to describe the coarse and fine portion of the size distribution.

Afterwards, size distributions results are plotted on log-normal paper for size distribution function validation.

Finally, outlet trunnion pressure versus air flow rate is investigated for further monitoring algorithm development to stabilize suction air flow inside the mill cylindrical shell.

3.0 BALL MILLING PROCESS CHARACTERIZATION

3.3.1 Effect of feed rate and air flow rate changes on product properties

The effect of feed rate step change on size distribution, density and charge was investigated, while keeping air flow rate constant. Samples were taken every 10 minutes during 2 hours for product property feedback. Three tests were performed:

1. m1: +1000 lb/hr (453.6kg/hr) at $t = 0$ followed by -2000 lb/hr (907.2kg/hr)
2. m2: +2000 lb/hr (907.2kg/hr) at $t = 0$ at $t = 60$ min
3. m3: -2000 lb/hr (907.2kg/hr) at $t = 0$

Test # m1: +1000 lb/hr (453.6kg/hr) feed rate increase followed by
-2000 lb/hr (907.2kg/hr) feed rate reduction

Product: S-1

Date: 16-02-2004 Time: 15:00

Initial conditions: $\dot{m} = 4350$ lb/hr (1973.1kg/hr) and $Q = 5400$ ACFM (2.549m³/sec)

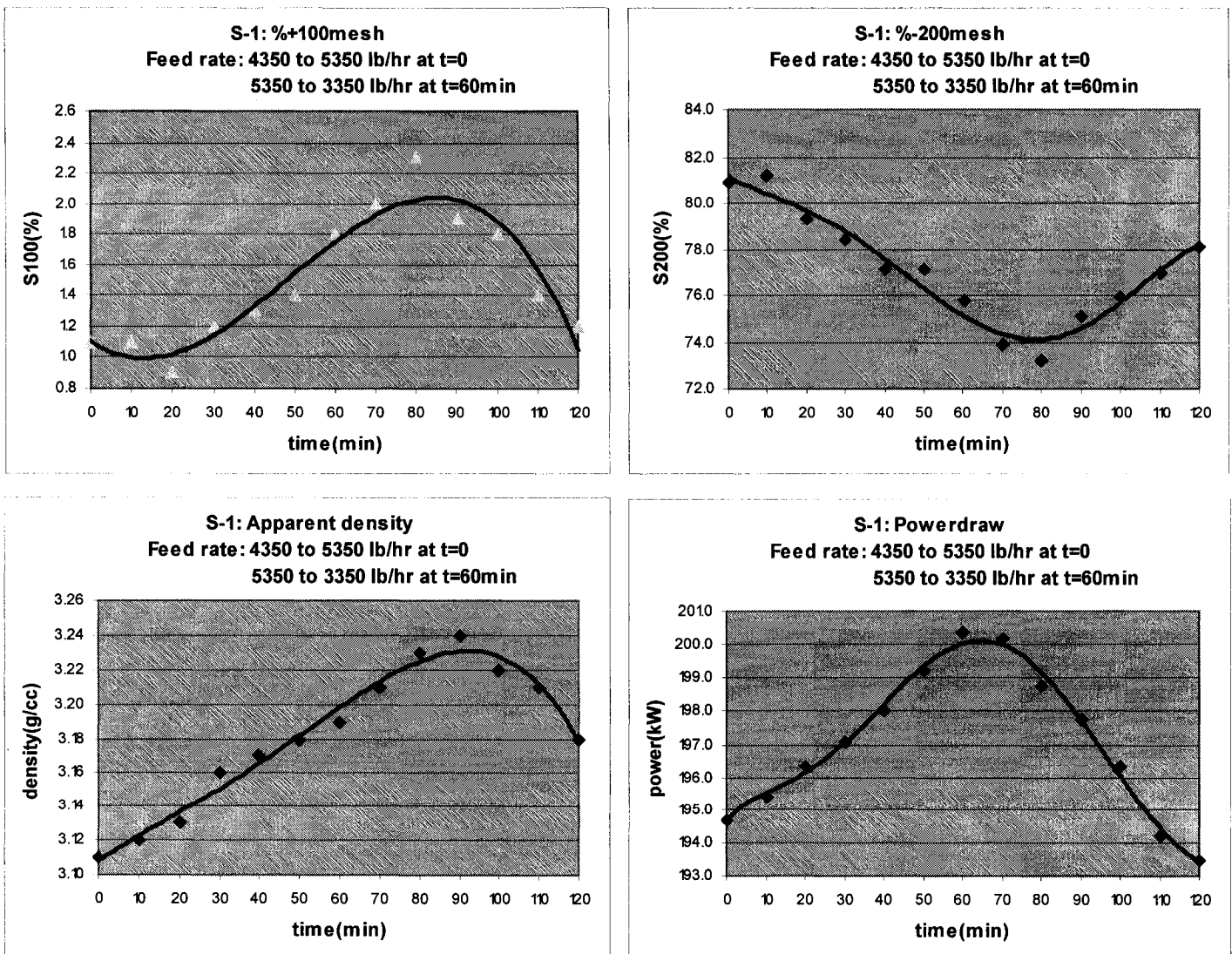


Figure 3.13: Feed rate trial # m1 results

Test m1 was performed during production of S-1. The feed rate was increased from 4350 to 5350 lb/hr (1973.1 to 2426.7kg/hr) at $t=0$ and decreased from 5350 to 3350 lb/hr (2426.7 to 1519.5kg/hr) at $t=60$ min. In figure 3.13, we can clearly see that as the feed rate is increased, charge increases (Powerdraw), the coarse portion of the ground product (+100mesh (+150 μ m)) increases and the fine portion (-200mesh (-75 μ m)) decreases. On the other hand, the feed rate reduction generates a decrease in charge, consequently reducing the +100mesh (+150 μ m) and increasing the -200mesh (-75 μ m). We can also see the inertial effect that lasts approximately 30 min from $t=60$ min to $t=90$ min, where the ball mill is in transition phase, passing from an emptying mode to a filling mode. This is confirmed by the local maximum on the powerdraw curve with related local maximum on the +100mesh (+150 μ m) and density curves and local minimum on the -200mesh (-75 μ m) curve.

Using the repeatability (within a laboratory) and reproducibility (between laboratories) limits of the apparent density and sieve analysis, the response time and powder charge sensitivity of the system with actual grinding conditions are defined. The minimum size distribution variation needed to differentiate between two ground products is defined by the maximum between the repeatability and reproducibility limits of the +100mesh (+150 μ m) and -200mesh (-75 μ m) results. Using MPIF 05 equations presented in Appendix 2,

$$r_{\max} = 0.4 + 0.03 SF = 0.4 + 0.03 (73\%) = 2.6\%$$

$$R_{\max} = 2.2\%$$

where, r_{\max} and R_{\max} are the maximum repeatability and reproducibility limits respectively.

Examining the -200mesh (-75 μ m) graph of figure 3.13, and using the maximum limit of 2.6%, we find the product response time T_R to be approximately 33 min. The powder charge sensitivity $M_{p(\min)}$ can be calculated using,

$$M_{p(\min)} = T_R \times \Delta \dot{m} \quad (3.37)$$

$$= 0.55 \text{ hr} \times 1000 \text{ lb/hr} \quad \Delta \dot{m} = \text{feed rate step change}$$

$$= 550 \text{ lb} \quad (249.5 \text{ kg})$$

3.0 BALL MILLING PROCESS CHARACTERIZATION

$M_{p(\min)}$ and T_R are defined respectively as minimum powder charge variation and time required to significantly affect product properties.

Test # m2: +2000 lb/hr (907.2kg/hr) feed rate increase

Product: S-3

Date: 22-02-2004

Time: 16:00

Initial conditions: $\dot{m} = 3500$ lb/hr (1587.6kg/hr) and $Q = 4500$ ACFM (2.124m³/sec)

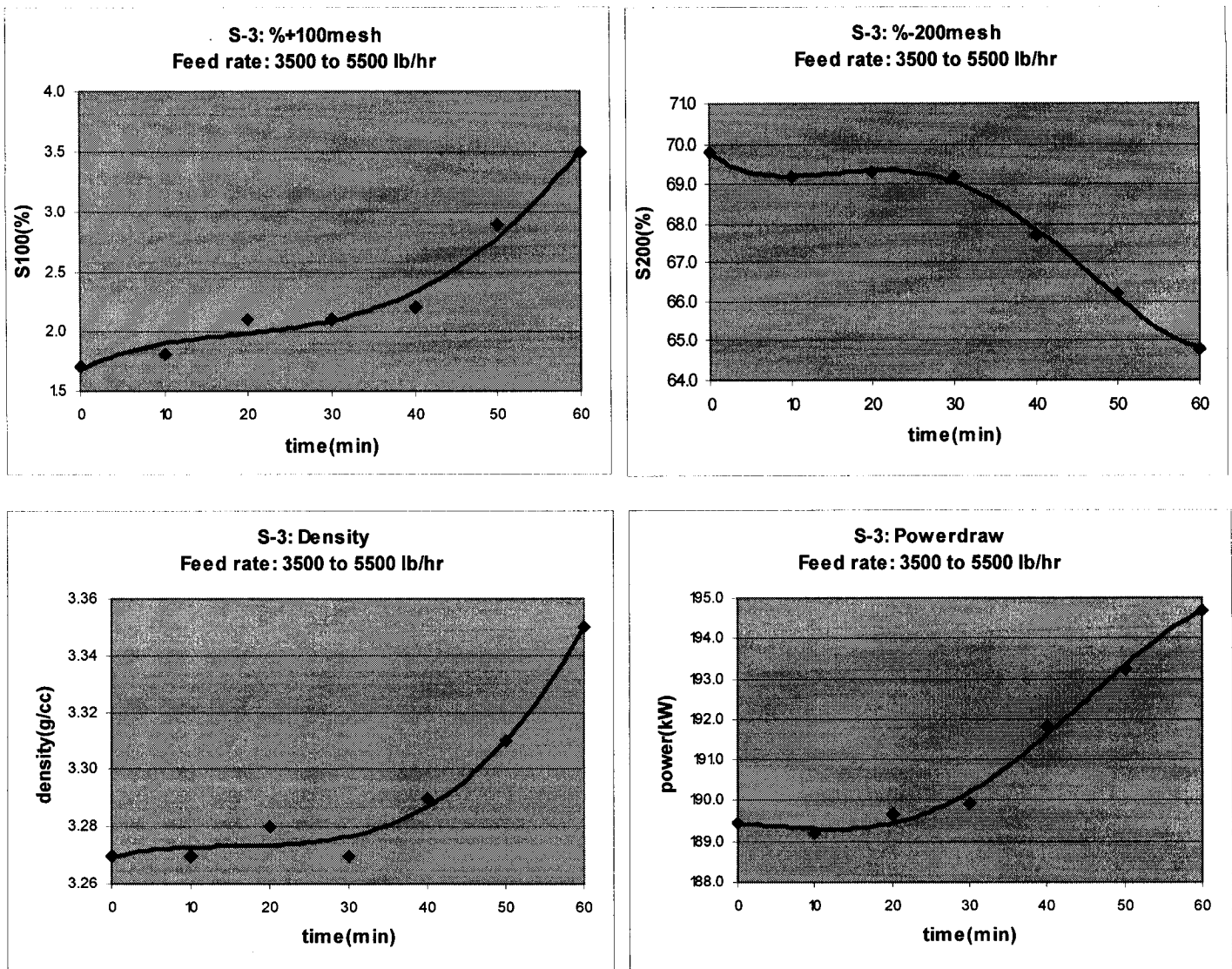


Figure 3.14: Feed rate trial # m2 results

Test m2 was performed during production of S-3. The feed rate was increased from 3500 to 5500 lb/hr (1587.6 to 2494.8kg/hr) at t=0. Looking at figure 3.14, we find that as the feed rate is incremented, powder charge increases, the coarse portion of the ground product (+100mesh (+150 μ m)) increases and the fine portion (-200mesh (-75 μ m)) decreases. The product is therefore getting coarser. However, discussing with the operator during the trials, it was found that the mill was in emptying mode, the starting -200mesh (-75 μ m) at 70% being lower than the desired 74% of product specification. This is seen by the straight portion on the curves of the previous 4 graphs of figure 3.14 from 0 to 30 min. It took 30 minutes to reverse from an emptying mode to a filling mode.

Similarly, the maximum repeatability and reproducibility limits are calculated:

$$r_{\max} = 0.4 + 0.03 SF = 0.4 + 0.03 (70\%) = 2.5\%$$

$$R_{\max} = 2.2\%$$

Using the maximum value of 2.5 % and -200mesh (-75 μ m) graph of figure 3.14, we find the product response time to be 0.72hr. The powder charge sensitivity is:

$$\begin{aligned} M_{p(\min)} &= T_R \times \Delta \dot{m} \\ &= 0.72hr \times 2000 lb/hr \\ &= 1440 lb \quad (653.2 kg) \end{aligned}$$

3.0 BALL MILLING PROCESS CHARACTERIZATION

Test # m3: -2000 lb/hr (907.2kg/hr) feed rate reduction

Product: S-2

Date: 22-03-2004

Time:16:00

Initial conditions: $\dot{m} = 7150$ lb/hr (3243.2kg/hr) and $Q = 6500$ ACFM (3.068m³/sec)

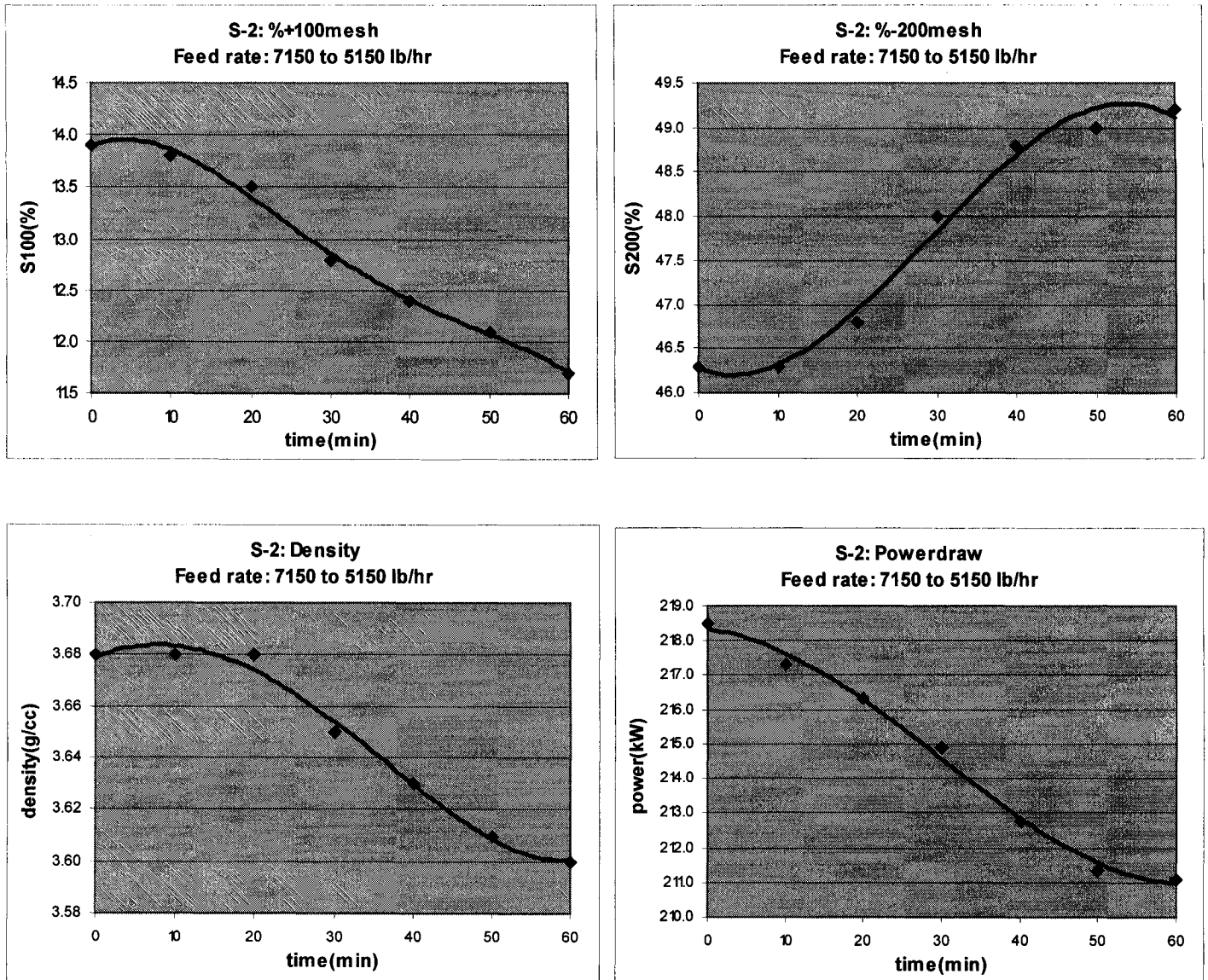


Figure 3.15: Feed rate trial # m3 results

Test m3 was performed during production of S-2. The feed rate was decreased from 7150 to 5150 lb/hr (3243.2 to 2336.0 kg/hr) at $t=0$. In figure 3.15, we can clearly see that as the feed rate is decreased, the charge decreases, the +100mesh (+150 μm) reduces and the -200mesh (-75 μm) increases. The product is therefore getting finer.

Once again, the maximum repeatability and reproducibility limits are calculated:

$$\begin{aligned} r_{\max} &= 0.4 + 0.03 SF = 0.4 + 0.03 (49.5\%) = 1.9\% \\ R_{\max} &= 2.2\% \end{aligned}$$

Using the maximum value of 2.2 % and -200mesh (-75 μm) graph of figure 3.15, we find the product response time to be 0.58hr. The powder charge sensitivity is:

$$\begin{aligned} M_{p(\min)} &= T_R \times \Delta \dot{m} \\ &= 0.58 \text{ hr} \times 2000 \frac{\text{lb}}{\text{hr}} \\ &= 1160 \text{ lb} \quad (526.2 \text{ kg}) \end{aligned}$$

Reviewing tests m1, m2 and m3, we can confirm that increasing feed rate increases powder charge. Moreover, the residence time decreases, allowing the input material to receive less breaking action, keep its original shape more and reach the exit faster to be swept away by the suction air flow, generating a product with higher density and coarser size distribution. However, at lower feed rate, the powder charge decreases, consequently increasing the ball/powder ratio. The particles are subject to higher residence time and receive more breakage action. The greater number of impacts produces ground particles with low density and finer size distribution. This is summarized below:

$$\begin{aligned} \uparrow \dot{m} &\Rightarrow \uparrow M_p \Rightarrow \text{coarser product} \\ \downarrow \dot{m} &\Rightarrow \downarrow M_p \Rightarrow \text{finer product} \end{aligned}$$

3.0 BALL MILLING PROCESS CHARACTERIZATION

Table 3.7 compares the powder charge M_p , product response time T_R and powder charge sensitivity $M_{p(\min)}$ for the performed feed rate tests:

Table 3.7: Powder charge, product response time and powder charge sensitivity results
for the feed rate tests

<u>Test</u>	<u>Product</u>	<u>M_p (lb)</u>	<u>T_R (hr)</u>	<u>$M_{p(\min)}$ (lb)</u>
m1	S-1	10000 (4535.9kg)	0.55	550 (249.5kg)
m2	S-3	9000 (4082.3kg)	0.72	1440 (653.2kg)
m3	S-2	12500 (5669.9kg)	0.58	1160 (526.2kg)

Each grade has a specific powder charge sensitivity being mainly a function of input material chemistry and size, powder charge, feed rate and airflow.

Since,

$$T_R = \frac{M_{p(\min)}}{\Delta \dot{m}} \quad (3.38)$$

the response time is inversely proportional to the size of the feed rate change. Greater variation provides faster response times and vice-versa.

Now, consider the effect of air flow rate variations on size distribution, density and charge, while keeping feed rate constant. Samples were taken every minute during 10 minutes for product property feedback. Two tests were performed:

1. Q1: -500 ACFM ($0.236\text{m}^3/\text{sec}$) at $t=0$
2. Q2: +700 ACFM ($0.330\text{m}^3/\text{sec}$) at $t=0$

Test # Q1: -500 ACFM ($0.236\text{m}^3/\text{sec}$) air flow rate reduction

Product: S-2

Date: 29-01-2004

Time: 15:15

Initial conditions: $\dot{m} = 4800 \text{ lb/hr}$ (2177.2kg/hr) and $Q = 5500 \text{ ACFM}$ ($2.596\text{m}^3/\text{sec}$)

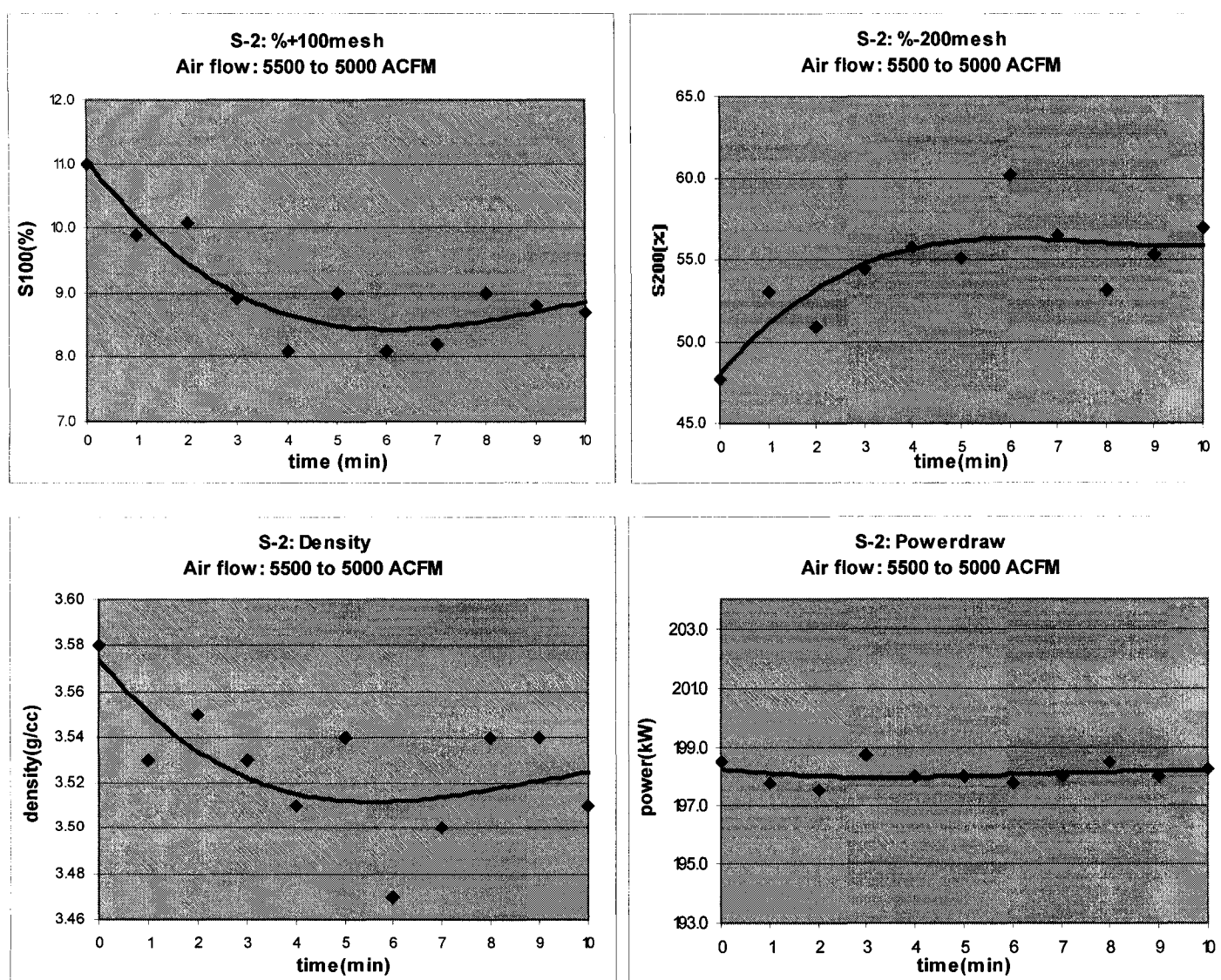


Figure 3.16: Air flow rate trial # Q1 results

3.0 BALL MILLING PROCESS CHARACTERIZATION

Test # Q2: +700 ACFM (0.330m³/sec) air flow rate increase

Product: S-4

Date: 9-02-2004

Time: 15:15

Initial conditions: $\dot{m} = 4800$ lb/hr (2177.2kg/hr) and $Q = 5500$ ACFM (2.596m³/sec)

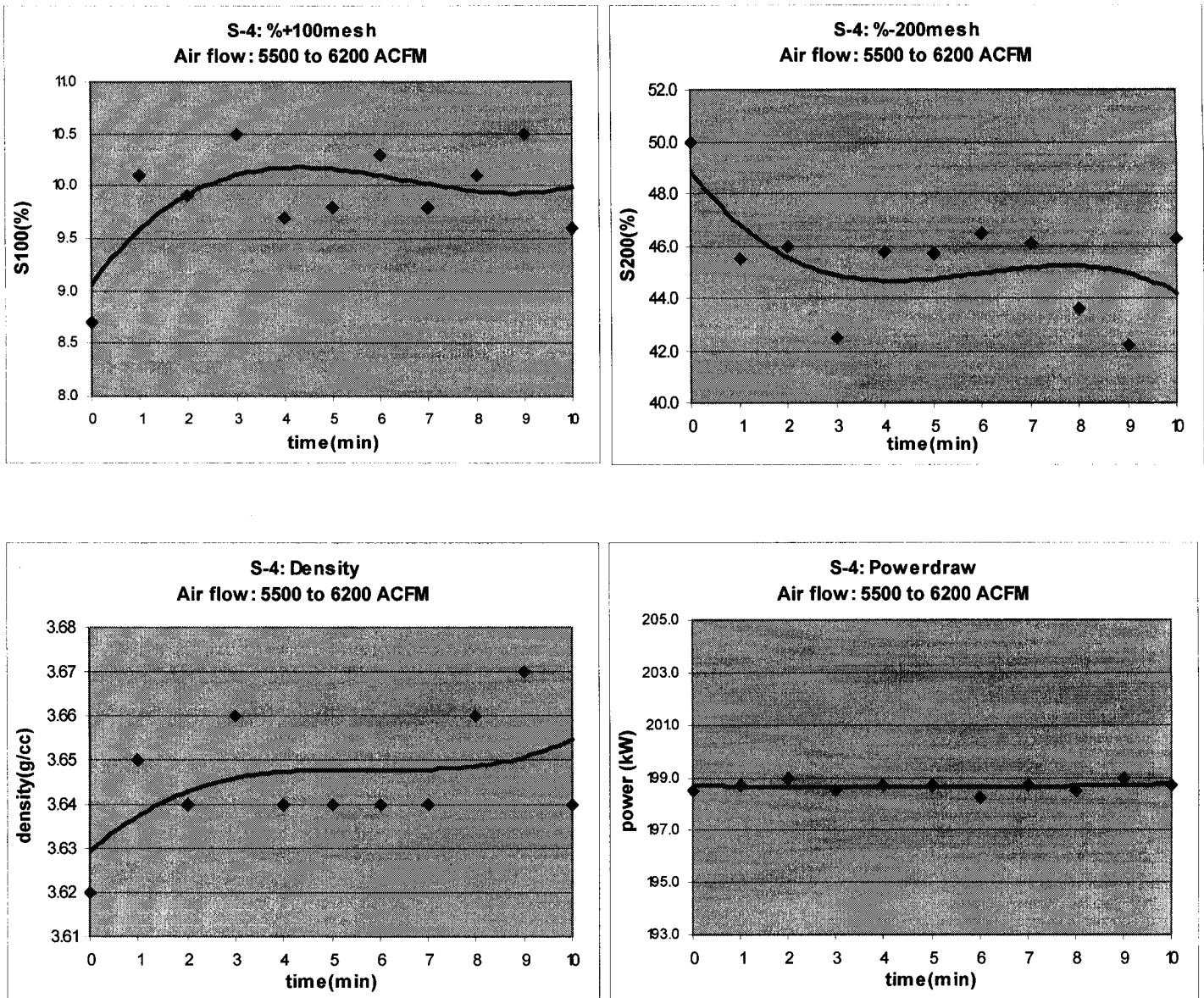


Figure 3.17: Air flow rate trial # Q2 results

Test Q1 was performed during production of S-2. The air flow rate was decreased from 5500 to 5000 ACFM (2.596 to 2.360 m³/sec) at t=0. Figure 3.16 shows that as the air flow rate is decreased, the coarse fraction (+100mesh (+150μm)) of the material decreases while the fine fraction (−200mesh (−75μm)) increases. On the other hand, looking at figure 3.17 of test Q2, which was done during production of S-4, we find that an increased air flow rate produces coarser ground shot: increased +100mesh (+150μm) and reduced −200mesh (−75μm). In both cases, examining powerdraw graphs, we realize that powder charge is not affected by air flow rate variation for small time intervals. However, for longer times, the powder charge would be affected by changes in air flow rate. For constant charge, changing the feed rate accordingly compensates for suction air flow rate variations:

$$\begin{aligned} &\text{for constant } M_p: \\ &\text{if } \uparrow Q \Rightarrow \uparrow \dot{m} \\ &\text{if } \downarrow Q \Rightarrow \downarrow \dot{m} \end{aligned}$$

Now, the maximum repeatability and reproducibility limits are calculated for tests Q1 and Q2:

$$r_{\max} = 0.4 + 0.03 SF = 0.4 + 0.03 (57\%) = 2.1\%$$

$$R_{\max} = 2.2\%$$

Using the maximum value of 2.2 % and the +100mesh (+150μm), −200mesh (−75μm) and density graphs of figure 3.16 and 3.17, the product response time to a step change in air flow rate is:

$$T_R = 4 \text{ minutes}$$

The size distribution of the product coming out of the mill is dictated by the air flow rate inside the cylindrical shell. A stronger air flow rate provides higher air velocity to pull out coarser and denser ground shot. On the other hand, a smaller air flow rate will sweep finer product. Moreover, the air flow rate influences powder charge: stronger flow emptying the mill faster and vice-versa.

The response time discovered in tests Q1 and Q2 was utilized to determine the air flow rate sensitivity ΔQ_{\min} , which is the minimum air flow rate variation to significantly affect product size distribution:

$$\Delta Q_{\min} = 100 \text{ ACFM}$$

3.0 BALL MILLING PROCESS CHARACTERIZATION

This minimum change usually generates a variation of approximately 0.75% on the product % passing a 200 mesh (75 μ m) sieve.

Examining feed rate and air flow rate trials apparent density graphs, the density is directly related to size distribution. The apparent density is proportional to the +100mesh (+150 μ m) fraction and inversely proportional to the -200mesh (-75 μ m) fraction. A coarser size distribution generates higher density and vice-versa.

3.3.2 Validation of size distribution function

There is no general agreement on what should constitute the minimum adequate characterization of the product size distribution from a ball milling circuit. Many powders exhibit straight line behavior on the log-normal plot. Hence, the particle size distribution can be reduced to 2 parameters, such as, the +100mesh (+150 μ m) and -200mesh (-75 μ m). Cumulative size distributions from feed rate and air flow rate tests are plotted on log-normal paper to determine the shape of the distribution and the sufficient number of points to reasonably characterize the product. Feed rate and air flow rate trial results plotted on log-normal paper are shown in Appendix 3. Feed rate test m1 cumulative distribution results at t=0 and t=50 min are presented in table 3.8 and shown on a log-normal plot in figure 3.18.

Table 3.8: Feed rate test m1 cumulative distribution results

Product: S-1
@ t = 0 , \dot{m} : 4350 \rightarrow 5350 lb/hr (1973.1 \rightarrow 2426.7 kg/hr)
@ t = 50 min, \dot{m} = 5350 lb/hr (2426.7 kg/hr)

<u>Sieve size (μm)</u>	<u>Cumulative weight undersize (%)</u>	
	<u>0 min</u>	<u>50 min</u>
45	52.7	47.3
75	80.9	77.1
106	94.5	93.0
150	98.9	98.6
180	99.8	99.9
250	100	100

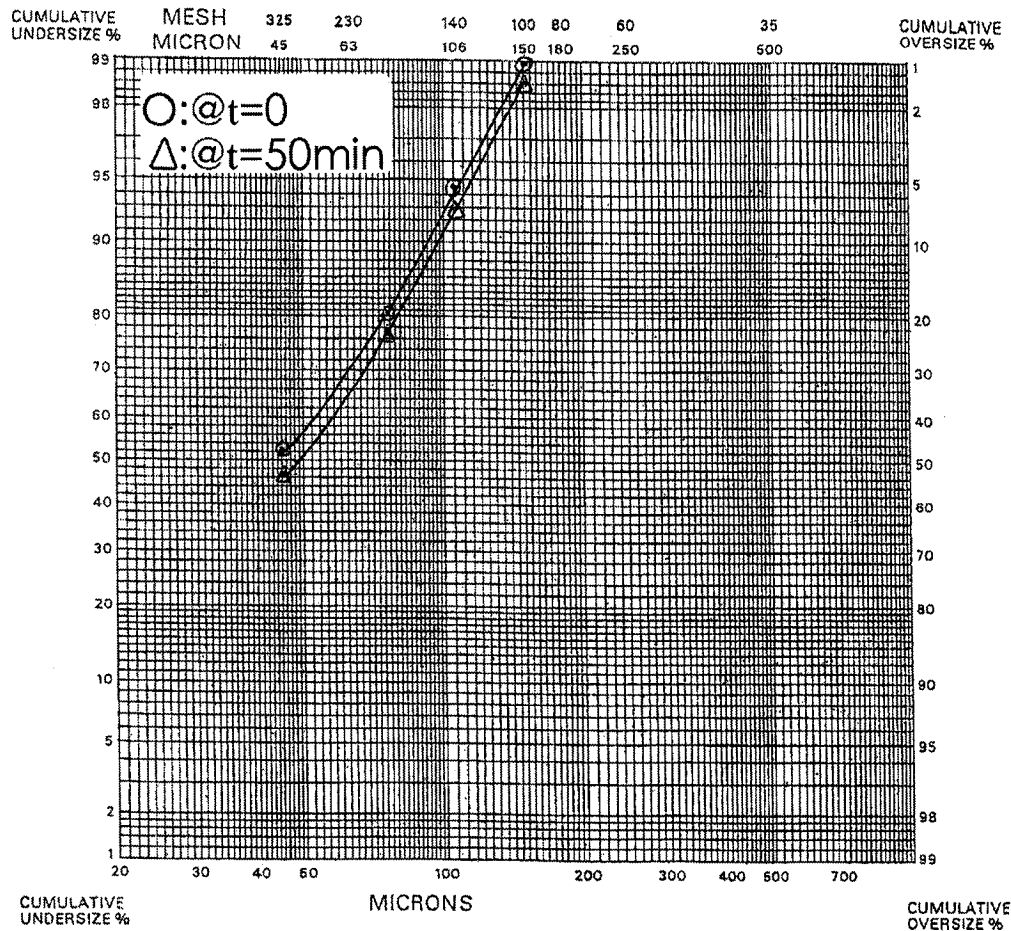


Figure 3.18: Feed rate test m1 cumulative distribution results on log-normal paper

Looking at figure 3.18 and similar results in Appendix 3, feed rate, air flow rate and powder charge are not affecting the shape of the distribution for the same product. The log-normal distribution is therefore very useful when dealing with metal powders. As previously explained in section 2.3, an extended region of the results can be fitted by a series of straight lines. As the product gets coarser, the line shifts downward. On the other hand, finer results show an upward shift of the distribution.

Hence, two point measurements are sufficient to characterize ball mill product size distributions. With the two points, the slope and position of the line can be determined. This confirms Domfer's approach of measuring the +100mesh (+150 μm) and -200mesh (-75 μm) for process control.

3.0 BALL MILLING PROCESS CHARACTERIZATION

3.3.3 Suction air flow monitoring

The strength of the suction flow inside the mill cylindrical shell dictates the size of the product. This was previously demonstrated with Q1 and Q2 trials, where strong and weak air flow rates generate coarser and finer product respectively. However, air flow rate control actions are taken based on flow transmitter signals from the blower output conduit. Auxiliary equipment between the transmitter and the mill may offset air flow rate inside the mill.

Trials dp1 and dp2 were executed to develop a relation between the outlet trunnion vacuum pressure and blower air flow rate, which was varied from 2000 to 6500 ACFM (0.944 to 3.068 m³/sec) using 500 ACFM (0.236 m³/sec) steps. The resulting outlet pressure was measured:

Test #: dp1
Product: S-4
Date: 10-02-2004
Time: 14:00
Initial conditions:
 $\dot{m} = 4100 \text{ lb/hr (1859.7 kg/hr)}$
 $Q = 5500 \text{ ACFM (2.596 m}^3\text{/sec)}$
 $P = 188.5 \text{ kW}$

Test #: dp2
Product: S-1
Date: 9-03-2004
Time: 11:00
Initial conditions:
 $\dot{m} = 4900 \text{ lb/hr (2222.6 kg/hr)}$
 $Q = 6100 \text{ ACFM (2.879 m}^3\text{/sec)}$
 $P = 200.9 \text{ kW}$

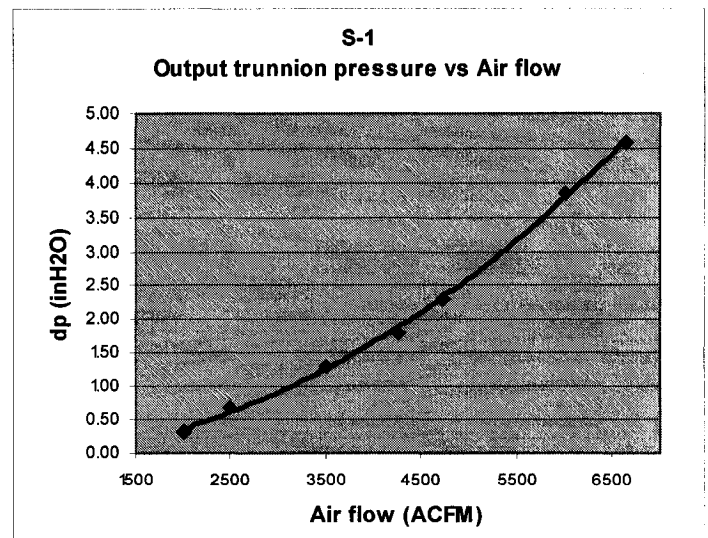
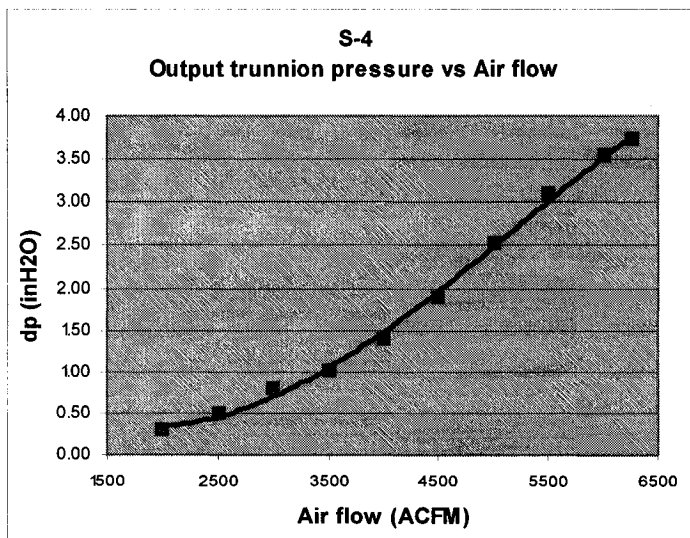


Figure 3.19: Outlet trunnion pressure trials # dp1 and dp2 results

During normal production and within operating limits, from 3500 to 6500 ACFM (1.652 to 3.068 m³/sec), outlet trunnion pressure is proportional to air flow rate.

If the pressure signal is too low, possible causes are:

1. R-413 discharge valve leak
2. Air lock valve leak
3. Suction circuit leak
4. Dirty dust collector cartridges

The lower air flow rate inside the mill produces out of specifications (too fine) ground material.

For higher pressure signals, dust collector cartridges are inspected since a broken cartridge reduces air circuit resistance drastically. This results in product quality problems (too coarse) accompanied by environmental issues.

3.4 Conclusion

From the size reduction theory presented in chapter 2, the ball milling process was characterized. The measurement and control of the parameters were described as a foundation for multivariable controller design. The plant trials determined the effect of parameter variations on product size distribution and density and validated the size distribution function. This provides fundamentals for process model development to follow in chapter 5. However before proceeding, it is important to address again size distribution measurability particularly with respect to sampling period and its effect on product quality.

4.0 PRODUCT SIZE FEEDBACK

The research focuses on optimizing the ball milling process of metal powders. The objectives are aimed at reducing process variations. Ball mill product quality is defined by precise and stable size distribution and apparent density. The performance of a model-based controller is greatly influenced by the frequency at which product properties are inputted to the control model. However, resource limitations restrict the frequency at which samples are taken and tested to only every 3-4 hours. Consequently, inertial problems are created since the effect of parameters adjustments are seen only after few hours. The plant trials described in section 3.3 show that apparent density is directly proportional to size distribution. Hence, size results are sufficient to characterize and control ball mill product properties. An automatic sampler is therefore created to work in conjunction with a fully automated sieve analyzer, providing frequent feedback of product size distribution.

4.1 Automatic sampler design

As described in section 3.2.12, the location where the most representative sample is collected is inside the inclined pipe connecting the impact tank and the ground shot tanks bucket elevator. An automated sampler improves and standardizes the manual scooping inside the inclined pipe performed by the operator, providing a more stable, precise, repetitive and, most importantly, representative sample at the required frequency. Complete investigation over major sampler manufacturing companies (Gustafson, Glen Mills, Metso Minerals Industries, InterSystems, Quality Control Equipment Co., G R Sprenger Engineering, etc) was done to find an appropriate automatic sampler. However, the existing samplers had design flaws or did not suit the application. The decision was therefore taken to create a new product sampler for metal powder ball milling.

Because of the highly competitive nature of most companies, reducing the total cost is one of the major concerns. A good starting point in cost reduction is in the design itself. The best design alternatives are often determined by an analysis of design costs. A study

4.0 PRODUCT SIZE FEEDBACK

of tolerances, surface finishes, processes, materials and equipment is necessary in designing for function, interchangeability, quality and economy.

A good and economical design is performed following general design rules, which are of great importance:

1. Design for simplicity in functional and physical characteristics.
2. Design for the most economical production methods.
3. Select materials with low-cost production and design requirements.
4. Design for the minimum number of separate operations in machining, casting, molding, forming, finishing, fabrication and assembly.
5. Eliminate handling and fixturing problems by designing for ease of location, set up and hold parts.
6. Specify surface roughness and accuracy no greater than needed.
7. Minimize maintenance and replacement parts.

The components of the design should be as symmetrical as possible, have the least possible number of important directions, be consistent in the dimensions used to orientate and locate them, and be designed for easy manual assembly.

The sampler should have a datum surface on which to base the assembly with location points. It should be designed so that one component can be placed on top of another. It should not need to be turned over during assembly and all assembled parts should be visible or accessible to checking devices. It should be made of standard parts and consist of a minimum number of separate components and fastenings.

Sampler design is presented in figure 4.1. Complete detailed drawings and component specifications are shown in Appendix 4. The sampler is located under the impact tank as illustrated in figure 4.2. It consists of the following parts:

- | | |
|------------------|--------------------------|
| 1. Main body | 5. Clevis base |
| 2. Holding parts | 6. Retaining ring |
| 3. Sampling part | 7. Non-rotating cylinder |
| 4. Sleeve | |

The main body is installed directly on the inclined pipe using standard flanges. A precisely machined bronze sleeve is fitted perpendicular to product flow inside the main body. The sleeve is positioned and maintained in place using two dowel pins and a retaining ring. With the holding parts, a non-rotating pneumatic cylinder is fixed to the main body. Using the clevis base, the sampling part that slides inside the sleeve is linked to the cylinder. A 5-way 3-position electrically operated directional valve is coupled with the cylinder to control the sampling part position. A cylinder stroke adjuster provides precise positioning of the sampling part. Extracted and retracted positions are confirmed using limit switches mounted on the cylinder. The retract and extract speeds are adjusted using flow control valves connected to the outlets of the directional valve. The sampler is controlled using digital input and output cards on the PLC for the limit switch signals and directional valve solenoids.

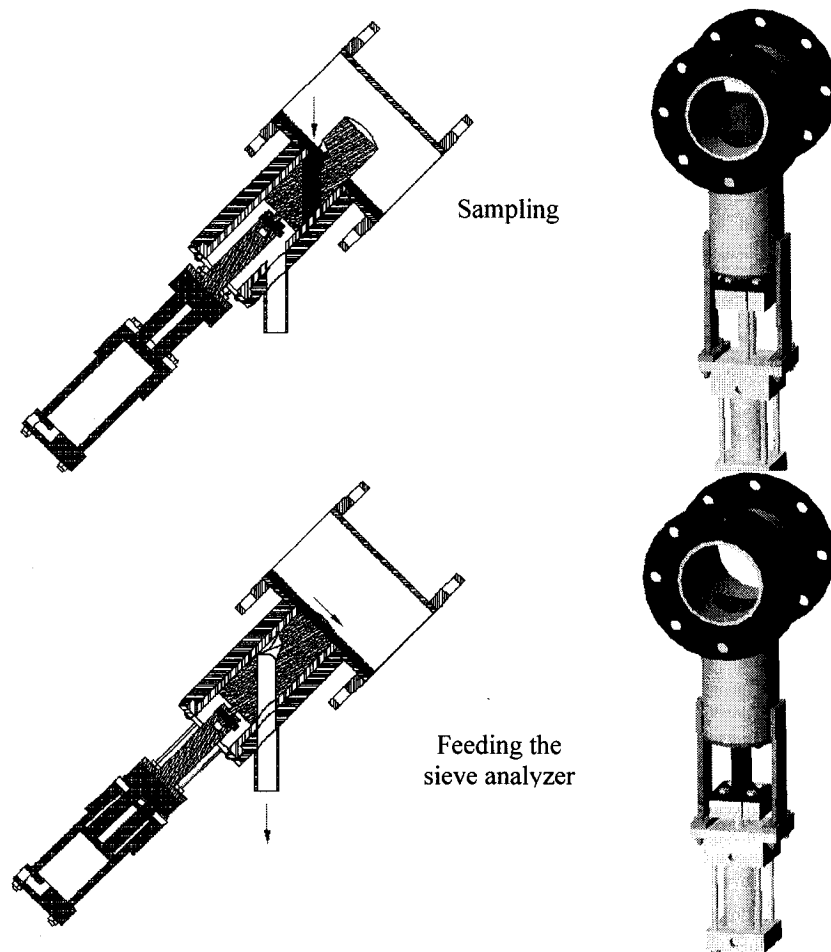


Figure 4.1: Automatic sampler design

4.0 PRODUCT SIZE FEEDBACK

The hardened steel sampling part was precisely machined to have an inside volume of 45cm^3 . This volume is a little above the prescribed test specimen volume from MPIF standard 04 to accommodate for partial filling of the sampling part. The sampler is shown in operation at the top of figure 4.1. The cylinder extracts the sampling part in position to intercept product flow. Once the inside volume is filled (less than 0.2 sec at actual product rates), the sampling part is retracted and the collected sample is emptied by gravity towards the sieve analyzer (bottom of figure 4.1). Product density and sampling volume variations provide samples from 100 to 170g.

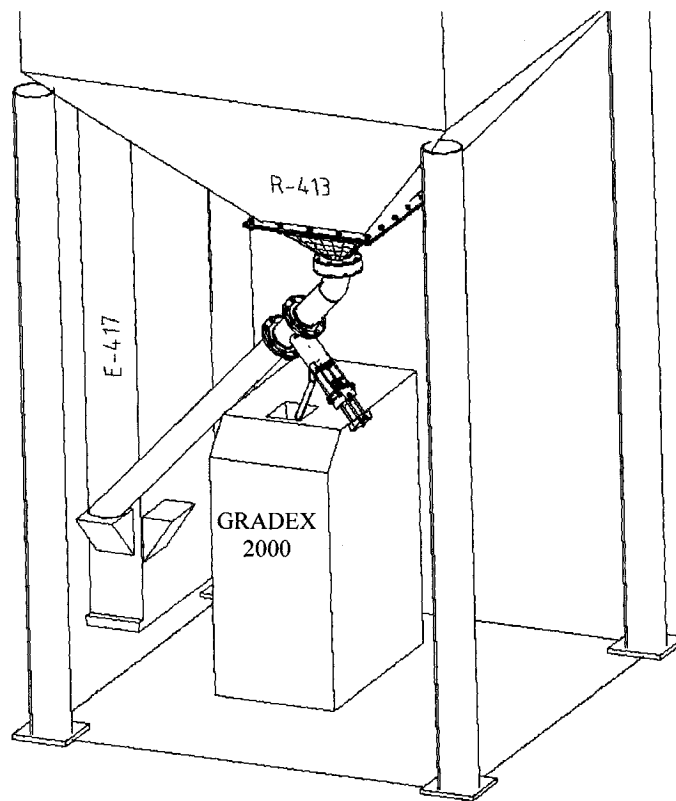


Figure 4.2: Sampler location

The major mechanical design issues for the sampler design project were sleeve and sampling part fits and material combinations. For assembled parts to function properly and to allow for interchangeable manufacturing, it is necessary to permit only a certain amount of tolerance on each of the mating parts and a certain amount of allowance

between them. To permit the sampling part to reciprocate inside the sleeve, a running fit is needed to provide sliding performance with suitable lubrication allowance. More precisely, an RC6 (H9/d9) medium running fit was selected since this fit is intended for higher running speeds and/or where temperature variations are likely to be encountered. Moreover, the main body was designed of substantial size to provide higher heat capacitance, reducing dimensional change caused by ambient temperature variations. The sampling part is composed of hardened steel to provide high wear resistance. On the other hand, the sleeve is fabricated from a softer material, such as bronze, to allow good sliding between the two parts.

During the plant trials described in section 3.3, product flow inside the inclined pipe was observed. It was found that turbulence increases approaching the 45° elbow below the impact tank. A minimum distance along the pipe axis, approximately 18 inches (45.7cm) from the elbow, is needed to let the product settle to the bottom of the pipe and become continuous and stable. This minimizes segregation and the sample contains all size ranges for further analysis.

4.2 Particle sizing

Particle sizing methods have evolved rapidly over the past 15 years. This evolution has led to new technologies and major improvements in the existing methods. The ASTM E-1919-03 document covers particle characterization methods in detail [52]. Newer particle sizing methods and improved older methods are:

- Sedimentation, Classification, Gravity, Centrifugal
- Surface Area and Porosity Measurements
- Sieving Analysis
- Electrical Sensing
- Laser diffraction
- Photon Correlation
- Image Analysis
- Single Particle Light Interaction
- Small Angle X-Ray Scattering

It is difficult to resolve a wide range of particles sizes simultaneously during an analysis. Almost all devices have limited size range that can be accurately resolved and analyzed. Each technique has a range of optimum suitability and if the size distribution is broader than that, the methods are not accurate. For sieves, it is generally above 400mesh (38 μ m). Optical microscopy is restricted to particles above approximately 1 μ m. Techniques such as sedimentation are only applicable to a narrow size range because of limitations imposed by the fundamental physics. In general, finer particle sizes are poorly characterized by sieving techniques. For image analysis techniques, when more than one particle is in the detection zone, they are sized as one large particle. Consequently, the particle size distribution becomes artificially skewed toward the coarse particle sizes. Also, agglomeration causes fine particles to appear as coarser particles. Deagglomeration requires agitation, milling and chemical treatments to maintain particle dispersion. Streaming techniques assume a uniform random dispersion of particles in the feedstock for the detector. The measurements become biased because of preferential settling of the coarse particles.

Although more analyzers using new particle sizing methods are becoming available, the factors needed to select a new analyzer haven't changed [53]:

1. Material characteristics: material particle size range, compatibility of the material with the analyzer surfaces, amount of material available for size analysis.
2. Performance: accuracy, repeatability, ability to detect all particles in a sample, nature and form of the desired sizing results.
3. Time: analysis speed required for the process, sampling time, operator training, calibration time.
4. Cost: analyzer, sampler, analysis, wasted sample material.
5. Maintenance: troubleshooting, supplier's service and repair, replacement parts.

Major metal powders manufacturing companies, such as Höganäs, Hoeganaes, Kobelco, Pyron, Quebec Metal Powders and Domfer Metal Powders, use a particle size range varying from 325 to 40mesh (45 to 425 μ m) to characterize their finished product. The attributes of powder metallurgy products are very dependent on the size distribution of

the metal powders used. Particles over 60mesh (250 μ m) in size are detrimental to the dies (scratching) during compaction and to bonding between the powder particles during the sintering process. However, the effect of the distribution of finer particles (below 400mesh (38 μ m)) on P/M product final properties is not well known. In many instances, ignoring this is not warranted since finer particles possess a greater surface area and kinetic activity. It takes 15625 of the smallest particles to equal the mass of one of the largest particles at a size ratio of 25. In general, the P/M industry uses a sink interval: -325mesh (45 μ m). Moreover, Domfer's knowledge base of the effect of size distribution on final product properties lies within -325 to +60mesh (-45 to +250 μ m).

The plant trials described in section 3.3 show the following minimum product response time to control parameter variations:

- Air flow rate: $T_R = 4$ min
- Feed rate: $T_R = 33$ min

The feed rate minimum response time of 33 minutes is for an aggressive step change of 1000 lb/hr (453.6 kg/hr). Fine tune adjustments in the order of ± 100 lb/hr (45.4 kg/hr) are expected to significantly affect the ground shot only after few hours. Hence, the size analysis speed required for the process is approximately between 5 and 30 minutes. More frequent size results are not representative of the process since the ball mill needs sufficient time to react and stabilize after parameter changes.

A leading screening equipment and technology company called ROTEX manufactures a fully automated sieve analyzer called the GRADEX 2000TM, which minimizes correlation between automated and manual size analysis results and provides product feedback at the desired accuracy, repeatability and frequency. The analyzer is a patented PC-controlled device which fully automates the sieve analysis process and follows MPIF standard 5. The analyzer is designed to utilize a stack of standard 8in (20.32 cm) round test sieves. These test sieves can be easily changed to suit specific test requirements. Sieving action is provided by the same rotary shaking/tapping motion used on typical manual sieve shakers. On-line testing is conducted in conjunction with the new automatic sampler that provides the test specimens. The analyzer automatically classifies and weighs each sieve

4.0 PRODUCT SIZE FEEDBACK

fraction, calculates and stores weight values and reports the data to the controller. The analyzer is shown in figure 4.3 along with specifications in appendix 4.

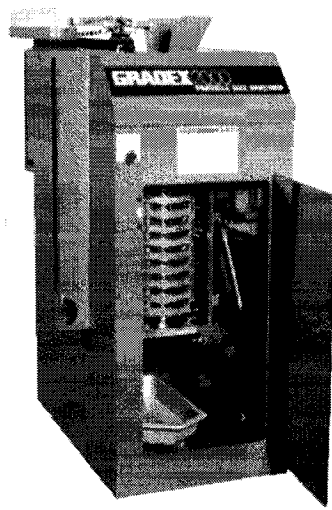


Figure 4.3: Fully automated sieve analyzer

By fully automating the entire sieve analysis process, the product can be analyzed on a more frequent and timely basis (every 15min when following MPIF 05). Further, it frees technicians and/or operators to perform other work, while, at the same time, improving test accuracy and repeatability over manual methods by eliminating operator error and bias.

The analyzer reduces costs and frees manpower through automatic, frequent and timely analysis: frees operators to perform other work, increases testing capacity without additional manpower and enables testing to move to the point of sample. Also, test quality is improved by eliminating operator error: manual steps where errors often occur are eliminated, repeatability is improved by avoiding sieve damage due to overbrushing since the sieves are brushed evenly and consistently, and transposition and calculation errors are eliminated by electronic data transfer. The analyzer can accept feed directly from the processing line, analyze the sample automatically, and transfer the results to the PLC. The analyzer control software is self-contained, and a PC is connected for remote data collection and software maintenance.

4.3 Conclusion

Based on the measurability and controllability of the product properties and the plant trials presented in chapter 3, an automatic metal powder sampler was created to work with a fully automated sieve analyzer to supply frequent feedback of product size distribution. It is expected that the performance of the model-based control system, described in chapter 5, is greatly influenced by the frequency at which product sizes are inputted to the control model.

5.0 PROCESS MODEL DEVELOPMENT

The goal of this research is to develop model-based control for the ball milling process of metal powder. The objectives are aimed at reducing product size variations while maximizing throughput. From the size reduction theory, ball milling characterization and sampler design explained in the previous chapters, process model development is now detailed. First, a process modelling background is presented. Then, the new control strategy is described, followed by the architecture used to integrate the control system. Finally, the created ball mill model is outlined.

5.1 Process modelling background

Advanced process control is used to achieve a variety of objectives. It is very important that appropriate objectives and correspondingly appropriate control strategies be chosen for implementation on ball milling circuits. Nowadays, strategies can be used to stabilize milling circuits to the extent that milling circuits can be made to grind continuously for long periods without danger to humans, too many stoppages and damage to equipment. The control strategies currently being developed emphasize the optimization of the milling operation with stabilization being just one of the consequences. The principal objective of ball milling control might be viewed as the maximization of the financial profits of a company by the manipulation of control actions on the grinding circuit. Unfortunately, the effects of milling on the ultimate profits are not easily quantified. Many factors can come into play, and these would include the prevailing economic conditions, the availability of various resources and the characteristics of upstream and downstream processes. The above principal objective is too unruly to be implemented as an automated on-line strategy, and is more suitably implemented by management as the top level of a hierarchy of objectives.

Most processes downstream of the milling process respond in a very non-linear way to the size of the ground product, giving rise to large variations in the final product properties and leading to financial losses. The best solution to the interrelated requirements of size and throughput is the specification of a long term rate of production

with a specific objective defined as the maximization of throughput while product size is controlled at a set point.

Mathematical models of milling circuits are presently used as the basis of process analysis, control and optimization. The complexity of the process has resulted in the development of several different types of models, each of which has its strong points and limitations. Much research has been conducted into mechanistic modelling of milling circuits. A model incorporating recent technologies can be expressed in terms of a multitude of non-linear algebraic and differential equations that can be solved only by numerical techniques on super-computers. For those models, mathematical relationships for all the relevant physical mechanisms that can reasonably occur need to be developed. The fundamental concepts of selection (*S*) and breakage (*b*) functions have been frequently used [54] and present-day models generally incorporate these functions with enhancements to account for more detailed specifications of functional forms. Some of the functions representing rates and distributions of breakage are still given in functional forms that are not measured or derived, but guessed by intuition.

Many factors influence the selection of control techniques for grinding circuits [55].

1. The nature of the process determines the general type of theory required (linear, non-linear, multivariable, stochastic, etc). However, when a process is simulated by a complex model and some aspects of the process are not fully understood, the interpretation of the requirements is subjective and biased by assumptions made about the process and the object of control.
2. Only some of the important process variables in milling circuits can be measured by accurate and reliable on-line instruments. Furthermore, in practice there are fewer manipulatable variables than needed. As a result, compromises are required and subjective decisions on observability and controllability have to be made.
3. The control techniques must be aimed at the achievement of practical objectives. Various criteria, such as minimum variance, fastest response and regulation of key variables can be chosen for incorporation into the hierarchy of objectives for optimization.

4. Management must be convinced that the techniques used are practical and beneficial. The cost of the investment should be less than the expected return on investment.
5. The operators must have sufficient understanding and confidence in the control system, and must find it convenient to use.
6. The availability of software (computer-aided-design packages) and hardware (instrumentation and computer systems) can influence the choice of control techniques.
7. The appropriate control technique requires that sufficient attention be given to the metallurgical process and control technologies.

Techniques applied to the control of milling circuits range from single-loop proportional-integral (PI) control to several types of modern advanced systems such as multivariable controllers and expert systems.

Single-variable control is a technique in which one control action is used to control one plant variable. The control action may depend on many plant outputs, but because there is only one control action, there can only be one primary set point. As described previously in section 3.2.2 and 3.2.9, two PI control loops are used to control the feed rate and air flow rate of the ball milling operation.

However, ball milling is a multivariable process since it has a number of inputs and outputs. Multivariable control requires the manipulation of the inputs of the multivariable process so that the outputs of the process are controlled to desired values. The ball milling process is interactive since a control action significantly affects more than one of the process controlled outputs. A multivariable controller compensates for interactions in the multivariable process that it controls. This is performed by calculating suitable control action combinations that induce the required responses in the process outputs. A deviation in one of the process outputs can sometimes be corrected by a combination of input changes that has no significant net effect on the other outputs. This decoupling is desirable in many instances. Many limitations in classical control strategies are caused by

a lack of information about the magnitude of controlled variable responses to manipulated variable changes and the nature of the interactions between variables.

Frequency-based methods, which are linear control techniques, make use of the computational power and insight obtained using Laplace transforms and transfer functions. This includes the classic techniques such as Bode plots, root-locus and Nyquist methods. The extension of the Nyquist techniques has produced multivariable frequency-domain methods, such as the inverse Nyquist array (INA), the direct Nyquist array and the characteristic locus techniques. INA techniques can be used in the design of a pre-compensator that decouples the output variables of the multivariable process it controls. This decoupling provides independent single-variable control loops associated with each process output. INA techniques can be applied when representative transfer functions are developed with linearization over the region of operation.

Changes in the dynamic characteristics of a process are taken into account using an adaptive control strategy. The changes may be due to variations in input product properties or to characteristics of the process that are time variant. One of the advantages of adaptive control is that it can be installed for process control without the requirement for periodic retuning to compensate for changes in operating levels during subsequent years of operation.

Furthermore, a great deal of work is being done towards the development of computer software that is able to mimic human intelligence. Expert systems are capable of learning, storing and using very human-like terms. These types of control systems can monitor measurements, accept and remember advice from human operators and experts and make adjustments to control actions in much the same way as an experienced human operator. Expert systems should not be viewed as replacements for control strategies based on mathematical models. In fact, the two technologies are very useful for different problems in process control and they can complement each other very well if combined suitably.

5.2 Control strategy

As has been mentioned, model-based control has never been used in open-circuit dry ball milling of metal powders. Moreover, there is no general framework for the synthesis of practically implementable non-linear feedback controllers for particulate processes that allow attaining desired particle size distributions. The models and control systems already developed [2-12] are for closed-circuit wet ball milling. Also, references [6-9] describe mining industry grinding circuits consisting of primary open-circuit SAG mills followed by closed-circuit ball mills. Reference [13] outlines modeling and control of closed-circuit cement mills.

The goal of this research is to develop model-based control for the optimization of the ball milling process of metal powder. The research objectives are aimed at reducing product size variations while maximizing throughput. However, powder quality, energy cost, personnel cost, and operating cost are also improved. A new control strategy is developed to achieve Domfer ball milling specifications, presented in table 2, at 99.7% confidence interval ($\pm 3\sigma$). This provides improved downstream equipment controllability and reduces by 50% the number of rejected final product lots.

Mathematical models of ball milling circuits are presently used as the basis of process analysis, control and optimization. As described in section 2.2, the batch size-mass rate balance equation may be applied to the particle breakage process occurring in a ball mill:

$$\frac{d[w_i(t)M_p]}{dt} = -S_i w_i(t)M_p + \sum_{j=1, j \neq i}^{i-1} b_{ij} S_j w_j(t)M_p, \quad n \geq i \geq j \geq 1 \quad (5.1)$$

This equation gets complicated very quickly when the following aspects are considered: breakage functions, selection functions, residence time distributions for all sizes of particles, effect of missing screen sizes and effect of operating variables.

Grinding is governed by two independent functions: breakage (***b***) and selection (***S***). The breakage distribution function describes the production of daughter particles by a single breakage event. The breakage element b_{ij} is the weight fraction of particles in size interval i formed by the breakage of larger particle in size interval j . The size fraction with $i=1$ is the top size fraction and with $i=n$ is the pan fraction. The selection function (***S***) measures the rate at which breakage events occur for each particle size. If there are n screen sizes, there are $(n-j)$ breakage elements b_{ij} for each parent size j , and there are n parent sizes. It is impractical to estimate all of these elements independently. Consequently, it is assumed that the elements fit a smooth function which can be parameterized by a number of constants.

Three different breakage distribution functions matching product size distribution results are presented below [28]:

$$b_{ij} = B_{i-1,j} - B_{i,j} \quad (5.2)$$

where,

$$B_{i,j} = b_1 \left(\frac{x_i}{x_j} \right)^{b_2} + (1 - b_1) \left(\frac{x_i}{x_j} \right)^{b_3} \quad (5.3)$$

or,

$$B_{i,j} = b_1 \left(\frac{x_0}{x_j} \right)^{b_4} \left(\frac{x_i}{x_j} \right)^{b_2} + \left(1 - b_1 \left(\frac{x_0}{x_j} \right)^{b_4} \right) \left(\frac{x_i}{x_j} \right)^{b_3} \quad (5.4)$$

or,

$$B_{i,j} = b_1 \left(\frac{x_0}{x_j} \right)^{b_4} \left(\frac{x_i}{x_j} \right)^{e_1} + \left(1 - b_1 \left(\frac{x_0}{x_j} \right)^{b_4} \right) \left(\frac{x_i}{x_j} \right)^{e_2} \quad (5.5)$$

$$e_1 = b_2 + b_5 \left(\frac{\ln x_j}{\ln R} \right), \quad e_2 = b_3 + b_6 \left(\frac{\ln x_j}{\ln R} \right)$$

x_i is the geometric mean size of size fraction i , x_j the geometric mean size of size fraction j , x_0 the reference size and R the screen size ratio ($\sqrt{2}/2$).

The increased flexibility of the functions with more parameters provides better predicted size distributions and lower error and minimizes the risk of biasing the production mill model [28].

Grinding mill behavior can be described by the determination of selection functions over a range of operating conditions. Unfortunately, the breakage functions themselves can cause significant changes in mill selection functions. This indicates that the proper selection of a breakage function requires advance experimentation to correlate with actual plant results.

Consider a ball mill where 30% of the feed particles leave in less than two minutes, 50% leave between two and five minutes, and 20% leave between five and ten minutes after entering the mill. This simple residence time distribution is shown in figure 5.1. It is a statistical description of how long particles stay inside the mill.

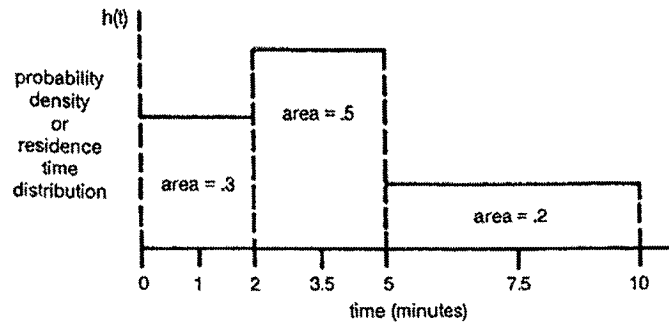


Figure 5.1: Simple residence time distribution [28]

The batch size-mass balance equation applies only to batch mills and idealized continuous mills exhibiting plug flow behavior. With residence time probability distribution, equation 5.1 can extend to continuous mills. A reasonable model might predict the product size distribution of a continuous mill, $w_i M_p^C$, as the weighted average of size distributions produced by batch grinding $w_i M_p$ for 1 minute, 3.5 minutes and 7.5 minutes [28].

$$\begin{aligned} w_i M_p^C &= 0.3w_i M_p(1 \text{ min}) + 0.5w_i M_p(3.5 \text{ min}) + 0.2w_i M_p(7.5 \text{ min}) \\ &= \sum [h(t)\Delta t] w_i(t)M_p \end{aligned} \quad (5.6)$$

The exact model uses vanishingly-narrow time intervals (dt), so that the summation becomes an integral [56]:

$$w_i M_p^C = \int_{t=0}^{\infty} h(t) w_i(t) M_p dt \quad (5.7)$$

where, $h(t)$ is the residence time distribution function and $w_i(t)M_p$ the solution of the size-mass rate balance equation.

This equation implicitly ignores the possibility of different residence time distributions for particles of different sizes. Moreover, this equation assumes that the breakage and selection functions do not change as particles move through the mill as grinding progresses.

Production mill selection functions cannot be directly calculated. They can only be estimated and used to predict product size distributions that fit the measured size distribution as closely as possible. The continuous size-mass balance equation 5.7 is used to calculate product size distributions. In addition to an estimated selection function, the equation also requires a breakage function and residence time distribution. If either is incorrect, an incorrect best selection function is chosen. The simplest selection function fits a power function similar to a Schuhmann distribution:

$$\ln(S_i) = \ln(s_1) + s_2 \ln\left(\frac{x_i}{x_0}\right) \quad (5.8)$$

However, this equation does not have sufficient flexibility to fit most measured size distribution. Therefore, more complex extensions are used to match experimental data, such as quadratic, cubic and modified Schuhmann selection functions [25]:

$$\ln(S_i) = \ln(s_1) + s_2 \ln(x_i/x_0) + s_3 [\ln(x_i/x_0)]^2 \quad (5.9)$$

and,

$$\ln(S_i) = \ln(s_1) + s_2 \ln(x_i/x_0) + s_3 [\ln(x_i/x_0)]^2 + s_4 [\ln(x_i/x_0)]^3 \quad (5.10)$$

and,

$$S_i = \frac{s_1 (x_i/x_0)^2}{1 + [(x_i/x_0)/s_3]^{s_4}} \quad (5.11)$$

The constants are determined to minimize differences with measured product size distributions. The selection functions can simulate the predicted product size distribution for specific size distribution ranges. For example, the power distribution is effective for medium-sized particles. The modified Schuhmann distribution is better than the simple Schuhmann to predict coarse size fractions.

In discrete size analysis, the properties of all particles in a size fraction are lumped together and averaged. Serious calculation errors are introduced if the size interval is too large to discriminate important changes in the properties of the particles. For any finite difference formulation, the size interval must be small enough to define the curvature of the continuous functions. It is recommended that a complete $\sqrt{2}$ sieve series be used.

A quantitative knowledge of $S_i w_i M_p$ and b_{ij} is crucial to predicting ball mill behavior. The effect of the operating variables on the selection and breakage functions biases product size distribution simulation. The parameters of the selection and breakage functions should be correlated to variable changes: feed size distribution and chemistry, feed rate, powder charge, ball charge, charge motion and air flow rate. However, there are no existing reliable correlations between any of the variables.

When considering feed and product rate in continuous ball milling, the batch size-mass rate balance equation can extend to equation 5.12 with the following statement involved:

The net rate production of size i material **equals** the sum rate of appearance from all larger sizes **plus** the rate of fresh fed material of size i **minus** the rate of disappearance of size i **minus** the rate of mill product of size i .

The final balance is: (5.12)

$$\frac{d[w_i(t) M_p(t)]}{dt} = \sum_{j=1, i>1}^{i-1} b_{ij} S_j w_j(t) M_p(t) + \dot{m} w_i^*(t) - S_i w_i(t) M_p(t) - (\dot{m}_o + \dot{m}_{D415}) w_i^{**}(t)$$

$$n \geq i \geq j \geq 1$$

where b_{ij} is the weight fraction of products from j to i , S_i the specific rate of breakage of size i , S_j the specific rate of breakage of size j , w_i the fraction of material of size i , w_j the fraction of material of size j , w_i^* the fraction of fresh fed material of size i , w_i^{**} the fraction of mill product of size i , M_p the powder charge, \dot{m} the feed rate, \dot{m}_o the product rate and \dot{m}_{D415} the dust rate.

As described in section 3.3, the plant trials performed on ball mill 408 demonstrated the effect of feed rate and air flow rate on product size distribution and powder charges. By examining figures 3.13 to 3.17, we can clearly see the non-linear relation between feed rate, air flow rate and product size distribution. Moreover, powder charge exhibits non-linear behavior with respect to step feed rate changes.

As shown in table 3.5, Domfer uses 7 size intervals from +60 to -325mesh (+250 to -45 μ m) as a knowledge base and for quality control. The particle size reduction process inside the mill would need to be described using 7 non-linear differential equations with the general form of equation 5.12. If residence time distribution was considered, the 7 size intervals solutions $w_i M_p$ would then be used in equation 5.7 and integrated with the selected residence time function. The non-linear differential equations would not be representative of Domfer ball milling process for the following reasons:

1. The input material size distribution is not known in real time.
2. It is impractical to estimate all the elements of equations 5.7 and 5.12.
3. Breakage and selection functions are estimated to fit size distribution results.
4. Breakage functions can cause significant changes in mill selection functions.
5. Production mill selection functions cannot be directly calculated.
6. The parameters are determined to minimize differences between simulated and measured product sizes.
7. Residence time distributions are much more complex when considering different particle sizes and longitudinal position inside the mill.
8. The presently used mathematical models were not developed for open circuit dry ball milling of metal powders.

9. There are no reliable correlations of the effect of the operating variables on the breakage and selection functions. The simulation would therefore be biased.

Although grinding circuits exhibit nonlinear dynamic behavior, controller design has largely been investigated from a linear controller perspective, such as PID control. Modern and classical linear controller design techniques require the use of linear process models. As rigorous ball milling mathematical models are necessarily non-linear, these nonlinear models need to be linearised and control limited to this linearised region of the state space. The robustness of the linear controller cannot be guaranteed since the operation strays from the linearised region. INA techniques cannot be applied since the transfer functions are not representative of the process. Moreover, the differential equations are time variant with respect to operating parameter variations and ball mill conditions.

A new ball milling process model is therefore proposed. It integrates process sub-models composed of rules, equations and heuristics. Following interviews with Domfer's most experienced ball mill operators, optimized rule-based sub-models for feed rate and air flow rate were created. Heuristic and logical rules are used in sequential decisions that lead to the invention of feasible and plausible control structure [57]. The creation of fuzzy sets can involve direct participation of plant personnel who otherwise might be precluded from the process because of their limited knowledge of mathematics. These sets are then used in rules to interpret plant operating conditions and to generate new set points for the process or advice for the operating crew [58]. Plant trials were performed to develop reliable correlations between key operating variables, validate product size distribution function and define overall system behavior. The created equations are simple, based on plant data and, most importantly, representative of the process. The model is implemented using an agent based architecture.

5.3 Agent based architecture

Model based control allows the estimation of process dynamics based on an overall process model which integrates sub-models of many process phenomena with different

time scales. For real time control, information is needed simultaneously with respect to many variables of the ball milling process as well as from the final product. The variables of interest are non-linear time variant and some of them cannot be directly measured.

Agent based architectures have features that are favorable for creating a model-based control system for metal powder ball milling. A multi-agent system can deal with multiple data streams and many process sub-models of different sizes and operating time scales.

The main steps for the development of model based control are:

- Create the process model
- Design an architecture capable of executing the model
- Implement the controller so that control parameters are calculated from the outputs of the process model

An agent based architecture developed by Thomson *and al.*[15] is utilized to implement the ball mill model for process control. The architecture is presented in figure 5.2.

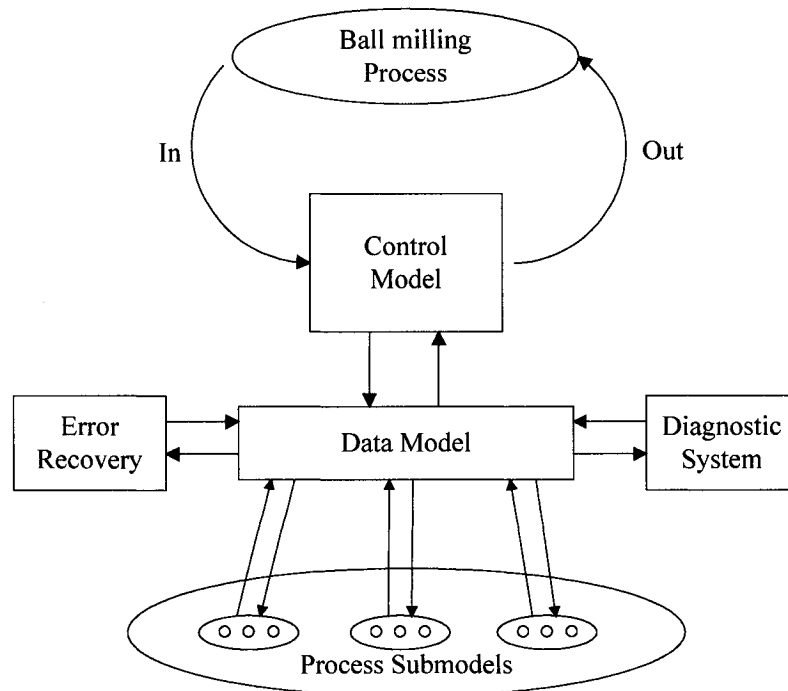


Figure 5.2: Agent based architecture [15]

The control model performs 3 tasks:

1. Acquisition of sensor data
2. Calculation of control parameters from process model variables by operating on the data model
3. Transmission of parameter values to control the real process

The data model stores sensor data, process model variables and control parameters, and allows the integration of data from all process models.

The control system depends on an integrated process model composed of many sub-models for the calculation of specific state variables. The control model continuously operates the cycle from acquiring sensor data to sending control parameters to the physical process at the fastest cycle time.

The overall ball milling process model continuously calculates state variables from the given sensor data. The model is a loosely coupled network of related process sub-models. Each process sub-models performs at its own cycle time by reading input data from and placing output variables into the data model for the control model. Individual agents are used to manage, calculate or control each data stream. Task execution by agents is predefined by powder grades for action.

Sensor data and state variables from the data model are continuously evaluated by the diagnostic system to determine whether sensor data have errors, processes are in control, state variables are moving out of acceptable ranges, or control parameters are approaching limits. The control model interprets the diagnostics for action. Disturbances induced in the process are back propagated to the input, so that faults that may appear are more easily interpretable as variations in the input data [59].

When an error occurs, only the affected sub-models are halted. Determination is made if the production process can continue with reduced data. If yes, the exception is handled by

separate agents that execute predefined processes. For extreme difficulties, an operator is informed and intervention is requested.

Interrupts are generated by the diagnostic system indicating drifts from set points or a machine or process malfunction. These interrupts create error recovery agents to rehabilitate the process, then restart suspended agents, and finally, return full execution to the control agent.

A multi-agent system can cope with the complexity of multiple process models, various control tasks and ancillary processes: diagnostics and error recovery. The organization of execution can directly mimic the heterarchical nature of the phenomena to be controlled [15].

5.4 Ball mill model

Using the agent based architecture previously described, the ball mill model deals with all the variables of the process and applies the various rules and relations as appropriate. The rules are developed based on the knowledge of most experienced ball mill operators and plant trial results. Moreover, the model architecture allows adaptive control using agents for product recipes and process variations. The consideration of a multivariable process helped to identify the key model parameters and gave insight into the problem. This led to the understanding that the key parameters could be decoupled due to the large time frame differences, i.e., for the main variables (feed rate, air flow rate, ball feed rate, ball and powder charges, and liner wear), the problem decomposed into several single parameter sub-models.

The detailed ball mill model is now presented. It is composed of model statements and features of the agent based architecture: control model, data model, process sub-models, diagnostic system and error recovery.

5.4.1 Model statements

1. Grinding is a first-order rate process:
$$\frac{d[w_i(t)M_p(t)]}{dt} \propto w_i(t)M_p(t)$$

2. Ball milling is governed by 2 functions: breakage b and selection S . These functions are mill dependent and related to each other.
3. The powder charge term of the continuous size-mass rate balance equation (5.12) is non-linear time variant with respect to feed rate and air flow rate variations.
4. The product size distribution function is governed by ball size distribution. A steady ball size distribution provides constant product size distribution function.
5. Stable ball size distribution and ball bed height enable single point measurement to characterize and control the product size distribution coming from the ball mill.
6. Liner wear is constant for overall liner life.
7. Inferential measurement of powder charge is performed using powerdraw sensor data.
8. Increasing total charge for constant powerdraw with respect to liner wear favors stable strain energy applied to the particles. With higher volume and consequently greater ball charge, the powder charge must be increased for constant ball/powder ratio.
9. Stable input material properties, ball/powder ratio, ball size distribution, mean residence time and product size distribution provide consistent product apparent density and shape.
10. Process disturbances are interpreted as variations in the input data.
11. Control strategy:
 - Maximize breakage rates with feed rate variations.
 - Control product size distribution with air flow rate adjustments.

5.4.2 Control model

The control model performs the acquisition of sensor data, the calculation of control parameters from process model variables by operation on the data model and the transmission of parameter values to control the real process at the fastest cycle time: 30ms/cycle for ball mill 408 programmable logic controller.

The sensor variables acquired by the control model are:

- Product % retained by a 100 mesh sieve, $S100$
Product % passing a 200 mesh sieve, $S200$
- Mill powerdraw, P
- Outlet trunnion pressure, dP_o
- Rotational speed, ω
- Babbits temperatures, $T_{bab,in}$ and $T_{bab,out}$
Fluid drive temperature, T_{fd}
Speed reducer temperature, T_{sr}
Dust 415 temperature, T_{D415}

After tests and measurements, the following parameters are entered by the operators and/or foreman on the human machine interface (HMI):

- Product apparent density, ρ_o
- Ball bed height, H
Campaign run time, T_{camp}

As well, the process engineer enters the subsequent variables in the system:

- Ball bulk density, ρ_b
M-408 ball usage, $M_{ub(408)}$
M-408 run time, T_{408}
- Total wear volume, ΔV_L
Wear volume with respect to balls, $\Delta V_{L(ball)}$
Inlet liner life, T_{Lin}
Outlet liner life, T_{Lout}

The atomizing plant supplies the following data:

- Input material size distribution, $S20$
Input material apparent density, ρ_i
Input material chemistry, %C and %Si

Finally, the product grade (1, 2, 3, 4) is entered on the HMI. A correlation table in the PLC provides the following parameters with respect to powder grades:

- Optimum product % passing a 200 mesh sieve, $S200_{opt}$
- Optimum powerdraw, P_{opt}
- Maximum product % retained by a 100 mesh sieve, $S100_{max}$
- Starting feed rate and air flow rate: \dot{m}_{start} and Q_{start}
- Allowable powerdraw, feed rate and air flow rate ranges: P_r , \dot{m}_r and Q_r

The process sub-models calculate state variables from input data. Each process sub-model performs at its own cycle time by reading input data from and placing output parameters into the data model for the control model. The following output control variables are sent to the physical process:

- Powder feed rate, \dot{m}
- Air flow rate, Q
- Ball feed rate, \dot{m}_b
- Dust 415 pulses duration and intervals: $t_{D415,pulse}$ and $t_{D415,intr}$

The rule-based process sub-models of feed rate and air flow rate give feed rate and air flow rate set points, $\dot{m}_{set\ point}$ and $Q_{set\ point}$, for the robust PI controllers described in section 3.2.2 and 3.2.9. The two controllers operate at the fastest cycle time and are shown in figure 5.3.

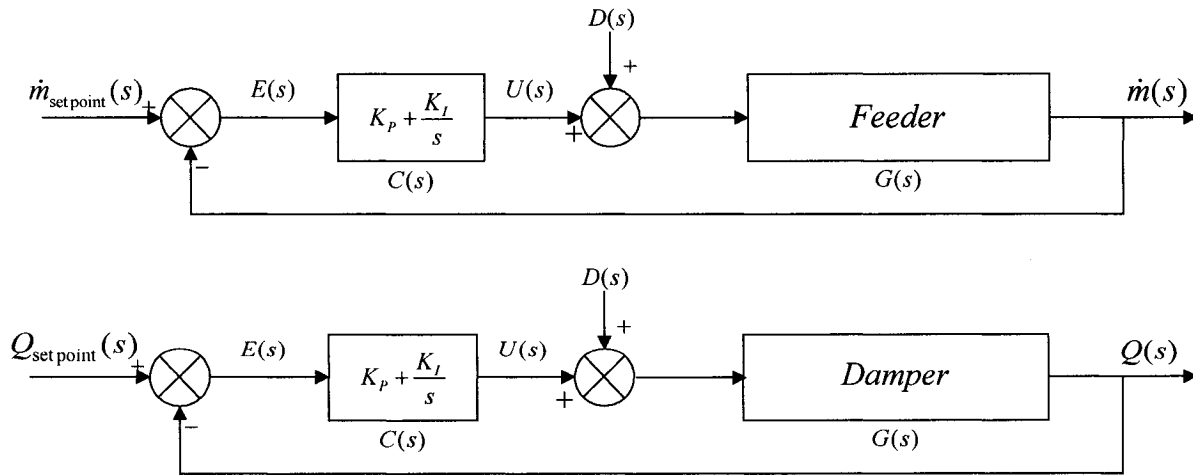


Figure 5.3: PI controllers for feed rate and air flow rate output control parameters

5.0 PROCESS MODEL DEVELOPMENT

Ball feed rate output parameter is calculated using equation 3.14:

$$\dot{m}_b = \dot{m}_{b(408)}^* + \Delta\dot{m}_b$$

The ball feed rate to compensate ball and liner wear $\dot{m}_{b(408)}^*$ and the ball feed rate correction factor $\Delta\dot{m}_b$ are computed by the process sub-models.

5.4.3 Data model

The data model stores sensor data, process sub-model variables and control parameters, and enables the integration of data from all process models.

The state variables are:

- Liner wear, W_L
Liner wear with respect to balls, $W_{L(ball)}$
Ball feed rate to compensate liner wear, $\dot{m}_{b(408)}^{**}$
- Empty mill powerdraw, $P_{no\ load}$
Mill powerdraw attributable to balls, P_b
Mill powerdraw attributable to powder, P_p
- Powder charge, M_p
Ball charge, M_b
- Product rate, \dot{m}_o
- Mean residence time, τ

The control parameters are:

- Desired powder feed rate, $\dot{m}_{set\ point}$
- Desired air flow rate, $Q_{set\ point}$
- Ball feed rate to compensate ball and liner wear, $\dot{m}_{b(408)}^*$
Ball feed rate correction factor, $\Delta\dot{m}_b$

The most influential variables of the ball milling process are presented below and ordered by increasing time required to significantly affect product properties:

Air flow rate, Q	4 minutes
Powder feed rate, \dot{m}	30 minutes
Ball feed rate, \dot{m}_b	24 hours
Liner wear, W_L	1 week
Powder charge, M_p	$f(\dot{m})$
Ball charge, M_b	$f(\dot{m}_b)$
Powerdraw, P	$f(\dot{m}, \dot{m}_b)$
Mean residence time, τ	$f(M_p, \dot{m})$
Product rate, \dot{m}_o	$f(\dot{m})$

The mathematical equations that determine the liner wear, ball feed rate, powder charge and residence time contribute to the control model, but it is the AI models for feed and air flow rate that are the heart of the control system. This is because the output of the powder grinding process is dominated by the near time frame factors. The parameters able to significantly affect product properties for a single powder grade campaign are air flow rate, powder feed rate and ball feed rate. Therefore, control actions are taken on these parameters at their corresponding process response times.

5.4.4 Process sub-models

The ball mill model is composed of a loosely coupled network of related process sub-models operating at different cycle times. Each sub-model reads input data from the data model, calculates state variables and places output variables in the data model for the control model. The sub-models are described below.

5.4.4.1 Liner wear

Inside grinding volume augmentation as a function of liner wear must be calculated in order to include liner wear in ball height control. The created 3-D model of the mill interior shell with new and used liners shown in figure 3.9 is used for liner wear calculation. Constant liner wear for all liner life is assumed since the liner hardness is constant across thickness and the new liners aggressive shape projects the ball charge against the unprotected wall to create wear rate equivalent to used liners with an

increased sliding friction. Moreover, the effect of liner wear on charge motion (grinding dynamics) is negligible for a single grade production run. Liner wear is calculated using equation 3.8:

$$\begin{aligned}
 W_L &= \frac{\Delta V_{Lin}}{T_{Lin}} + \frac{\Delta V_{Lout}}{T_{Lout}} \\
 &= \frac{\Delta V_L / 2}{T_{Lin}} + \frac{\Delta V_L / 2}{T_{Lout}} \quad \text{where: } \Delta V_{Lin} + \Delta V_{Lout} = \Delta V_L \\
 &= \frac{30.5 \text{ ft}^3}{6500 \text{ hr}} + \frac{30.5 \text{ ft}^3}{9000 \text{ hr}} \quad \Delta V_{Lin} = \Delta V_{Lout} @ T_L \\
 &= 13.96 \frac{\text{in}^3}{\text{hr}} \quad (228.76 \frac{\text{cm}^3}{\text{hr}}) \\
 &= 13.96 \frac{\text{in}^3}{\text{hr}} \times 0.28 \frac{\text{lb}}{\text{in}^3} = 3.9 \frac{\text{lb}}{\text{hr}} \quad (1.77 \frac{\text{kg}}{\text{hr}})
 \end{aligned}$$

The parameters are fed to the sub-model after multi-point measurement of worn liners during half-set liner change every 6 months. Similarly, liner wear with respect to ball bed at rest is calculated using equation 3.10:

$$\begin{aligned}
 W_{L(ball)} &= \frac{\Delta V_{Lin(ball)}}{T_{Lin}} + \frac{\Delta V_{Lout(ball)}}{T_{Lout}} \\
 &= \frac{\Delta V_{L(ball)} / 2}{T_{Lin}} + \frac{\Delta V_{L(ball)} / 2}{T_{Lout}} \quad \text{where: } \Delta V_{Lin(ball)} + \Delta V_{Lout(ball)} = \Delta V_{L(ball)} \\
 &= \frac{8.5 \text{ ft}^3}{6500 \text{ hr}} + \frac{8.5 \text{ ft}^3}{9000 \text{ hr}} \quad \Delta V_{Lin(ball)} = \Delta V_{Lout(ball)} @ T_L \\
 &= 3.89 \frac{\text{in}^3}{\text{hr}} \quad (63.75 \frac{\text{cm}^3}{\text{hr}})
 \end{aligned}$$

Using $W_{L(ball)}$, the ball feed rate required to maintain a constant charge inside ball mill 408 despite liner wear is calculated using equation 3.11:

$$\begin{aligned}
 \dot{m}_{b(408)**} &= W_{L(ball)} \times \rho_b \\
 &= 3.89 \frac{\text{in}^3}{\text{hr}} \times 0.172 \frac{\text{lb}}{\text{in}^3} \\
 &= 0.67 \frac{\text{lb}}{\text{hr}} \quad (0.30 \frac{\text{kg}}{\text{hr}})
 \end{aligned}$$

The ball bulk density ρ_b is also supplied to the sub-model after liner change every 6 months.

5.4.4.2 Ball feed rate

The continuous ball feed rate to compensate for ball and liner wear on ball mill 408 is determined using equation 3.6:

$$\begin{aligned}
 \dot{m}_{b(408)*} &= \frac{M_{ub(408)}}{T_{408}} \\
 &= \frac{\left(\frac{\dot{m}_{(408)}}{\varepsilon \dot{m}_{(108)} + \dot{m}_{(208)} + \dot{m}_{(308)} + \dot{m}_{(408)}} \right) B}{T_{408}} \\
 &= \frac{\left(\frac{4100 \text{ lb/hr}}{0.25(2000 \text{ lb/hr}) + 1350 \text{ lb/hr} + 1550 \text{ lb/hr} + 4100 \text{ lb/hr}} \right) (83444 \text{ lbs})}{6000 \text{ hrs}} \\
 &= 7.6 \frac{\text{lb}}{\text{hr}} \quad (3.45 \frac{\text{kg}}{\text{hr}})
 \end{aligned}$$

$M_{ub(408)}$ and T_{408} are ball usage and run time for a year.

After each product campaign, ball bed height is verified to confirm and adapt equation 3.6 to actual grinding conditions. The goal is to regulate ball bed height to favor a constant strain energy applied to the particles with respect to liner wear. Using equations 3.12 and 3.13 along with the ball mill 3-D model of figure 3.9, the ball feed rate correction factor $\Delta \dot{m}_b$ is computed. First, the ball bed height is measured by the operator after each campaign:

$$H - 10\text{in} = \Delta H$$

Then, from the 3-D model, the ball volume offset is determined:

$$\Delta H \rightarrow \Delta V_b$$

With the ball volume offset, ball bulk density and campaign run time, the correction factor is calculated:

$$\Delta \dot{m}_b = \rho_b \frac{\Delta V_b}{T_{camp}}$$

A new correction factor is provided at least every 7 days, which corresponds to the longest single grade production run.

Also, the ball charge state variable M_b is computed using the following equation:

$$M_b = \rho_b V_{b(start)} + \dot{m}_{b(408)}(T_{run\ time}) + \rho_b \Delta V_b \quad (5.13)$$

$V_{b(start)}$ is the starting ball volume with new liners found using ball mill 3-D model and $T_{run\ time}$ is the run time from which the new liners were installed. The ball charge is calculated at the fastest cycle time with corrected ball charge ($\rho_b \Delta V_b$) supplied after a product campaign (3-7 days).

5.4.4.3 Powder charge

Breakage rates of most of the sizes are greatly affected by ball/powder ratio. At low powder filling, much of the energy is spent in ball-to-ball contact, giving rise to low breakage rates and over grinding of the fines. However, at high powder charge, the powder cushions the breakage action, decreasing grinding efficiency. The rates of breakage reach a maximum when all the effective spaces where collisions between tumbling balls are taking place get filled with powder. Ball mill performance is greatly influenced by powder and ball load. However, direct measurement of charge is not practically feasible. Hence, inferential measurement becomes a very attractive option. A soft-sensor system can estimate inaccessible process variables using a mathematical model employing measurable variables. Inference of powder charge is accomplished with direct measurement of powerdraw and using equation 3.23:

$$P = P_{no\ load} + kP_{charge} = P_{no\ load} + k(P_b + P_p)$$

First, after a liner change (every 6 months), the empty mill powerdraw is determined:

$$P_{no\ load} = P \quad @ \quad P_b, P_p = 0 \quad (5.14)$$

Then, after a product campaign with a maximum duration of one week, the mill powerdraw attributable to ball charge is verified to validate ball bed height measurement and determine the lumped mill powerdraw parameter k :

$$P_b = \frac{P - P_{no\ load}}{k} \quad @ \quad P_p = 0 \quad (5.15)$$

Finally, powder charge is estimated using the mill powerdraw attributable to powder:

$$P_p = \frac{P - P_{no\ load} - kP_b}{k} \quad (5.16)$$

The maximum breakage rates are obtained approximately at maximum powerdraw, depending on liner condition and ball load. This maximum powerdraw attributable to powder corresponds to the optimum powder charge, $M_{p_{opt}}$.

At maximum breakage rates, further addition of powder increases the hold-up without increasing productivity because the collision zones are already saturated and more powder just accumulates in the mill. Powerdraw with respect to powder charge variation is plotted in figure 5.4. Overfilling reduces powerdraw since the center of gravity of the charge approaches the longitudinal axis of the mill. The ball-powder bed expands to give poor powder-ball-powder nipping collision and reduce breakage rates. Drastically overfilling the mill may cause severe blockage problems. It is therefore prudent to operate the mill at an optimum powerdraw just below the maximum powerdraw, or as seen in figure 5.4, to the left side of $M_{p_{opt}}$. In this region of operation, increasing feed rate will increase powerdraw and vice versa.

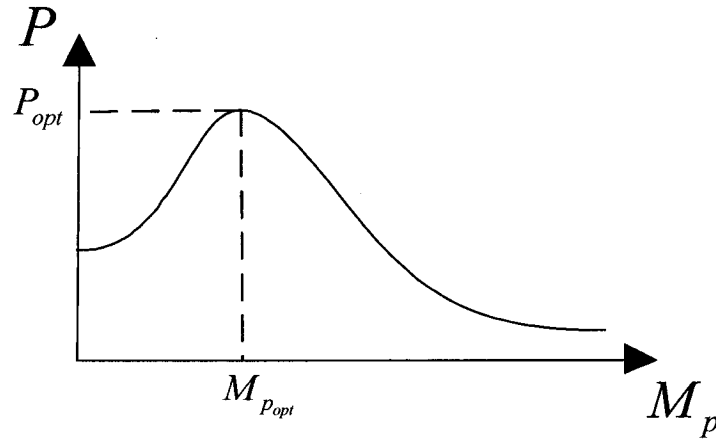


Figure 5.4: Powerdraw versus powder charge

Mill powerdraw readings are provided at the fastest cycle time (30ms/cycle). An averaging function was needed to filter powerdraw variations occasioned by charge motion. 60 PLC cycles power reading average was sufficient to provide a stable and representative signal. The powerdraw input is therefore refreshed every 1.8sec.

5.4.4.4 Residence time

Residence time is a fundamental concept of the ball milling process that dictates the number of impacts providing disintegration and attrition of the particles and that significantly influences product shape. Residence time distributions are very complex and require more experimentation to correlate with plant results when considering particles of different sizes and longitudinal position inside mills with high L/D ratio.

Consequently, the mean residence time equation is utilized:

$$\tau = \frac{M_p}{\dot{m}}$$

This simple equation is widely used and provides sufficient insight on breakage action duration. The residence time sub-model performs at fast cycle time corresponding to the cycle time of powder charge and feed rate (~2sec).

5.4.4.5 Product rate

The research objectives are specified as the maximization of throughput while controlling product size distribution to a set point. As described in section 3.2.11, the product rate is defined as:

$$\dot{m}_o = \dot{m} - \dot{m}_{D415} - \frac{dM_p}{dt}$$

At the beginning of a new campaign, the powder charge inside the mill increases,

$$\frac{dM_p}{dt} > 0$$

However, once production is completed, the mill is emptied,

$$\frac{dM_p}{dt} < 0$$

Powder charge is kept constant once the optimum quantity is attained, which will maximize breakage rates of all sizes. So,

$$\frac{dM_p}{dt} = 0$$

During normal operating conditions, the dust rate \dot{m}_{D415} is proportional to feed rate and averages to:

$$\dot{m}_{D415} = 0.02 \dot{m}$$

By weighing the dust collector discharge bucket after each production run (max. once per week), the dust rate is verified. Any malfunction of the air separator is detected. Product rate state variable is provided at the cycle time of feed rate and powder charge (~2sec) with corrected dust rate every 3-7 days.

5.4.4.6 Powder feed rate

Feed rate is a very important output control variable since it dictates productivity, residence time and powder charge. Moreover, feed rate variations can significantly affect product properties within 30 minutes. The control strategy is to reach as fast as possible and maintain an optimum powder charge that maximizes throughput and quality. Powder charge is interpreted in a set of rules to generate new feed rate set points for the process.

The rules were created according to the knowledge of ball mill operators (over 15 years experience), lab director (25 years experience) and R&D foreman (20 years experience). Afterwards, plant trials described in section 3.3 verified the knowledge base and allowed the development of an optimized sub-model.

The rules are presented below:

<i>if</i> $P \leq P_{opt} - 17$	<i>then</i> $\dot{m}_{sp} = \dot{m}_{sp} + 400$
<i>if</i> $P_{opt} - 17 < P \leq P_{opt} - 12$	<i>then</i> $\dot{m}_{sp} = \dot{m}_{sp} + 300$
<i>if</i> $P_{opt} - 12 < P \leq P_{opt} - 7$	<i>then</i> $\dot{m}_{sp} = \dot{m}_{sp} + 200$
<i>if</i> $P_{opt} - 7 < P \leq P_{opt} - 2$	<i>then</i> $\dot{m}_{sp} = \dot{m}_{sp} + 100$
<i>if</i> $P_{opt} - 2 < P < P_{opt} + 2$	<i>then</i> $\dot{m}_{sp} = \dot{m}_{sp}$
<i>if</i> $P_{opt} + 2 \leq P < P_{opt} + 7$	<i>then</i> $\dot{m}_{sp} = \dot{m}_{sp} - 100$
<i>if</i> $P_{opt} + 7 \leq P < P_{opt} + 12$	<i>then</i> $\dot{m}_{sp} = \dot{m}_{sp} - 200$
<i>if</i> $P_{opt} + 12 \leq P < P_{opt} + 17$	<i>then</i> $\dot{m}_{sp} = \dot{m}_{sp} - 300$
<i>if</i> $P \geq P_{opt} + 17$	<i>then</i> $\dot{m}_{sp} = \dot{m}_{sp} - 400$

$$[P, P_{opt}] = \text{kW}$$

$$[\dot{m}_{sp}] = \text{lb/hr (kg/hr)}$$

Evidently, increasing feed rate increases the powerdraw attributable to powder and vice versa. Once P falls between $P_{opt}-2$ and $P_{opt}+2$, the feed rate set point is maintained. Also, based on the operator's knowledge and past plant results, different starting feed rates \dot{m}_{start} are supplied depending on the grade produced. Typical values are shown in table 3.6. Starting at a feed rate close to ideal to maintain optimum powder charge improves product response time.

Plant trial results show that the powder charge sensitivity is mainly function of input material chemistry and size, powder charge, feed rate and air flow rate. As shown in equation 3.38, the response time is inversely proportional to the size of the feed rate change:

$$T_R = \frac{M_{p(\min)}}{\Delta \dot{m}}$$

Trial m1 shows a response time of approximately 30 minutes for an aggressive feed rate step change of 1000 lb/hr. The smaller feed rate changes of the rule-based system requires more time to significantly affect powder charge. A cycle time of 30 minutes is selected for sub-model execution to supply a new feed rate set point to the PI controller of the control model. This allows process stabilization and sufficient time to significantly affect powder charge, and, consequently, product properties.

The powder feed rate PI controller operates at the fastest cycle time (30ms/cycle) with some averaging (~2sec/cycle) to filter disturbances occasioned by powder irregularities and structural vibrations. As discussed in section 3.2.2, the settling time to feed rate set point step change is below 3 minutes.

The feed rate rules allow the adaptation to input material properties. For example, a higher amount of carbon in the atomized shot makes the input material more brittle. Less grinding energy is required for size reduction before the material gets swept away by the air flow. Therefore, the sub-model increases feed rate set points to maintain the optimum powerdraw. Thus, throughput is maximized and residence time decreased.

5.4.4.7 Air flow rate

The most critical output control parameter of the ball milling process is the air flow rate since it prescribes product size distribution. In addition, air flow rate variations can significantly affect product properties within 4 minutes. The control strategy is to regulate the air flow rate to achieve product size specifications at a 99.7% confidence interval. Product size feedback is interpreted in a set of rules to generate new air flow rate set points for the process.

The rules were created based on plant personnel knowledge and trial results. A stronger air flow rate pulls out coarser and denser ground shot. On the other hand, smaller air flow rate sweeps finer and less dense product. It is explained in section 3.3 that the minimum air flow rate change to affect product properties is 100 ACFM with product response time of 4 minutes. This dictates the minimum airflow set point variation applied in the rules and sub-model cycle time.

Cumulative size distributions from feed rate and air flow rate tests were plotted on log-normal paper to determine the distribution function and the sufficient number of points needed to reasonably characterize the product. Looking at the results of figure 3.18 and Appendix 3, we find that feed rate, air flow rate and powder charge variations are not affecting the shape of the distribution per product. This confirms model statement 4: the

product size distribution function is governed by ball size distribution. An extended region of the results can be fitted by a series of straight lines defined by 2 parameters: the slope and intercept. The lines shift up or down depending on product size results. The ball size distribution and ball bed height are regulated via the ball feed rate sub-model to preserve a steady size distribution function. As a result, the slope on the log-normal plot does not change. A single point (intercept) can therefore be used to characterize and control product size distribution: product percent passing a 200 mesh sieve, $S200$. This simplifies the rule-based air flow rate sub-model implementation and plant personnel understanding. Moreover, operator's knowledge for output variables control is based on $S200$ results.

The rules are presented below:

<i>if</i> $S200 \leq S200_{opt} - 4$	<i>then</i> $Q_{sp} = Q_{sp} - 500$
<i>if</i> $S200_{opt} - 4 < S200 \leq S200_{opt} - 3$	<i>then</i> $Q_{sp} = Q_{sp} - 300$
<i>if</i> $S200_{opt} - 3 < S200 \leq S200_{opt} - 2$	<i>then</i> $Q_{sp} = Q_{sp} - 200$
<i>if</i> $S200_{opt} - 2 < S200 \leq S200_{opt} - 1$	<i>then</i> $Q_{sp} = Q_{sp} - 100$
<i>if</i> $S200_{opt} - 1 < S200 < S200_{opt} + 1$	<i>then</i> $Q_{sp} = Q_{sp}$
<i>if</i> $S200_{opt} + 1 \leq S200 < S200_{opt} + 2$	<i>then</i> $Q_{sp} = Q_{sp} + 100$
<i>if</i> $S200_{opt} + 2 \leq S200 < S200_{opt} + 3$	<i>then</i> $Q_{sp} = Q_{sp} + 200$
<i>if</i> $S200_{opt} + 3 \leq S200 < S200_{opt} + 4$	<i>then</i> $Q_{sp} = Q_{sp} + 300$
<i>if</i> $S200 \geq S200_{opt} + 4$	<i>then</i> $Q_{sp} = Q_{sp} + 500$

$$[S200, S200_{opt}] = \%$$

$$[Q_{sp}] = \text{ACFM}$$

The optimum product percentage passing a 200 mesh sieve, $S200_{opt}$, is the mean value of Domfer ball milling product specification shown in table 1.2. Once $S200$ is between $S200_{opt}-1$ and $S200_{opt}+1$, the air flow rate set point is maintained. Also, based on operator's knowledge and past plant results, different starting air flow rates Q_{start} are prescribed depending on the grade produced. Typical values are shown in table 3.6. Starting at an air flow rate close to optimum to reach specific product size greatly increases product size response time.

The cycle time of the sub-model follows product size feedback frequency. As discussed in section 4.2, the size analysis speed required for the process is approximately between 5 and 30 minutes when considering minimum product response time to output control parameter variations. More frequent size results are not representative of the process since the ball mill requires sufficient time to react and stabilize following parameter changes. Using the automated sampler and sieve analyzer and following MPIF standard 05, product size analysis results are inputted to the sub-model every 15 minutes. If the product is sampled and tested by the operator, the cycle is 3-4 hours. It is obvious that more frequent feedback would greatly maximize overall control system performance.

The air flow rate PI controller operates at the fastest cycle time (30ms/cycle) with some averaging (~2sec/cycle) to filter disturbances occasioned by flow turbulence. As discussed in section 3.2.9, the settling time to air flow rate set point step change is below 1.5 minutes.

The decoupled arrangement of the air flow rate sub-model eliminates controller interactions and enables adaptation with respect to liner wear. As discussed in section 2.4, 2.5 and 2.6, the smoother cross section of used liners affects charge motion to favor attrition grinding and increase breakage rates of the fines. In this case, the higher *S200* is detected by the sub-model that increases the air flow rate set point to sweep out coarser product and maintains constant product size distribution with respect to wear.

5.4.5 Diagnostic system and error recovery

Sensor data and state variables from the data model are continuously monitored by the diagnostic system to evaluate whether sensor data have errors, the process is in control, state variables are moving out of acceptable ranges, or control parameters are approaching limits. The diagnostics are elucidated by the control model for action. The diagnostic system generates interrupts to create error recovery agents for process rehabilitation. Only the affected sub-models are stopped when an error occurs. If the production process can continue with reduced data, the exception is handled by agents

that execute predefined processes. The operator is informed and intervention is requested for extreme difficulties. Once the error is fixed, the suspended agents are restarted and full execution is returned to the control agent.

5.4.5.1 Size distribution function

As discussed in section 2.3 and demonstrated in section 3.3.2, metal powders exhibit straight line behavior on the log-normal plot. Hence, the particle size distribution can be reduced to just 2 parameters, the slope and intercept. As the product gets coarser, the line is shifted downward and as the product gets finer, the line is shifted upward. For a specific grade, once the optimum $S200$ is achieved, an $S100$ range is expected with an upper control limit shown in ball mill product specifications of Appendix 1. For example, when S-1 grade is produced, $S200_{opt}$ is 67% with a maximum of 6% on the $S100$. If $S100$ is above 6%, this shows that the slope of the line on the log normal plot has changed, which identifies a change in the shape of the product size distribution. Single point measurement for the air flow rate sub-model is no longer valid. A possible reason is the lower ball charge accompanied with ball size distribution variation. The reduced amount of 2in (5.08cm) diameter new steel balls provides less breaking energy to the larger particles that reach the exit without being fractured enough. Intervention is therefore requested for ball bed height verification to fine tune the ball feed rate sub-model. The product % retained by a 100mesh (150 μ m) sieve is monitored every 15 minutes or 3-4 hours, depending on product size feedback cycle time.

5.4.5.2 Product apparent density

Product apparent density is determined with the MPIF standard 04. Plant trials described in section 3.3.1 proved that density is directly proportional to size distribution. A coarse size distribution engenders higher density and vice-versa. This input parameter was decoupled from the sub-models to simplify the control strategy and deal with different time scales.

However, density deviation can be seen for the following reasons:

1. Input material size distribution and shape variations due to atomization process variations.
2. Input material size distribution variations caused by segregation in the feeding tanks.

Input material size influences the residence time. Finer particles spend less time being deformed to conserve their initial spherical shape to allow better arrangement for apparent density whereas coarser particles need to receive more breakage action to produce irregular shape with lower apparent density. Moreover, more irregular and hollowed atomized shot particles produce a different output shape that arranges itself differently giving rise to biased product density results. Plant personnel are advised of out of specification product every 3-4 hours, following apparent density tests performed by ball mill operators.

5.4.5.3 Outlet trunnion pressure

Product size is dictated by air flow rate inside the mill rotating cylindrical shell. However, robust air flow rate control actions are taken using the flow element feedback installed after the blower. Any malfunction between the flow element and the mill offset the strength of the suction air flow: cyclone variable flow restriction, dust collector cartridges, impact tank discharge valve and suction circuit conduit leaks. Consequently, the effectiveness of the sweeping action is monitored using a pressure transmitter connected to the suction circuit just after the outlet trunnion.

It was demonstrated in the plant trials explained in section 3.3.3 that outlet trunnion pressure dP_o is proportional to air flow rate Q . For a specific air flow rate, if the outlet pressure strays out of the acceptable range ($\pm 25\%$), the air flow rate sub-model is affected and the following offsets are applied:

$$\begin{array}{lll} \text{if } dP_o \downarrow & \text{then} & Q \uparrow \\ \text{if } dP_o \uparrow & \text{then} & Q \downarrow \end{array}$$

5.0 PROCESS MODEL DEVELOPMENT

A decrease in outlet pressure is compensated by an air flow rate increase and vice-versa to regulate suction air flow throughout the campaign. Also, dust 415 pulse durations and intervals, $t_{D415,pulse}$ and $t_{D415,intr}$, are intensified to accentuate the cleaning of clogged cartridges.

For extreme deviations, intervention is requested to investigate the following possible causes:

for low outlet pressures: R-413 discharge valve leak
Cyclone air lock valve leak
Suction circuit conduit leak
Clog dust collector cartridges

for high outlet pressures: Broken dust collector cartridge

In the above cases, the dust rate calculated from the product rate sub-model is verified to confirm that \dot{m}_{D415} is still equal to 2% of \dot{m} .

The outlet trunnion pressure is monitored at the fastest cycle time with a longer averaging (10sec/cycle) to alleviate turbulence in the suction circuit that induces vacuum pressure signal variations. Outlet pressure diagnostics allow adaptive control of the air flow rate with respect to circuit resistance changes. Once again, the decoupled approach simplifies the implementation of adapted new air flow rate set points for the control model.

5.4.5.4 Loading and emptying phases

Every 3-7 days, between different product campaigns, the ball mill is emptied to prevent cross-contamination. Plant results from the past years show out-of-specification size distributions at the beginning of a new campaign for periods as long as 8 hours. One can easily imagine the detrimental effect of 48000lb (21772.8kg) (8hr X 6000lb/hr (2721.6kg/hr)) off specification ground shot over a 432000 lb (195955.2kg) (3days X 24hr/day X 6000lb/hr (2721.6kg/hr)) product campaign. As discussed in section 3.2.5, the powder charges for all grades vary from 9000 to 12500lb (4082.3 to 5669.9kg). Hence, if

a campaign is started at a feed rate in the region of the acceptable feed rate range \dot{m}_{range} , the time required to reach the optimum powder charge is too long. At low powder filling, much of the energy of the tumbling balls is taken up in steel-to-steel contact giving low breakage rates and overgrinding of the particles.

At startup, the diagnostic system suspends the feed rate rule-based sub-model and applies the maximum feed rate:

$$\dot{m} = \dot{m}_{max} = 12000 \text{ lb/hr} \quad (5443.1 \text{ kg/hr})$$

Once the powerdraw is above or equal to P_{opt} , the halted feed rate sub-model is restarted at \dot{m}_{start} and full execution is returned to the control agent. This minimizes the duration at which the mill is underfilled. The diagnostic executes at the cycle time of the powder feed rate PI controller (~2sec/cycle).

During the emptying phase at the end of the campaign, the air flow rate sub-model adapts to the decreasing powder charge by increasing the air flow rate. The rules increase air flow rate set points based on product feedback results, which tend to become finer as the mill is emptying.

5.4.5.5 Powerdraw, feed rate and air flow rate ranges

During normal grinding operation with product size within upper and lower control limits, powerdraw, feed rate and air flow rate parameters must lie within a specific range (P_r , \dot{m}_r and Q_r) function of the grade produced. This is shown in table 5.1.

Table 5.1: Allowable powerdraw, feed rate and air flow rate ranges

	P_r (kW)	\dot{m}_r (lb/hr), (kg/hr)	Q_r (ACFM), (m ³ /sec)
MP3	195 ± 19.5	3500±875, (1587.6±396.9)	4500±900, (2.124±0.425)
MP1	200 ± 20.0	4000±1000, (1814.4±453.6)	5400±1080, (2.549±0.510)
MP4	214 ± 21.4	5500±1375, (2494.8±623.7)	6500±1300, (3.068±0.614)
MP2	226 ± 22.6	6000±1500, (2721.6±680.4)	6500±1300, (3.068±0.614)

If any of the parameters drift out of range, intervention is requested with key process equipment and variables to verify:

- P out of range: power factor, ball mill motor, fluid drive, speed reducer, gears
- \dot{m} out of range: automatic input material feeder, input material chemistry (%C, %Si) and size distribution.
- Q out of range: suction circuit, dust collector, fan

5.4.5.6 Powerdraw vs feedrate

The maximum breakage rates are achieved around maximum powerdraw, depending on ball charge and liner shape. Further addition of powder increases hold-up without increasing productivity since the collision zones are already saturated and more powder just accumulates. Overfilling approaches the center of gravity of the charge towards the longitudinal mill axis to reduce powerdraw. Severe blockage problems can be induced by large overfilling. Actual powder charge must be kept below the powder charge at maximum powerdraw to conserve the relation between feed rate and powerdraw attributable to powder and consequently the feed rate rule-based sub-model effectiveness:

$$\begin{aligned}\uparrow \dot{m} &\Rightarrow \uparrow P_p \\ \downarrow \dot{m} &\Rightarrow \downarrow P_p\end{aligned}$$

Otherwise, if the powder charge is increased above the optimum charge, the feed rate and powerdraw relation are inverted. This leads to overfilling and reduction of effective collisions by powder cushioning to diminish breakage rates of all sizes. This phenomenon can be seen on the graph of figure 5.4, with maximum powerdraw P_{max} being the local maximum located at optimum powder charge Mp_{opt} . The desired region of operation is on the left side of the local maximum. The feed rate powerdraw relation is monitored every 30 minutes, which corresponds to the cycle time of the powder feed rate sub-model.

If a feed rate increase provokes a reduction in powerdraw, the powder feed rate sub-model is suspended and a separate agent reduces feed rate to recover the region of operation at which all the effective spaces where collisions between tumbling balls are occurring are filled with powder. Then, a new lower optimum powerdraw P_{opt} is utilized, and full execution is returned to the feed rate sub-model.

Input material availability is also monitored every 2 seconds. Lack of input material is seen because of an empty or blocked feeding tank. This is detected by a combination of maximum output on the feeder and 0 lb/hr as actual powder feed rate. Operator intervention is therefore requested.

5.4.5.7 Product size verification

The derivative of product size with respect to time dS/dt is investigated to confirm that the control system is effective and reaching the desired properties. This is shown in figure 5.5.

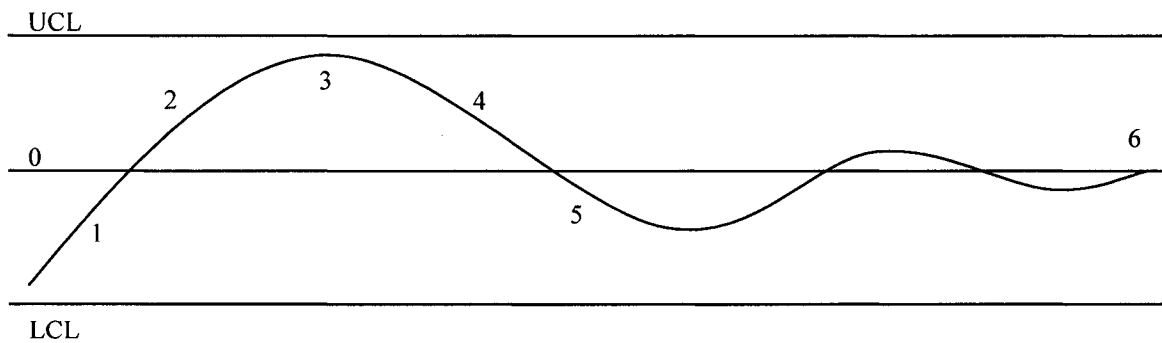


Figure 5.5: Product size derivative with respect to time

Depending on the control region and product size variation tendency, the following diagnostics are made:

1: $dS/dt > 0$ in LCL region	\Rightarrow	O.K.
2: $dS/dt > 0$ in UCL region	\Rightarrow	Bad direction Intensify control action
3: $dS/dt = 0$ in LCL or UCL regions	\Rightarrow	Stabilization with error Change in direction
4: $dS/dt < 0$ in UCL region	\Rightarrow	O.K.
5: $dS/dt < 0$ in LCL region	\Rightarrow	Bad direction Intensify control action
6: $dS/dt = 0$ at 0	\Rightarrow	O.K. Desired value obtained

The product size diagnostic operates at a cycle time of 30 minutes, just as the powder feed rate sub-model, to allow process stabilization and sufficient time for significant product property changes. If the product size is not responding well to a control action, an

error recovery agent is created for process rehabilitation. The agent intensifies the control action to recover product size set point convergence. If the error is not fixed, the affected sub-model is stopped, operator intervention is requested and it is determined if the production process can continue.

5.4.5.8 Equipment

The Domfer grinding process is composed of equipment with specific tasks: raw material feeding tanks, input material feeder, steel balls feeder, ball mill, receiving tank, cyclone separator, dust collector, damper, blower and filter. The ball mill 408 grinding circuit is shown in figure 3.1.

Any malfunction is detected and the control model interprets the diagnostics for action:

- Input material feeder conveyor and/or bucket elevator faults
Action: Continue process and request intervention
Suspend feed rate sub-model
- Ball feeder blockage and/or motor faults
Action: Pause ball feed rate sub-model, continue process and request intervention
- Ball mill motor fault
Action: Stop process and request intervention
- Ball mill babbits, fluid drive and speed reducer temperatures out of range
Action: Halt powder charge sub-model, continue process with reduced data and request intervention
- Receiving tank and cyclone blockage
Action: Stop process and request intervention
- Blower motor fault
Action: Stop process and request intervention
- Dust collector broken cartridges and/or high temperature
Action: Stop process and request intervention

The detailed ball mill model is shown in figure 5.6 with key variables and control architecture.

The key sensor variables acquired from the process are:

- Product % retained by a 100 mesh sieve, $S100$
Product % passing a 200 mesh sieve, $S200$
- Mill powerdraw, P

After tests and measurements, the following key parameters are entered by the operators on the human machine interface:

- Product apparent density, ρ_o
- Ball bed height, H
Campaign run time, T_{camp}

The rule-based process sub-models of feed rate and air flow rate give feed rate and air flow rate set points, $\dot{m}_{\text{set point}}$ and $Q_{\text{set point}}$, for the PI controllers.

- Powder charge is interpreted to generate new feed rate set points.
- Product size feedback is interpreted to generate new air flow rate set points.

The ball feed rate to compensate ball and liner wear $\dot{m}_{b(408)}$, and the ball feed rate correction factor $\Delta\dot{m}_b$ are computed by the process sub-models.

The following output control variables are sent to the physical process:

- Powder feed rate, \dot{m}
- Air flow rate, Q
- Ball feed rate, \dot{m}_b

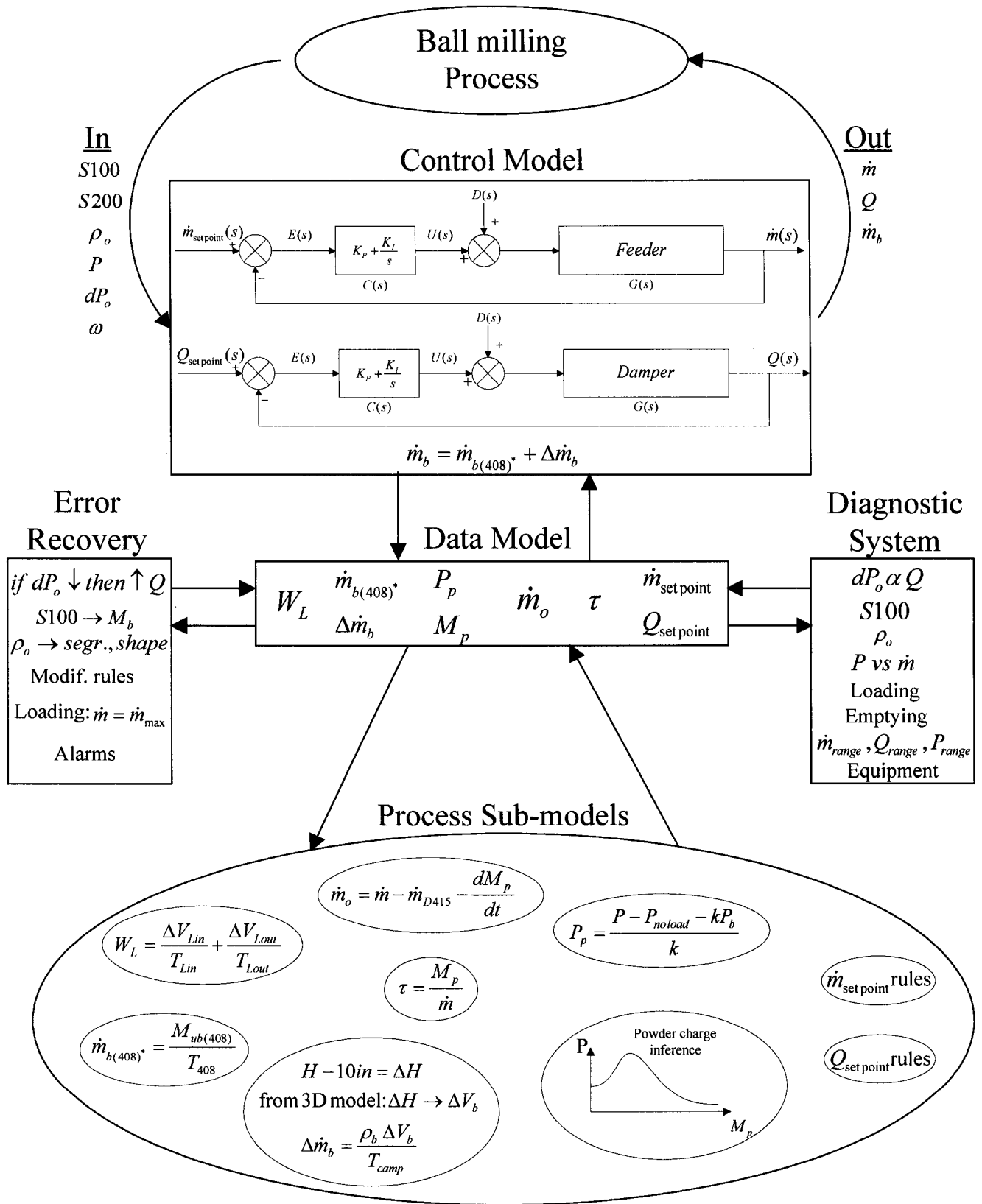


Figure 5.6: Ball mill model

5.5 Conclusion

The multi-agent system that was designed is expected to cope with the complexity of the ball milling process, which is composed of multiple data streams and many sub-models of different sizes and operating time scales. The model based approach enabled the estimation of process physics by integrating an overall process model composed of sub-models of process phenomena. An agent based architecture with the following features was utilized: input/output parameters from the process, control model, data model, process sub-models, diagnostic system and error recovery. The variables of interest are non-linear, time variant (product sizes, powder charge) and some of them were measured using soft sensors (powerdraw, ball bed height). The consideration of a multivariable process helped to identify the key model parameters, and gave insight into the problem. This led to the understanding that the key parameters could be decoupled due to the large time frame differences, i.e., for the variables (feed rate, air flow rate, ball feed rate, ball and powder charges, and liner wear), the problem decomposed into several single parameter sub-models. The mathematical equations that determine the liner wear, ball feed rate, powder charge and residence time contribute to the control model, but it is the AI models for feed and air flow rate that are the heart of the control system. This is because the output of the powder grinding process is dominated by the near time frame factors: air flow rate and powder feed rate.

6.0 CONTROL AND MONITORING

The ball mill model that was created integrates process sub-models composed of rules, equations and heuristics. For real time control, information is needed simultaneously for many variables of the process. The model based control system was developed using an agent based architecture. This multi-agent system deals with multiple data streams and process sub-models of different sizes and operating time scales. The control strategy decouples the process parameters to simplify the sub-model equations, reduce unwanted interactions and allow low-level computer control and monitoring. A multi-variable controller is required to implement the model architecture features and achieve research objectives with good performance. In this chapter, control and monitoring algorithms developed to implement the ball mill model are presented, followed by controller hardware design.

6.1 Background

System control and monitoring is accomplished using a programmable logic controller (PLC) which can easily handle multiple data streams and process sub-models of different time scales. The following are the key advantages of using low-level programmable logic controllers:

- Very robust and stable
- Rugged design for an industrial environment
- Flexible architecture adaptable to specific applications
- Good performance (small cycle time)
- Widely used
- Cost friendly

Very few industries exist today that do not employ programmable controllers. Almost every business in the manufacturing sector, and many in the service sector, use PLCs in abundance. It is little wonder that the relatively rapid integration of the PLC into the manufacturing sector has been called the second industrial revolution [60].

A PLC is basically a CPU (central processing unit) containing a program and connected to input and output (I/O) devices. The program controls the PLC such that when an input signal from an input device changes state, the appropriate response is made. The response involves activating an output signal to an output device. The PLC uses a form of PC logic called ladder-diagram programming. The contact-ladder diagram is the most widely used low-level PC language [61]. A ladder diagram consists of one line running to the left side with lines branching off to the right. The left line is called the bus bar and the branching lines are instruction lines or rungs. On the instruction lines are placed conditions that lead to instructions on the right hand side. The logical conditions dictate when and how the instructions at the right are executed. A ladder diagram is shown in figure 6.1.

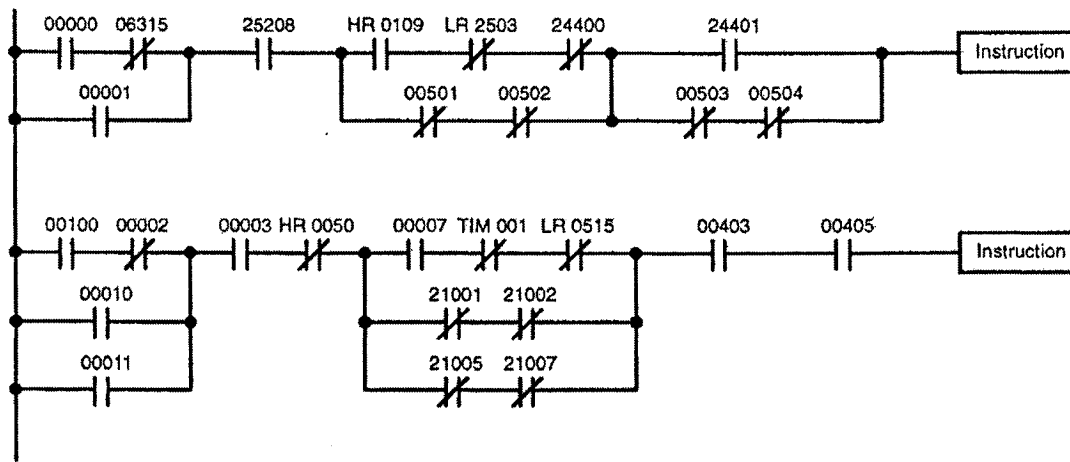


Figure 6.1: Basic ladder diagram

The instruction lines can branch apart and join back together. The vertical pairs of lines are conditions. The conditions without diagonal lines through them are normally open conditions and may correspond to a LOAD, AND, or OR instruction. Conditions with diagonal lines through them are normally closed conditions and correspond to LOAD NOT, AND NOT, or OR NOT instruction. The numbers above each condition show the operand bit for the instruction. The status of the bit associated with each condition determines the execution condition for the following instruction. Each condition in a ladder diagram is either ON or OFF depending on the status of the operand bit that is associated with it.

In ladder programming, the logical combination of ON and OFF conditions before an instruction determines the resulting condition under which the instruction is executed. This condition (ON or OFF) is the execution condition for the instruction, since all instructions other than the load instruction have execution conditions.

The operands for any of the ladder instructions can be any bit in the memory areas of the PLC. The conditions in a ladder diagram can be determined by I/O bits, flags, work bits, timers/counters, etc. The instructions of the ladder diagram can be performed on bits, words and double words in the memory areas of the PLC.

Ladder diagram instructions are presented in Appendix 5.

The ladder diagram cannot be directly inputted to the PLC. It is necessary to convert it to mnemonic code, which contains exactly the same information as the ladder diagram, but in a format that can be directly typed into the PLC. The program is inputted into addresses in the program memory. Each address holds one instruction and all of the definers and operands required for that instruction. The program memory addresses start at 00000 and run until the capacity of the program has been reached.

Several basic steps should be followed when writing a ladder diagram program:

1. Create a list of the I/O devices and I/O points that are assigned to them and construct a table showing the I/O bit allocated to each I/O device.
2. Determine what words are available for work bits and create a table in which they can be allocated as being used.
3. Draw the ladder diagram following the logical conditions and operations desired.
4. Input the program to the PLC.
5. Check the program for syntax errors and memory area conflicts.
6. After the entire control system has been installed, execute the program, check for execution errors and fine tune if required.

It is important to understand the internal operation of the PLC to efficiently program the control strategy. The operating sequence is continuously executed by the PLC, as shown in figure 6.2.

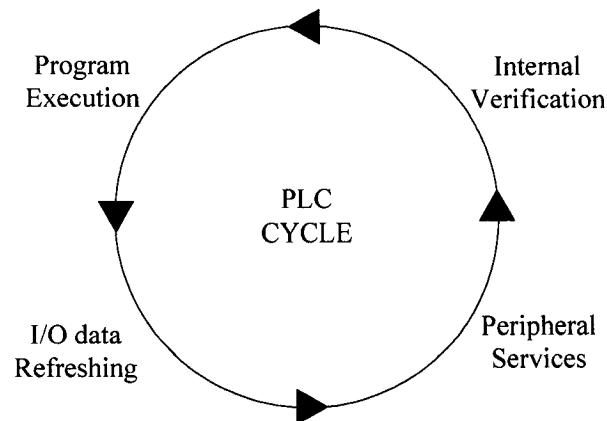


Figure 6.2: Programmable logic controller cycle

The following operations are executed every cycle:

1. Internal verification: I/O bus and memory verification, watchdog timer, etc.
2. Program execution: the program instructions are executed in sequence using input and memory data to control output and memory data.
3. I/O data refreshing: input data read and copy to memory, output data command from memory.
4. Peripheral services: Programming console, Host Link module, communication boards, etc.

The major factors in determining program timing are the cycle time and the I/O response time. One run through all required CPU unit operations is called a cycle, the time required for each cycle is called the cycle time.

The PLC architecture diagram is presented in figure 6.3. We can see that the architecture provides all the features needed to implement the multi-variables control system.

Each block performs the tasks required by the agent based architecture described previously in section 5.3:

1. Input module: acquisition of sensor data
2. User program:
 - Calculate the control parameters from process model variables by operating on the data model
 - Execute agent defined tasks
 - Perform process sub-models
 - Monitor sensor data and state variables
 - Recover errors
3. Data memory and I/O data tables:
 - Sensor data, process model variables and control parameters storage
 - Integration of data from all process sub-models
4. Output module: Transmission of parameter values to control the real process

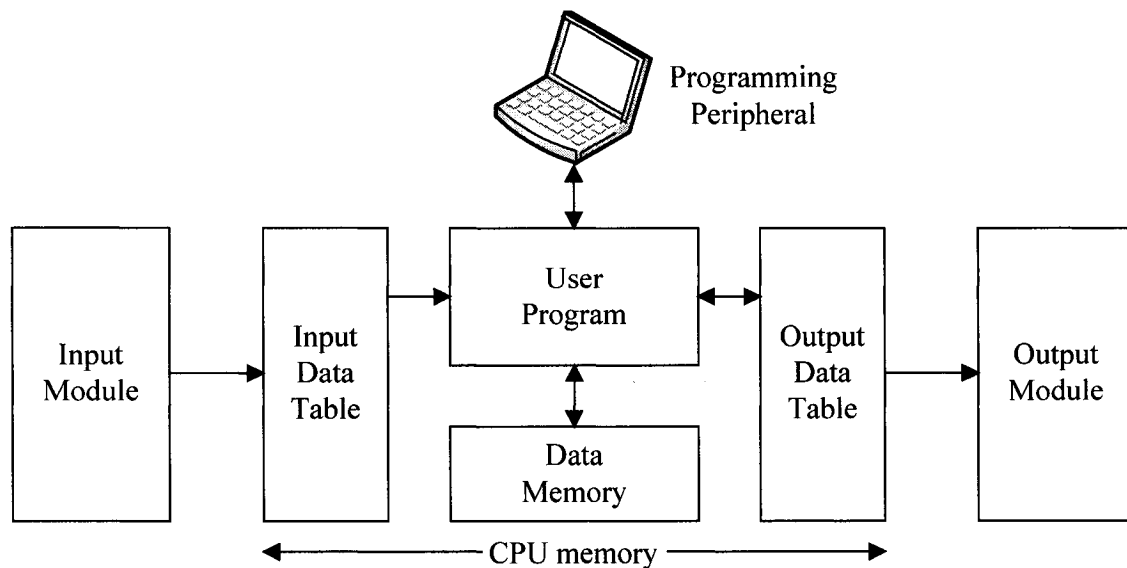


Figure 6.3: PLC architecture diagram

The most important control and monitoring algorithms used to integrate the ball mill model features are now presented. The algorithms are developed in low-level PC language. After that, controller hardware with specifications is described.

6.2 Control algorithms

Control algorithms are developed to calculate control parameters from process sub-model variables. The following output control parameters are sent to the physical process:

- Powder feed rate, \dot{m}
- Air flow rate, Q
- Ball feed rate, \dot{m}_b

The rule-based process sub-models of feed rate and air flow rate provide feed rate and air flow rate set points, $\dot{m}_{\text{set point}}$ and $Q_{\text{set point}}$, for the robust PI controllers described in section 3.2.2 and 3.2.9. A ladder diagram of the control algorithm used to implement the PI controllers is presented in figure 6.4. It operates at the fastest PLC cycle time (30ms).

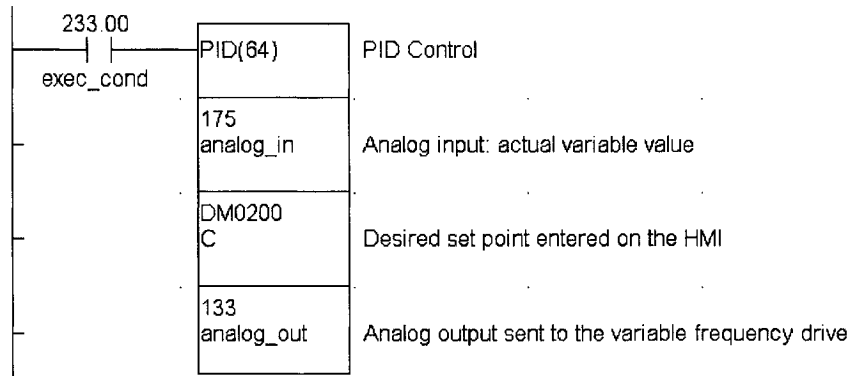


Figure 6.4: Feed rate and air flow rate control algorithm

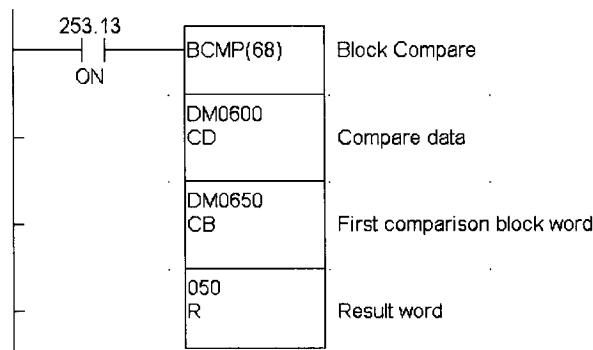
When the execution condition is OFF, PID is not executed. When the execution condition is ON, the function carries out PID control according to the designated parameters. It takes the specified input range of binary data from the content of the input word *analog_in* and carries out the PID operation according to the parameters that are set. The results are then stored as the operation output amount in the output word *analog_out*.

PID parameter words range from C through C+32 and are configured as presented below:

Word	15 to 12	11 to 8	7 to 4	3 to 0
C	Set point			
C+1	Proportional band			
C+2	Integral time/sampling period			
C+3	Derivative time/sampling period			
C+4	Sampling period			
C+5	Input filter coefficient			PID forward/ reverse
C+6	0	Input range	Time unit for sampling period and integral/ derivative times	Output range
C+7 to C+32	Work area (Cannot be accessed directly from the program)			

The sub-models are integrated in a low-level PC language. The rules *if/then* statements are computed using PLC functions: block compare (BCMP), binary coded decimal add (ADD) and binary coded decimal subtract (SUB).

The ladder symbol of the block compare function is:

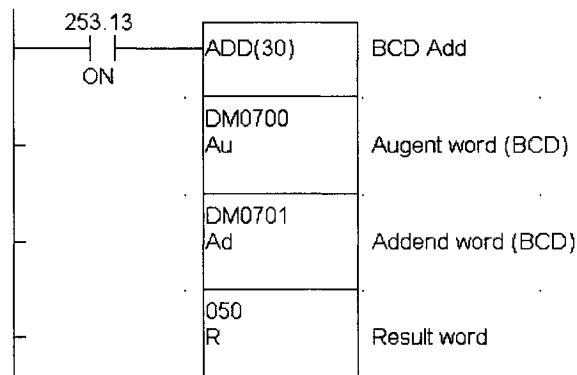


When the execution condition is OFF, BCMP is not executed. When the execution condition is ON, BCMP compares CD to the ranges defined by a block consisting of CB, CB+1, CB+2,..., CB+31. Each range is defined by two words, the first one providing the lower limit and the second word providing the upper limit. If CD is found to be within any of these ranges (inclusive of the upper and lower limits), the corresponding bit in R is set. The rest of the bits in R are turned OFF.

The comparisons that are made and the corresponding bit in R that is set for each true comparison are shown below:

$CB \leq CD \leq CB+1$	Bit 00
$CB+2 \leq CD \leq CB+3$	Bit 01
$CB+4 \leq CD \leq CB+5$	Bit 02
$CB+6 \leq CD \leq CB+7$	Bit 03
$CB+8 \leq CD \leq CB+9$	Bit 04
$CB+10 \leq CD \leq CB+11$	Bit 05
$CB+12 \leq CD \leq CB+13$	Bit 06
$CB+14 \leq CD \leq CB+15$	Bit 07
$CB+16 \leq CD \leq CB+17$	Bit 08
$CB+18 \leq CD \leq CB+19$	Bit 09
$CB+20 \leq CD \leq CB+21$	Bit 10
$CB+22 \leq CD \leq CB+23$	Bit 11
$CB+24 \leq CD \leq CB+25$	Bit 12
$CB+26 \leq CD \leq CB+27$	Bit 13
$CB+28 \leq CD \leq CB+29$	Bit 14
$CB+30 \leq CD \leq CB+31$	Bit 15

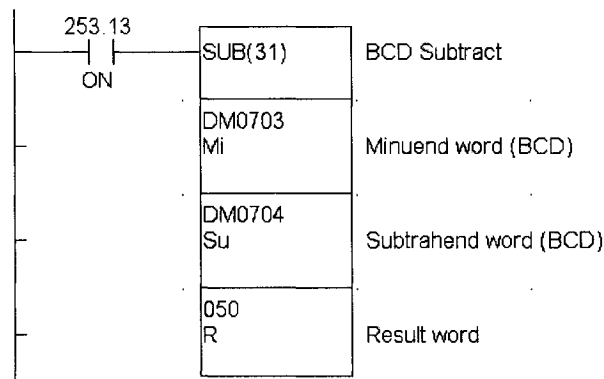
The ladder symbol of the binary coded decimal add function is shown below:



When the execution condition is OFF, ADD is not executed. When the execution condition is ON, the function adds the contents of Au, Ad and CY and places the result in R. Carry (CY) is set if the result is greater than 9999.

$$Au + Ad + CY \rightarrow CY, R$$

The ladder symbol of the binary coded decimal subtract function is shown below:



When the execution condition is OFF, SUB is not executed. When the execution condition is ON, the function subtracts the contents of Su and CY from Mi and places the result in R. If the result is negative, CY is set and the 2's complement of the actual result is placed in R. To convert the 2's complement to the true result, subtract the content of R from zero.

$$Mi - Su - CY \rightarrow CY, R$$

As previously described in section 5.4.4.6, powder charge is interpreted in a set of rules to generate new feed rate set points for the process. The control strategy is to reach as fast as possible and maintain an optimum powder charge that maximizes throughput and quality. The created control algorithm is presented in figure 6.5. The condition part of the rules is executed by BCMP where the mill power is compared to the ranges defined in the comparison block words. The corresponding bit in the result word is set and the action is taken on the feed rate: increase (ADD) *if* power is low or decrease (SUB) *if* power is high. The differentiated instruction is used when an @ is placed in front of the instruction, such as @ADD and @SUB. This ensures that the instruction is executed only once, i.e., when the execution condition changes from OFF to ON.

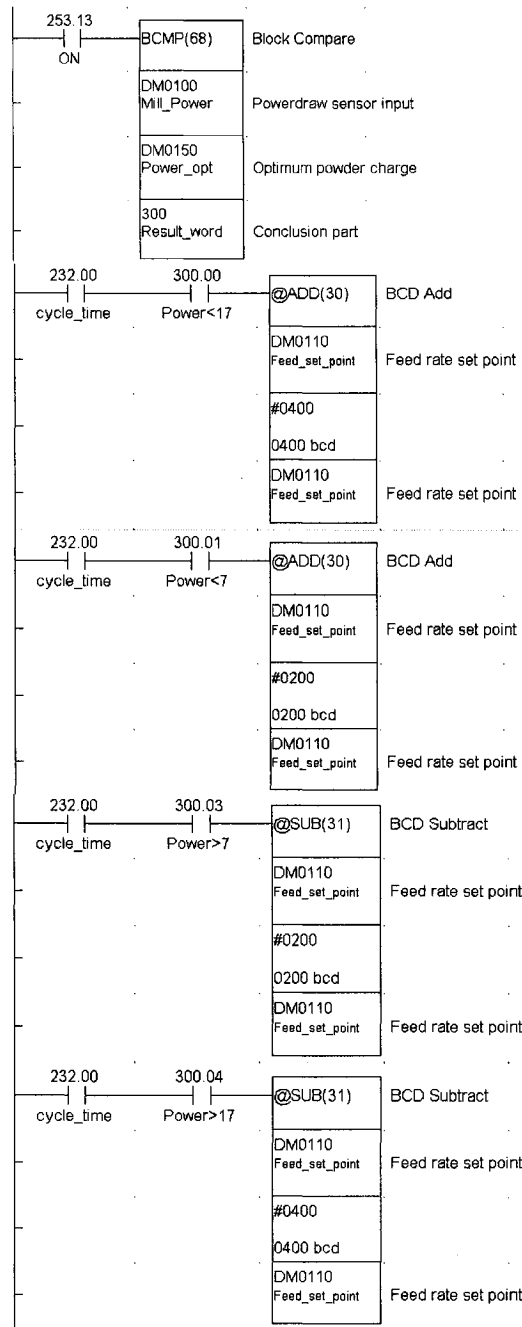


Figure 6.5: Powder feed rate sub-model control algorithm

As described in section 5.4.4.7, product size feedback is interpreted in a set of rules to generate new air flow rate set points for the process. The control strategy is to regulate air flow rate to achieve product size specifications at a 99.7% confidence interval. The created control algorithm is presented in figure 6.6. The condition part of the rules is

executed by the BCMP where the product percent passing a 200mesh (75 μ m) sieve *S200* is compared to the ranges defined in the comparison block words. The corresponding bit in the result word is set and action is taken on the air flow rate: reduce (SUB) *if* product is coarse or increase (ADD) *if* product is fine.

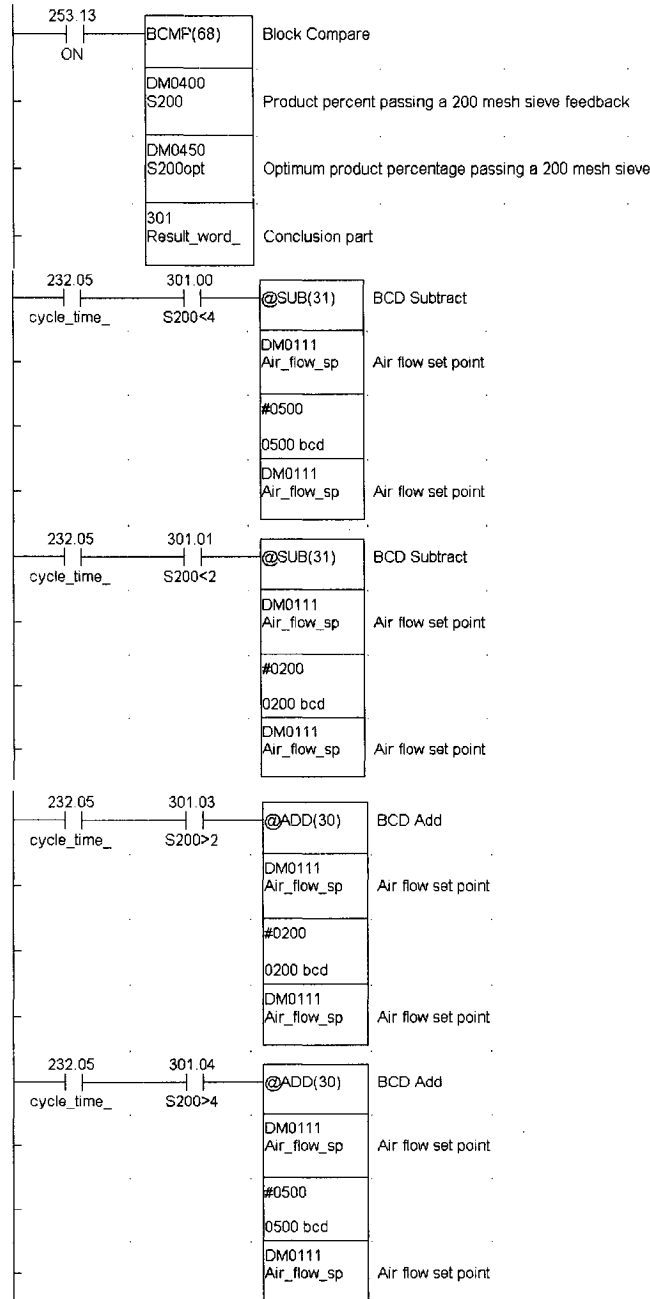


Figure 6.6: Air flow rate sub-model control algorithm

Up to 16 ranges can be defined in the BCMP function which permits 16 condition parts or rules for the powder feed rate and air flow rate sub-models. The algorithms are executed at the cycle times of the sub-models: 30 minutes for feed rate, 15 minutes or 3-4 hours for air flow rate.

As described in section 3.2.4 and 5.4.2, the ball feed rate output parameter is calculated using:

$$\dot{m}_b = \dot{m}_{b(408)*} + \Delta\dot{m}_b$$

The equation is converted to ladder diagram and presented in figure 6.7.

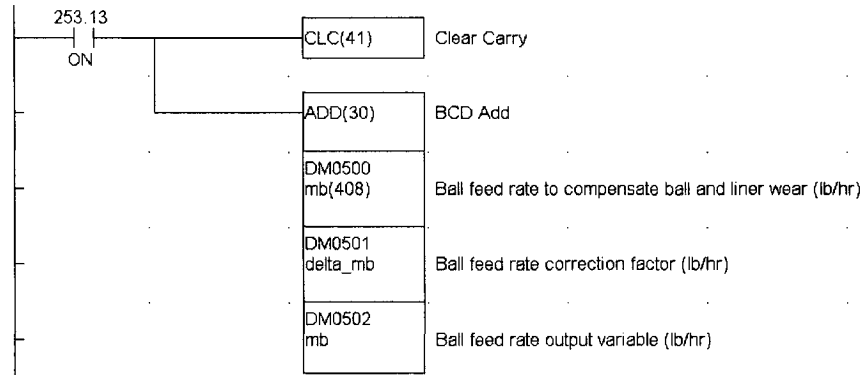


Figure 6.7: Ball feed rate control algorithm

The clear carry function CLC is used to reset CY to 0. This ensures that any carry from other program operations are not included in the addition. The program clears CY with CLC, adds the content of $\dot{m}_{b(408)*}$ and $\Delta\dot{m}_b$ and places the result in \dot{m}_b . This is executed at the fastest cycle time (30ms) with $\dot{m}_{b(408)*}$ and $\Delta\dot{m}_b$ refreshed once a year and once a week respectively, as prescribed by the ball feed rate sub-model cycle times.

6.3 Monitoring algorithms

Monitoring algorithms are developed to monitor sensor data and state variables from the data model and assess whether sensor data have errors and the process is in control. The diagnostics are evaluated by the control model for action and error recovery agents are created for process rehabilitation.

The first and most important variable to be monitored is the product percent passing a 100mesh (150 μ m) sieve *S100* to confirm the slope of the size distribution on the log-normal plot, as explained in section 5.4.5.1. As shown in ball mill product specifications of Appendix 1, a *S100* range is expected with an upper control limit. The ladder diagram of the created algorithm is presented in figure 6.8.

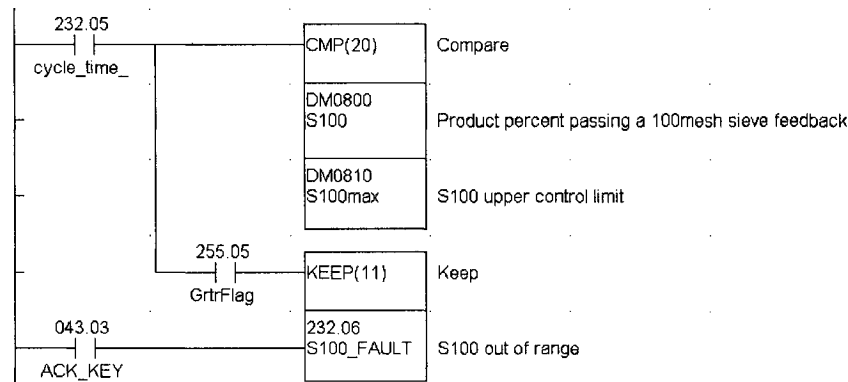


Figure 6.8: *S100* monitoring algorithm

When the execution condition is OFF, compare (CMP) is not executed. When the execution is ON, the function compares *S100* and *S100max* and outputs the result to the GR (greater), EQ (equal) and LE (less) flags.

Flags: EQ \rightarrow ON if *S100* equals *S100max*

LE \rightarrow ON if *S100* is less than *S100max*

GR \rightarrow ON if *S100* is greater than *S100max*

KEEP is used to maintain the status of the designated bit *S100_FAULT* based on two execution conditions: the set input S and the reset input R. KEEP operates like a latching relay that is set and reset. When S turns ON, the designated bit will go ON and stay ON until reset, regardless of whether S stays ON or goes OFF. When R turns ON, the

designated bit will go OFF and stay OFF until set, regardless of whether R stays ON or goes OFF.

So when *S100* goes above the upper control limit *S100_{max}*, the greater flag turns ON to set the designated bit *S100_FAULT*. Intervention is then requested on the HMI for ball bed height verification. Once the error is fixed, the operator resets the designated bit by pressing the *ACK_KEY* on the HMI. Full execution is then returned to the control agent. The monitoring algorithm executes every 15 minutes or 3-4 hours, depending on product feedback cycle time.

The second monitored key variable is product apparent density, which is part of Domfer ball mill product specifications presented in Appendix 1. As explained in section 5.4.5.2, this input parameter was decoupled from the sub-models to simplify the control strategy and cope with different time scales. Moreover, plant trials described in section 3.3.1 demonstrated that density is proportional to size distribution. The ladder diagram of the monitoring algorithm is presented in figure 6.9.

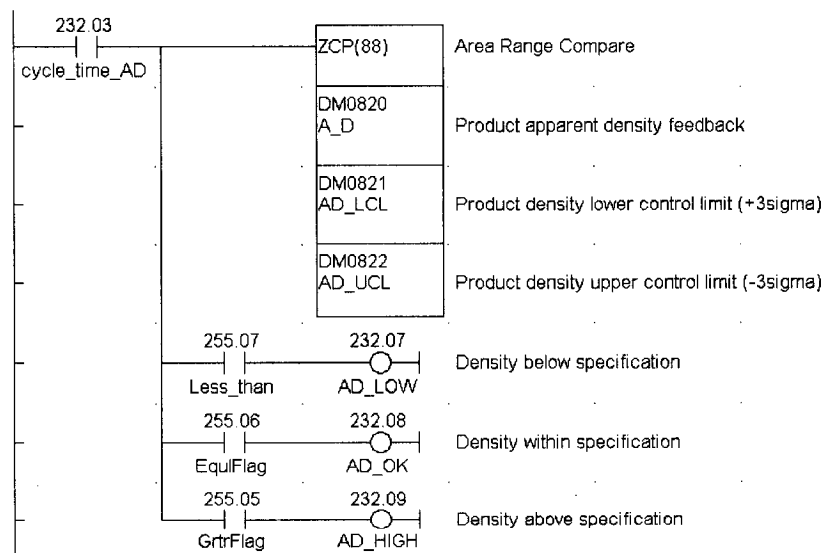


Figure 6.9: Product apparent density monitoring algorithm

When the execution condition is OFF, area range compare ZCP is not executed. When the execution condition is ON, ZCP compares A_D to the range defined by the lower and upper limits of product apparent density specification and outputs the result to the GR, EQ and LE flags.

Flags: EQ \rightarrow ON if $AD_LCL \leq A_D \leq AD_UCL$

LE \rightarrow ON if $A_D < AD_LCL$

GR \rightarrow ON if $A_D > AD_UCL$

When A_D goes above or below the control limits, ZCP turns ON the GR or LE flags and the designated bits are set: AD_HIGH or AD_LOW . Intervention is requested on the HMI:

1. Verify input material size distribution.
2. Check feeding tanks.

Once product apparent density falls back into the specified range, AD_OK is set and full execution is returned to the control agent. Plant personnel are advised every 3-4 hours, which corresponds to the algorithm cycle time that follows product density tests performed by the operators.

The outlet trunnion pressure is also monitored to verify air flow rate inside the mill which dictates product size. It was demonstrated in section 3.3.3 that outlet trunnion pressure dP_o is proportional to air flow rate Q . A decrease in outlet pressure is compensated by an air flow rate increase and vice versa to maintain suction air flow constant throughout the campaign. The ladder diagram of the algorithm is shown in figure 6.10.

When the execution condition is OFF, ZCP is not executed. When the execution condition is ON, ZCP compares dP_o to the range defined by the lower and upper control limit of outlet trunnion pressure at specific air flow rate and outputs the result to the GR, EQ and LE flags. When dP_o goes above dP_o_UCL , ZCP turns ON the GR flag and SUB subtracts 100ACFM (0.0472m³/sec) to Air_flow_sp . On the other hand, when dP_o goes below dP_o_LCL , ZCP turns ON the LE flag and ADD adds 100ACFM (0.0472m³/sec) to Air_flow_sp . A corrected air flow rate set point $Air_flow_sp_C$ can therefore be supplied to the air flow rate PI controller. The algorithm allows adaptation to suction circuit

resistance variations and operates every 10 seconds to alleviate pressure signal noise induced by turbulence.

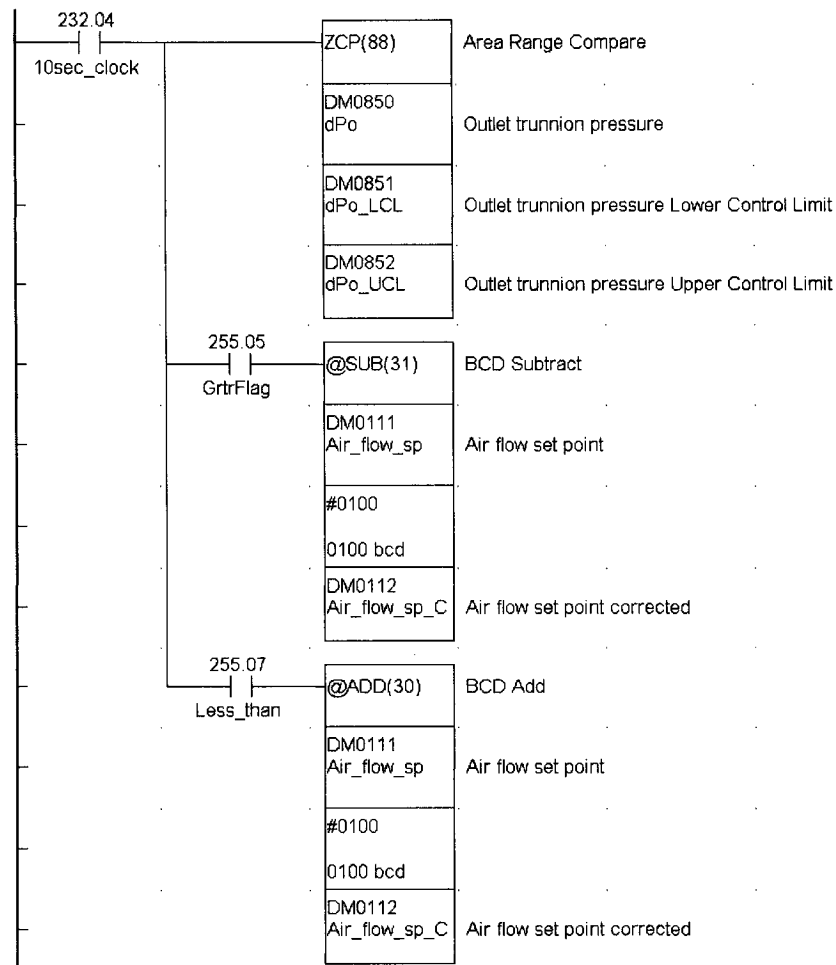


Figure 6.10: Outlet trunnion pressure monitoring algorithm

The ball mill is emptied after each product campaign to prevent cross-contamination. As discussed in section 5.4.5.4, if a campaign is started in the region of the acceptable feed rate range, the time required to reach the optimum powder charge is too long. Out of specification ground shot is produced for as long as 8 hours since at low powder filling, much of the energy of the tumbling balls is taken in steel-to-steel contacts to overgrind the particles. An algorithm, shown in figure 6.11, is created to suspend the feed rate rule-based sub-model and PID control algorithm and apply maximum feed rate. Once the

powerdraw is above P_{opt} 2kW, the halted feed rate sub-model is restarted at \dot{m}_{start} and full execution is returned to the control agent.

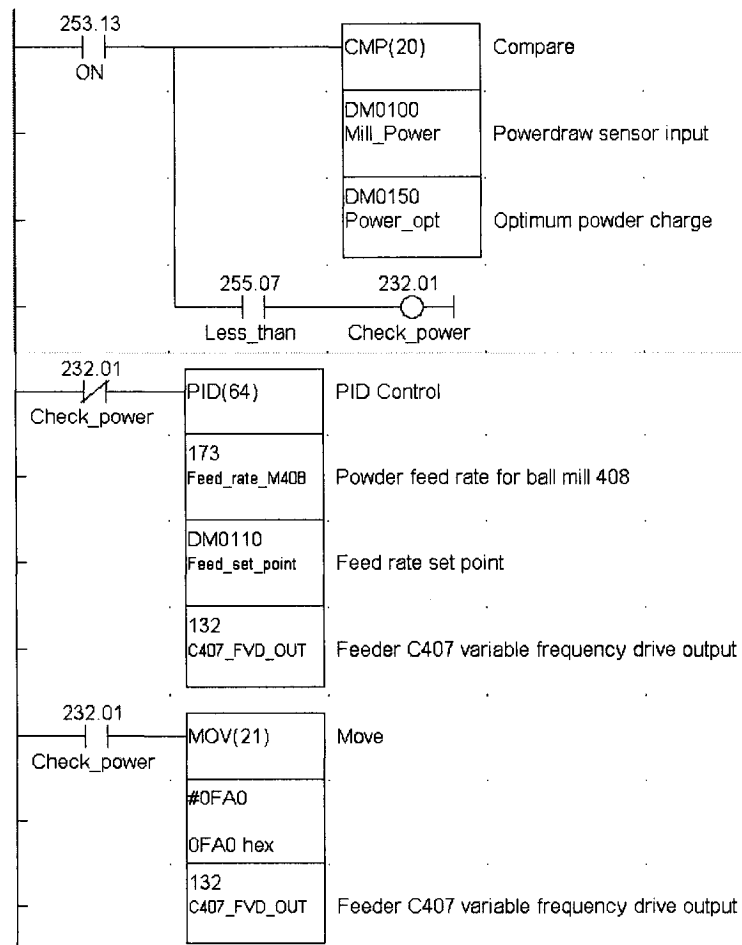


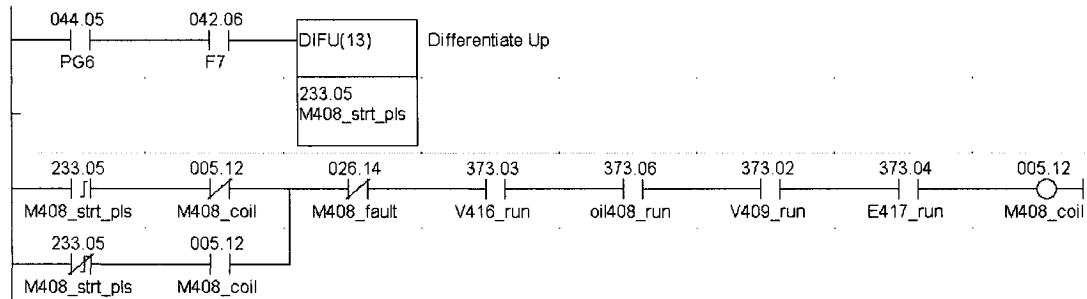
Figure 6.11: Loading phase monitoring algorithm

When the execution condition is OFF, CMP is not executed. When the execution condition is ON, CMP compares *Mill_Power* and *Power_opt* and outputs the result to the GR, EQ and LE flags. At startup, when *Mill_Power* is below *Power_opt*, CMP turns ON the LE flag to set *Check_power* that will suspend the PID function and force maximum output: FA0hex in *C407_VFD_OUT* to supply 20mA to the variable frequency drive (maximum speed). Once the optimum powerdraw is reached, CMP resets *Check_power* and full execution is returned to the PID function.

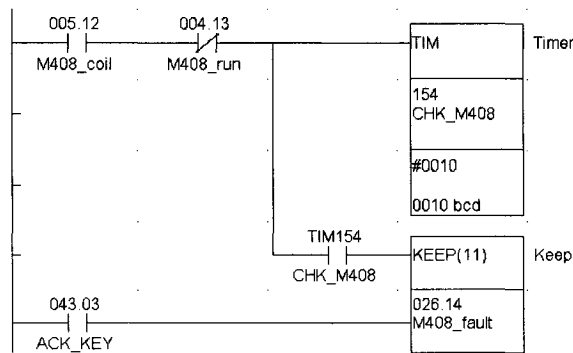
6.0 CONTROL AND MONITORING

Finally, as described in section 5.4.5.8, any equipment malfunction of the grinding process is detected and the control model interprets the diagnostics for action. The equipment monitoring algorithms operate at fastest PLC cycle time (30ms).

Examine ball mill 408 motor holding relay:



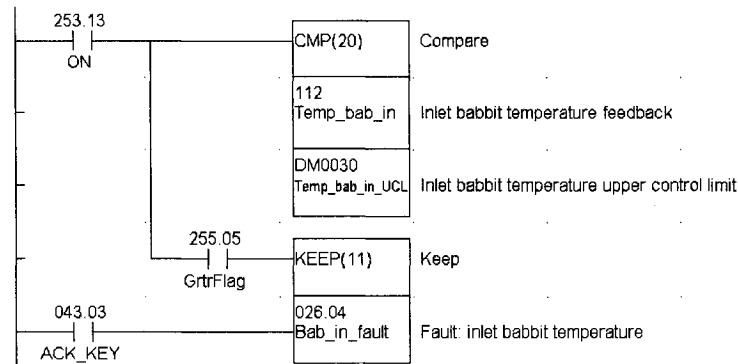
Once the execution condition are set (*V416_run*, *oil408_run*, *V409_run*, *E417_run*), the operator can start *M408_coil* by pressing the F7 key while being on page 6 on the HMI. As shown below, *M408_run* is monitored to ensure that the motor starter is working properly.



When *M408_coil* is set, the run confirmation relay *M408_run* must turn ON to confirm good operation. Any motor malfunction is detected by the overload protection of the starter and *M408_run* does not turn ON with an energized starter coil. A timer is activated when its execution condition goes ON (*M408_coil* ON AND *M408_run* OFF) and is reset when the execution condition goes OFF. Once activated, TIM measures in units of 0.1sec from the set value: 1.0sec for overload protection. If the execution remains long enough for TIM to time down to zero, the completion flag *CHK_M408* for the timer

number used turns ON and remains ON until TIM is reset, i.e., until its execution condition goes OFF. When *CHK_M408* turns ON, KEEP sets ON the designated bit *M408_fault*. Intervention is requested on the HMI and the process is stopped: *M408_fault* ON resets the holding relay of BM408 motor. Once the error is fixed, the operator resets *M408_fault* with the *ACK_KEY* on the HMI. Full execution is returned to the control agent and BM408 motor can be restarted.

Ball mill babbitt temperatures are monitored to validate powder charge sub-model:



When *Temp_bab_in* goes above the upper control limit *Temp_bab_in_UCL*, the greater flag turns ON to set *Bab_in_fault*. Intervention is requested on the HMI for babbitt lubrication verification and the powder charge sub-model is halted. The process continues with reduced data. Once the fault is corrected, the operator resets *Bab_in_fault* with the *ACK_KEY* on the HMI and full execution is returned to the control agent.

Similar algorithms have been programmed for fluid drive and speed reducer temperature monitoring.

6.4 Controller hardware

The ball mill process model is integrated using a programmable logic controller manufactured by Omron. The controller hardware architecture is composed of a central processing unit (CPU), communication board, backplane, I/O digital units, I/O analog units, temperature sensor units, DeviceNet master unit, remote I/O digital units, remote I/O analog units, remote temperature input unit and a human machine interface (HMI). The PLC components are presented below along with specifications and related sensor variables.

- CPU: C200HG-CPU43
 - Operating system: firmware Omron
 - Clock speed: 25MHz
 - Program capacity: 15.2K words
 - Basic instruction execution time: 0.15µsec
 - Ball mills program scan time \approx 30ms
 - Slotted on the backplane
- Communication board: C200HW-COM06-EV1
 - RS-422/485 port, RS-232C port
 - Slotted on the CPU unit
 - Variables: *S100* and *S200*
 - RS-485 communication with automatic sieve analyzer
- Backplane: C200HW-BC101
 - 10 I/O unit slots

The following units are slotted on the CPU's backplane.

- Digital input unit: C200H-ID212
 - 16 input points 24VDC +10%/-15%
 - Input response time: 1.5ms max.
 - Variables:
 - Powder feeder run confirmation
 - Ball mill run confirmation
 - Ball feeder inputs
 - High level dust collector
 - Ball mill gear oil flow
 - Low level oil ball mill gear

- Digital output unit: C200H-OC225
 - 16 relay output points
 - 250VAC max or 24VDC max
 - 2A/pt. or 8A/16pt. max. load current
 - Output response time: 10ms max.
 - Variables:
 - Powder feeder variable frequency drive starter
 - Ball mill motor starter
 - Ball feeder outputs

- Analog input unit: C200H-AD003
 - 8 analog current inputs: 4-20 mA
 - Resolution: 1/4000 (full scale)
 - Converted output data: 16-bit binary data
 - Accuracy: $\pm 0.6\%$ of full scale (0° to 55°C)
 - Conversion time: 1.0 ms/point
 - Variables:
 - Mill powerdraw
 - Outlet trunnion pressure
 - Powder feed rate
 - Air flow rate

- Analog output unit: C200H-DA004
 - 8 analog current outputs: 4-20 mA
 - Resolution: 1/4000 (full scale)
 - Set data: 16-bit binary data
 - Accuracy: $\pm 0.8\%$ of full scale (0° to 55°C)
 - Conversion time: 1.0 ms/point
 - Variables:
 - Blower damper
 - Powder feeder

- Temperature sensor unit: C200H-TS001
 - Temperature sensor: thermocouple type K, J, and L
 - 4 input points/unit
 - Output code to PLC: 4-digit BCD
 - Accuracy: $\pm(1\% \text{ full scale} + 1^{\circ}\text{C})$
 - Conversion time: 1.2 sec max. per point
 - Variables:
 - Fluid drive temperature
 - Babbit temperatures
 - Dust collector temperature

- DeviceNet master unit: C200HW-DRM21-V1
 - Connection method: Multi-drop and T-branch
 - Communication baud rates and network distances:
 - 500000 bps: 100m max.
 - 250000 bps: 250m max.
 - 125000 bps: 500m max.
 - Max. number of connecting nodes: 64 (1 master unit and 63 slave units)
 - 1600 I/O points (800 input and 800 output points)

DeviceNet is a low-cost open protocol communication link to connect industrial devices (such as limit switches, photoelectric sensors, valve manifolds, motor starters, process sensors, bar code readers, variable frequency drives, and panel displays) to a network and eliminate expensive hardwiring. The direct connectivity provides improved communication between devices as well as important device-level diagnostics not easily accessible or available through hardwired I/O interfaces. DeviceNet is a simple networking solution that reduces the cost and time to wire and install industrial automation devices, while providing interchangeability of like components from multiple vendors. The following units are linked to the DeviceNet network.

- Remote transistor input unit: DRT1-ID16
 - 16 input points 24VDC +10%/-15%
 - Input response time: 1.5ms max.
 - Variables:
 - Feeding tank elevator run confirmation
 - Powder feeder elevator run confirmation
 - Blower run confirmation
 - Ground shot tank elevator run confirmation
 - Speed reducer cooling blower run confirmation
 - Ball mill gear oil pump run confirmation
 - Ball mill cooling water pump run confirmation
 - Ball mill motor cooling blower run confirmation

- Remote transistor output unit: DRT1-OD16
 - 16 relay output points
 - Supply voltage 24VDC +10%/-15%
 - 0.3A/pt. or 2.4A/16pt. max. output current
 - Output response time: 1.5ms max.
 - Variables:
 - Feeding tank elevator motor starter
 - Powder feeder elevator motor starter
 - Blower motor starter
 - Ground shot tank elevator motor starter
 - Speed reducer cooling blower motor starter
 - Ball mill gear oil pump motor starter
 - Ball mill cooling water pump motor starter
 - Ball mill motor cooling blower motor starter

- Remote analog input unit: DRT1-AD04H
 - 4 analog current inputs: 4-20 mA
 - Resolution: 1/30000 (full scale)
 - Converted output data: 0 to 7530hex full scale
 - Accuracy: $\pm 0.8\%$ of full scale (0° to 55°C)
 - Conversion time: 250 ms/4 points

- Remote analog output unit: DRT1-DA02
 - 2 analog current outputs: 4-20 mA
 - Resolution: 1/6000 (full scale)
 - Set data: 0 to 1770hex full scale
 - Accuracy: $\pm 0.8\%$ of full scale (0° to 55°C)
 - Conversion time: 4 ms/2 points
 - Variable:
 - Blower variable frequency drive

- Remote temperature input unit: DRT1-TS04T
 - Thermocouple type K, J, L, T and E
 - 4 input points/unit
 - Output code to PLC: 4-digit hexadecimal
 - Accuracy: $\pm(1\% \text{ full scale} + 1^{\circ}\text{C})$
 - Conversion time: 250ms/4 points
 - Variable:
 - Speed reducer temperature

The programmable logic controller configuration is presented in figure 6.12.

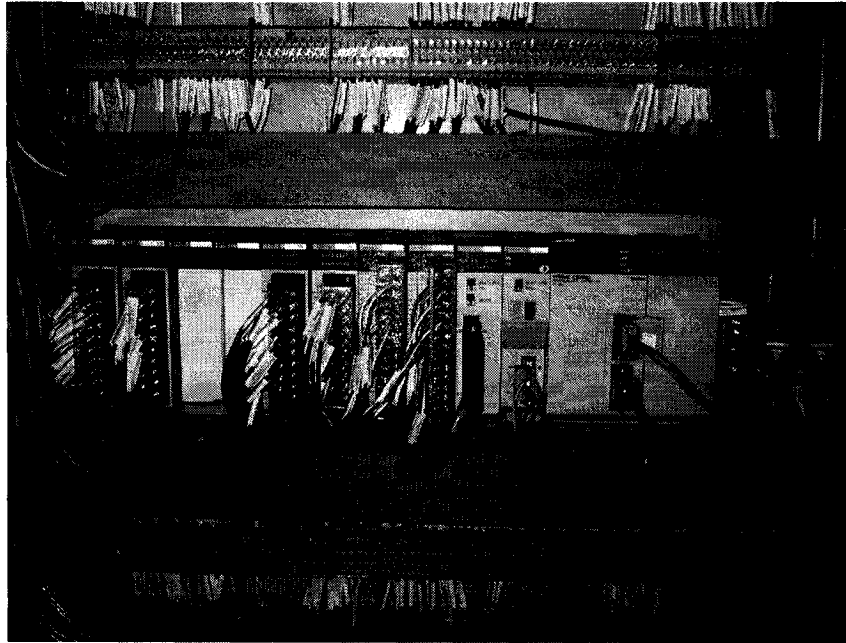


Figure 6.12: Programmable logic controller configuration

The CX-Programmer software is designed for use with Omron programmable logic controllers. It provides a straightforward method of creating, maintaining and testing programs, either offline or connected to a PLC. CX-Programmer runs in the Microsoft Windows environment and offers a comprehensive range of facilities such as:

1. New program creation
2. Program storage and editing
3. Uploading and downloading code to a PLC
4. Program status during execution by the PLC
5. Commenting programs (symbolic addresses, symbolic block and network names, comments)
6. Maintenance of library files
7. On-line editing
8. Function blocks

PLC programs can be constructed in ladder diagrams and a special statement list editor allows PLC programs to be seen and checked in mnemonic format.

A human machine interface is utilized by the operator for visualizing and controlling the ball mill process. It provides a simple way of presenting data from and inputting data to the PLC. Many features can be presented on the screen: motor statuses, actual rates,

alarms, messages, parameters, etc. The operator can perform tasks on the screen such as: starting or stopping motors, acknowledging alarms, entering desired values, choosing specific paths and parameters, etc. Ball mill 408 human machine interface page is presented in figure 6.13.

The human machine interface (HMI) is manufactured by EXOR:

UniOP – Universal Operator Panel Family: Model MKDR25-0045

Linked to the peripheral CPU port using a CPM1-CIF11 unit that converts the peripheral port to RS-422 communication protocol.

The following parameters are entered by the operator on the HMI:

- Product apparent density
- Ball bed height
- Campaign run time
- Product grade

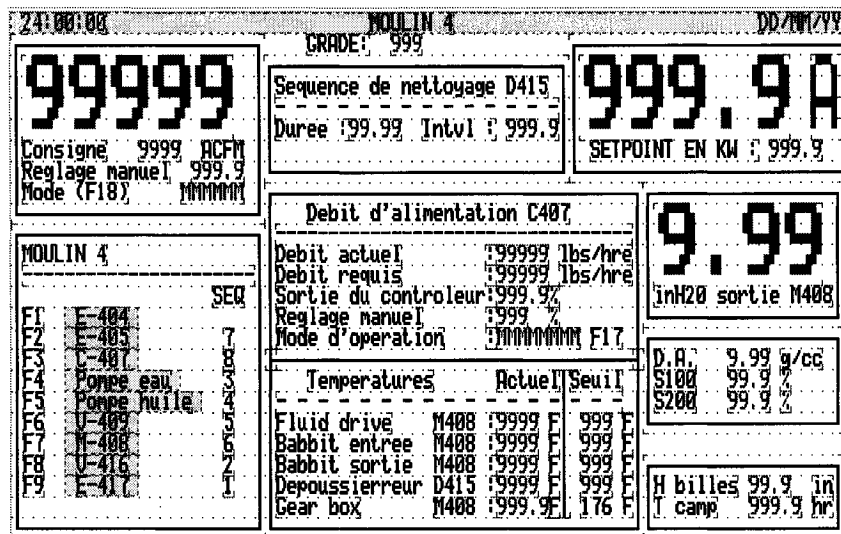


Figure 6.13: Ball mill 408 human machine interface page

The HMI is programmed using software called UniOP Designer. Figure 6.13 can be interpreted as follows: black numbers and letters represent passive text, red numbers 9 display actual values related to PLC addresses in numeric format, and red letters M and green rectangles show messages or states linked to bit status (ON or OFF) of the PLC.

Controller hardware specifications are presented in Appendix 6.

6.5 Conclusion

In this chapter, control and monitoring algorithms were created to integrate the ball mill model. The algorithms were developed in ladder diagram low-level PC language. The control algorithms calculate control parameters from process sub-models variables. The monitoring algorithms verify sensor data and state variables from the data model and assess whether sensor data have errors and the process is in control. The controller hardware architecture was designed using a PLC which implements the model architecture and handles multiple data streams and sub-models of different time scales.

7.0 RESULTS AND DISCUSSION

A new ball mill model was designed to integrate process sub-models composed of rules, equations and heuristics. The model-based control system was developed using an agent based architecture. This multi-agent system deals with multiple data streams and process sub-models of different sizes and operating time scales. The control strategy decouples the process parameters to simplify the sub-model equations, reduces unwanted interactions and allows low-level programming. Control and monitoring algorithms were developed in ladder diagram PC language. The controller hardware architecture was designed using a PLC which provides all the features needed to implement the multi-variables control system.

System performance was tested on ball mill 408 to validate the control strategy and demonstrate that ball milling product specifications are achieved at a 99.7% confidence interval ($\pm 3\sigma$). The reduction of size variations was greatly influenced by the frequency at which product properties were inputted to the controller. Therefore, product size results obtained by manual sampling and testing at the sieve analyzer designed frequency (every 15 minutes) were fed to the model for action.

Trial results are now presented, followed by future development recommendations to maximize ball milling process controllability.

7.1 Validation of the control system

In order to demonstrate control system performance, product properties were measured according to MPIF standard 04 and 05, as described in section 3.2.12, 3.3 and Appendix 2, and inputted into the process model during the production of grade S-1 on ball mill 408.

First, examine the graphs of figure 7.1 showing ball mill 408 product property results obtained without the model-based controller from April 14th 2005 to April 21st 2005. The

7.0 RESULTS AND DISCUSSION

x-axis represents the sample number, having a time scale of 3-4 hours, depending on operator's testing frequency.

Three different grades were produced:

S-1 (samples 2693 to 2697): $S200_{opt} = 63\%$, $\rho_o = 3.20\text{g/cm}^3$
S-4 (samples 2698 to 2704): $S200_{opt} = 53\%$, $\rho_o = 3.50\text{g/cm}^3$
S-2 (samples 2705 to 2712): $S200_{opt} = 48\%$, $\rho_o = 3.50\text{g/cm}^3$
S-1 (samples 2713 to 2722): $S200_{opt} = 63\%$, $\rho_o = 3.20\text{g/cm}^3$

Product specifications are shown in table 1.2 and Appendix 1.

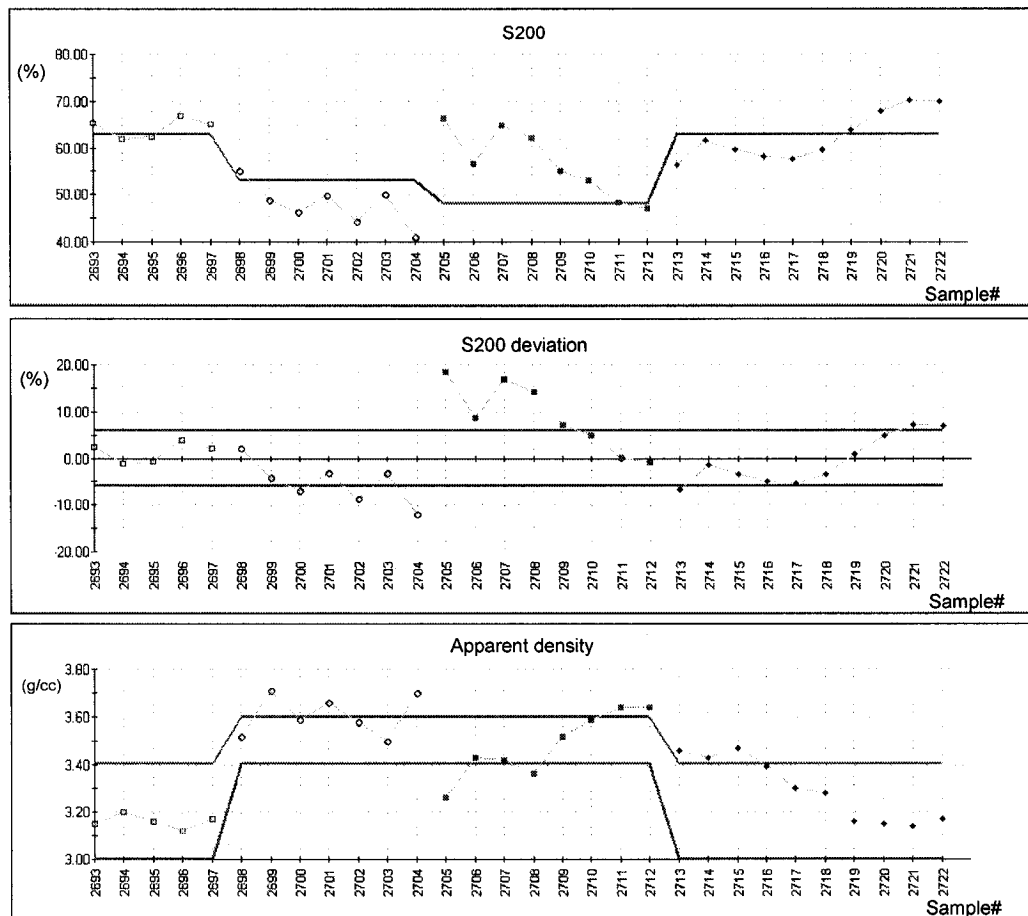


Figure 7.1: Ball mill 408 product property results

We can clearly see that the ball milling operation generates large product property variations similar to the ones presented earlier in table 1.1. Moreover, the properties are out of specification in many cases.

Now examine in more detail grade S-1 campaign #538 produced from samples 2713 to 2722 (last curves on the right side of the graphs of figure 7.1). The total campaign lasted 3 days, from 5pm April 19th2005 to 4am April 21st2005. Campaign results were ($\mu \pm 3\sigma$):

Product apparent density: $\rho_o = 3.30 \pm 0.41 \text{ g/cm}^3$

Product % passing a 200 mesh sieve: $S200 = 62.5 \pm 15.7 \%$

Once again, we find that the campaign shows large off-specification variations that reflect on all downstream operations and, therefore, on the final powder properties.

The model-based control system was applied to the ball milling process during campaign #538 from 1pm to 5pm on April 20th2005, between sample 2718 and 2719 of figure 7.1. The controller varied the output parameters according to the developed control strategy described in chapter 5:

- Maximize breakage rates using feed rate rule-based sub-model
 - Maintain P_{opt} with \dot{m} variations
- Adjust product size distribution using air flow rate rule-based sub-model
 - Control $S200$ with Q variations

Performance trial results are presented below:

Test # : Performance 1
 Date : 20-04-2005
 Time: 13:00 to 17h00
 Equipment: Ball mill 408
 Campaign #: 538
 Product : S-1

Control parameters:

$S200_{opt} = 63 \pm 4\%$ $P_{opt} = 214.2\text{kW}$
 $S100_{max} = 10\%$ $\rho_o = 3.20 \pm 0.20 \text{ g/cm}^3$
 $\dot{m}_{start} = 4000 \text{ lb/hr (1814.14 kg/hr)}$
 $Q_{start} = 5000 \text{ ACFM (2.360 m}^3\text{/sec)}$

Initial conditions @ t = 0: $\dot{m} = 3600 \text{ lb/hr (1632.9 kg/hr)}$
 $Q = 5200 \text{ ACFM (2.454 m}^3\text{/sec)}$

7.0 RESULTS AND DISCUSSION

Air flow rate variation with respect to $S200$ is presented in figure 7.2 along with $S100$ and ρ_o results. Adjustments are executed according to air flow rate sub-model rules described in section 5.4.4.7 and 6.2. Stronger air flow rate provides higher air velocity to pull out coarser and denser shot whereas smaller air flow rate sweeps finer and less dense product. Samples were taken every 15 minutes for product properties feedback. The sub-model therefore generated a new air flow rate set point every 15 minutes for the PI controller of the control model. The initial conditions were actual feed rate and air flow rate used by the operator at the beginning of the trial.

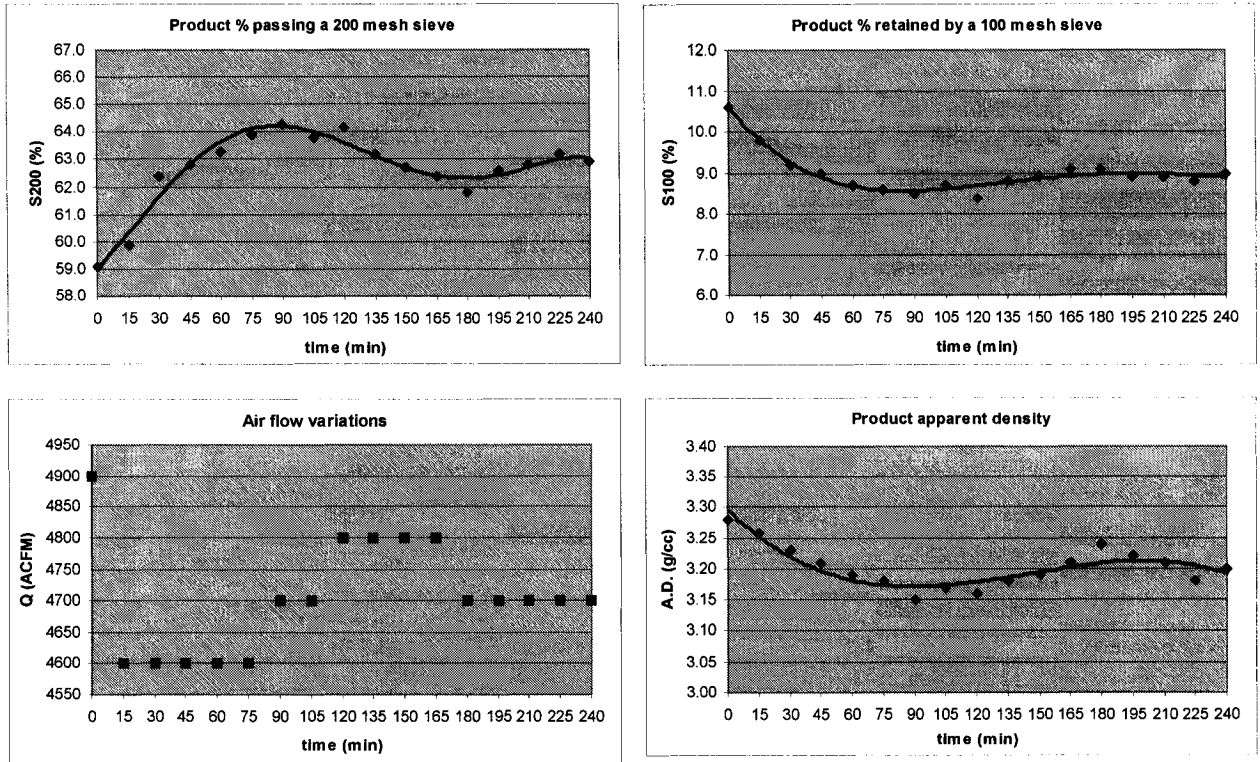


Figure 7.2 : Air flow rate variations with respect to $S200$

The air flow rate was changed according to the rule condition parts:

$$@ t = 0: S200 = 59.1\%$$

$$\text{if } S200_{opt} - 4 < S200 \leq S200_{opt} - 3 \text{ then } Q_{sp} = Q_{sp} - 300$$

$$Q = 5200 \rightarrow 4900 \text{ ACFM} \quad (2.454 \rightarrow 2.313 \text{ m}^3/\text{sec})$$

@ t = 15 min: $S200 = 59.9\%$

if $S200_{opt} - 4 < S200 \leq S200_{opt} - 3$ then $Q_{sp} = Q_{sp} - 300$
 $Q = 4900 \rightarrow 4600$ ACFM (2.313 \rightarrow 2.171 m³/sec)

@ t = 30 min: $S200 = 62.4\%$

if $S200_{opt} - 1 < S200 < S200_{opt} + 1$ then $Q_{sp} = Q_{sp}$
 $Q = 4600$ ACFM (2.171 m³/sec)

and so forth...

Looking at product property graphs of figure 7.2, we can observe that settling time from out to in specification using the controller is approximately 30 minutes. From 0 to 30 minutes, the fine portion of the ground product $S200$ increases to reach $S200_{opt}$ and the coarse portion $S100$ decreases below $S100_{max}$. Moreover, $S100$ also stabilizes around 9% in 30 minutes to confirm model statement 4. This was already expected from size distribution function validation results of section 3.3.2.

From 30 to 240 minutes, product properties are maintained with the following accuracy and precision ($\mu \pm 3\sigma$) :

$$\rho_o: 3.19 \pm 0.08 \text{ g/cm}^3$$

$$S200: 63.1 \pm 2.1 \%$$

For campaign 528, ρ_o and $S200_{opt}$ were $3.20 \pm 0.20 \text{ g/cm}^3$ and $63 \pm 4\%$ respectively.

The decoupled $S200$, $S100$ and ρ_o functions are similar to impulse responses of second order systems with poles in the left half S -plane of the Laplace domain. This behavior exhibits system stability.

After that, feed rate variations with respect to mill powerdraw are shown in figure 7.3. Adjustments are performed according to the rule-based feed rate sub-model described in section 5.4.4.6 and 6.2. The control strategy is to reach the optimum powder charge as fast as possible and to maintain it in order to maximize throughput and quality. Higher

7.0 RESULTS AND DISCUSSION

feed rate increases powerdraw attributable to powder and vice versa. Every 30 minutes, the sub-model supplies a new feed rate set point to the PI controller of the control model.

Powder charge was interpreted in a set of rules to generate new feed rates for the process:

@ t = 60 min: $P = 211.1\text{kW}$

if $P_{opt} - 7 < P \leq P_{opt} - 2$ *then* $\dot{m}_{sp} = \dot{m}_{sp} + 100$
 $\dot{m} = 3600 \rightarrow 3700 \text{ lb/hr}$ (1632.9 \rightarrow 1678.3 kg/hr)

@ t = 90 min: $P = 211.3\text{kW}$

if $P_{opt} - 7 < P \leq P_{opt} - 2$ *then* $\dot{m}_{sp} = \dot{m}_{sp} + 100$
 $\dot{m} = 3700 \rightarrow 3800 \text{ lb/hr}$ (1678.3 \rightarrow 1723.7 kg/hr)

and so forth...

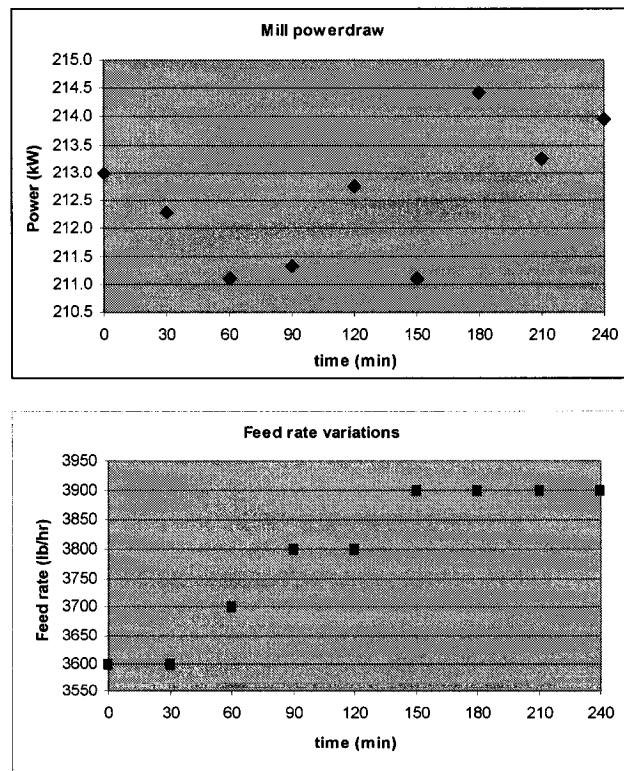


Figure 7.3 : Feed rate variations with respect to mill powerdraw

When the controller took command of the ball milling process, the mill was in emptying mode since most operators tend to vary feed rate while maintaining the air flow rate constant to achieve requested product size. Campaign #538 was started at a feed rate of 4800lb/hr (2177.2kg/hr) (sample 2713 on figure 7.1) and reduced down to 3600 lb/hr (1632.9 kg/hr) to grind finer. However, we know from plant trials explained in section 3.3 that product response time from air flow rate changes is much faster compared to feed rate changes. Inertial problems are therefore created since the effect of feed rate changes is seen only after few hours. This is seen on figure 7.1, where some grades were off-specification for as long as 12 hours (3-4 samples).

The developed control strategy regulates product size distribution with air flow rate and maximizes breakage rates with feed rate. The controller corrected product size in 30 minutes and optimized productivity by increasing feed rate from 3600 to 3900 lb/hr to reach and maintain P_{opt} , as presented in figure 7.3.

Model-based controller results correspond well with the required specific objectives presented in table 1.2. Domfer ball milling specifications are achieved at a 99.7% confidence interval ($\pm 3\sigma$). Moreover, the very good density results obtained using single point measurement to characterize product size distribution and to apply control actions confirm model statements 5, 8 and 9 presented in section 5.4.1.

Plant results obtained without and with the model-based control system for grade S-1 production are:

<u>Without controller ($\mu \pm 3\sigma$)</u>	<u>Model-based control system ($\mu \pm 3\sigma$)</u>
$\rho_o = 3.30 \pm 0.41 \text{ g/cm}^3$	$\rho_o = 3.19 \pm 0.08 \text{ g/cm}^3$
$S200 = 62.5 \pm 15.7 \%$	$S200 = 63.1 \pm 2.1 \%$
	Settling time: $T_s = 30$ minutes
	The model-based control system is stable.

This section shows the validation of the control system. Domfer is in the process of installing the required sensors and system. However, manual testing was done only once, and further validation is necessary for longer periods of time.

7.2 Future development

As presented in section 7.1, the model based control system created in this thesis performs very well and achieves the required objectives and product specifications. However, a number of recommendations are made for future development to maximize process variable controllability, and consequently, product quality.

First, the used impact tank discharge valve is a butterfly valve held partially open which causes a leak in the suction circuit and generates a upward air flow rate in the tank. Installing a new airlock rotary valve to replace the butterfly valve would have the following advantages:

1. Maximum air flow rate inside the mill increased by 10%.
2. Fines settling at the bottom of the impact tank greatly optimized.
3. Dust rate decreased by 50%.
4. Size distribution of product discharging by gravity from the tank stabilized to favor more representative samples for optimum control.
5. Suction circuit resistance variations reduced to decrease air flow rate standard deviation and allow better control precision (smaller ΔQ_{min}) for product size fine tuning.

Second, putting in place a new heat exchanger designed to cool the oil of the fluid drive at high percentage slip would enable ball mill rotational speed variation with respect to liner wear. The control strategy would be to start with a new set of inlet and outlet liners at minimum rotational speed ($\phi_c = 0.71$), then increase the speed gradually as the lifting efficiency decreases with liner wear, up to maximum speed ($\phi_c = 0.77$) for a worn out set, in order to keep constant charge motion and applied strain energy to the particles. Moreover, the increased rotational speed with respect to liner wear would maximize mill powerdraw and breakage rates.

Third, an absolute vacuum pressure transmitter should be installed on the suction circuit just after the outlet trunnion to monitor the effectiveness of the sweeping action. This transmitter would be independent of atmospheric pressure changes, which are quite high inside the plant, and would provide better air flow rate surveillance from the diagnostic system.

Fourth, the effect of input material properties on the milling dynamics should be evaluated to adapt the process sub-models for each grade produced. Atomized shot chemistry, apparent density and size distribution would be inputted to the control model for action. Any change in the feed material size distribution directly affects the grinding media size distribution and hence the breakage rates. For ball mills, coarse breakage rates decrease as the feed size increases. The coarser feed contributes less as a grinding media and is instead a burden which requires to be ground. This reflects on ball mill performance, where a feed size reduction results in an augmentation of throughput. Moreover, carbon and silica are known to increase the hardness of the shot particles which become more brittle. Therefore, less strain energy per ton is required for size reduction, which also results in an increase of throughput.

Finally, with stable upstream and downstream processes, the effect of ball mill product properties on finished powder properties should be investigated. Table 7.1 shows a comparison between MP2 and MP3 final product properties.

Table 7.1: MP2 and MP3 final product properties

	<u>Density (g/cm³)</u>	<u>Compressibility (g/cm³)</u>	<u>Green Strength (psi)</u>	<u>Flow (sec)</u>
MP 2	2.94	6.76	1150 (7929 kPa)	28
MP 3	2.61	6.66	1246 (8591 kPa)	32

MP2, which is the grade with the lowest residence time (Table 3.3 and 3.6), has the highest bulk density and compressibility with lower green strength and flow. Since the particles spend less time being deformed, the initial sphericity of the atomized shot is conserved allowing better particle arrangement for bulk density and compressibility and providing a faster flow to fill the dies. However, this is detrimental to green strength

7.0 RESULTS AND DISCUSSION

since the particles do not have enough attachment points to hold for green machining. In that case, MP3, with a more irregular shape, provides better green strength.

Moreover, dimensional change after sintering is directly affected by the size distribution of the ball milled products. After compaction, the sintering process provides solid-state diffusion and bonding between the powder particles. If a substance reacts chemically and the reaction occurs at constant temperature and constant pressure, then the Gibbs function is:

$$(dG)_{T,P} \leq 0 \quad (7.1)$$

A criterion for chemical equilibrium for a reaction that occurs in a closed system at constant temperature and pressure is that the Gibbs function be a minimum:

$$(dG)_{T,P} = 0 \quad (7.2)$$

The reaction can continue only as long as the Gibbs function continues to decrease. The reaction cannot proceed if the Gibbs function increases, because a violation of the second law of thermodynamics would occur.

The Gibbs function that needs to be minimized is expressed as:

$$G = G_o + \gamma A \quad \text{where } \begin{array}{l} G = \text{free Gibbs energy} \\ G_o = \text{initial energy of the system} \\ \gamma = \text{surface energy} \\ A = \text{free surface} \end{array} \quad (7.3)$$

Also,

$$dG = \gamma dA \quad (7.4)$$

In the case of multiple surfaces,

$$\sum \gamma_i A_i \Rightarrow \text{minimize} \quad (7.5)$$

Assuming that γ is constant for all particles, we find that A has to be minimized. Diffusion and bonding between the powder particles allows reduction of free surfaces during sintering. The driving force of the reaction is to minimize free surfaces. A finer product having greater free surface reduction potential reacts faster, expands less or even

tends to shrink. This is seen in table 7.2 by comparing MP2 with MP1, where MP1 shows less growth after sintering.

Table 7.2: MP2 and MP1 dimensional change comparison

	<u>-200mesh (75μm) (%)</u>	<u>Dimensional change(in/in)</u>
MP2	48	0.0020 (0.051 mm/mm)
MP1	62	0.0002 (0.005 mm/mm)

7.3 Conclusion

In this chapter, the control system was validated on ball mill 408 at Domfer Metal Powders during the production of grade S-1. Initially, trials showed large off-specification variations that reflected on all downstream operations and, therefore, on final properties. Once the controller was activated, the required product property specifications were achieved within 30 minutes at a 99.7% confidence interval. Very good apparent density results were attained using single point measurement to apply control actions, which confirmed the model statements. However, manual testing was done only once, and further validation is necessary for longer periods of time. Finally, recommendations were made for future development to maximize process variable controllability, and, insights were given on the effect of ball mill product properties on finished powder properties for further evaluation.

8.0 CONTRIBUTION TO KNOWLEDGE AND BENEFITS TO INDUSTRY

8.1 Contribution to knowledge

The phenomena of interest in the ball milling process tend to be dynamic and non-linear, and the variables that can be measured are not the ones that lead to direct control of the process. Traditional control architectures based on PID control mechanisms do not cope well with this type of process, since the mechanisms typically assume relatively stable processes that are fixed, linear, and time-invariant. For the most part, present day control of manufacturing processes is non-adaptive and based on maintaining control variables at or near fixed points [15]. Model-based control built on the integration of process know-how allows the estimation of process dynamics based on first principles and a highly adaptive control system can be implemented.

The non-linear and oscillatory behavior of many particulate processes, such as metal powder ball milling, implies the need to implement non-linear model-based feedback controllers to ensure a stable and efficient operation. In spite of the rich literature on population balance modeling, numerical solution, and dynamical analysis of particulate processes, research on model-based control of such processes has been very limited [62].

This thesis provides a general framework for the creation of practically implementable, non-linear feedback controllers for particulate processes that allow the achievement of desired particle size distributions. Examples of particulate processes include the crystallization of proteins for pharmaceutical applications, the emulsion polymerization reactors for the production of latex, the aerosol synthesis of titania powder used in the production of white pigments, the thermal spray processing of nanostructured coatings, crystallizers, aerosol reactors, cell cultures, cement production, and, obviously, metal powder manufacturing processes.

Powder metallurgy has become a proven method of parts production and is now considered to be a good alternative in the manufacture of many components. Areas of

rapid growth include aerospace applications, advanced composites, electronic components, magnetic materials and metalworking tools. The powder metallurgy process generally consists of four basic steps: metal powder manufacturing, mixing, compacting and sintering. The attributes of powder metallurgy products are very dependent on the characteristics of the metal powders used. Chemistry and purity, particle size distribution, particle shape and surface texture are important properties and characteristics of the metal particles.

The creation of a model-based control system for ball milling optimizes the overall metal powder manufacturing process. The reduction in product size variations provides a stable input material that enhances the controllability of downstream processes, which reflects on final powder properties, and, therefore, on the quality of powder metallurgy products.

This thesis, which is the first industrial application of model-based control using an agent-based architecture, serves as a guideline for other areas of research using the same architecture, such as advanced control of forming processes [15].

New techniques were developed to include metal powder ball mill physics into design and computer models:

- Multi-point measurement of used liners to create a 3-D model of the inside grinding volume and to allow ball feed rate corrections based on ball bed height verification.
- Product rate inference using feed rate, dust rate and the variation of powder charge with respect to time.
- Using the repeatability and reproducibility limits of apparent density and sieve analysis results to determine product response time and minimum powder charge and air flow rate variations to significantly affect product properties.
- Size distribution function validation to enable two point measurement for ball mill product size characterization and control.

These techniques can be applied to improve other milling processes in the cement and mining industries.

The approach of decoupling ball mill process variables can be followed to simplify model development, improve process controllability, eliminate unwanted controller interactions, deal with different time scales and allow low-level programming in the development of practically implementable model-based controllers.

A new control strategy was established:

1. Maximize breakage rates with feed rate variations based on inferential measurement of powder charge using powerdraw sensor data.
2. Control product properties with air flow rate adjustments based on size results.

The low-level control and monitoring algorithms developed can be easily implemented on widely used and cost friendly controllers. Newly developed artificial intelligence controllers can use the ladder diagram programming of the rule-based sub-models. Moreover, controller hardware design can be a reference to integrate process models with similar control architectures and strategies.

Heuristic control systems have already been done for closed-circuit (coarse particle recirculation) wet ball milling [2,7], secondary cone crushing [58] and cement milling [13]. This is the first heuristic control system applied for dry metal powder grinding.

Complete investigation over major sampler manufacturing companies was achieved to find an appropriate automatic sampler. However, the existing samplers had design flaws or did not suit the application. A new automatic sampler for metal powder, working in conjunction with a sieve analyzer, was therefore created to supply product feedback at a faster frequency. The rugged and flexible design can be utilized in many other powder manufacturing applications.

8.2 Benefits to industry

The Canadian economy has historically been based on natural resources. Nowadays, areas of rapid growth in powder metallurgy provide Canadian companies with the opportunity to compete worldwide in metal powder manufacturing processes. To be

competitive, a high-level of sophisticated automation is required to produce large quantities of metal powder at the lowest cost and highest quality. Advanced control is the core of an optimum modern manufacturing operation.

The Domfer process is unique. Worldwide, it is the only metal powder manufacturing process where cast iron shot is ball milled. The irregular shape of the ground particles provides very good green strength, which is required to maintain smooth surfaces, sharp corners, and intricate details during ejection from the compacting die or tooling and the subsequent transfer to the sintering operation. Also, the production of cast iron powders is very promising for infiltration, impregnation and friction applications. Brake pads manufactured with the use of cast iron powders show high wear resistance, high friction factor and good polymer-powder cohesion.

Domfer Metal Powders will greatly benefit from advanced control technologies, especially model-based control, since it represents a breakthrough in the way complex machinery is operated. This Canadian technology, if exploited properly, will endow Domfer with a serious lead on the competition.

In addition to using the method of model-based control for ball milling, Domfer can apply the new technology for other complex equipment, such as electrical decarburizing furnaces and attrition mills, to upgrade their overall process and to create a new line of products of the highest quality.

9.0 CONCLUSION

The ball milling operation is critical since it determines many characteristics of the final products: density, dimensional change, green strength and compressibility. Based on the size distribution and density results, the operator adjusts feed rate, air flow rate and level of balls. The quality of the powder coming out of the ball mill is a function of operator experience and expertise since he has to simultaneously adjust all the variables for a desired size distribution and density. Highly variable input material properties constantly change the milling dynamics on the product. Also, samples are taken only every 3-4 hours, which cause inertial problems since the effect of parameter changes are seen only after a few hours. We saw in table 1.1 that the ball milling operation generates large variations in powder properties. Moreover, advances in testing tools and process know-how in the field of mixing, compacting and sintering in powder metallurgy has enabled Domfer's customers to test the powders more rigorously.

The goal of the research was to develop model-based control for the ball milling of metal powder. The objectives were: develop techniques to include process physics into design and computer models, develop process monitoring and fault diagnosis techniques, develop control strategies for model-based control and develop computer architectures for real-time model-based control. The research objectives were aimed at reducing product size variations while maximizing throughput, improving powder quality, and reducing energy cost, personnel cost and operating cost.

The literature on advanced process dynamics and control, size reduction theory, ball mill models and other existing grinding models was reviewed. It was found that model-based control had never been used in open-circuit dry ball milling of metal powder. The phenomena of interest in the ball milling process are dynamic and non-linear, and the measurable variables are not the ones that lead to direct control of the process. Traditional control architectures based on PID control mechanisms do not cope well with the ball milling process, since these mechanisms typically assume relatively stable processes that are fixed, linear and time-invariant. Process modelling permits the

9.0 CONCLUSION

estimation of ball milling dynamics based on first principles and a highly adaptive control system can be implemented if a good understanding of the process physics is available.

First, ball mill size reduction theory was presented as a basis for process characterization. Definitions, laws of grinding, powder characterization, performance trends, charge motion and media wear were outlined.

Then, the Domfer ball milling process was characterized. Process physics was described along with the measurability and controllability of the variables: input material properties, powder feed rate, grinding balls, liners, ball and powder charges, residence time, powerdraw, rotational speed, air flow rate, outlet trunnion pressure, product rate and product properties. Plant trials were executed on ball mill 408 to define overall system behavior and performance specifications of variables and sensors. The effect of feed rate and air flow rate on product properties was determined:

$$\text{Feed rate: } T_R = \frac{M_{p(\min)}}{\Delta \dot{m}}$$

$$\text{Air flow rate: } T_R = 4 \text{ min}$$

$$\Delta Q_{\min} = 100 \text{ ACFM}$$

There was no general agreement on what should constitute the minimum adequate characterization of product size distribution from a ball milling circuit; so, the size distribution function was validated. On a log-normal plot, ground shot exhibited a straight line behavior. An extended region of the results fitted a series of straight lines. Hence, it was demonstrated that two point measurement, the slope and intercept, is sufficient to characterize ball mill size distributions.

Next, an automatic sampler was created to work in conjunction with a fully automated sieve analyzer. The sampler fits on the inclined pipe under the impact tank and is mainly composed of a main body, holding parts, sampling part, sleeve, clevis base, retaining ring and non-rotating cylinder. From the plant trial results on product response time, the entire

sieve analysis process was fully automated to provide frequent product size feedback: every 15 minutes according to MPIF 05.

Most importantly, a new ball mill model was created. It integrates process sub-models composed of rules, equations and heuristics. The equations are simple, based on plant data and, most importantly, representative of the process. The model was implemented using an agent based architecture that can deal with multiple data streams and a loosely coupled network of related process sub-models of different sizes and operating time scales. A new control strategy was established:

- Maximize breakage rates with feed rate variations based on inferential measurement of powder charge using powerdraw sensor data.
- Control product properties with air flow rate adjustments based on size results.

The consideration of a multivariable process helped to identify the key model parameters, and gave insight into the problem. This led to the understanding that the key parameters could be decoupled due to the large time frame differences, i.e., for the main variables (feed rate, air flow rate, ball feed rate, ball and powder charges, and liner wear), the problem decomposed into several single parameter sub-models.

The model is composed of statements and the features of the agent based architecture, such as the control model, data model, process sub-models, diagnostic system and error recovery. The following sub-models were developed: liner wear, ball feed rate, powder charge, residence time, product rate, feed rate and air flow rate. As well, diagnostics and error recovery were developed for the size distribution function, product apparent density, outlet trunnion pressure, loading and emptying phases, parameter ranges, powerdraw vs feed rate, product size verification and equipment. The mathematical equations that determine the liner wear, ball feed rate, powder charge and residence time contribute to the control model, but it is the AI models for feed and air flow rate that are the heart of the control system. This is because the output of the powder grinding process is dominated by the near time frame factors: air flow rate and powder feed rate.

9.0 CONCLUSION

For real time control, information is needed simultaneously with respect to many of the process variables. The control strategy decouples process parameters to simplify the sub-model equations, reduce unwanted interactions and allow low-level computer control and monitoring. A programmable logic controller was selected to implement the model architecture features and achieve research objectives with good performance.

Furthermore, algorithms were developed in low-level PC language. Control algorithms were created to calculate output control parameters from process sub-models: powder feed rate, air flow and ball feed rate. Also, monitoring algorithms were created to monitor sensor data and state variables from the data model and assess whether sensor data have errors and the process is in control. The diagnostics are evaluated by the control model for action and error recovery agents are generated for process rehabilitation. Finally, controller hardware architecture was designed using a PLC manufactured by Omron. It is composed of a central processing unit, communication board, backplane, I/O digital units, I/O analog units, temperature sensor units, DeviceNet master unit, remote I/O digital units, remote I/O analog units, and remote temperature units. A human machine interface manufactured by Exor is linked to the PLC to allow the operator to visualize and control the ball milling process.

System performance was tested on ball mill 408 at Domfer Metal Powders during the production of grade S-1 to verify the control strategy. The reduction of size variations is greatly influenced by the frequency at which product properties are inputted to the controller. Product size results obtained by manual sampling and testing at the sieve analyzer designed frequency were fed to the model for action. Plant trial results obtained without and with the model-based control system are:

Without controller ($\mu \pm 3\sigma$)

$$\rho_o = 3.30 \pm 0.41 \text{ g/cm}^3$$

$$S200 = 62.5 \pm 15.7 \%$$

Model-based control system ($\mu \pm 3\sigma$)

$$\rho_o = 3.19 \pm 0.08 \text{ g/cm}^3$$

$$S200 = 63.1 \pm 2.1 \%$$

Initially, the trials showed large off-specification variations that reflected on all downstream operations and, therefore, on the final properties. Once the controller was

activated, the required product property specifications were achieved within 30 minutes and maintained with the above accuracy and precision. Moreover, the system exhibited stability. Model-based controller results corresponded well with the required specific objectives presented in table 1.2. Domfer ball milling specifications were attained at a 99.7% confidence interval. In addition, very good product apparent density results were achieved using single point measurement to apply control actions, which confirmed the model statements.

The control system was validated. Domfer is in the process of installing the required sensors and system. However, manual testing was done only once, and further validation is necessary for longer periods of time.

Recommendations were made for future development to maximize process variable controllability, and consequently, product quality: an air lock rotary valve at the bottom of the impact tank, a new heat exchanger for ball mill fluid drive, an absolute vacuum pressure transmitter to monitor sweeping action, and the evaluation of input material properties on the milling dynamics. Insights were given on the effect of ball mill product properties on finished powder properties (density, compressibility, green strength, flow and dimensional change) for further evaluation.

The research objectives were accomplished. A new model-based control system was created for metal powder ball milling. This thesis provides a general framework for the creation of practically implementable, non-linear feedback controllers for particulate processes that allow the achievement of desired particle size distributions. The system optimizes the metal powder manufacturing process. The reduction in size variation produces a stable input material that enhances the controllability of downstream processes, which reflects on final powder properties, and, therefore, on powder metallurgy product quality. This project is the first industrial application of model-based control using an agent-based architecture. It supplies a guideline for other areas of research using the same architecture.

9.0 CONCLUSION

New techniques were developed to include metal powder ball mill physics into design and computer models:

- Multi-point measurement of used liners to create a 3-D model of the inside grinding volume and to allow ball feed rate corrections based on ball bed height verification.
- Product rate inference using feed rate, dust rate and the variation of powder charge with respect to time.
- Using the repeatability and reproducibility limits of apparent density and sieve analysis results to determine product response time and minimum powder charge and air flow rate variations to significantly affect product properties.
- Size distribution function validation to enable two point measurement for ball mill product size characterization and control.

The low-level control and monitoring algorithms developed can be easily implemented on widely used and cost friendly controllers. Newly developed artificial intelligence controllers can apply the ladder diagram programming of the rule-based sub-models. Moreover, controller hardware design can be a reference to integrate process models with similar control architectures and strategies in other applications. Very few industries exist today that do not employ programmable logic controllers. The PLC uses ladder diagram PC logic which is the most widely used low-level PC language.

Domfer Metal Powders will greatly benefit from this advanced control technology since it represents a breakthrough in the way complex machinery is operated. If exploited properly, this Canadian technology will endow Domfer with a serious lead on the competition with respect to product quality and competitiveness. Moreover, Domfer can apply the new technology for other complex equipment, such as electrical decarburizing furnaces and attrition mills to upgrade their overall process and to create a new line of powders with the highest quality.

REFERENCES

1. DeGarmo, E.Paul, J Temple Black and Ronald A. Kohser, 1988, Materials and Processes in Manufacturing, Macmillan Publishing Company, p.376-392.
2. Conradie, A.V.E and C. Aldrich, 2001, Neurocontrol of a ball mill grinding circuit using evolutionary reinforcement learning, Minerals Engineering, Vol.14, No.10, p.1277-1294.
3. Galan, O., G.W. Barton, J.A. Romagnoli, 2002, Robust control of a SAG mill, Powder technology, Vol.124, p.264-271.
4. Herbst, J.A., W.T. Pate and A.E. Oblad, 1992, Model-based control of mineral processing operations, Powder Technology, Vol. 69, p.21-32.
5. Valery, W. and S. Morrell, 1995, The development of a dynamic model for autogenous and semi-autogenous grinding, Minerals Engineering, Vol.8, No.11, p.1285-1297.
6. Pomerleau, André, Daniel Hodouin, André Desbiens and Éric Gagnon, 2000, A survey of grinding circuit control methods : from decentralized PID controllers to multivariable predictive controllers, Powder Technology, Vol.108, p.103-115.
7. Spring, R. and M. Franklin, 1991, Intuitive process control system programming, IFAC Expert Systems in Mineral and Metal Processing, Espoo, Finland, p.7-11.
8. Elber, L., D. Thomson, and G. Johnson, 1994, Development of a control system for a SAG-B-C grinding circuit, Minerals Engineering, Vol.7, No.2-3, p. 153-167.

9. Ivezic, Dejan D. and Trajko B. Petrovic, 2003, New approach to milling circuit control – robust inverse Nyquist array design, International Journal of Mineral Processing, Vol.70, p.171-182.
10. Apelt, T.A., S.P. Asprey and N.F Thornhill, 2001, Inferential measurement of SAG mill parameters, Minerals Engineering, Vol.14, No.6., p.575-591.
11. Apelt, T.A., S.P. Asprey and N.F Thornhill, 2002, Inferential measurement of SAG mill parameters II: state estimation, Minerals Engineering, Vol.15, p.1043-1053.
12. Apelt, T.A., S.P. Asprey and N.F Thornhill, 2002, Inferential measurement of SAG mill parameters III: inferential models, Minerals Engineering, Vol.15, p.1055-1071.
13. Topalov, Andon Venelinov and Okyay Kaynak, 2004, Neural network modeling and control of cement mills using a variable structure theory based on-line learning mechanism, Journal of Process Control, Vol.14, p.581-589.
14. Christofides, Panagiotis D., 2002, Model-based control of particulate processes, Kluwer Academic Publishers, p.1-7.
15. Thomson, Vincent, Benoit Boulet, Robert DiRaddo and Patrick Girard, 2004, An Agent Based Architecture for Model Based Control, IEEE Systems, Man and Cybernetics, Oct04 Conference, The Hague.
16. Rumpf, H., 1977, Physical Aspects of Comminution and New Formulation of a Law of Comminution, Powder Technology, Vol. 7, p.145-159.
17. Austin, L.G., R.R. Klimpel and P.T. Luckie, 1984, Process Engineering of Size Reduction: Ball Milling, Society of Mining Engineers, p.3-70.

18. Mailer, P. de W., 1988, The feasibility of on-line measurement of the size distribution of a slurry, 1st IFAC Workshop on Applied Measurements in Mineral and Metallurgical Processing, South Africa.
19. Austin, L.G., R.R. Klimpel and P.T. Luckie, 1984, Process Engineering of Size Reduction: Ball Milling, Society of Mining Engineers, p.9-11.
20. Cho Heechan and Leonard G. Austin, 2002, The equivalence between different residence time distribution models in ball milling, Powder Technology, Vol. 124, p.112-118.
21. Watanabe, Hiroshi and Yoshihito Kondo, 1998, A study on critical rotational velocity in ball-milling, ATM, Vol.1 No.1, p.1-7.
22. Rittinger, R. P. von, 1857, Lehrbuck der Aufbereitungskunde, Ernst u. Korn, Berlin.
23. Rose, H.E., 1967, Proceedings, 2nd European Symposium Zerkleinern, H. Rumpf and W. Pietsch, eds., Dechema Monographien 57, Nr. 993-1026, Verlag Chemie, Weinheim, p.27-62.
24. Bond, F.C., 1960, Crushing and Grinding Calculations, British Chemical Engineering, Vol.6, p.378-391, 543-548.
25. Austin, L.G., R.R. Klimpel and P.T. Luckie, 1984, Process Engineering of Size Reduction: Ball Milling, Society of Mining Engineers, p.62-63.
26. Scarlett, Brian, 2002, Particle Populations – to balance or not to balance, that is the question!, Powder Technology, Vol 125, p.1-4.
27. Austin, L.G., R.R. Klimpel and P.T. Luckie, 1984, Process Engineering of Size Reduction: Ball Milling, Society of Mining Engineers, p.69-71.

28. Spring, R., C. Larsen and A. Mular, 1985, Industrial Ball Mill Modelling: Documented Application of the Kinetic Model, Canada Centre for Mineral and Energy Technology, p.1-35.
29. German, Randall M., 1994, Powder Metallurgy Science, Metal Powder Industries Federation, p.51-64.
30. Morrell, S., W.M. Finch, T. Kojovic and H. Delboni Jr., 1996, Modelling and simulation of large diameter autogeneous and semi-autogeneous mills, International Journal of Mineral Processing, 44-45, p.289-300.
31. Zeng, Yigen and Eric Forssberg, 1993, Monitoring grinding parameters by signal measurements for an industrial ball mill, International Journal of Mineral Processing, 40, p.1-16.
32. Teke, E., M. Yekeler, U. Ulusoy and M. Canbazoglu, 2002, Kinetics of dry grinding of industrial minerals: calcite and barite, International Journal of Mineral Processing, 67, p.29-42.
33. Radziszewski, P., 1999, Comparing Three DEM Charge Motion Models, Minerals Engineering, Vol.12, No.12, p.1501-1520.
34. Radziszewski, P. and S. Morrell, 1998, Fundamental Discrete Element Charge Motion Model Validation, Minerals Engineering, Vol.11, No.12, p.1161-1178.
35. Dong, H. and M.H. Moys, 2003, Load behavior and mill power, International Journal of Mineral Processing, Vol. 69, p.11-28.
36. Mishra, B.K., Rajamani R.K., 1994, Simulation of charge motion in ball mills, Part 1: experimental verifications, International Journal of Mineral Processing, Vol.40, p.171-186.

37. Mishra, B.K., Rajamani R.K., 1994, Simulation of charge motion in ball mills, Part 2: numerical simulations, International Journal of Mineral Processing, Vol.40, p.171-186.
38. Malghan, 1982, Methods to reduce steel wear in grinding mills, Minerals Engineering, Vol. 32, p.684-690.
39. Hlungwani, O., J. Rikhotso, H. Dong and M.H. Moys, 2003, Further validation of DEM modeling of milling: effects of liner profile and mill speed, Minerals Engineering, Vol. 16, p.993-998.
40. Radziszewski, Peter, 1997, Predictive model for ball mill wear, Canadian Metallurgical Quarterly, Vol.36, No.2, p.87-93.
41. Kelly, E.G., and D.J. Spottiswood, 1982, Introduction to Mineral Processing, Wiley, Toronto.
42. Radziszewski, P., 1991, Étude de l'automatisation du procédé de la comminution dans un broyeur à boulets, Thèse de Doctorat, Université Laval.
43. Radziszewski, P. and S. Tarasiewicz, 1993, Modelling and simulation of ball mill wear, Wear, 160, p.309-316.
44. Radziszewski, P. and S. Tarasiewicz, 1993, Simulation of ball charge and liner wear, Wear, 169, p.77-85.
45. Djordjevic, N., 2003, Discrete element modelling of the influence of lifters on power draw of tumbling mills, Minerals Engineering, Vol.16, p.331-336.
46. Rail, Alexandre, 1999, Integration of automated weighing system for metal powders, Master Thesis, Mechanical Engineering, McGill University.

47. Austin, L.G., R.R. Klimpel and P.T. Luckie, 1984, Process Engineering of Size Reduction: Ball Milling, Society of Mining Engineers, p.79-117.
48. Moys, M.H., M.A. van Nierop and I. Smit, 1996, Progress in measuring and modelling load behavior in pilot and industrial mills, Minerals Engineering, 9 (12), p.1201-1214.
49. Herbst, J.A. and W.T. Pate, 1999, Object components for comminution system softsensor design, Powder Technology, 105, p.424-429.
50. Napier-Munn, T.J., S. Morrell, R.D. Morrison and T. Kojovic, 1996, Mineral comminution circuits, Julius Kruttschnitt Mineral Research Centre, Australia.
51. American Davidson, 1983, Getting to know Gyrol Fluid Drives, Michigan Corporation.
52. ASTM E-1919-03, 2003, Standard Guide for Worldwide Published Standards Relating to Particle and Spray Characterization, American Society for Testing and Materials.
53. Pohl, Michael, 2004, Particle sizing: A quick look at new and improved methods, Powder and Bulk Engineering, Vol 18, No.2, p.21-27.
54. Austin, L.G., R.R. Klimpel and P.T. Luckie, 1984, Process Engineering of Size Reduction: Ball Milling, Society of Mining Engineers.
55. Hulbert, D.G., 1989, The state of the art in the control of milling circuits, IFAC Automation in Mining, Mineral and Metal Processing, Buenos Aires, Argentina.

56. Gupta, V.K., D. Hodouin and R.Spring, 1985, SPOC Manual Chapter 7.2: FINDBS computer program for breakage and selection functions determination in the kinetic model of ball mills, Report SP85-1/7.2, CANMET, Energy, Mines and Resources Canada.
57. Kookos, Ioannis K. and John D. Perkins, 2002, An algorithmic method for the selection of multivariable process control structures, Journal of Process Control, Vol. 12, p.85-99.
58. Meech, J.A. and L.A. Jordon, 1993, Development of a self-tuning fuzzy logic controller, Minerals Engineering, Vol.6, No.2, p.119-131.
59. Mao, W., 2003, Qualitative Model-based Fault Diagnosis Applied to Extrusion Blow Molding, Master Thesis, McGill University.
60. Batten, George L. Jr., 1994, Programmable Controllers: Hardware, Software & Applications, McGraw-Hill, p.4.
61. Batten, George L. Jr., 1994, Programmable Controllers: Hardware, Software & Applications, McGraw-Hill, p.81.
62. Christofides, Panagiotis D., 2002, Model-based control of particulate processes, Kluwer Academic Publishers.

Appendix 1

Domfer ball mill 408 technical drawings and specifications

Grenaille brute	But visé (%) -200 m	Maximum (%) +100 m	Guide densité	Moulins à billes	Autres grenailles
S-1	63 ± 4	6 %	3.20 ± 0.20	# 408, 308	S-14/15
S-2	48 ± 4	8 %	3.60 ± 0.20	# 408	S-16
S-3	70 ± 4	7 %	3.20 ± 0.20	# 408	-
S-4	53 ± 4	6 %	3.60 ± 0.20	# 408	-
S-5	65 ± 4	7 %	3.10 ± 0.20	# 208	-
S-6	48 ± 4	7 %	3.50 ± 0.20	# 208	-
S-7	65 ± 4	7 %	3.10 ± 0.20	# 208	-
S-8	48 ± 4	8 %	3.20 ± 0.20	# 208	-
S-9	50 ± 4	8 %	3.20 ± 0.20	# 208	-
S-10	40 ± 4	8 %	3.50 ± 0.20	# 208	-
S-11	80 ± 4	6 %	3.30 ± 0.20	# 308, 208, 408	S-17
S-12	25 ± 4	50 %	3.80 ± 0.20	# 308	S-18
S-13	80 ± 4	2 %	3.00 ± 0.20	# 308, 408	-

CHANGEMENT DE GRADE (TOUS LES MOULINS ET TOUS LES GRADES)

- 1) Laissez fonctionner le moulin sans alimentation pendant 2 heures.
- 2) Notez l'ampérage à vide sur les chartes de contrôle de la base de données.

APRES LA PRODUCTION DE S-3 & S-4

- 1) Même chose que lors d'un changement de grade.
- 2) Produire 5,000 lbs de MP 11 avec de la grenaille S-1 / S-2.

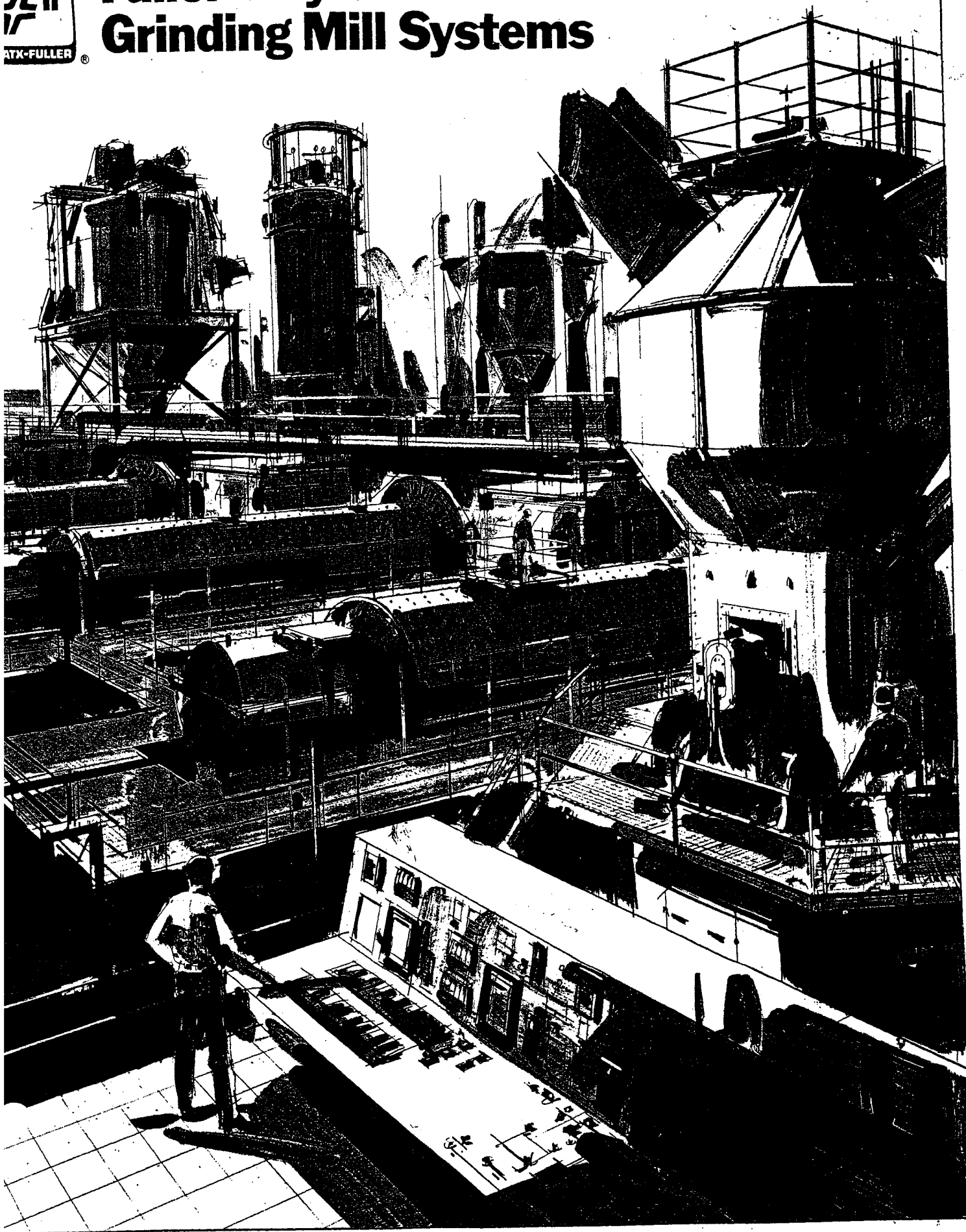
Approbation:

MAQ

SU

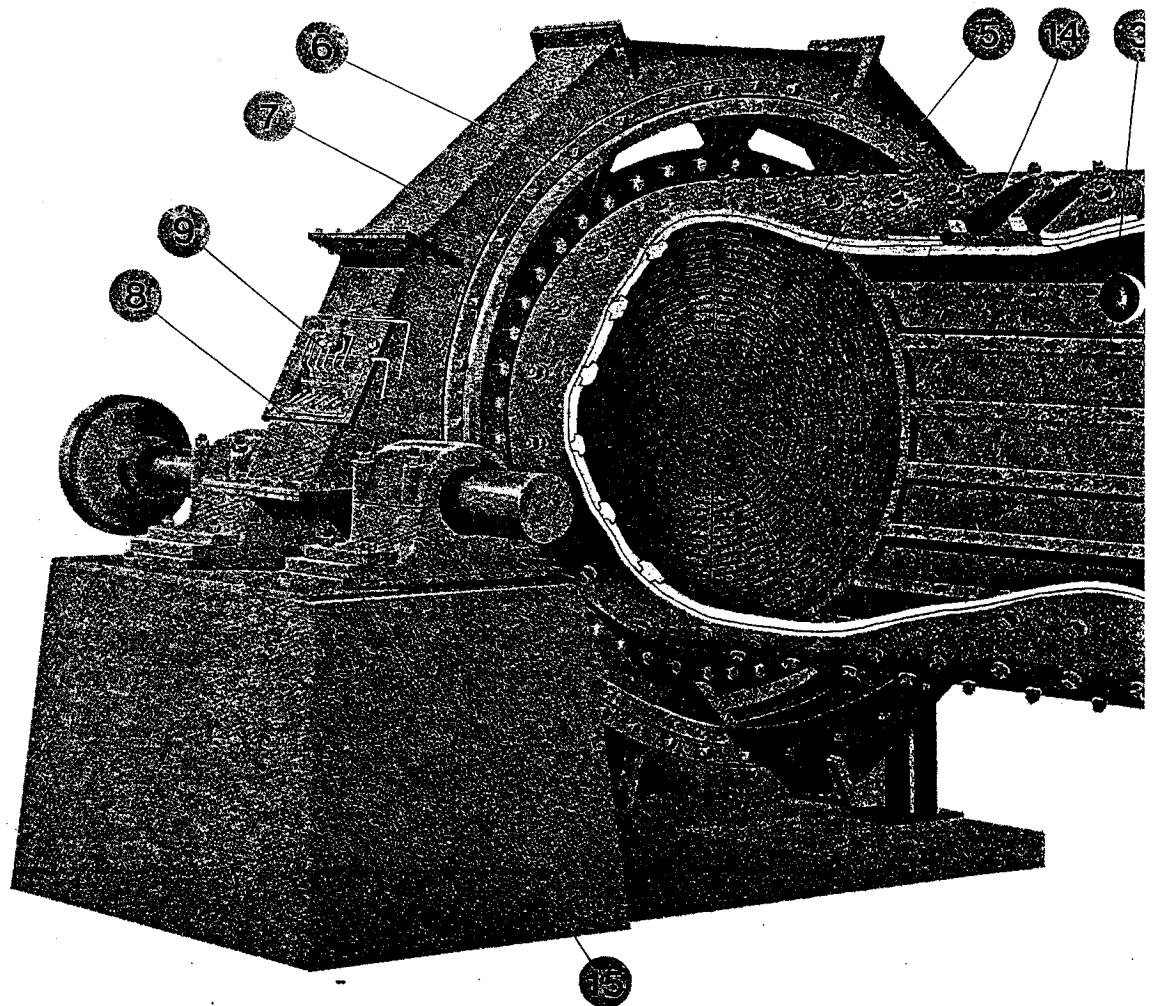


Fuller[®] Traylor[®] Grinding Mill Systems



Features and Benefits

- 1 **Bearing** is heavy ball and socket design arranged for continuous oil lubrication. The water cooled socket is provided with poured lead-tin babbitt.
- 2 **Shell** is welding quality steel, accurately rolled and drilled to insure easy liner installation.
- 3 **Liners** are available in many configurations designed for each application to insure longest possible life and maximum mill production.
- 4 **Compartment Diaphragm** Assembly consists of grate plates on the feed side and wear plates on the discharge side. The frame is of heavy-duty steel and each piece is designed to enter the shell through the manhole.
- 5 **Discharge Grate Assembly** consists of slotted segments, each is designed to enter the shell through the manhole for ease of maintenance.
- 6 **Single Helical Gears** of the most efficient design are precision cut to insure long life and reliable service.
- 7 **The Gear Guard** encloses the gear and pinion and is provided with a close contact seal for protection against dust. Doors are provided for convenient inspection.



The Pinion is forged integral with its shaft; it is symmetrical and reversible for longer life. The bearings housings are provided with heavy duty spherical roller bearings. A circulating oil system is supplied where needed for proper bearing lubrication and low operating temperatures.

The Gear and Pinion is equipped with an automatic spray lubrication system to provide the correct amount of grease at the proper time.

The Feed Pipe is supplied with a replaceable abrasion resistant half round liner.

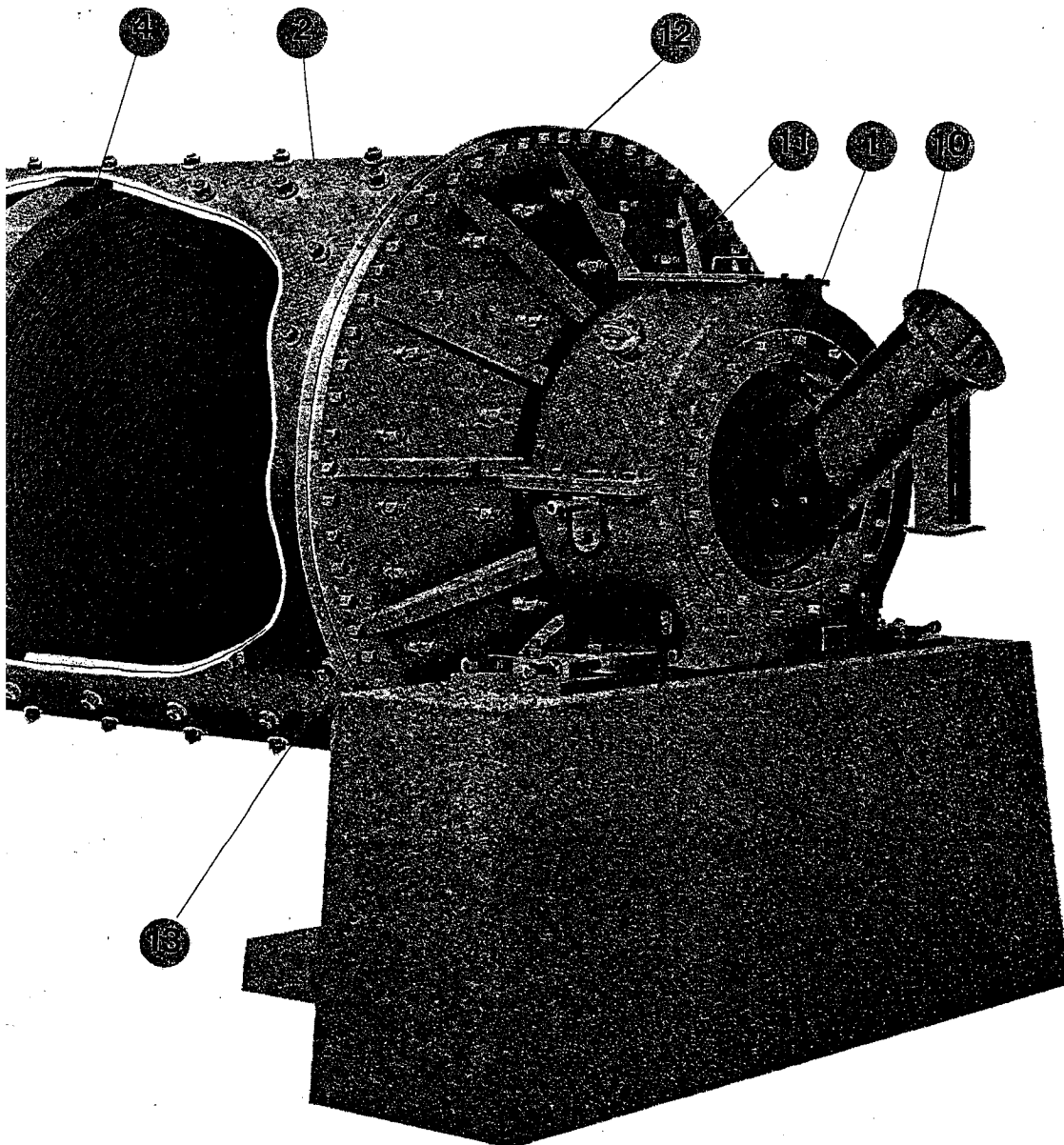
Observation ports are supplied in the bearing housing so that inspection is simplified.

12 Shell Flanges are welded to the shell plate, then machined to insure accurate alignment for the trunnions and true concentricity of the shell, thereby guaranteeing long bearing life and reliable service.

13 The heads are cast with the trunnions integral. They are faced to fit the flanges on the shell and drilled to assure interchangeability.

14 Manholes are provided for access in each compartment. Each manhole is designed so that the largest part installed inside the shell can be removed and reinstalled.

15 Sole Plates are provided for the bearings and extend under the pinion. The sole plates are provided with adjusting screws for alignment of the mill.



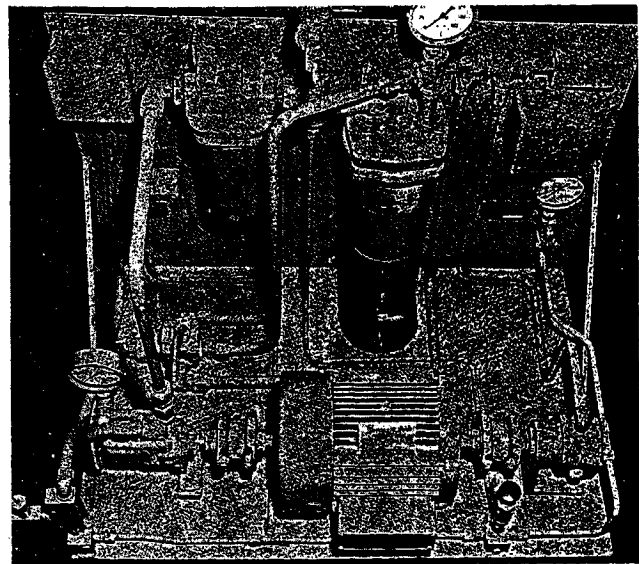
Main Bearing Features

Main Bearing Lubrication System

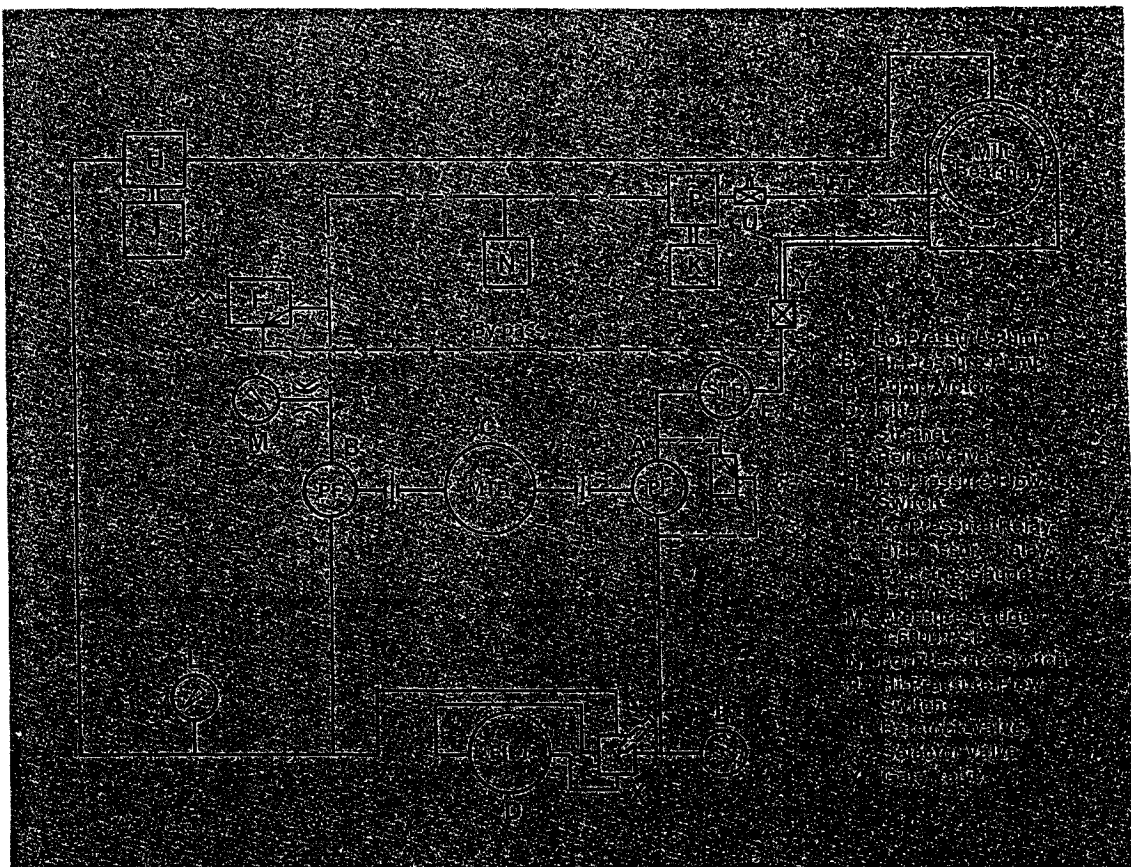
Each bearing is equipped with dual lubrication systems. The high pressure lift system is designed to lift the mill trunnion from the bearing surface before the mill is rotated. This system may be turned off after the starting sequence has been satisfied; although most operators keep the system running continually.

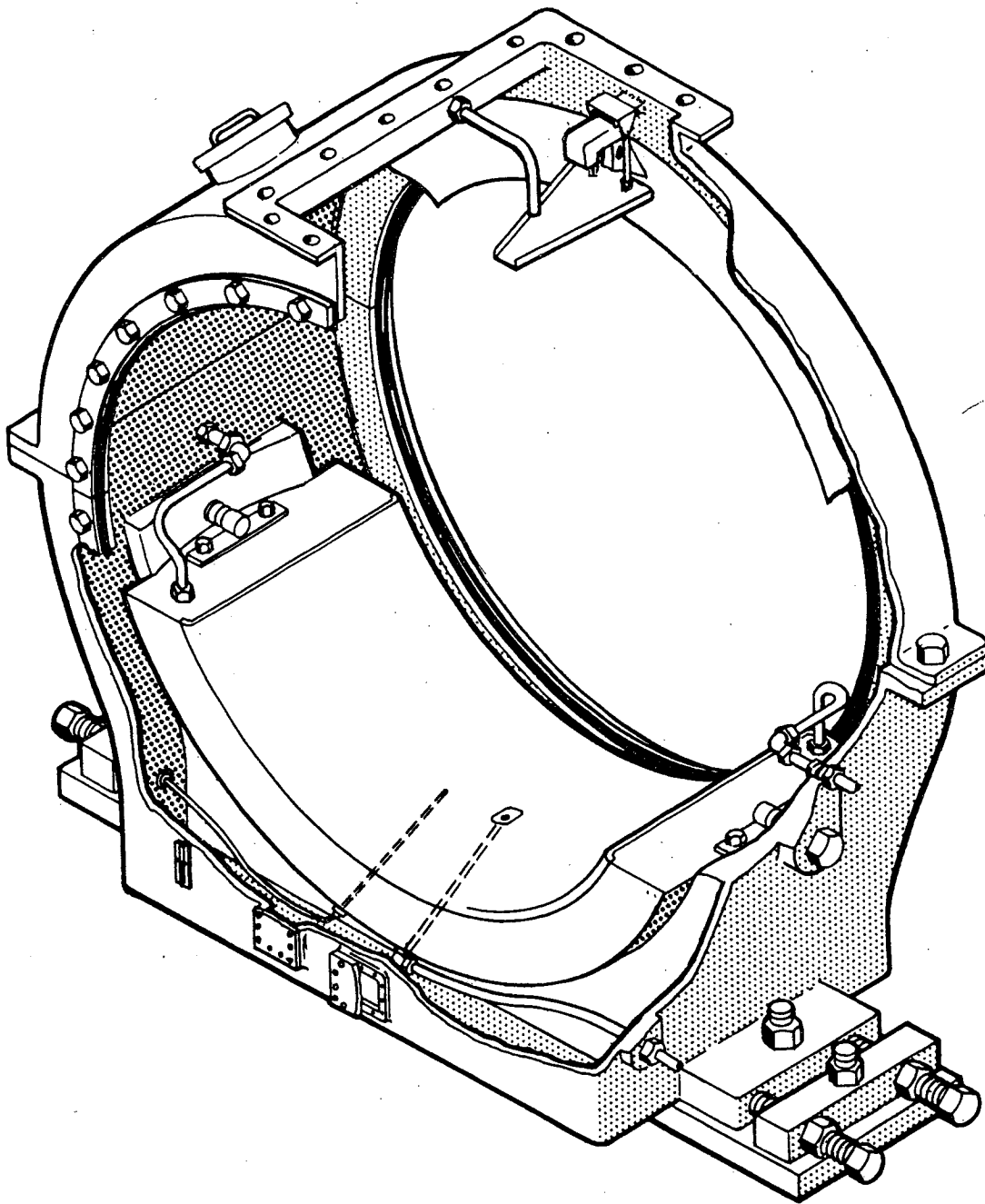
A separate low pressure recirculating system supplies oil heating and conditioning where required. The oil is pumped from the sump and returned on the top of the bearing housing. An internal oil ring with wipers also transmits oil to the trunnion, thereby assuring sufficient oil to the bearing at all times.

An optional manual high pressure pump can be supplied for use in maintenance or during erection.



Schematic of oil flow showing check valves, regulators, etc., on high pressure and low pressure temperature.





Main Bearing

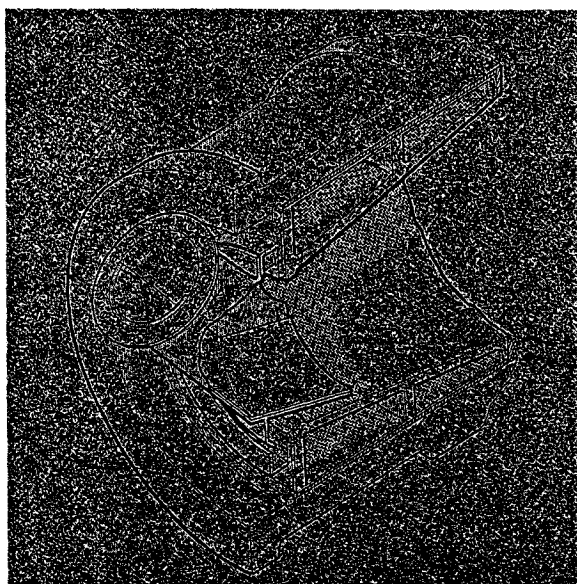
The self-aligning ball and socket arrangement assures consistent bearing alignment. The socket is provided with a poured-in-place babbitt liner, while the bearing is arranged for continuous self-oil lubrication. The oil is lifted by means of a disc attached to the trunnion. A hinged wiper removes the oil from the disc, and the spout directs it to the center of the trunnion, assuring lubrication across the bearing surface.

The ends of the bearings are fitted with split closure type seal rings to prevent escape of lubricant and entrance of grit. Welded steel sole plates are provided for the bearings. They are arranged with adjusting screws for alignment. When the mill is being supplied with a ring gear and pinion drive, the main bearing sole plates extend under the pinion base.

Mill Components

Spout Feeders

Spout feeders are used where the total feed has sufficient elevation to be spouted directly through this feeder into the trunnion opening of the mill. Most operators prefer this arrangement because of its simple and inexpensive maintenance.



DRY FEED A labyrinth type seal is used on dry grinding mills allowing sufficient air to be drawn thru the mill for proper venting.



WET FEED The packing gland provides an adjustable seal to prevent slurry spill back on all wet grinding mills.

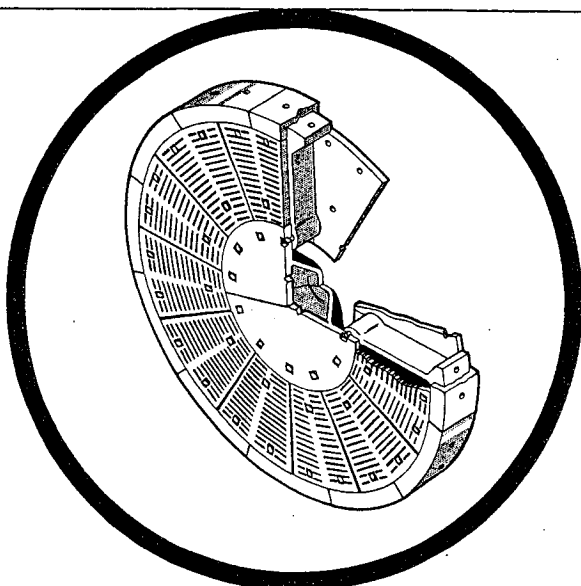
Discharge Arrangement With Trunnion Connected Drive

The torque tube is attached to the mill trunnion flange and to the drive through a low speed coupling. Sufficient openings are supplied in the torque tube for material discharge into the discharge housing.

The discharge housing is constructed of steel plate. Mounting brackets are provided on both sides of the housing for connection to the foundation. Adjustable felt seals are attached to the housing. This rubbing seal contacts the torque tube and insures suitable dust control.

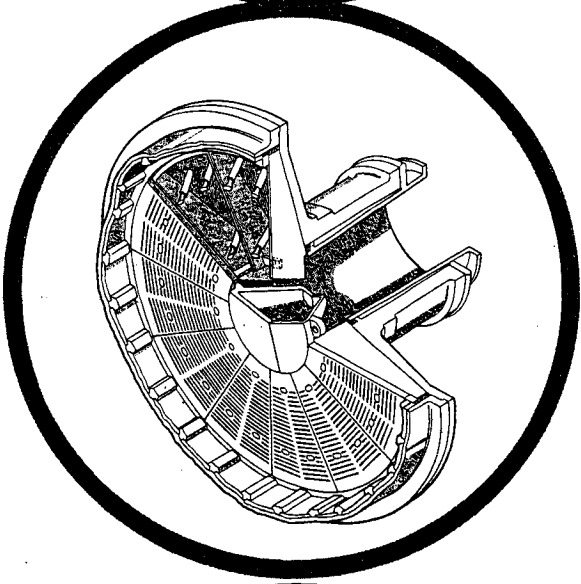
The discharge housing has a flanged connection on the bottom for attaching a material conveyor. A flanged connection is provided on top of the housing for connecting the mill vent system.





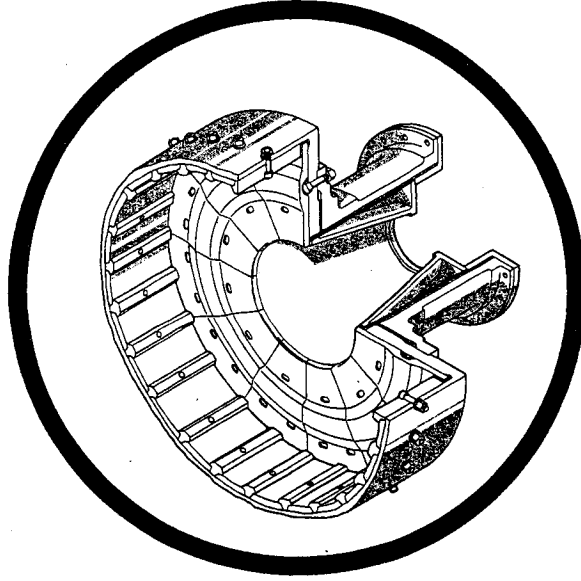
Diaphragm

The compartment diaphragm is designed to contain balls and oversize particles. It is also used to lift the material to approximately mill center line to help the flow of material in the following compartment. The frame is fabricated and the liners and grates are cast construction. All pieces are designed to pass thru the mill manhole opening, thereby assuring ease of replacement. The grates have tapered self-cleaning holes to minimize plugging.



Discharge Grate

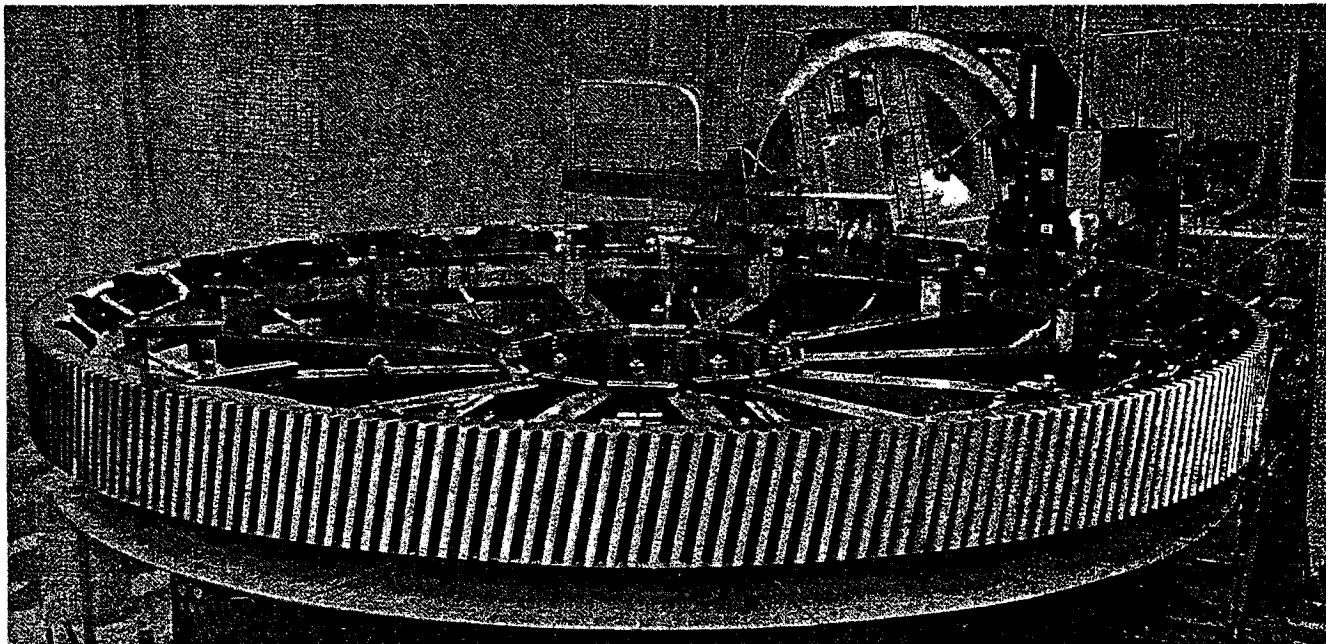
The discharge grate is of cast construction, sectionalized so that it may be replaced thru the manhole opening. The grates are supported on fabricated lifters that are bolted to the discharge head. Tapered self-cleaning holes minimize plugging.



Internal Flange Head

Large diameter mills require special designs due to restrictions imposed by availability of castings as well as shipping limitations. The inside flange mill is designed to help alleviate this problem. The shell flange is turned in toward the trunnion. The flange is extended into the trunnion opening diameter, providing an excellent surface for liner mounting. The head mounting bolts are completely protected by the head liners. This simple design assures the user of many years of trouble-free operation with a minimum of maintenance hours required to replace the liners.

Mill Drives



This mammoth gear cutting facility at Fuller's Allentown, Pa. plant is capable of cutting high-precision gears as large as 288 inches O.D. and as small as 10 inches O.D. and can handle gears to 55 tons in weight. The gear cutter is equipped with internal gear cutting attachments to cut large high-quality internal gears with maximum tip circle diameters of 270 inches and minimums of 16 inches. The machine is capable of cutting spur, single-helical, and double-helical gears to AGMA 12 standards and can cut high-quality gears to 400 Brinell hardness. In addition, capabilities of the gear cutting machine are complemented by Fuller's large-capacity, modern machine shop, which is equipped with boring mills to 24 feet in diameter, 60-inch x 30-foot lathes, 9 x 30-foot openside planer mills, and other modern equipment.

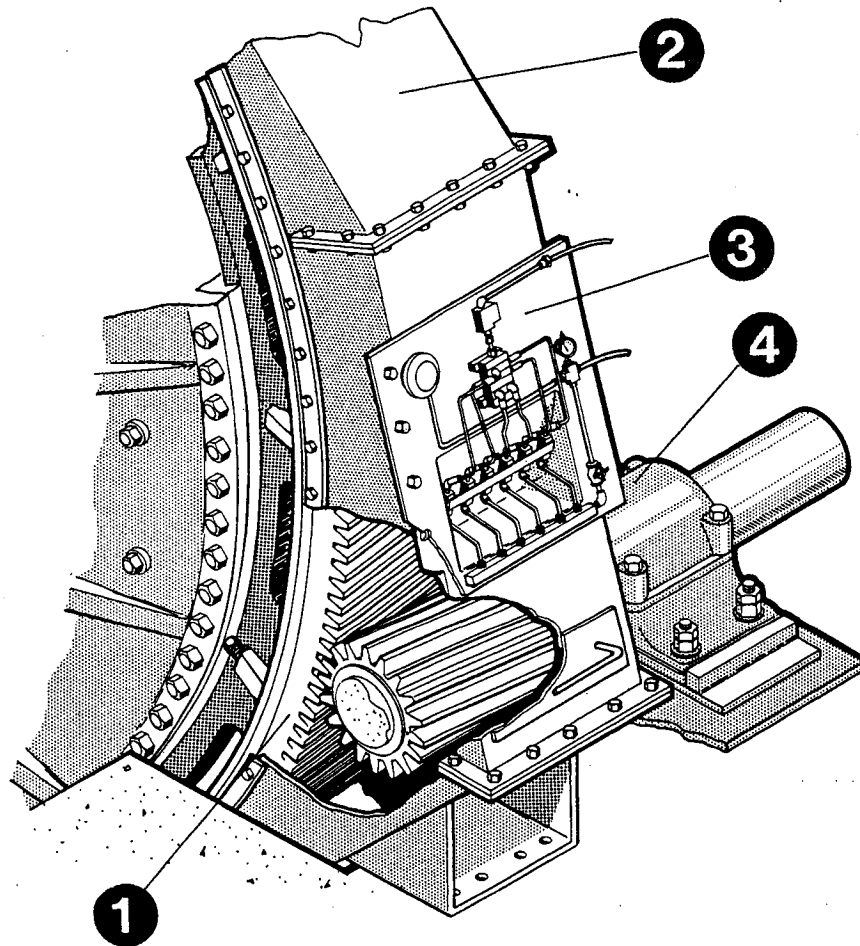
Alternate Drives

Traylor Mills are also supplied with trunnion connected drives. Other drive systems are available for large mills, these include ring gear with multiple pinions as well as gearless drives incorporating the latest technology in

the electrical industry. A complete study of the electrical system is a prerequisite for the proper choice of mill drives as they approach the 10,000-15,000 HP range. New drive concepts are continually being evaluated to keep Traylor systems among the leaders.

Ring Gear and Pinion

- 1.** The girth gear is single helical with accurately generated teeth. It is made from cast steel in two halves for ease of installation. The flange is accurately machined on both sides to precisely fit the mill shell flange. The gear is reversible so that each face of the gear can be used. Extended rim flanges are located on the gear to be used as sealing surface for the gear guard.
- 2.** The gear guard is manufactured from welded steel plate, it encloses the gear face as well as the pinion assembly. An annular seal mounted on the guard contacts the gear rim flange, providing a positive means of preventing escape of lubricating medium as well as keeping abrasive dust from entering the gear mesh.
- 3.** The automatic spray lubrication panel is mounted on the gear guard. This panel contains the metering valves and the spray nozzles. The system includes a barrel pump, a timer, air control panel, hydraulic control valves, hose assemblies, metering valves, and spray nozzles. The system gives the operator assurance that the gears and pinion are properly lubricated.
- 4.** The driving pinion is forged alloy steel and is forged integral with the pinion shaft. The shaft is symmetrical and reversible so that both faces of the pinion may be worn. The shaft is provided with spherical roller bearing pillow blocks. The bearings can be lubricated by either oil or grease.



SEE 10 FLANGE

7'-0" INS. DIA.

10'-0"

CUT EXISTING GRATES
TO SUIT NEW SLEEVE +
WELD

13'

SEGMENTED GRATES 2 1/4" THICK
10-14 % MANGANESE FACT N° 6856-1
TO BE WELDED TOGETHER RADIALLY
3" RUNS @ 12"
CONTINUOUS WELD TO SLEEVE

2'-3"

2'-3"
4'-7 1/2"
1'-9 1/2"
TO BE VERIFIED IN FIELD

1 1/2"
1/2" RING
2'-3" DIA.
TO BE VERIFIED IN FIELD

TACK WELD
1/8" RING

SPIRAL BAR 1/2" x 1"
WELD TO NEW SLEEVE

FEED END

A. HOLE
OF 1/4" SCREWS

STD 20" x 12" ECCENTRIC
WELD REDUCER

3' 0" O.D.
2' 9" B.C.
17 1/2" I.D.
1 1/2"

DISCHARGE END

SEE DETAIL BELOW

RUBBER BELT

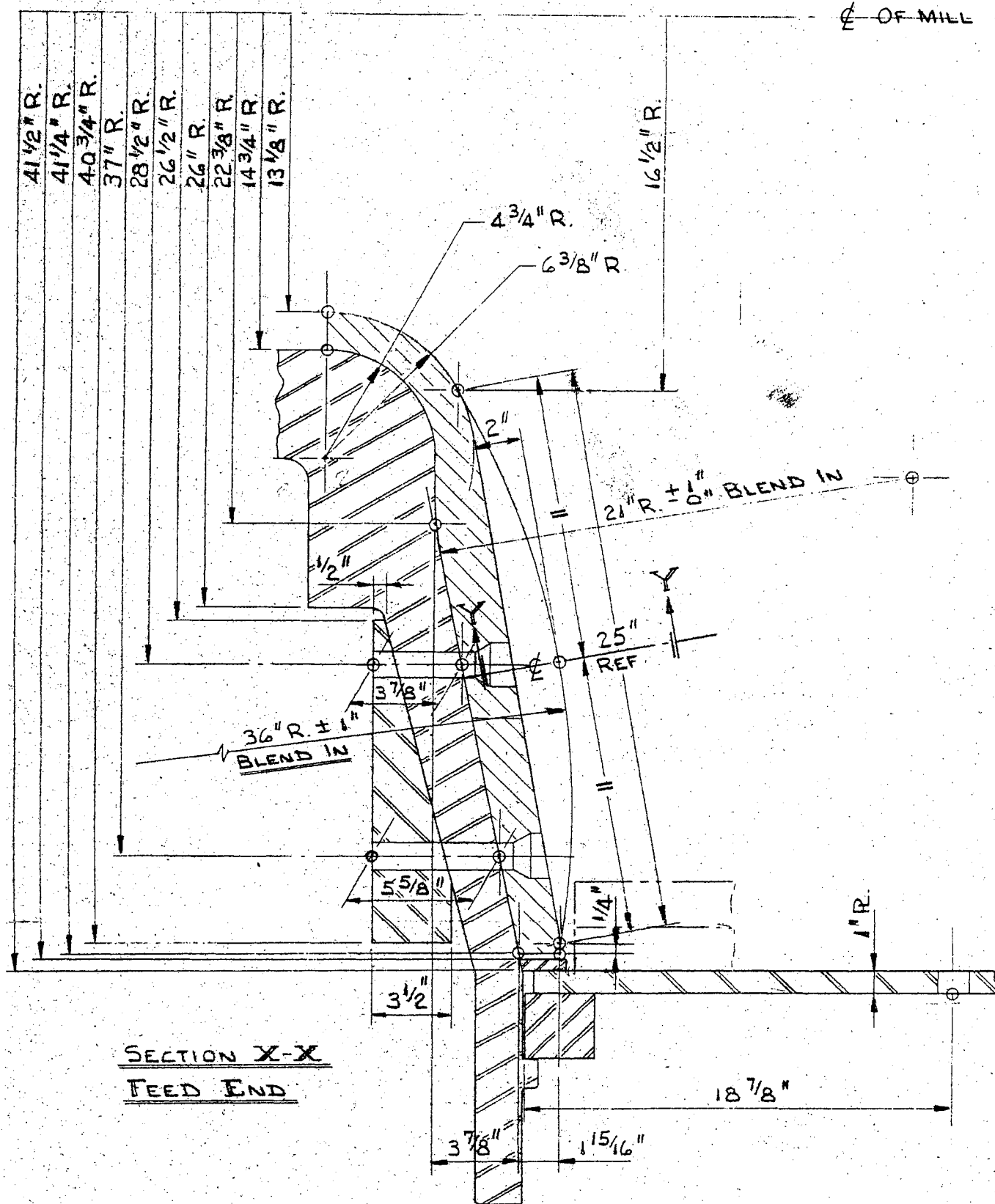
1/2" t.

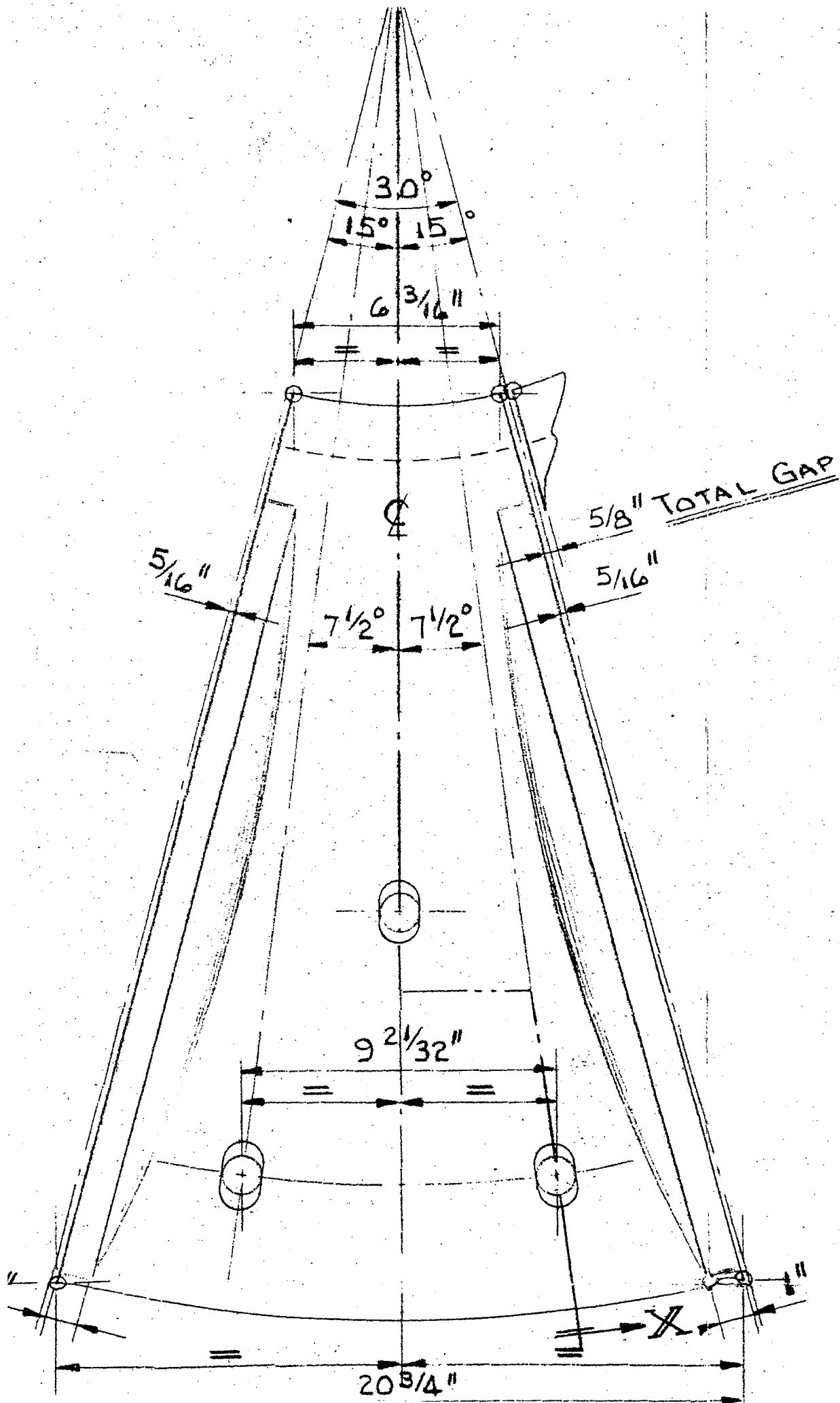
20" INS. DIA.

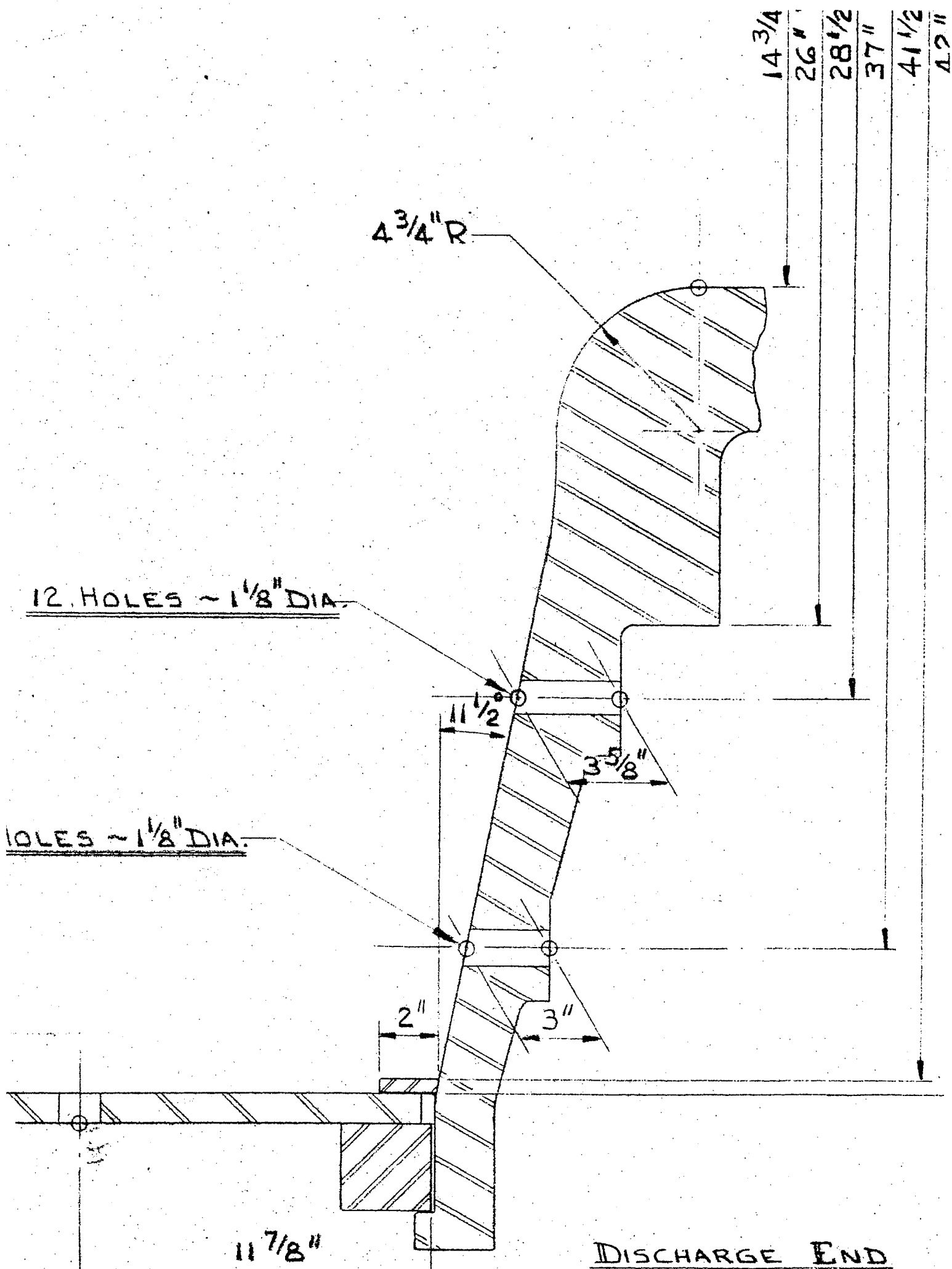
1" x 1/2" BARS @ 1/2" c/c.
TACK WELD TO EXIST. CONE

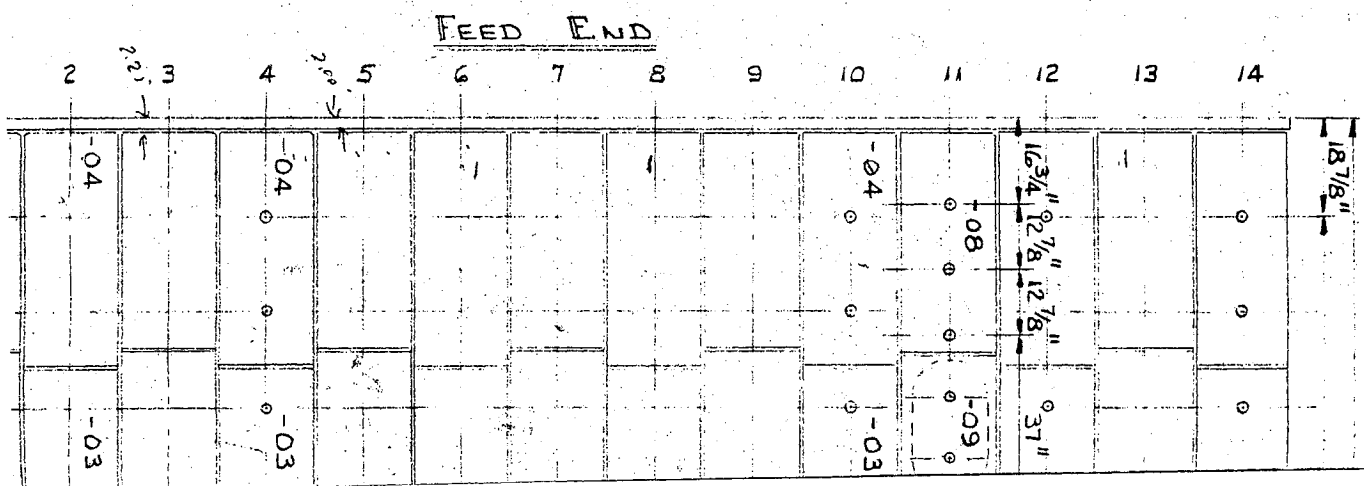
WELD 1" x 1" x 1/8" EACH
SIDE AROUND CIRCUMFERENCE

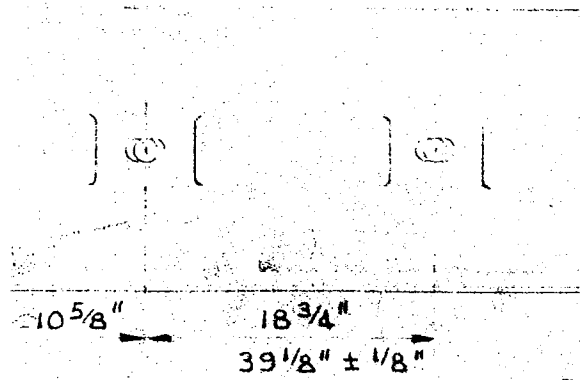
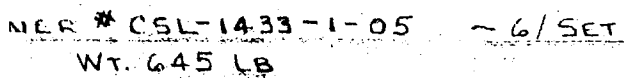
φ OF BALL MILL



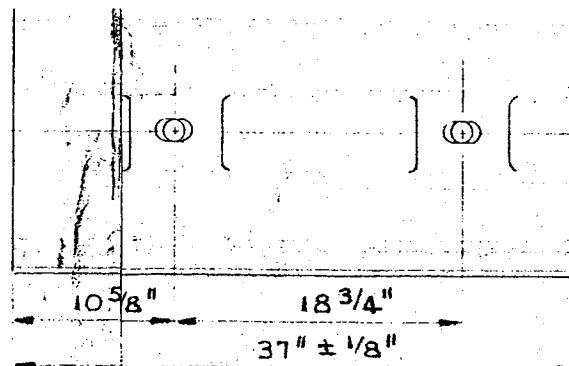




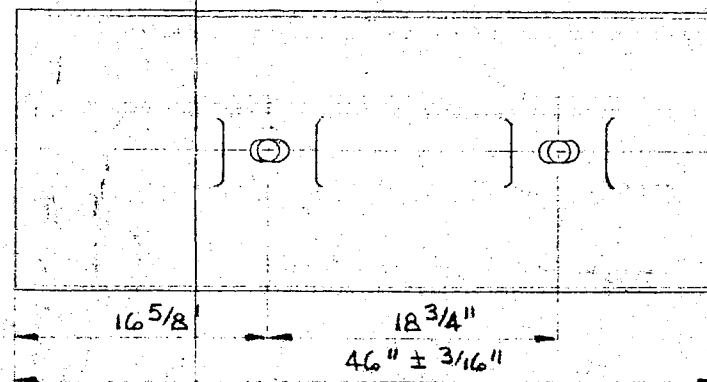




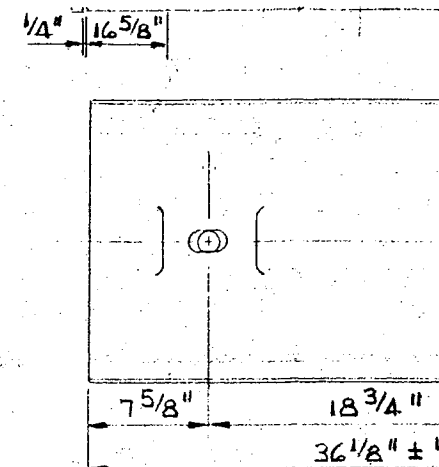
JER # CSL-1433-1-02 ~ 7/SET
WT. 590 LB.



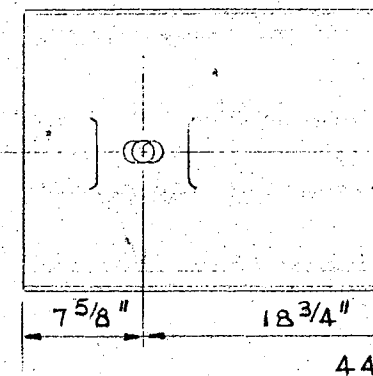
LINER # CSL-1433-1-03 ~ 80/SET
 WT 555 LB.



LINER * CSL-1433-1-04 ~ 7/SET
WT. 690 LB.



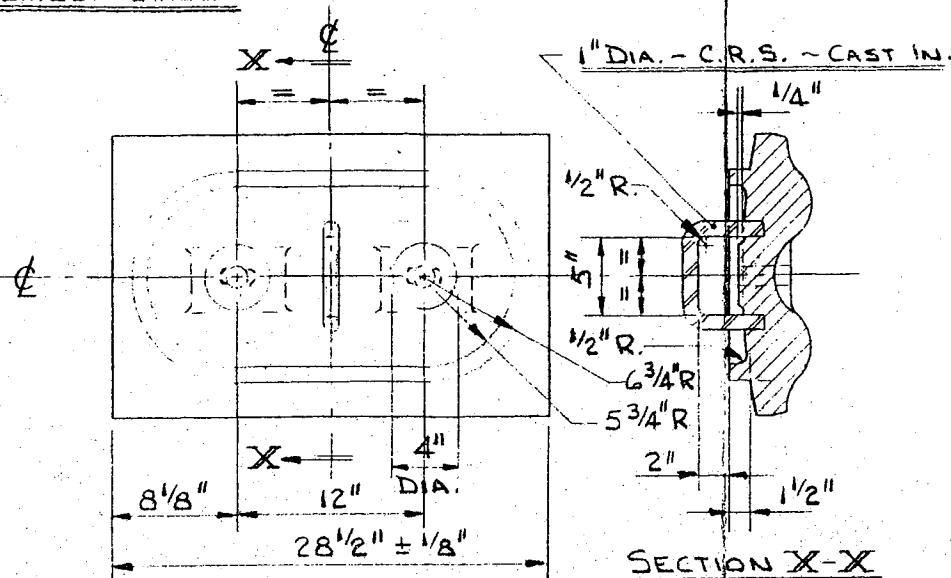
WT. 545 LB.



LINER # CSL-1433-1-
WT. 670 LB.

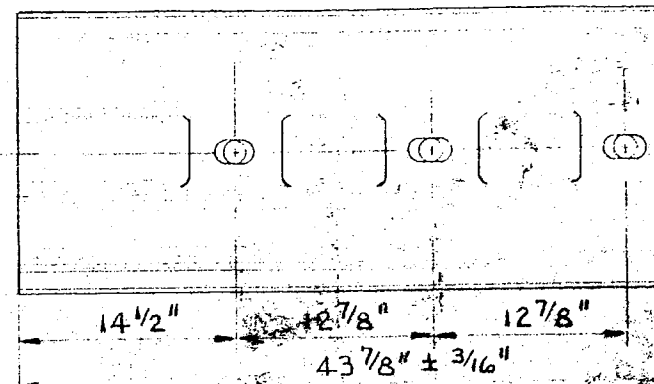
[illegible]

SCALE 1/2"=1'-0"
ASSEMBLY LAYOUT



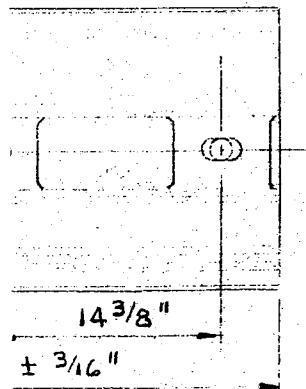
DOOR LINER # CSL-1433-1-09 ~ 2/SET
WT. 465 LB.

LINER # CSL-1433-1-06 ~ 1/SET
WT. 560 LB.



LINER # CSL-1433-1-08 ~ 1/SET
WT. 665 LB.

~ 6/SET



~ 1/SET

UNLESS OTHERWISE SPECIFIED: - DIM. IN INCHES (") - IN MILLIMETRES (mm)
1. DIM. TOL. ± 1/16" 2. ANGLE TOL. ± 1° 3. SURFACE FINISH STD. FDRY. PRACTICE
4. FILLETS 1/4" MAX. 1/8" MIN. R OR 45° CHAMF. 5. ALL CORNERS 1/4" MAX. 1/16" MIN. R OR 45° CH.
6. MATERIAL NI HARD, TYPE I, CAST & STRESS RELIEVED

TITLE
DOUBLE WAVE SHELL LINER
FOR 7'-0" DIA. x 26'-0" LONG, TRAYLOR, BALL MILL
CUSTOMER DOMFER METAL POWDERS LTD., LA SALLE, QUEBEC
REF. # 29582-4

norcas

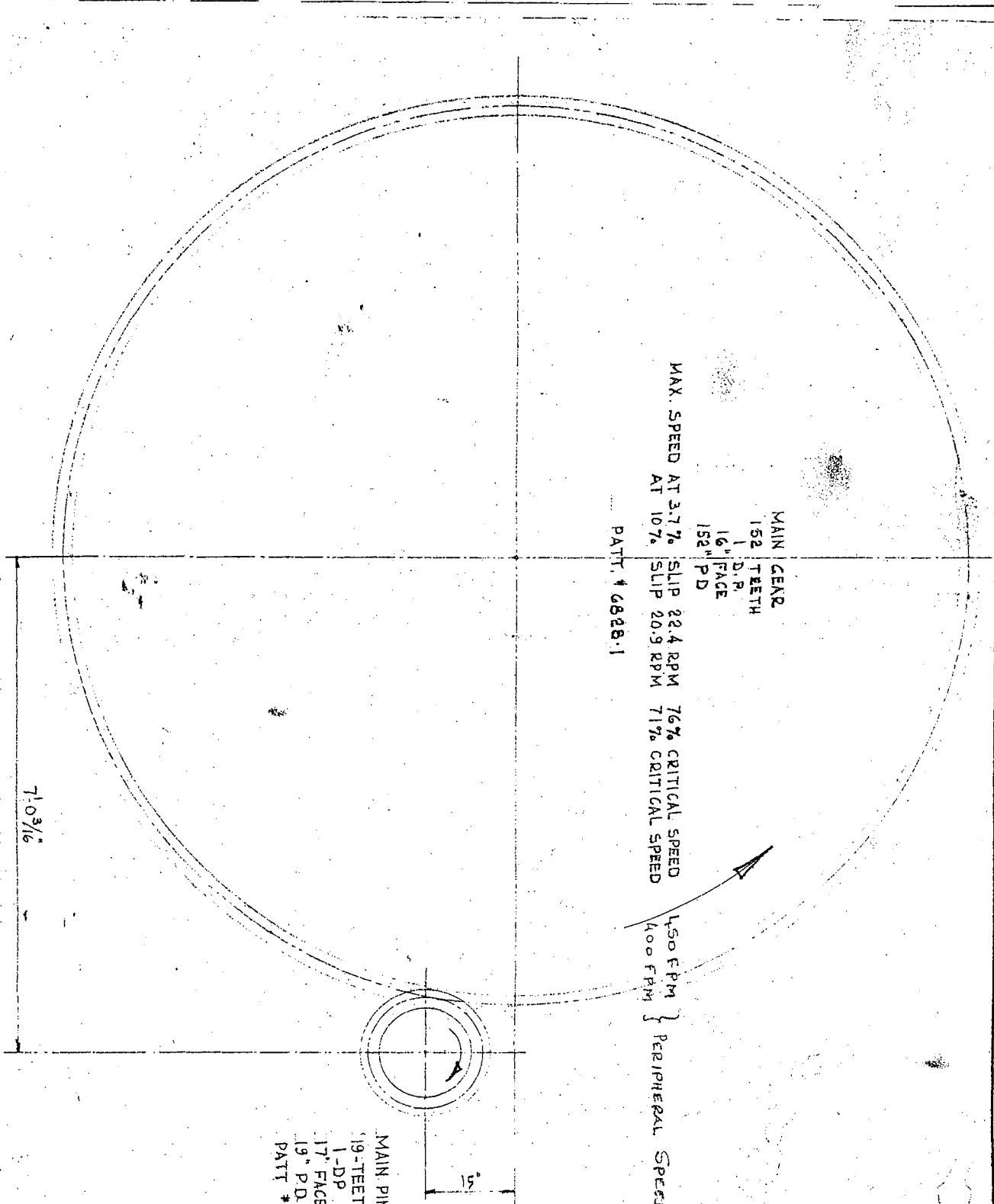
NORCAST INC. / TORONTO
Mont Joli Div. / Mont Jo
Wabi Div. / New Liskear

SCALE 1/2" / 1 1/2" / 3" = 1'

DWG. NO. CSL-1433-1

ISSUED - BY CUST. REQUEST MAR. 20. 86 W.T.

REVISIONS

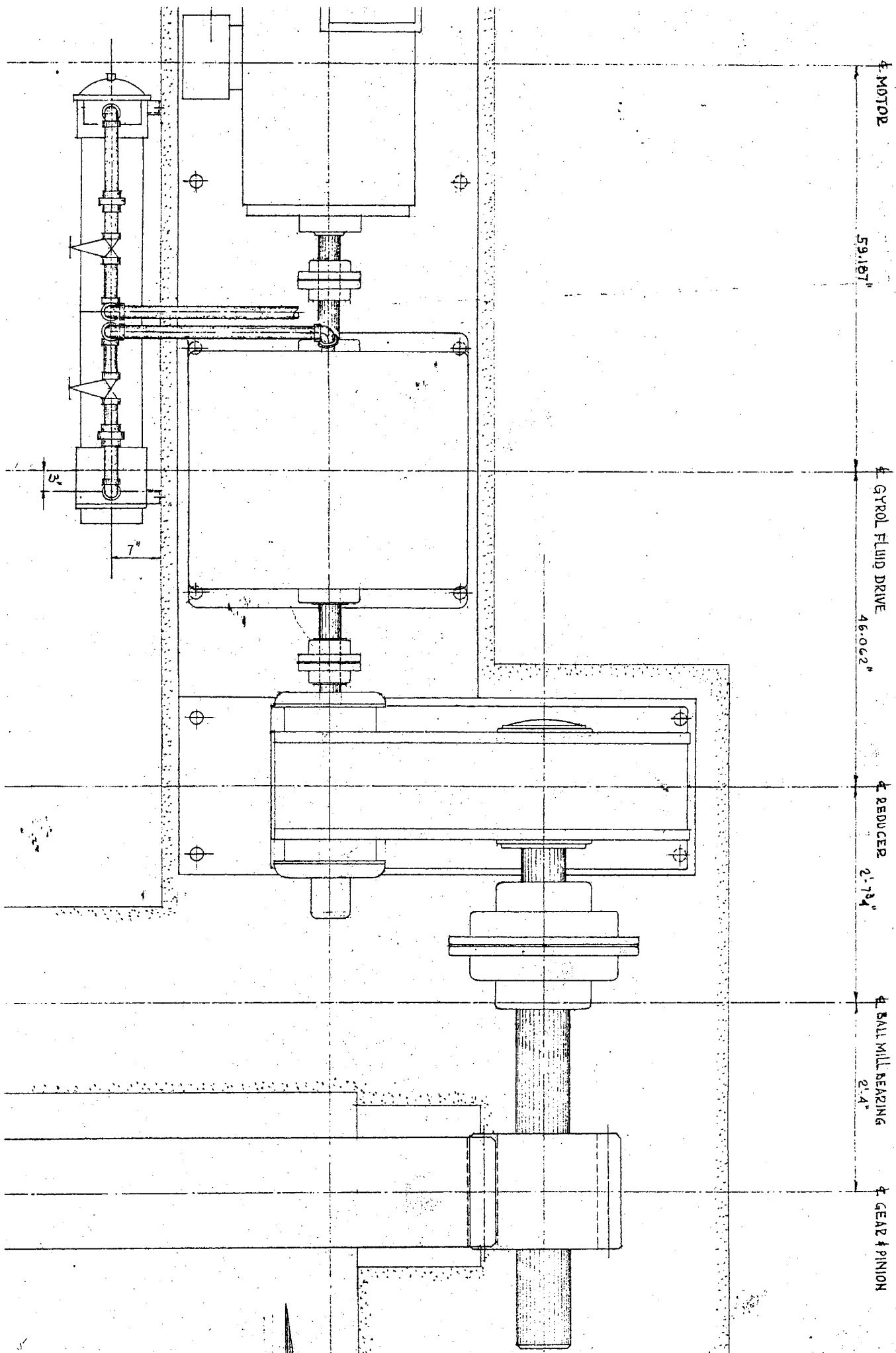


MAIN GEAR
152 TEETH
16" FACE
152" PD
MAX. SPEED AT 3.7% SLIP 22.4 RPM 76% CRITICAL SPEED
AT 10% SLIP 20.9 RPM 71% CRITICAL SPEED
PATT. # 6828-1

450 FPM } PERIPHERAL SPEED
400 FPM }

MAIN PINION
19-TEETH
1-DP
17" FACE
19" PD
PATT. # 6827-1

71.0316



MOTOR 500 H.P.
FRAME 8110Z
3-60-2300 VOLTS (2390V)
1775 R.P.M. FL SPEED
113 AMPS FL CURRENT
83% EFFICIENCY

FALK GEAR COUPLING
TYPE 25G10
P.O. 9010-9
DWG M. 202-1
1775 RPM

GYROL FLUID DRIVE
(AMERICAN STANDARD)
P.O. 9010-6
DWG MPR-PE2-M197

FALK GEAR COUPLING
TYPE 25G10
DWG M. 202-1
P.O. 9010-9
MAX. SPEED 1709 RPM
MIN. SPEED 855 PPM

2130Y2 PARALLEL SHAFT
FALK SPEED REDUCER
DWG MPR-PE2-M202
P.O. 9010-9
RATING 775
RATIO 9.55:1

FALK STEELFLEX COUPLING
TYPE 210F - P.O. 9010-9
DWG M 202-2

BLOWER

WT: 3000lbs

SHIM

STICK
CONTROL

2:1 SPEED REDUCTION
MAX. POSSIBLE
NORMAL 3.7% SLIP

WT. 4630

SHIM

1 1/2" GROUT

BEDPLATE (FALK CORP)
P.O. 9010-9 DWG M. 202-3

1 1/2"

1 1/2"

1 1/2"

1 1/2"

1 1/2"

1 1/2"

1 1/2"

1 1/2"

1 1/2"

1 1/2"

1 1/2"

1 1/2"

1 1/2"

1 1/2"

1 1/2"

1 1/2"

1 1/2"

1 1/2"

1 1/2"

1 1/2"

1 1/2"

1 1/2"

1 1/2"

1 1/2"

1 1/2"

1 1/2"

1 1/2"

1 1/2"

1 1/2"

1 1/2"

1 1/2"

1 1/2"

1 1/2"

1 1/2"

1 1/2"

1 1/2"

1 1/2"

1 1/2"

1 1/2"

1 1/2"

1 1/2"

1 1/2"

1 1/2"

1 1/2"

1 1/2"

1 1/2"

1 1/2"

1 1/2"

1 1/2"

1 1/2"

1 1/2"

1 1/2"

1 1/2"

1 1/2"

1 1/2"

1 1/2"

1 1/2"

1 1/2"

1 1/2"

1 1/2"

1 1/2"

1 1/2"

1 1/2"

1 1/2"

1 1/2"

1 1/2"

1 1/2"

1 1/2"

1 1/2"

1 1/2"

1 1/2"

1 1/2"

1 1/2"

1 1/2"

1 1/2"

1 1/2"

1 1/2"

1 1/2"

1 1/2"

1 1/2"

1 1/2"

1 1/2"

1 1/2"

1 1/2"

1 1/2"

1 1/2"

1 1/2"

1 1/2"

1 1/2"

1 1/2"

1 1/2"

1 1/2"

1 1/2"

1 1/2"

1 1/2"

1 1/2"

1 1/2"

1 1/2"

1 1/2"

1 1/2"

1 1/2"

1 1/2"

1 1/2"

1 1/2"

1 1/2"

1 1/2"

1 1/2"

1 1/2"

1 1/2"

1 1/2"

1 1/2"

1 1/2"

1 1/2"

1 1/2"

1 1/2"

1 1/2"

1 1/2"

1 1/2"

1 1/2"

1 1/2"

1 1/2"

1 1/2"

1 1/2"

1 1/2"

1 1/2"

1 1/2"

1 1/2"

1 1/2"

1 1/2"

1 1/2"

1 1/2"

1 1/2"

1 1/2"

1 1/2"

1 1/2"

1 1/2"

1 1/2"

1 1/2"

1 1/2"

1 1/2"

1 1/2"

1 1/2"

1 1/2"

1 1/2"

1 1/2"

1 1/2"

1 1/2"

1 1/2"

1 1/2"

1 1/2"

1 1/2"

1 1/2"

1 1/2"

1 1/2"

1 1/2"

1 1/2"

1 1/2"

1 1/2"

1 1/2"

1 1/2"

1 1/2"

1 1/2"

1 1/2"

1 1/2"

1 1/2"

1 1/2"

1 1/2"

1 1/2"

1 1/2"

1 1/2"

1 1/2"

1 1/2"

1 1/2"

1 1/2"

1 1/2"

1 1/2"

1 1/2"

1 1/2"

1 1/2"

1 1/2"

1 1/2"

1 1/2"

1 1/2"

1 1/2"

1 1/2"

1 1/2"

1 1/2"

1 1/2"

1 1/2"

1 1/2"

1 1/2"

1 1/2"

1 1/2"

1 1/2"

1 1/2"

1 1/2"

1 1/2"

1 1/2"

1 1/2"

1 1/2"

1 1/2"

1 1/2"

1 1/2"

1 1/2"

1 1/2"

1 1/2"

1 1/2"

1 1/2"

1 1/2"

1 1/2"

1 1/2"

1 1/2"

1 1/2"

1 1/2"

1 1/2"

1 1/2"

1 1/2"

1 1/2"

1 1/2"

1 1/2"

1 1/2"

1 1/2"

1 1/2"

1 1/2"

1 1/2"

1 1/2"

1 1/2"

1 1/2"

1 1/2"

1 1/2"

1 1/2"

1 1/2"

1 1/2"

1 1/2"

1 1/2"

1 1/2"

1 1/2"

1 1/2"

1 1/2"

1 1/2"

1 1/2"

1 1/2"

1 1/2"

1 1/2"

1 1/2"

1 1/2"

1 1/2"

1 1/2"

1 1/2"

1 1/2"

1 1/2"

1 1/2"

1 1/2"

1 1/2"

1 1/2"

1 1/2"

1 1/2"

1 1/2"

1 1/2"

1 1/2"

1 1/2"

1 1/2"

1 1/2"

1 1/2"

1 1/2"

1 1/2"

1 1/2"

1 1/2"

1 1/2"

1 1/2"

1 1/2"

1 1/2"

1 1/2"

1 1/2"

1 1/2"

1 1/2"

1 1/2"

1 1/2"

1 1/2"

1 1/2"

1 1/2"

1 1/2"

1 1/2"

1 1/2"

1 1/2"

1 1/2"

1 1/2"

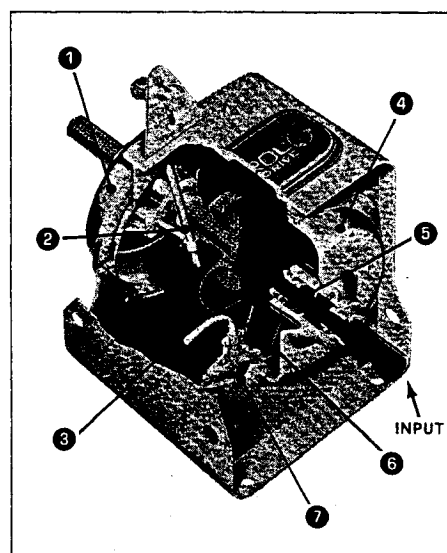
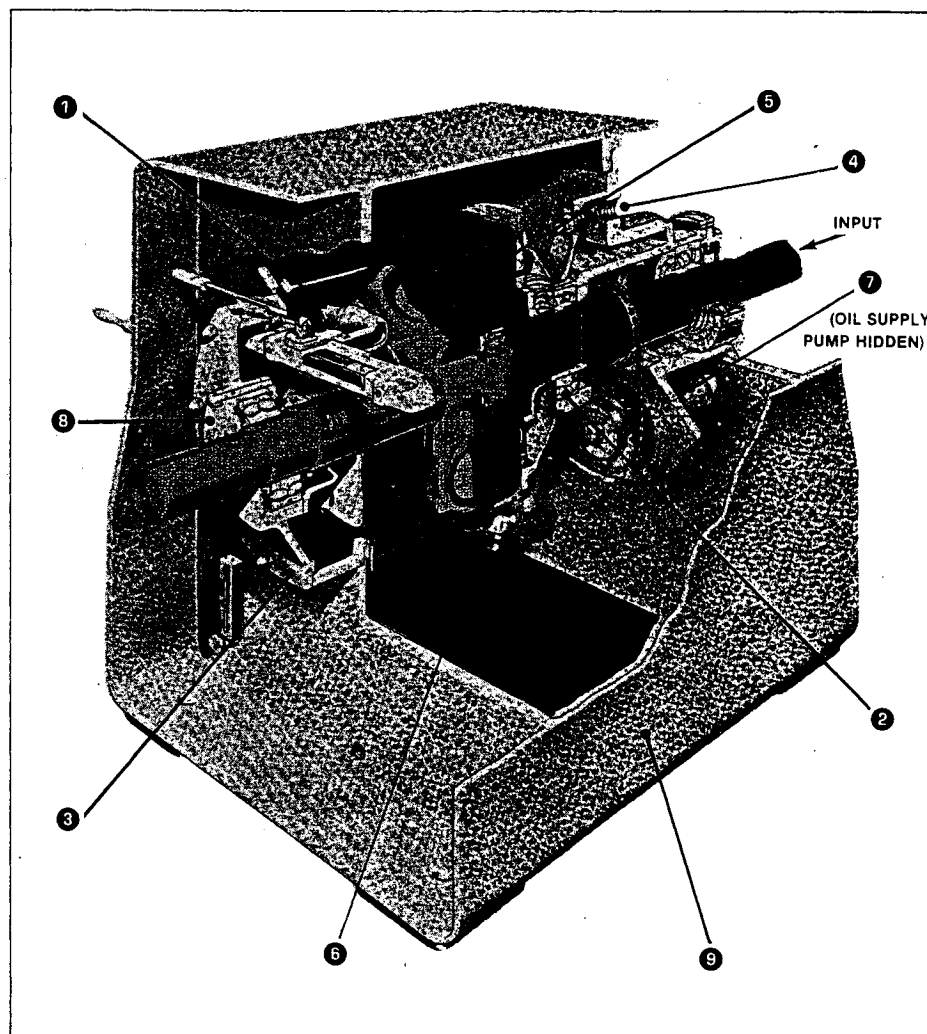
1 1/2"

Class 2 → SIZE 198

Class 2 fluid drives are available in various standard arrangements, with horsepower ratings from 1 to 2250. These drives work hard every day handling fans, conveyors, pumps and blowers in many industrial applications.

sizes 126 — 270
horsepowers to 1500
speeds to 1800 rpm

- Dual horizontal scoop tubes, between inner and outer casing, give stepless speed control for either direction of rotation.
- Two oil-lubricated anti-friction bearings support input shaft.
- End bell housing protects all working parts.
- Oil returns from heat exchanger . . . to transmit power, remove heat and lubricate all working parts.
- Impeller and runner are precision cast from high-quality aluminum for long life.
- Oil exits to external heat exchanger for cooling. (See heat exchanger note.)
- Oil supply pump (hidden) — driven from input shaft — supplies constant volume of oil for the working circuit . . . regardless of output speed or direction of rotation.
- Two oil lubricated, anti-friction bearings — one a pilot bearing between impeller and runner — support the output shaft.
- Rugged steel casing encloses rotating parts . . . serves as oil reservoir.



- 1 Two anti-friction, grease-lubricated bearings, mounted in the end bell, support the output shaft.
- 2 Vertical dual-tip scoop tube, located between runner and casing, gives stepless speed control for rotation in either direction.
- 3 Impeller and runner are precision die-cast from aluminum for long life.
- 4 End-bell type housing holds oil, encloses rotors, bearings, pump and scoop tube.
- 5 Two anti-friction, grease-lubricated bearings carry the input shaft.
- 6 Chain drive transmits drive power from the input shaft to the circulating pump.
- 7 Submerged, circulating pump supplies constant volume of oil for the working circuit, regardless of output speed or direction of rotation.

Note: We offer shell-and-tube exchangers as standard equipment for oil cooling duty. If you need to cool with air, we can offer air/oil heat exchangers.

sizes 55 — 107
horsepowers to 40
speeds to 3600 rpm

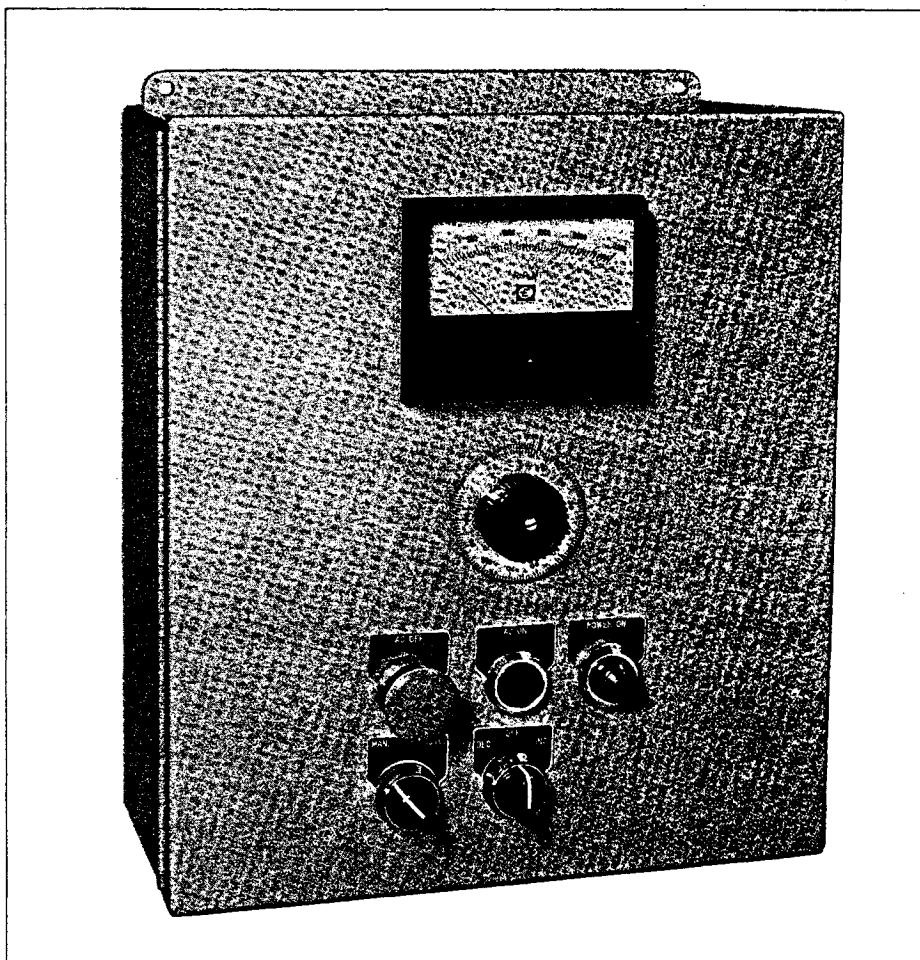
Gýroltrol® controllers provide precise automatic or manual control of output speed for Gýrol® fluid drives.

- Packaged in standard NEMA 12 dust-proof enclosure.
- Components and wiring meet J.I.C. standards for dependability.
- Motor starts under no-load conditions every time.
- Accuracy and repeatability within $\pm 1\%$ of maximum speed.
- Compact Gýroltrol controller takes little space.
- Wide range of options and accessories.
- Expert start-up service available.
- Very low control power required.

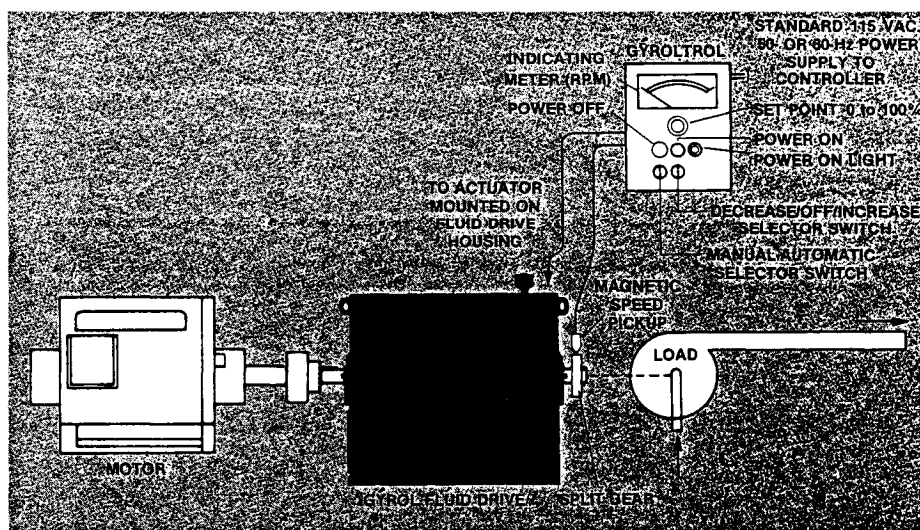
Gýroltrol® allows closed-loop automatic control with remote, automatic speed adjustment, direct readout of output speed, accurate control — regardless of load change.

Gýroltrol controller positions a rugged, heavy-duty industrial electrical actuator located on the fluid drive housing. The actuator moves the fluid drive scoop tube to control the output speed.

Gýrol fluid drives are ideal for process applications requiring automatic control. The Gýroltrol controller accepts any standard process control signal. You can control for speed, pressure, level, flow or torque . . . reliably.



Typical application, for constant speed control. With changing load conditions, the Gýroltrol system commands the fluid drive to maintain constant output speed.



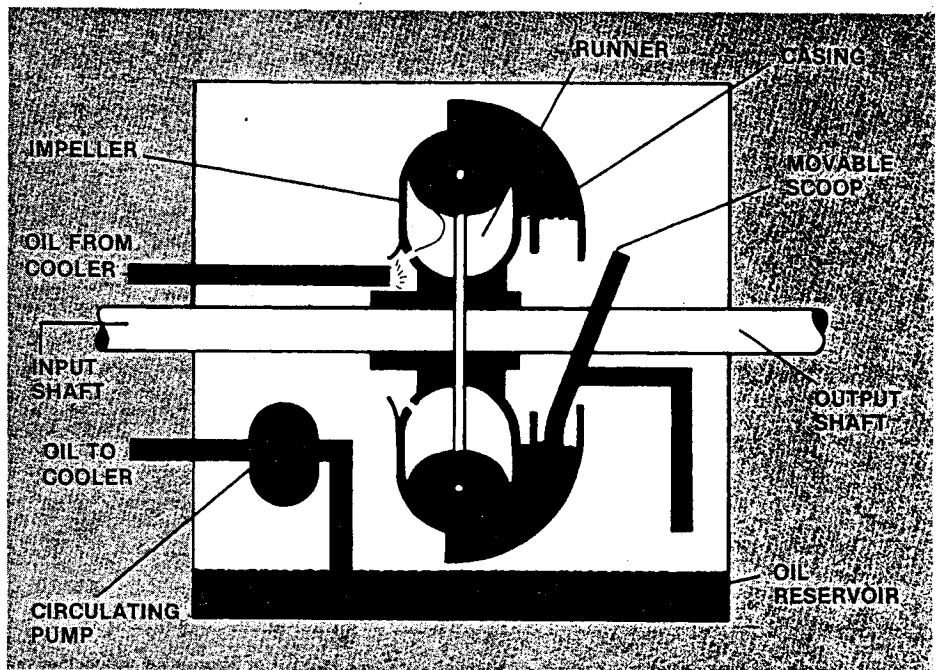
Gýrol® fluid drives . . . how they work.

Gýrol fluid drives transmit power smoothly and without shock, using a vortex of hydraulic oil. Oil particles are accelerated in the impeller (connected to the prime mover) and power is transmitted as they strike the blades of the runner (connected to the driven load). There is no mechanical connection between input and output shafts.

In a Gýrol fluid drive, you can change the amount of oil in the working circuit while the machine is operating. This ability to change the amount of oil gives you infinitely variable speed adjustment. You can easily adjust the output speed by manual or automatic control.

A circulating pump — usually driven from the input shaft — pumps oil from the housing reservoir through an external heat exchanger to remove excess heat, then returns it to the working elements (impeller and runner), is thrown outward where it takes the form of a toroid (doughnut shape).

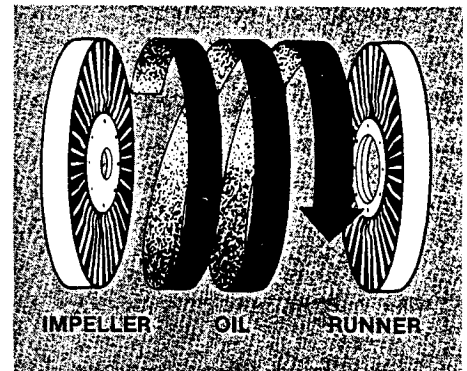
Varying the quantity (mass) of oil in this toroid varies the output speed. A movable scoop tube controls the amount of oil in the toroid. You can control the position of this scoop tube (and the amount of oil in the working circuit) either manually or with automatic control devices. The scoop tube returns the oil to the reservoir, where it starts once again through the pump, heat exchanger and back to the working circuit. The scoop tube gives you fast response and



smooth, stepless speed control over a wide range, i.e. 5:1 variable torque; 4:1 constant torque.

All moving parts in a Gýrol fluid drive are either submerged in oil or pressure-lubricated. The same oil transmits power, removes heat and lubricates.

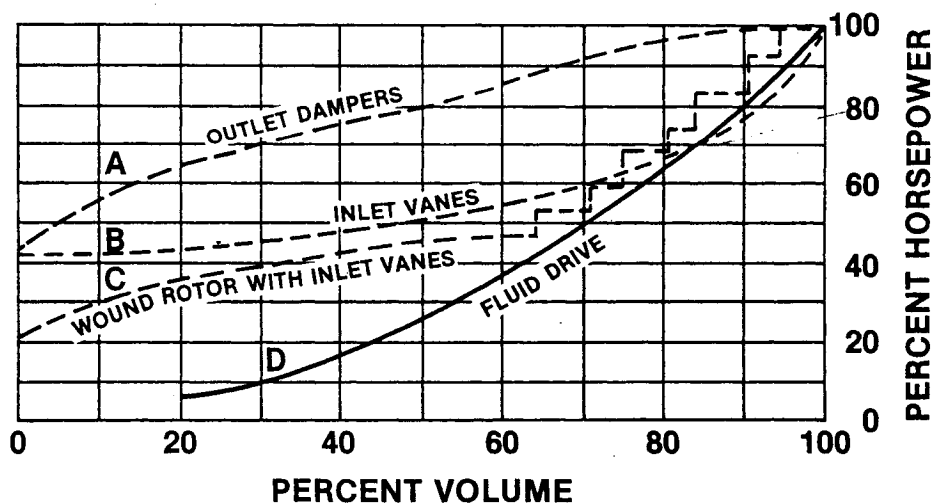
Gýrol fluid drives are simple, dependable power transmission devices which transmit the mechanical energy from the motor to the load at 95 % efficiency or better.



Gýrol® fluid drives save power.

By adjusting output speed, you can operate a fan or pump at reduced speed, which may be more efficient. For example, by operating a mechanical draft fan at the right speed to produce a desired air volume, you eliminate power losses without wasteful throttling from vanes or louvers. Similar power savings are found when you use a Gýrol fluid drive to vary the speed of centrifugal pumps, centrifugal compressors or other variable torque applications.

The curve shows the relative fan brake horsepower for various methods of controlling the volume of a typical mechanical draft fan. A — outlet dampers; B — inlet vanes; C — wound rotor with inlet vanes; D — fluid drive.



Appendix 2

MPIF apparent density and sieve analysis standard test methods

**2003
Edition**

Standard Test Methods for Metal Powders and Powder Metallurgy Products

**METAL POWDER
INDUSTRIES FEDERATION**



**Advancing
Powder
Metallurgy
& Powder
Materials
Worldwide**

Standard Test Methods for Metal Powders and Powder Metallurgy Products

Introduction

The Metal Powder Industries Federation

The Metal Powder Industries Federation (MPIF) is a voluntary-membership, not-for-profit trade association formed by the members of the P/M and particulate materials industry to promote the advancement of the metal powder producing and consuming industries and the practice of powder metallurgy and particulate materials (PM²) technologies. MPIF is a federation of six trade associations, each of which is concerned with some aspect of powder metallurgy, metal powders or particulate materials: the Powder Metallurgy Parts Association (PMPA), Metal Powder Producers Association (MPPA), Refractory Metals Association (RMA), Powder Metallurgy Equipment Association (PMEA), Advanced Particulate Materials Association (APMA), and the Metal Injection Molding Association (MIMA).

MPIF Standards

MPIF standards cover five categories:

1. P/M Nomenclature
2. Powder Testing Standards
3. P/M, P/F and MIM Materials Standards
4. Material (Product) Testing Standards
5. Safety Standards (ANSI/MPIF)

Certain trade associations within MPIF have established standards committees composed of technical people who are responsible for developing standards within their area of expertise and proposing them to the MPIF membership. Before a standard can be issued as an official MPIF standard, it must be approved by the MPIF corporate, voting membership as a whole. The standards contained in this book have all been adopted under this procedure.

Purpose and Use

MPIF standards are intended to present and clarify P/M technology so as to aid in the conduct of business. P/M materials specifications and test standards relate to those activities that concern designers and users of P/M parts as well as the manufacturer.

The use of any MPIF standard is entirely voluntary. Existence of an MPIF standard does not in any respect preclude any member of MPIF or non-member from manufacturing or selling products not included in this standard. Suppliers are at liberty to supply products or to use procedures other than those identified in any standard.

Disclaimers

Neither MPIF nor any of its federated trade association members assumes or accepts any liability resulting from use or non-use of any MPIF standard. In addition, neither MPIF nor any of its federated trade associations accepts any liability or responsibility for the compliance of any product with any standard or for the results of any testing or other procedure undertaken in accordance with any standard.

By publication of these standards, no position is taken with respect to the validity of any patent rights in connection therewith, and the Metal Powder Industries Federation does not undertake to insure anyone utilizing the standards against liability for infringement of any Letters Patent nor assume any such liability.

Availability

MPIF standards may be revised at any time by the group responsible for their creation. Users are cautioned to refer to the latest edition. Comments from any source concerning the standards or MPIF's standards programs are welcome.

No part of this publication may be reproduced, stored in a retrieval system, or transmitted, in any form or by any means, electronic, mechanical, photocopying, recording, or otherwise, without the prior permission of the publisher.

Published by
Metal Powder Industries Federation
105 College Road East
Princeton, New Jersey 08540-6692 U.S.A.
TEL: (609) 452-7700
FAX: (609) 987-8523
E-mail: info@mpif.org Website: www.mpiif.org



Copyright 2003

SBN No. 1-878954-94-6

Determination of Apparent Density of Free-Flowing Metal Powders Using The Hall Apparatus

MPIF Standard 04

Issued 1945, Adopted 1948

Revised 1972, 1980, 1985, 1992, 1998



STANDARD

04

1. SCOPE

- 1.1 This standard describes a method for determining the apparent density of free-flowing metal powders and is only suitable for those powders which will flow unaided through the specified Hall flowmeter funnel. See MPIF Standard No. 28 for apparent density of non-free-flowing metal powders.
- 1.2 *This standard may involve hazardous materials, operations and equipment. This standard does not purport to address all of the potential safety problems associated with its use. It is the responsibility of the user of this standard to establish appropriate safety and health practices and to determine the applicability of regulatory limitations prior to use.*

2. APPARATUS

- 2.1 Hall Flowmeter Funnel: A standard flowmeter funnel (Fig. 1) having an orifice 0.100 inch (2.54 mm) in diameter.
- 2.2 Density Cup: A cylindrical cup (Fig. 2) having a capacity of $25 \pm 0.03 \text{ cm}^3$, as measured by MPIF Standard No. 53, with an inside diameter of $28 \pm 0.5 \text{ mm}$.
- 2.3 Stand: A support (Fig. 3) to hold the flowmeter funnel concentric with the density cup so that the bottom of the orifice is approx. 1.0 inch (25 mm) above the top of the density cup when assembled (Fig. 4).
- 2.4 Base: A vibration-free table to support the flowmeter assembly.
- 2.5 Balance: A balance having a capacity of at least 200 g and a sensitivity of 0.01 g.

NOTE 1—Names of manufacturers of this apparatus are listed in General Information IV.

3. TEST SPECIMEN

- 3.1 The test specimen shall consist of a volume of approximately 30 to 40 cm^3 of metal powder, obtained in accordance with MPIF Standard 01, Sampling Finished Lots of Metal Powders.

4. PROCEDURE

- 4.1 The entire test specimen shall be carefully loaded into the flowmeter funnel and permitted to flow through the discharge orifice into the center of the density cup. The testing apparatus should not be moved during the filling.
- 4.2 When the powder completely fills and overflows the periphery of the density cup, the funnel shall be rotated approximately 90° in a horizontal plane so that the remaining powder falls away from the cup.
- 4.3 Using a non-magnetic spatula with the blade held perpendicular to the top of the cup, the powder shall be leveled off flush with the top of the density cup. Care must be taken to avoid jarring the apparatus at any time.
- 4.4 After the leveling operation, the density cup should be lightly tapped on the side to settle the powder to avoid spilling in transfer.
- 4.5 The powder shall be transferred to the balance and weighed to the nearest 0.1g. This is the mass M.

5. CALCULATIONS

- 5.1 Calculate the apparent density as follows:

$$\text{Apparent Density, } (\rho_a) = \frac{M}{V}$$

where:

M = mass of powder from the density cup in grams

V = the volume of the cup (as determined by the procedure in Standard 53)

NOTE 2—If the measured volume is $25 \pm 0.03 \text{ cm}^3$ it is permissible to use 25 cm^3 for V.

NOTE 3—While the specified volume of the density cup is $25 \pm 0.03 \text{ cm}^3$ it is permissible to use a cup with a volume from 24.8 to 25.2 cm^3 provided the actual measured volume is used to calculate the apparent density of the powder.

6. REPORT

- 6.1 Report the results as apparent density to the nearest 0.01 g/cm^3 .

7. PRECISION

- 7.1 The repeatability (r) and reproducibility (R) values were determined (1991) from an interlaboratory study analyzed statistically according to ASTM E 691 as follows:
- 7.1.1 Repeatability $r=1.5\%$. Duplicate analyses of unlubricated or lubricated metal powders by the same operator and same apparatus should not differ by more than 1.5% at the 95% confidence level.
- 7.1.2 Reproducibility $R=3\%$ for unlubricated and lubricated iron powder and $R=5\%$ for lubricated brass and bronze powders. The difference between two single and independent results obtained by different operators working in different laboratories on lubricated and unlubricated iron powders should not differ by more than 3% at the 95% confidence level. Analyses of lubricated brass and bronze metal powders should not differ by more than 5% at the 95% confidence level.

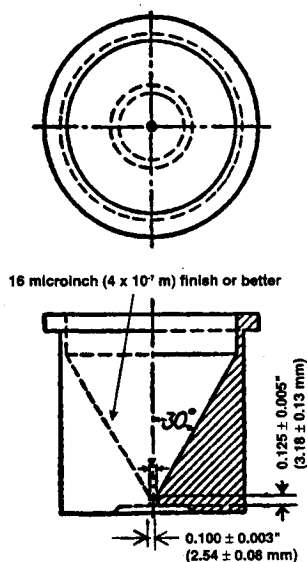


FIGURE 1: Hall Flowmeter Funnel

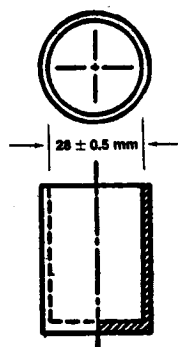


FIGURE 2: Density Cup ($25 \pm 0.03 \text{ cm}^3$)

APPENDIX

- A1. COMPARABLE STANDARDS
ASTM B 212
ISO 3923/1

Disclaimer

By publication of these standards no position is taken with respect to the validity of any patent rights in connection therewith, and the Metal Powder Industries Federation does not undertake to insure anyone utilizing the standards against liability for infringement of any Letters Patent nor assume any such liability.

MPIF standards are adopted in the public interest and are designed to eliminate misunderstandings between the manufacturer and the purchaser and to assist the purchaser in selecting and obtaining the proper material for his particular product. Existence of an MPIF standard does not in any respect preclude any MPIF member or non-member from manufacturing or selling products not included in this standard or from utilizing procedures or equipment other than those included in this standard.

The metric system conversion factors used in this standard are in accordance with IEEE/ASTM SI 10; "Standard for Use of the International System of Units (SI): The Modern Metric System". Recognized as an American National Standard (ANSI), the standard is published by the following organizations: ASTM, 100 Barr Harbor Drive, West Conshohocken, PA 19428-2959, USA; and Institute of Electrical and Electronics Engineers, Inc., 345 East 47th Street, New York, NY 10017, USA.

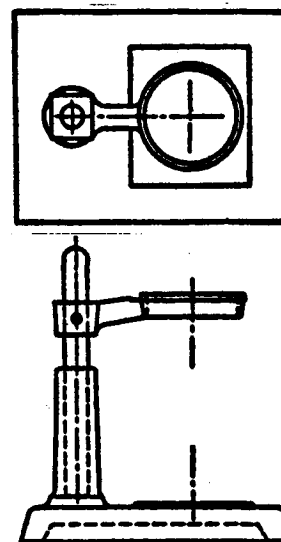


FIGURE 3: Stand

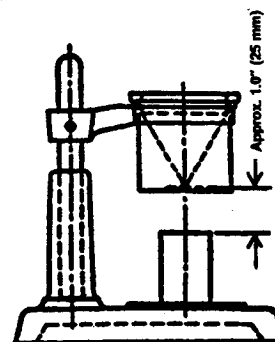


FIGURE 4: Assembly

This Standard, prepared by the Metal Powder Industries Federation, is subject to periodic revision. Suggestions for revision should be addressed to the Metal Powder Industries Federation, 105 College Road East, Princeton, N.J. 08540-6692. Users of Standards are cautioned to secure the latest editions. Complete edition of standards may be obtained from the Federation at the above address.

Method for

**Determination of Sieve Analysis
of Metal Powders**

MPIF Standard 05

Issued 1945, Revised 1949, Adopted 1949,
Revised 1962, 1973, 1985, 1992, Reaffirmed 1998

Edited 2003

**1. SCOPE**

- 1.1 This standard describes a method for determining the dry sieve analysis of granular metal powders.
- 1.2 *This standard may involve hazardous materials, operations and equipment. This standard does not purport to address all of the potential safety problems associated with its use. It is the responsibility of the user of this standard to establish appropriate safety and health practices and to determine the applicability of regulatory limitations prior to use.*

2. APPARATUS

- 2.1 Sieves: A set of calibrated sieves should be selected based upon the mesh size of powders being evaluated. The sieves shall be 8 in. (200 mm) in diameter and either 1 or 2 in. (25 or 50 mm) in depth and fitted with brass, bronze, stainless steel, or other suitable wire. The new U.S. Series standard sieves are the preferred series to use.

NOTE 1—For more detailed information, refer to ASTM Standard E 11.

NOTE 2—The new U.S. Series was adopted in 1970. The old U.S. Series standard sieves and equipment sieves manufactured by other companies, such as Tyler, may also be used if the new U.S. Series is not available. Care should be taken to make sure that sieve opening sizes are correct when performing standardization work.

Table 1 Testing Sieves According to the U.S. Standard Series and Tyler Standard Screen Scale Sieve Series.

Mesh Designation Number	Sieve Opening (μm)		
	New U.S. Series	Old U.S. Series	Tyler Series
20	850	840	833
35	—	—	417
40	425	420	—
60	250	250	250
80	180	177	175
100	150	149	147
140	106	105	—
150	—	—	104
200	75	74	74
230	63	62	—
250	—	—	63
325	45	44	45

- 2.2 Sieve Shaker: A mechanically operated single eccentric sieve shaker which imparts to the nest of sieves a rotary motion of 285 ± 15 rpm and a tapping action of 150 ± 10 taps per minute. The sieve shaker shall be fitted with a plug to receive the impact of the tapping device. The entire apparatus shall be mounted rigidly, and preferably shall be provided with an accurate time switch.

NOTE 3—Names of manufacturers of this apparatus are listed in General Information IV.

- 2.3 A balance having a capacity of at least 150 g and a sensitivity of 0.01 g.

NOTE 4—Use of a sound-proof enclosure is recommended.

3. TEST SPECIMEN

- 3.1 The test specimen, obtained in accordance with MPIF Standard 01 and having an apparent density greater than 1.5 g/cm^3 as determined by MPIF Standards 04 or 28, shall be 90–110 g. If the apparent density of the powder is less than 1.50 g/cm^3 , a 40–60 g sample shall be used.

4. PROCEDURE

- 4.1 The group of sieves selected shall be assembled in consecutive order based on size of openings. The sieve having the largest opening shall be placed at the top, and the assembly completed by a solid collecting pan placed below the bottom sieve. The test specimen shall be placed on the top sieve, and this sieve closed with a solid cover. The sieve assembly shall then be fastened securely in a suitable mechanical sieve shaking device and operated for 15 minutes.
- 4.2 The sieved fractions shall be removed from the nest of sieves by removing the coarsest sieve from the nest, gently tapping its contents to one side and pouring them on a glazed paper. Any material adhering to the bottom of the sieve and frame shall be brushed with a soft brush into the next finer sieve. The sieve just removed then shall be tapped upside down, on the paper containing the portion that had been retained on it. This fraction shall be weighed to within 0.1 g. This process shall be repeated for each sieve in the nest, and the fraction collected in pan shall also be removed and weighed. The sum of the masses of all the fractions shall be recorded. The difference

between the sum and the total sample mass shall be added to the mass of the fraction collected in the pan, provided the sum of all the fractions is not less than 99% of the original sample mass.

NOTE 5—If the sum is less than 99%, check for weighing errors, pin holes, etc. and repeat the test.

5. REPORT

- 5.1 The masses of the fractions retained on each sieve and the mass of the fraction collected in the pan shall be expressed as percentages of the test specimen mass to the nearest 0.1%. Powder specimen whose mass fraction is less than 0.1%, shall be reported as "trace". If fraction is absent, it shall be reported as "0.0".
- 5.2 Form for reporting test data of a typical 100 mesh powder.

Table 2 New U.S. Standard Series

Particle Size (μm)	Mesh Designation No.	Percentage By Mass
> 180	+ 80	
$\leq 180 > 150$	– 80 + 100	
$\leq 150 > 106$	– 100 + 140	
$\leq 106 > 75$	– 140 + 200	
$\leq 75 > 45$	– 200 + 325	
≤ 45	– 325	

Table 3 Old U.S. Standard Series

Particle Size (μm)	Mesh Designation No.	Percentage By Mass
> 177	+ 80	
$\leq 177 > 149$	– 80 + 100	
$\leq 149 > 105$	– 100 + 140	
$\leq 105 > 74$	– 140 + 200	
$\leq 74 > 44$	– 200 + 325	
≤ 44	– 325	

Table 4 Tyler Standard Screen Scale Sieve Series

Particle Size (μm)	Mesh Designation No.	Percentage By Mass
> 175	+ 80	
$\leq 175 > 149$	– 80 + 100	
$\leq 149 > 104$	– 100 + 150	
$\leq 104 > 74$	– 150 + 200	
$\leq 74 > 45$	– 200 + 325	
≤ 45	– 325	

- 5.3 Interpretation of this report should be made with reference to dimensional tolerance of the standard sieves as specified in ASTM E 11.

6. PRECISION

- 6.1 An interlaboratory study of the sieve analysis of

metal powders was run in 1993 and 1994 using the procedures contained in MPIF Standard 05 (1992). Each of twelve laboratories made three tests on four powder samples using each of two sets of sieves. One set of sieves was a standard set that was circulated to each laboratory in turn. A second set of sieves was chosen by each laboratory from its in-house sieve stock. ASTM Practice E 691 was followed for the design and analysis of the data. The details are given in MPPA Research Report MPPA R-05-95.

- 6.2 There were five U.S. Series standard sieves in each sieve nest: 80 mesh, 100 mesh, 140 mesh, 200 mesh, and 325 mesh plus a cover and a pan.
- 6.3 The precision information given below covers the percent retained between any pair of sieves, the percent retained on the coarsest sieve, the percent passing the finest sieve, and the cumulative percentages calculated from all sieves of greater openings above any sieve in the set.
- 6.4 The 95% repeatability limit, r , (within a laboratory) is represented by the equation:

$$r = 0.4 + 0.03 \times [\text{SF}], \text{ where}$$

[SF] is the % retained on the sieve of interest.

- 6.5 The 95% reproducibility limit, R , (between laboratories) is smaller for the circulated sieves than for the in-house sieves. For in-house sieves R can be calculated from the following equations:

$$R = 1.2 + 0.15 \times [\text{SF}] \text{ for } [\text{SF}] \text{ from } 0 \text{ to } 22, \text{ or}$$

$$R = 4.5 \text{ for } [\text{SF}] \text{ from } 22.1 \text{ to } 50, \text{ where}$$

[SF] is the % retained on the sieve of interest.

For circulated sieves (or by analogy matched sieves obtained by two laboratories) R can be calculated from the following equations:

$$R = 0.3 + 0.064 \times [\text{SF}] \text{ for } [\text{SF}] \text{ from } 0 \text{ to } 30, \text{ or}$$

$$R = 2.2 \text{ for } [\text{SF}] \text{ from } 30.1 \text{ to } 50, \text{ where}$$

[SF] is the % retained on the sieve of interest.

- 6.6 Duplicate results from the same laboratory should be considered acceptable at the 95% confidence level unless they differ by more than r , the repeatability interval.
- 6.7 Duplicate results from two different laboratories should be considered acceptable at the 95% confidence level unless they differ by more than R , the reproducibility interval.

APPENDIX

- A1. **Certified Sieves — Master Set**
Sieves conforming to ASTM Standard E 11 can be obtained from the sieve manufacturers, and arrangements can be made through them to have the sieves certified to NIST Standards. If used continually, the sieves will, after a period of time, become less accurate and might no longer be acceptable as certified sieves. The common practice, which would be considered acceptable according to this standard, would be to use the certified sieves as a master set for checking and calibrating other working sets of sieves.
- A2. **Matched Sieves**
The use of a matched set of sieves, established

through use of a standard powder is recommended when closer correlation of tests between supplier and consumer is desired.

A3.

Table 5 Suggested Sieve Series (New U.S.) for Metal Powders

Nominal Powder Mesh Size		20	40	60	100	140	200	325
New U.S. Sieve Series (Mesh Sizes)	20	✓	✓					
	40	✓	✓	✓				
	60	✓	✓	✓				
	80				✓			
	100	✓	✓	✓	✓	✓		
	140			✓	✓	✓	✓	
	200	✓	✓	✓	✓	✓	✓	✓
	230						✓	✓
	325		✓	✓	✓	✓	✓	✓
	Pan	✓	✓	✓	✓	✓	✓	✓

A4. Report on Precision and Accuracy of MPIF Standard 05. The complete report on this work, MPPA R-05-95, is available in the offices of the Metal Powder Industries Federation.

A5. COMPARABLE STANDARDS
ASTM B 214
ISO 4497

Disclaimer

By publication of these standards no position is taken with respect to the validity of any patent rights in connection therewith, and the Metal Powder Industries Federation does not undertake to insure anyone utilizing the standards against liability for infringement of any Letters Patent nor assume any such liability.

MPIF standards are adopted in the public interest and are designed to eliminate misunderstandings between the manufacturer and the purchaser and to assist the purchaser in selecting and obtaining the proper material for his particular product. Existence of an MPIF standard does not in any respect preclude any MPIF member or non-member from manufacturing or selling products not included in this standard or from utilizing procedures or equipment other than those included in this standard.

The metric system conversion factors used in this standard are in accordance with IEEE/ASTM SI 10; "Standard for Use of the International System of Units (SI): The Modern Metric System". Recognized as an American National Standard (ANSI), the standard is published by the following organizations: ASTM, 100 Barr Harbor Drive, West Conshohocken, PA 19428-2959, USA; and Institute of Electrical and Electronics Engineers, Inc., 345 East 47th Street, New York, NY 10017, USA.

This Standard, prepared by the Metal Powder Industries Federation, is subject to periodic revision. Suggestions for revision should be addressed to the Metal Powder Industries Federation, 105 College Road East, Princeton, N.J. 08540-6692. Users of Standards are cautioned to secure the latest editions. Complete edition of standards may be obtained from the Federation at the above address.

Appendix 3
Results of plant trials

M-408 trials: response time for a step change in feed rate

Test no. m1
 Date 16/2/2004
 Time 15:00
 Product S-1 D.A (g/cc) 2.90 to 3.50 S-200 (%) 58 to 66
 Feed rate (lb/hr) 4350
 Air flow (ACFM) 5400 3.25 inH2O
 Power (A) 81.8 81.8 82.1 82.5 82.8 83.2 83.7 84.2 84.1
 m Tr
 Step change in feed rate: 4350 to 5350 3min36sec 5350 to 3350 3min45sec

	time (min)							
mesh	0	10	20	30	40	50	60	70
no.60	trace	trace	trace	trace	trace	trace	trace	trace
no.80	0.2	0.1	0.1	0.1	0.1	0.1	0.3	0.4
no.100	0.9	1.0	0.8	1.1	1.2	1.3	1.5	1.6
no.140	4.4	4.4	4.8	4.9	5.2	5.6	5.8	6.2
no.200	13.6	13.3	15.0	15.5	16.4	15.9	16.6	17.9
no.325	28.2	27.9	28.8	31.1	31.1	29.8	29.9	30.7
pan	52.7	53.3	50.5	47.3	46.0	47.3	45.9	43.2

D.A. (g/cc)	3.11	3.12	3.13	3.16	3.17	3.18	3.19	3.21
	100.0	100.0	100.0	100.0	100.0	100.0	100.0	100.0
	52.7	53.3	50.5	47.3	46.0	47.3	45.9	43.2
S+100	1.1	1.1	0.9	1.2	1.3	1.4	1.8	2.0
S-200	80.9	81.2	79.3	78.4	77.1	77.1	75.8	73.9
S+140	5.5	5.5	5.7	6.1	6.5	7.0	7.6	8.2

Power (kW)	194.7	195.4	196.4	197.1	198.0	199.2	200.4	200.2
------------	-------	-------	-------	-------	-------	-------	-------	-------

83.5 83.1 82.5 81.6 81.3

m
3350 to 4350

80	90	100	110	120
trace	trace	trace	trace	trace
0.4	0.3	0.2	0.1	0.1
1.9	1.6	1.6	1.3	1.1
6.3	5.7	5.6	5.5	5.0
18.2	17.3	16.7	16.1	15.7
31.4	30.2	29.8	30.1	30.8
41.8	44.9	46.1	46.9	47.3

microns	0min	50min
45	52.7	47.3
75	80.9	77.1
106	94.5	93.0
150	98.9	98.6
180	99.8	99.9
250	100	100

3.23	3.24	3.22	3.21	3.18
100.0	100.0	100.0	100.0	100.0
41.8	44.9	46.1	46.9	47.3
2.3	1.9	1.8	1.4	1.2
73.2	75.1	75.9	77.0	78.1
8.6	7.6	7.4	6.9	6.2

198.7 197.8 196.4 194.2 193.5

M-408 trials: response time for a step change in feed rate

Test no. m2 Ball mill in emptying mode: at t=0, the -200mesh goal was 74%(new spec)
 Date 22/2/2004 Atomized shot has a higher carbon content: higher productivity, more brittle
 Time 16:00 To reduce quantity of shot in the mix due to scrap price increase

Product S-3 D.A (g/cc) 2.80 to 3.40 S-200 (%) 64 to 76

Feed rate (lb/hr) 3500
 Air flow (ACFM) 4500 1.83 inH2O 1.86 inH2O 1.83 inH2O 1.95 inH2O
 Power (A) 79.6 79.6 79.5 79.7 79.8 80.6 81.2 81.8

Step change in feed rate: 3500 to 5500 3min10sec 5500 to 3500 3min18sec

	time (min)						
mesh	0	10	20	30	40	50	60
no.60	trace	trace	trace	trace	trace	trace	trace
no.80	0.2	0.1	0.3	0.3	0.3	0.5	0.7
no.100	1.5	1.7	1.8	1.8	1.9	2.4	2.8
no.140	6.9	7.3	7.0	7.2	7.4	8.1	8.7
no.200	21.6	21.7	21.6	21.5	22.7	22.8	23.0
no.325	34.2	33.1	33.4	33.4	33.8	33.7	33.4
pan	35.6	36.1	35.9	35.8	33.9	32.5	31.4

D.A. (g/cc)	3.27	3.27	3.28	3.27	3.29	3.31	3.35
	100.0	100.0	100.0	100.0	100.0	100.0	100.0
	35.6	36.1	35.9	35.8	33.9	32.5	31.4
S+100	1.7	1.8	2.1	2.1	2.2	2.9	3.5
S-200	69.8	69.2	69.3	69.2	67.7	66.2	64.8
S+140	8.6	9.1	9.1	9.3	9.6	11.0	12.2
	189.4	189.2	189.7	189.9	191.8	193.3	194.7

M-408 trials: response time for a step change in feed rate

Test no. m3
Date 22/3/2004
Time 16:00

Since Q is high, the effect of feed rate is less predominant

Product S-2 D.A (g/cc) 3.20 to 3.80 S-200 (%) 42 to 54

From operator @ t=0: 2.57g/cc, 10.7%+100, 54.6%-200

Feed rate (lb/hr) 7150

Air flow (ACFM) 6500

dp (inH2O) 4.55 4.59 4.60 4.53 4.54 4.47 4.63 4.51

Power (A) 92.1 91.8 91.3 90.9 90.3 89.4 88.8 88.7

m Tr

Step change in feed rate: 7150 to 5150 3 min

	time (min)						
mesh	0	10	20	30	40	50	60
no.60	0.4	0.3	0.3	0.2	0.1	0.1	0.1
no.80	4.9	4.9	4.8	4.4	4.2	4.1	3.9
no.100	9.0	8.9	8.7	8.4	8.2	8.0	7.8
no.140	15.9	15.4	15.5	15.6	15.1	15.0	15.2
no.200	23.5	24.2	23.9	23.4	23.6	23.8	23.8
no.325	23.2	24.4	24.5	24.2	25.0	24.5	24.8
pan	23.1	21.9	22.3	23.8	23.8	24.5	24.4

D.A. (g/cc)	3.68	3.68	3.68	3.65	3.63	3.61	3.60
	100.0	100.0	100.0	100.0	100.0	100.0	100.0
	23.1	21.9	22.3	23.8	23.8	24.5	24.4
S+100	13.9	13.8	13.5	12.8	12.4	12.1	11.7
S-200	46.3	46.3	46.8	48.0	48.8	49.0	49.2
S+140	29.8	29.2	29.0	28.4	27.5	27.1	26.9

M-408 trials: response time for a step change in air flow (-500SCFM)

Test no. Q1
 Date 29/1/2004
 Time 15:15
 Product S-2 D.A (g/cc) S-200 (%)
 3.20 to 3.80 42 to 54
 Feed rate (lb/hr) 4800
 Air flow (ACFM) 5500
 Power (A) 83.2 83.4 83.1 83 83.5 83.2 83.2 83.1 83.2 83.4 83.2 83.3
 Step change in air flow: Q Tr
 5500 to 5000 1min50sec

mesh	time (min)										
	0	1	2	3	4	5	6	7	8	9	10
no.60	trace	trace	trace	trace	trace	trace	trace	trace	trace	trace	trace
no.80	3.5	3.0	2.9	2.5	2.3	2.3	2.4	2.4	2.5	2.4	2.4
no.100	7.5	6.9	7.2	6.4	5.8	6.7	5.7	5.8	6.5	6.4	6.3
no.140	15.7	13.9	14.2	13.6	12.9	13.6	11.7	12.8	13.4	13.0	12.7
no.200	25.6	23.1	24.8	23.0	23.3	22.3	20.0	22.5	24.4	22.9	21.7
no.325	25.8	25.3	25.3	25.9	27.2	25.1	24.6	25.8	26.7	25.9	24.6
pan	21.9	27.8	25.6	28.6	28.5	30.0	35.6	30.7	26.5	29.4	32.3

D.A. (g/cc)	3.58	3.53	3.55	3.53	3.51	3.54	3.47	3.50	3.54	3.54	3.51
-------------	------	------	------	------	------	------	------	------	------	------	------

S+100	11.0	9.9	10.1	8.9	8.1	9.0	8.1	8.2	9.0	8.8	8.7
S-200	47.7	53.1	50.9	54.5	55.7	55.1	60.2	56.5	53.2	55.3	56.9

198.5 197.8 197.5 198.7 198.0 198.0 197.8 198.0 198.5 198.0 198.3

M-408 trials: response time for a step change in air flow (+700SCFM)

Test no.	Q2												
Date	9/2/2004												
Time	16:00:00 PM												
Product	S-4	D.A (g/cc)	S-200 (%)										
		3.20 to 3.80	47 to 59										
Feed rate (lb/hr)	4800					Q	dp(inH2O)						
Air flow (ACFM)	5500					5500	3.22						
Power (A)	83.5					6200	3.75						
		83.4	83.5	83.6	83.4	83.5	83.5	83.3	83.5	83.4	83.6	83.5	
Step change in air flow:		Q	Tr										
		5500 to 6200	2min15sec										
	time (min)												
mesh	0	1	2	3	4	5	6	7	8	9	10		
no.60	trace	trace	trace	trace	trace	trace	trace	trace	trace	trace	trace		
no.80	2.4	2.8	2.7	2.7	2.6	2.4	2.8	2.6	2.7	3.0	2.5		
no.100	6.3	7.3	7.2	7.8	7.1	7.4	7.5	7.2	7.4	7.5	7.1		
no.140	14.5	16.1	16.3	17.6	16.2	16.2	15.3	15.9	16.8	17.1	15.8		
no.200	26.8	28.3	27.8	29.4	28.3	28.3	27.9	27.8	29.5	30.2	28.3		
no.325	27.6	27.6	27.4	27.6	27.3	27.3	28.0	27.1	27.8	27.4	27.4		
pan	22.4	17.9	18.6	14.9	18.5	18.4	18.5	19.0	15.8	14.8	18.9		
D.A. (g/cc)	3.62	3.65	3.64	3.66	3.64	3.64	3.64	3.64	3.66	3.67	3.64		
	100.0	100.0	100.0	100.0	100.0	100.0	100.0	99.6	100.0	100.0	100.0		
	22.4	17.9	18.6	14.9	18.5	18.4	18.5	19.4	15.8	14.8	18.9		
S+100	8.7	10.1	9.9	10.5	9.7	9.8	10.3	9.8	10.1	10.5	9.6		
S-200	50.0	45.5	46.0	42.5	45.8	45.7	46.5	46.1	43.6	42.2	46.3		
	198.5	198.7	199.0	198.5	198.7	198.7	198.3	198.7	198.5	199.0	198.7		

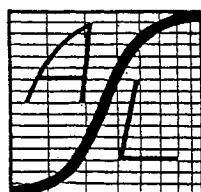
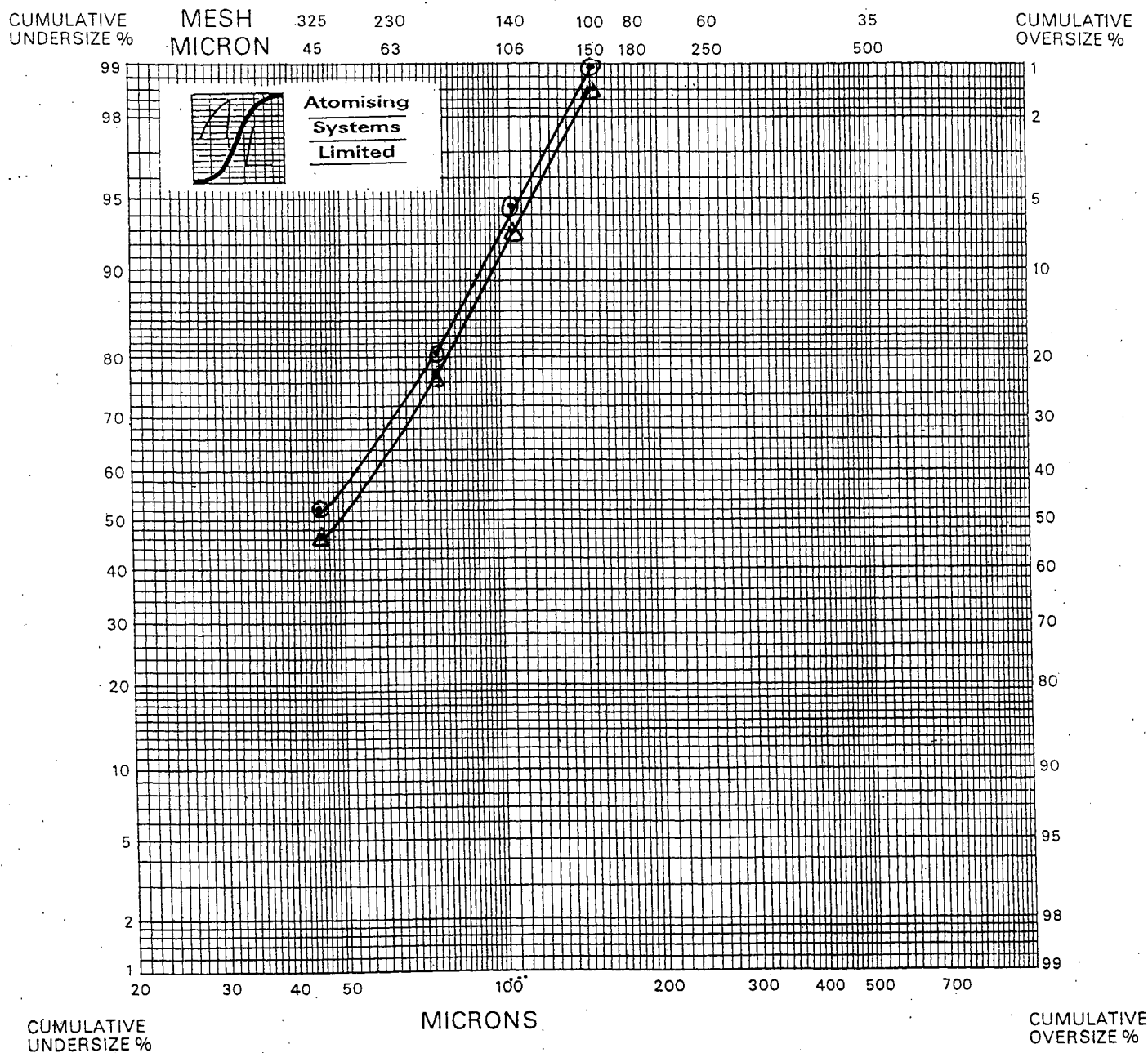
M-408 trials: output trunnion pressure vs Air flow

Test no.	dp1		Test no.	dp2	
Date	10/2/2004		Date	9/3/2004	
Time	14:00:00 PM		Time	11AM	
Product	S-4		Product	S-1	
Feed rate (lb/hr)	4100		Feed rate (lb/hr)	4900	
Air flow (ACFM)	5500		Air flow (ACFM)	6100	
Power (A)	79.2		Power (A)	84.4	
%out	Q(ACFM)	dp (inH2O)	%out	Q(ACFM)	dp (inH2O)
20.1	2000	0.30	15.1	2000	0.32
35.6	2500	0.49	31.2	2500	0.68
38.9	3000	0.80	38.9	3500	1.30
44.5	3500	1.02	52.3	4250	1.80
49.7	4000	1.40	65.4	4730	2.32
55.1	4500	1.90	75.3	6000	3.86
62.1	5000	2.53	100.0	6650	4.60
70.3	5500	3.10			
83.6	6000	3.54			
100.0	6270	3.73			

FEED RATE STEP CHANGE : +1000 lb/hr		RUN No.
AIR FLOW = 5400 ACFM	PRODUCT: S-1	M1
		DATE
		16/2/2004

① AT $t=0$, \dot{m} : 4350 \rightarrow 5350 lb/hr

Δ AT $t=50$ min, $\dot{m} = 5350$ lb/hr

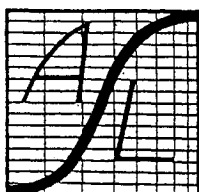
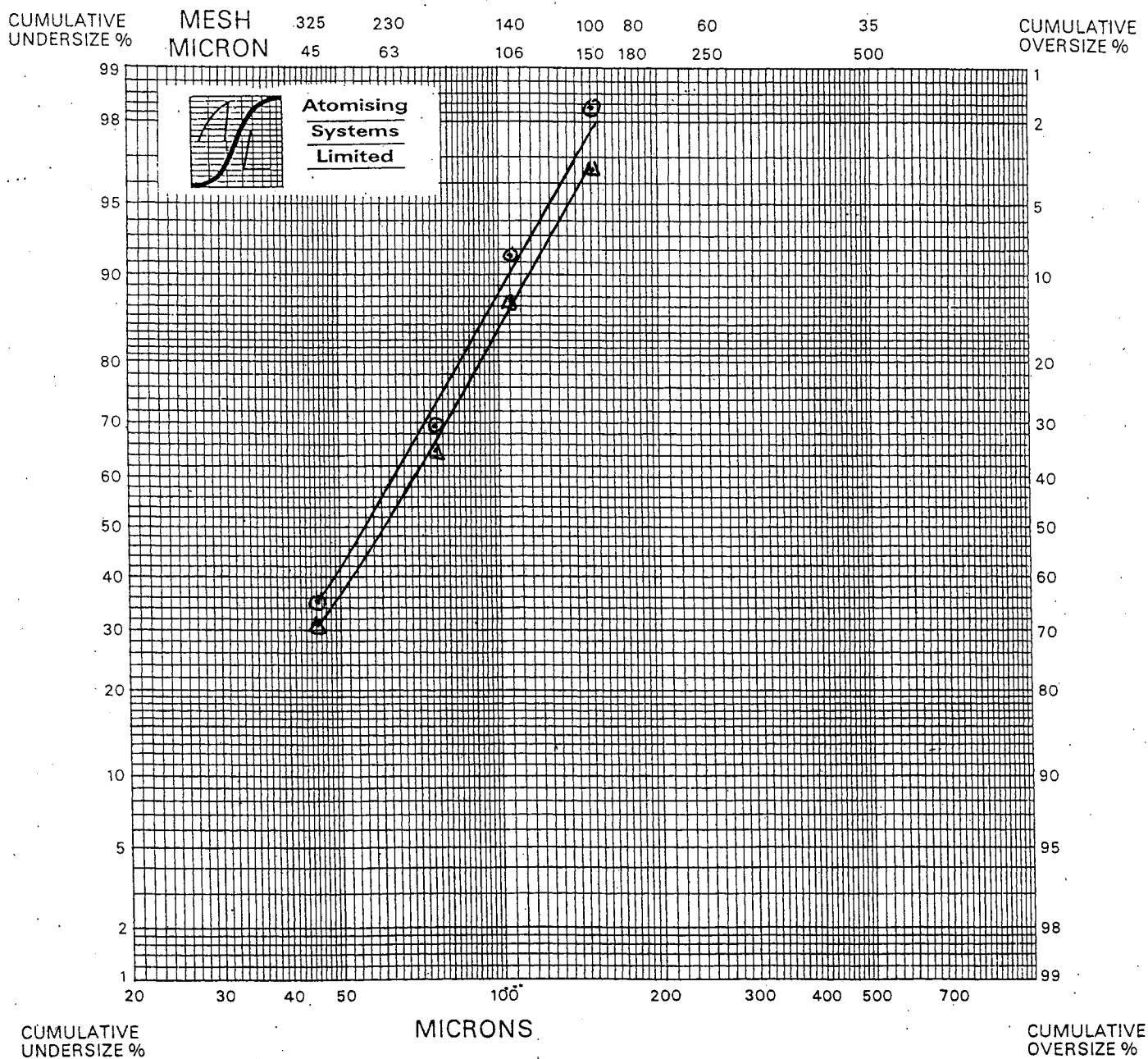


**Atomising
Systems
Limited**

FEED RATE STEP CHANGE: +2000 lb/hr		RUN No. 112
AIR FLOW=4500 ACFM	PRODUCT: S-3	
		DATE 22/2/2004

⊙ AT $t=0$, \dot{m} : 3500 \rightarrow 5500 lb/hr

Δ AT $t=60$ min, \dot{m} = 5500 lb/hr

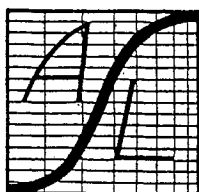
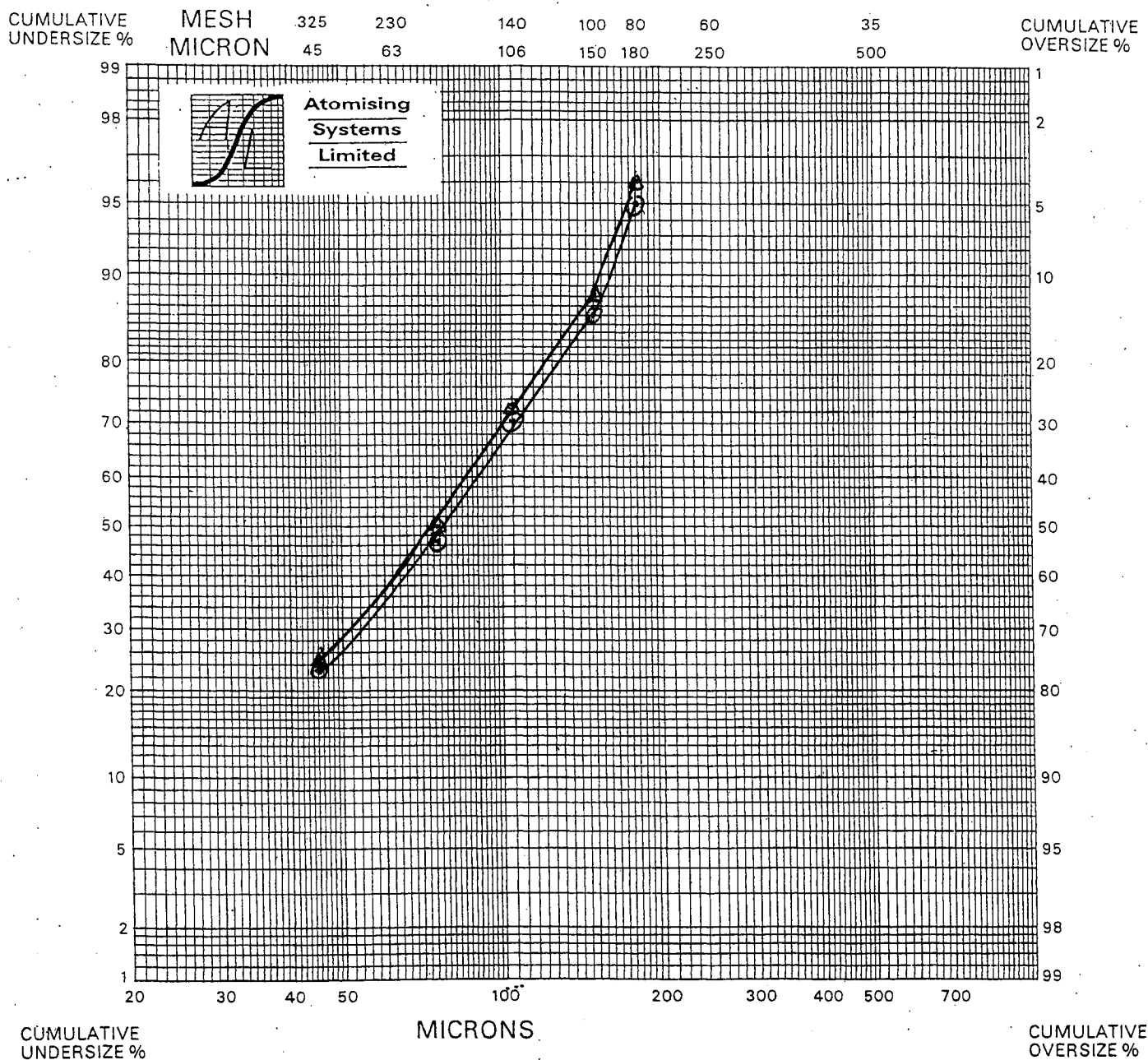


**Atomising
Systems
Limited**

FEED RATE STEP CHANGE! -2000 lb/hr		RUN No. M3
AIR FLOW=6500 ACFM	PRODUCT: S-2	
		DATE 22/3/2004

① AT $t=0$, \dot{m} : 7150 \rightarrow 5150 lb/hr

② AT $t=60$ min, \dot{m} = 5150 lb/hr

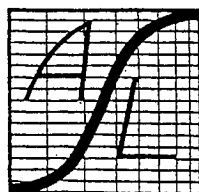
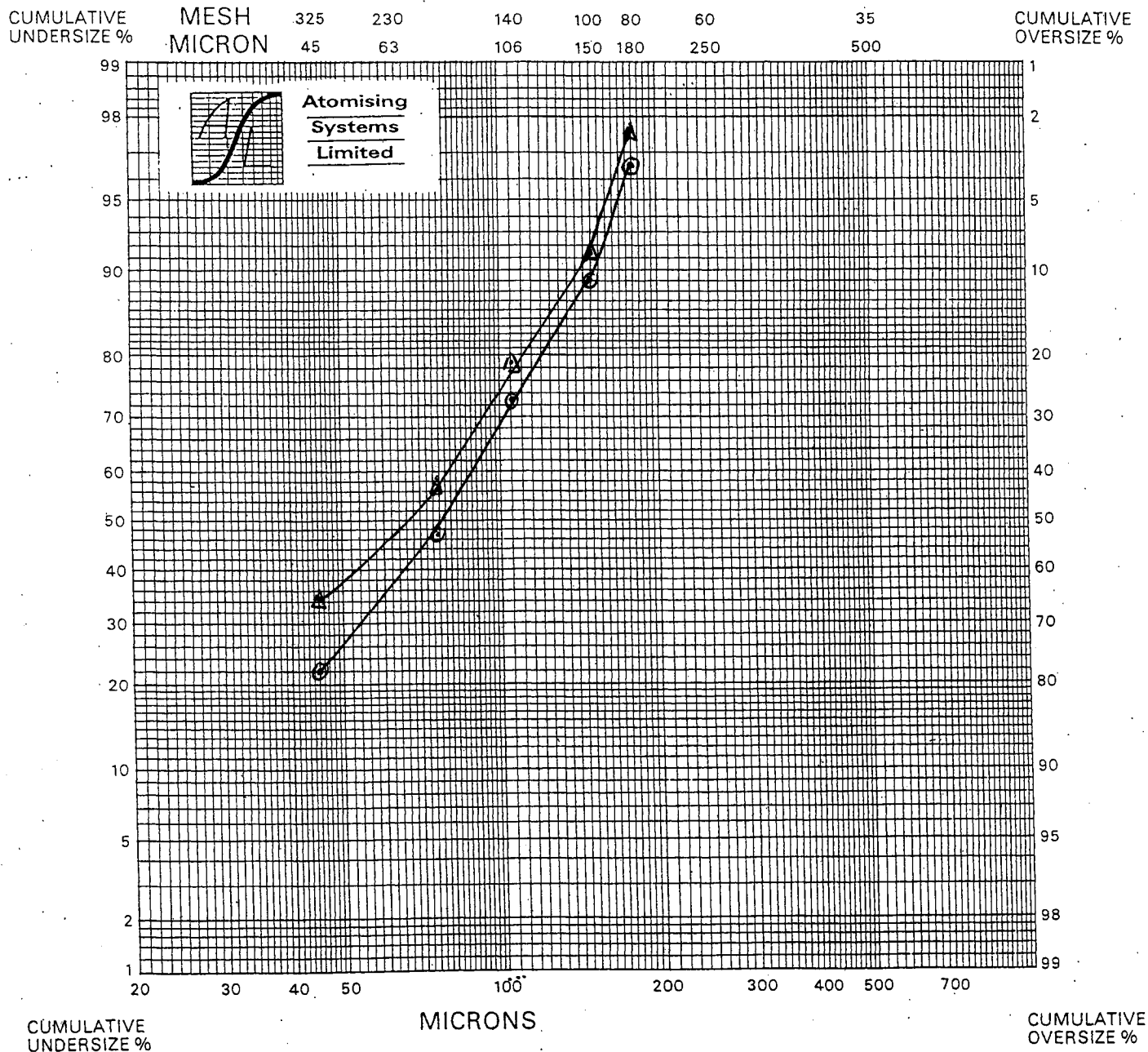


**Atomising
Systems
Limited**

AIR FLOW STEP CHANGE: -500 ACFM		RUN No. Q1
FEED RATE = 4800 lb/hr	PRODUCT: S-2	
		DATE 29/1/2004

① AT $t=0$, $Q: 5500 \rightarrow 5000$ ACFM

② AT $t=10$ min, $Q = 5000$ ACFM

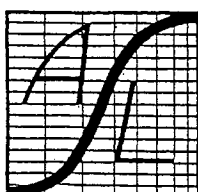
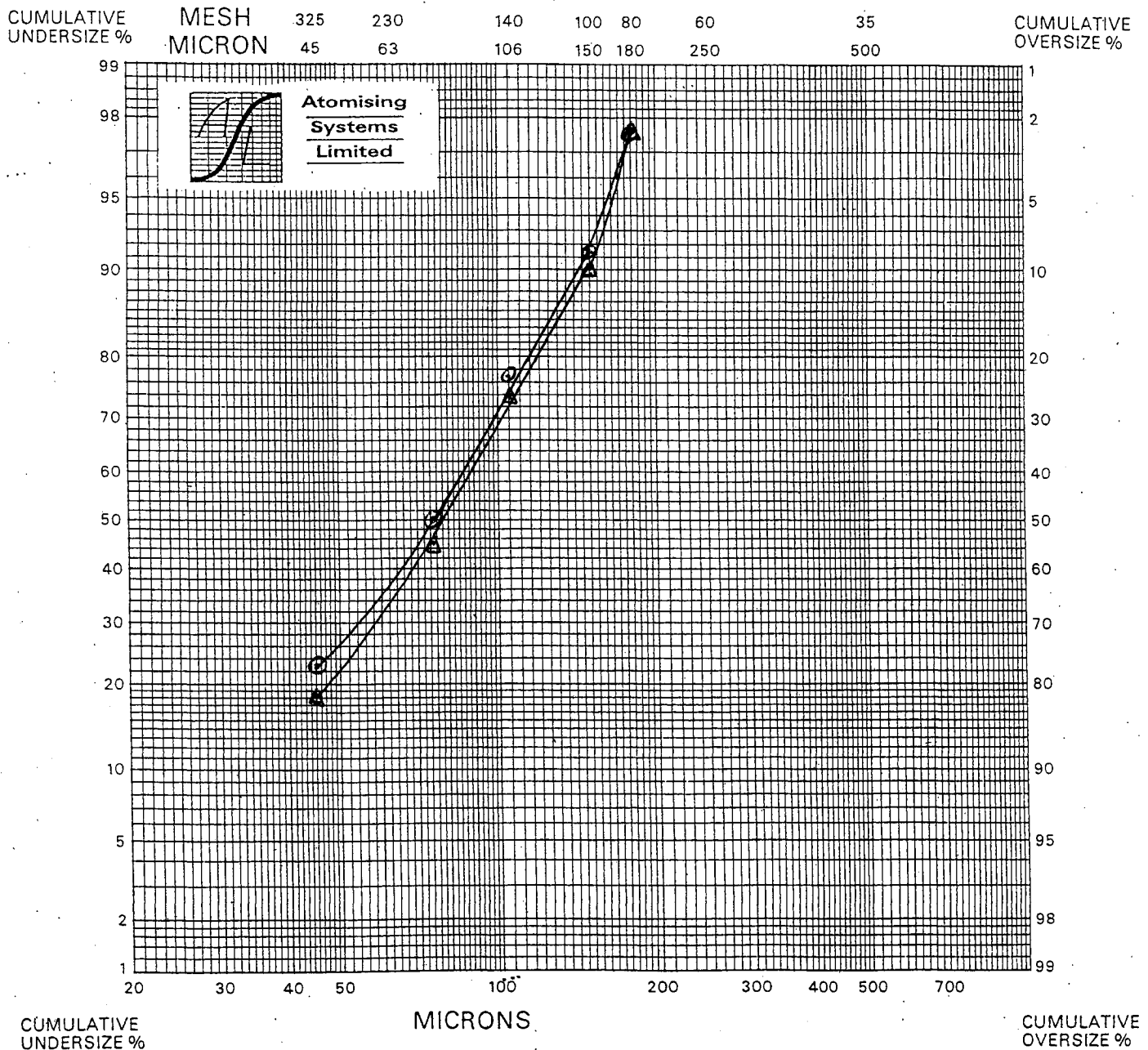


**Atomising
Systems
Limited**

AIR FLOW STEP CHANGE: + 700 ACFM		RUN No.
FEED RATE=4800 lb/hr	PRODUCT: S-4	Q2
		DATE 9/2/2004

Q AT $t=0$, $Q: 5500 \rightarrow 6200$ ACFM

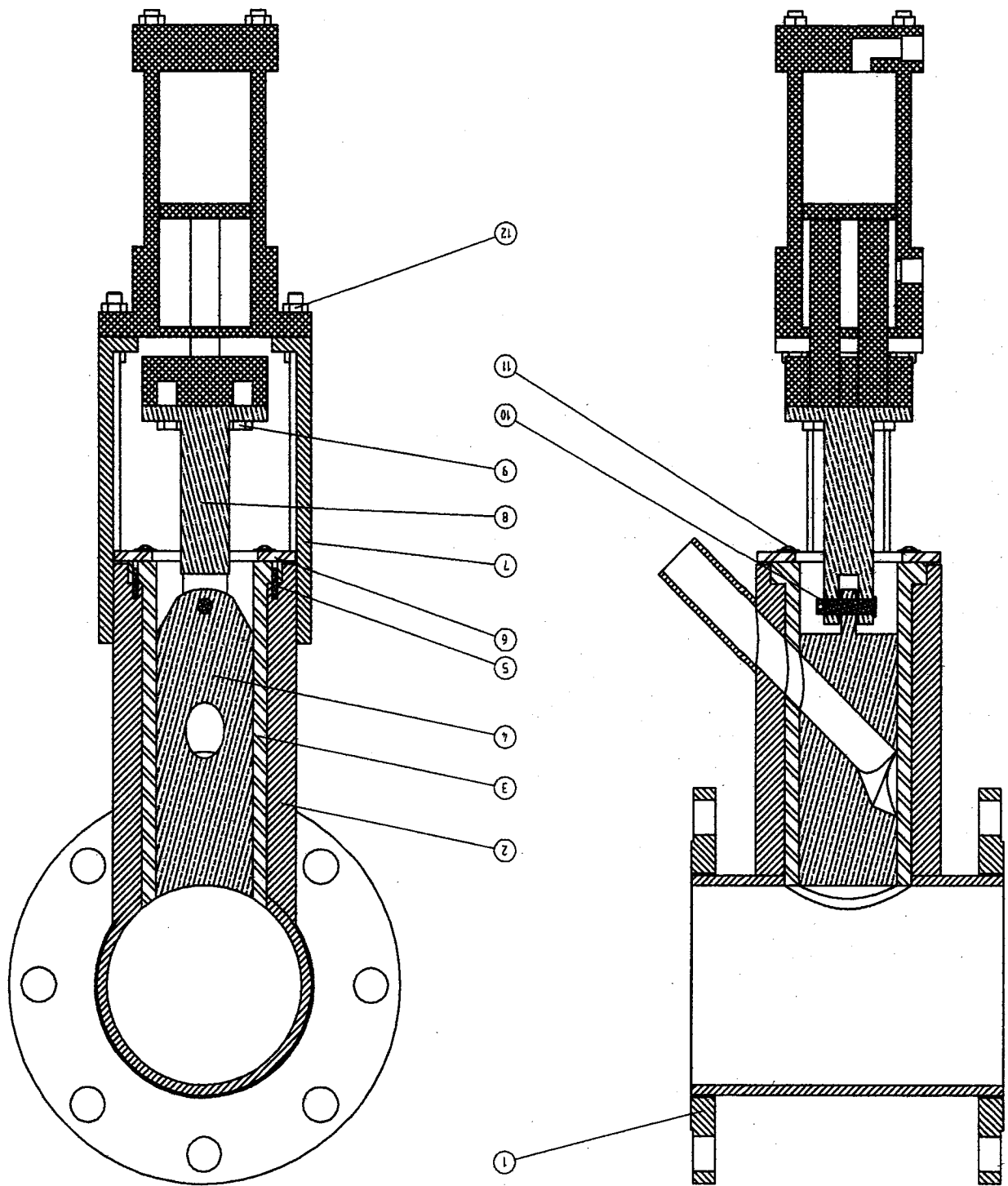
A AT $t=5$ min, $Q = 6200$ ACFM

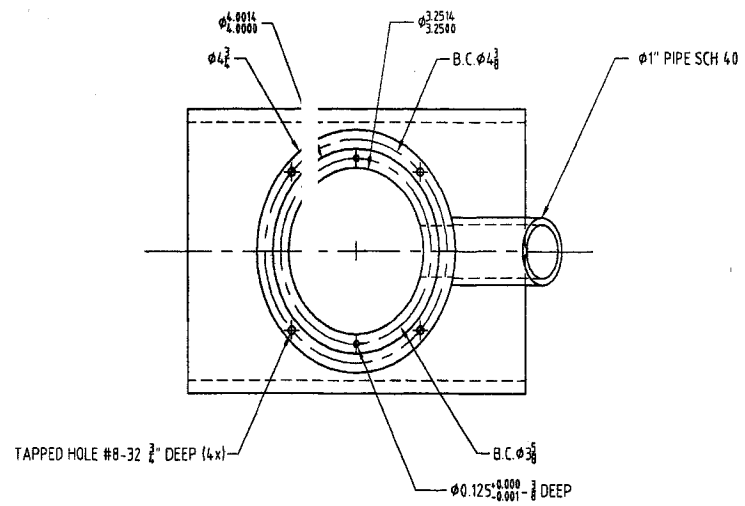
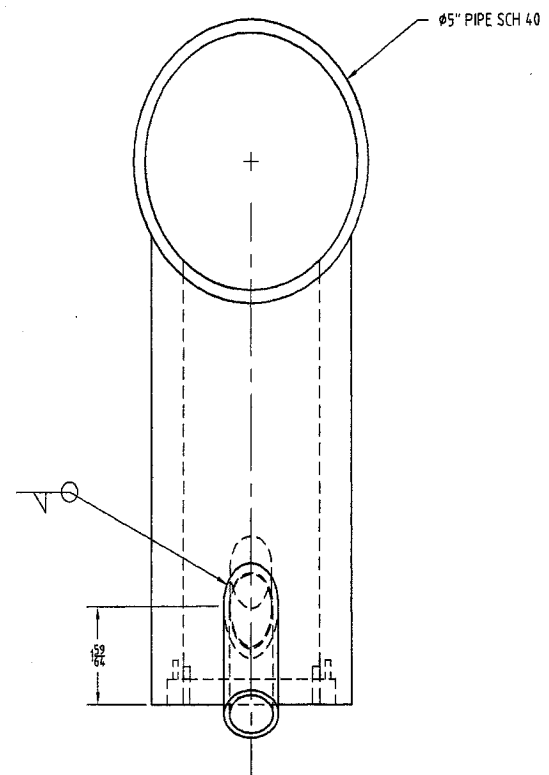
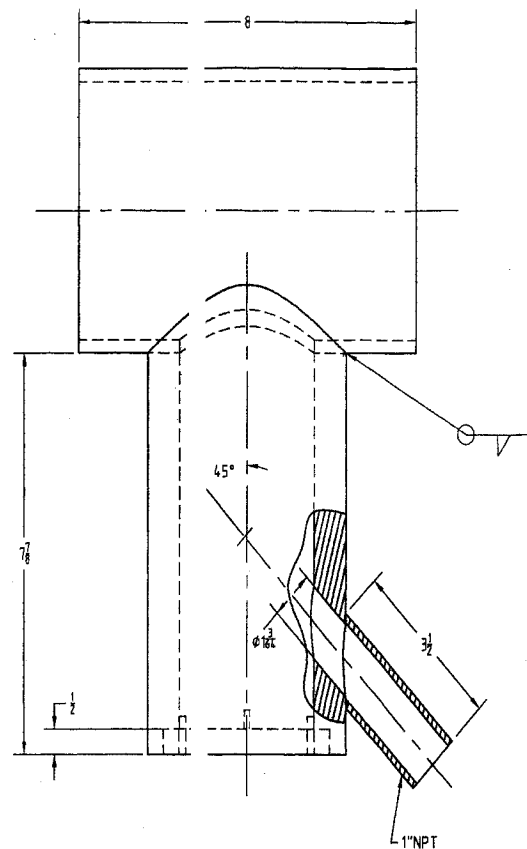


**Atomising
Systems
Limited**

Appendix 4

Automatic sampler detailed drawings and component specifications

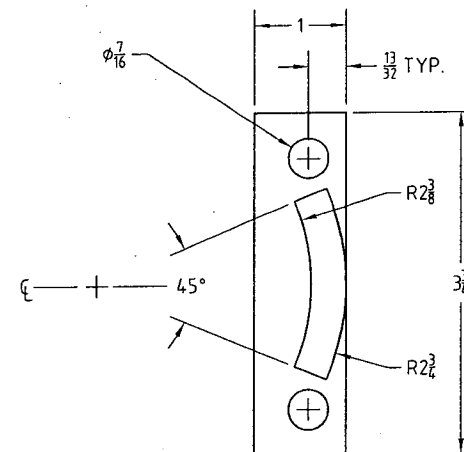
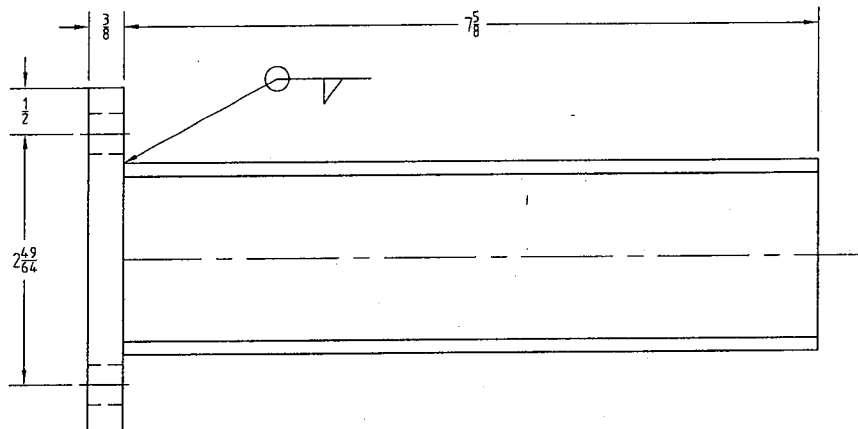




Handwritten signature and date: 8/18/2005

NO.	REVISED	DESCRIPTION	PART NO. PIÉCE	COUPLE / TORQUE	POIDS / WEIGHT
-----	---------	-------------	----------------	-----------------	----------------

A FOR CONSTRUCTION		P. TANGUAY	A. RAIL	04/03/18
ZONE	REV.	DESCRIPTION	REVISE PAR	APPROVÉ PAR
CE DOCUMENT EST LA PROPRIÉTÉ DE DOMFER POUDRES MÉTALLIQUES LTÉE. UTILISER TEL QUE PRÉSENTÉ PAR DOMFER POUDRES LTÉE. TOUTE REPRODUCTION, EN TOTALITÉ, OU EN PARTIE EST INTERDITE SANS LE CONSENTEMENT ÉCRIT DE DOMFER POUDRES MÉTALLIQUES LTÉE. / THIS DOCUMENT OWNED BY DOMFER METAL POWDERS LTD. USE AS PER DOMFER METAL POWDERS LTD. REQUIREMENTS. REPRODUCING IN TOTALITY OR PARTIALLY IS FORBIDDEN WITHOUT DIRECT AUTHORIZATION FROM DOMFER METAL POWDERS LTD.				
DOMFER DOMFER POUDRES MÉTALLIQUES LTÉE 4400, BOUL. NEUMANN, MONTRÉAL, QUÉBEC H3H 5R5 DEPT@DOMFER.COM TEL: 514.346.5511 FAX: 514.346.5511		TITRE / TITLE MAIN BODY AUTOMATIC SAMPLER MODEL BASED CONTROL		
DATE PAR / CREATED BY P. TANGUAY 2004/02/25		DISCIPLINE CODE MACHINE CODE M, M408, P122-02004, A		
ÉCHELLE / SCALE 1" = 2"		PAGE 2/7		



Handwritten signature/initials

A		FOR CONSTRUCTION		P. TANGUAY	A. RAIL	04/03/18
ZONE	NO.	DESCRIPTION		RÉVISÉ PAR	APPROUVÉ PAR	DATE
CE DOCUMENT EST LA PROPRIÉTÉ DE DOMFER POUDRES MÉTALLIQUES LTÉE. UTILISER TEL QUE PRÉSCRIT PAR DOMFER POUDRES MÉTALLIQUES LTÉE. TOUTE REPRODUCTION, EN TOTALITÉ, OU EN PARTIE EST INTERDITE SANS LE CONSENTEMENT EXPRES DE DOMFER POUDRES MÉTALLIQUES LTÉE. / THIS DOCUMENT OWNED BY DOMFER METAL POWDERS LTD. USE AS PER DOMFER METAL POWDERS LTD REQUIREMENTS. REPRODUCING IN TOTALITY OR PARTIALLY IS FORBIDDEN WITHOUT DIRECT AUTHORIZATION FROM DOMFER METAL POWDERS LTD.						
DOMFER DOMFER POUDRES MÉTALLIQUES LTÉE DOMFER METAL POWDERS LTD 6890, BOUL. NEWMAN, MONTRÉAL (QUÉBEC) H3N 2S3 DEPT. ENG@DOMFER.COM TEL: 514.345.8254 FAX: 514.345.8664				TITRE / TITLE HOLDING PART AUTOMATIC SAMPLER MODEL BASED CONTROL		
CRÉÉ PAR / CREATED BY P. TANGUAY		DATE 2004/02/25		DISCIPLINE CODE MACHINE CODE M M408		
RÉFÉRENCE / REFERENCE ---		ÉCHELLE / SCALE 3/4" = 1"		DWG NO. DE DESSIN P122-02004		REV. A

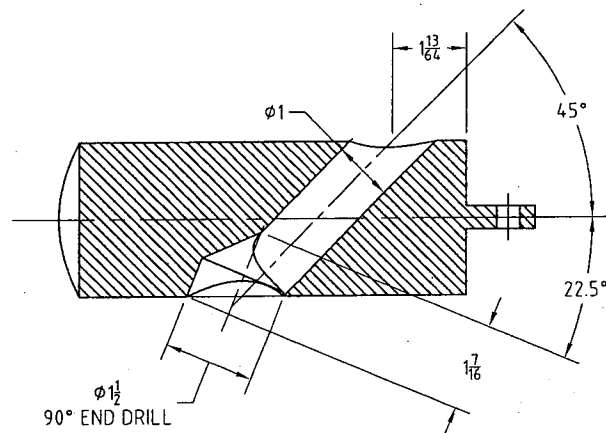
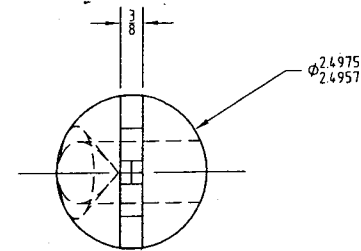
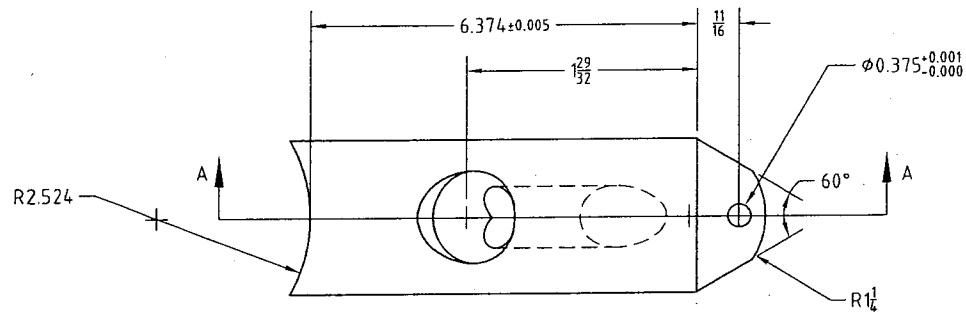
D

C

B

A

NO.	QTE/QTY	DESCRIPTION	PART NO. PIÉCE	COUPLE / TORQUE	POIDS / WEIGHT
-----	---------	-------------	----------------	-----------------	----------------



COUPE A-A

*Dr. Paul
8/8/2005*

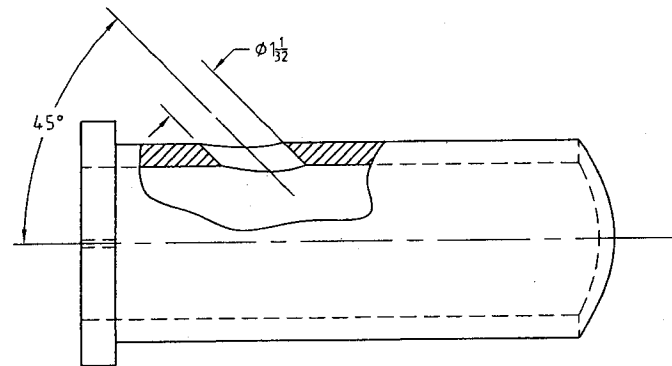
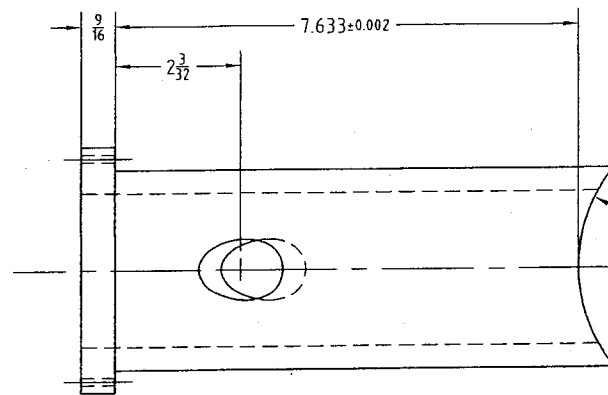
A		FOR CONSTRUCTION		P. TANGUAY	A. RAIL	04/03/18
ZONE	NO.	DESCRIPTION		RÉVISÉ PAR	APPROUVÉ PAR	DATE
CE DOCUMENT EST LA PROPRIÉTÉ DE DOMFER POUDRES MÉTALLIQUES LTÉE. UTILISER TEL QUE PRÉSCRIT PAR DOMFER POUDRES MÉTALLIQUES LTÉE. TOUTE REPRODUCTION, EN TOTALITÉ, OU EN PARTIE EST INTERDITE SANS LE CONSENTEMENT EXPRES DE DOMFER POUDRES MÉTALLIQUES LTÉE. / THIS DOCUMENT OWNED BY DOMFER METAL POWDERS LTD. USE AS PER DOMFER METAL POWDERS LTD REQUIREMENTS. REPRODUCING IN TOTALITY OR PARTIALLY IS FORBIDDEN WITHOUT DIRECT AUTHORIZATION FROM DOMFER METAL POWDERS LTD.						
DOMFER DOMFER POUDRES MÉTALLIQUES LTÉE DOMFER METAL POWDERS LTD 6690, BOUL. HENRI, MONTRÉAL (QUÉBEC) H3N 2S3 DEPT.ING@DOMFER.COM TEL: 514.345.8254 FAX: 514.345.8664		CRÉÉ PAR / CREATED BY P. TANGUAY DATE 2004/02/25		TITRE / TITLE SAMPLING PART AUTOMATIC SAMPLER MODEL BASED CONTROL		
		RÉFÉRENCE / REFERENCE ---		DISCIPLINE CODE MACHINE CODE M M408		
ÉCHELLE / SCALE 1" = 2"		PAGE 4/7		DWG NO. DE DESSIN P122-02004		
				REV. A		

D

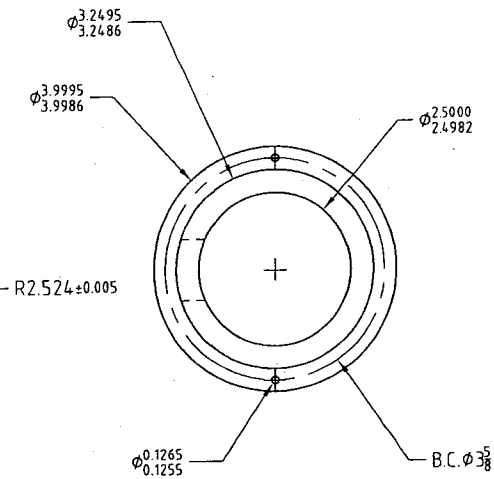
C

B

A



NO.	STÉ/QTÉ	DESCRIPTION	PART NO. PIÈCE	COUPLE / TORQUE	POIDS / WEIGHT
-----	---------	-------------	----------------	-----------------	----------------



A. Lef
8/8/2005

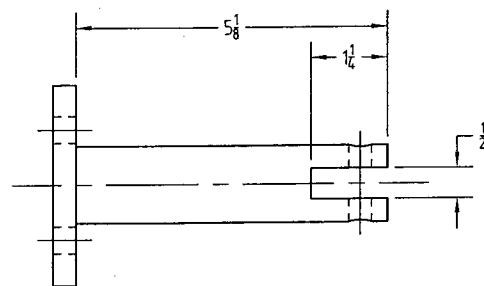
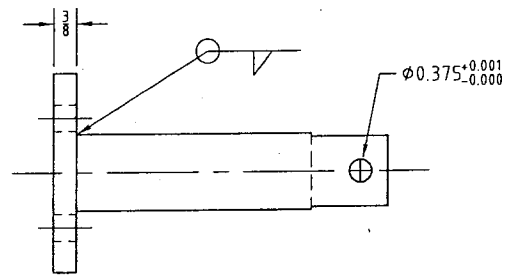
A		FOR CONSTRUCTION		P.TANGUAY	A.RAIL	04/03/18
ZONE	NO.	DESCRIPTION		RÉVISÉ PAR	APPROUVÉ PAR	DATE
CE DOCUMENT EST LA PROPRIÉTÉ DE DOMFER POUDRES MÉTALLIQUES LTÉE. UTILISER TEL QUE PRESCRIT PAR DOMFER POUDRES LTÉE. TOUTE REPRODUCTION, EN TOTALITÉ, OU EN PARTIE EST INTERDITE SANS LE CONSENTEMENT EXPRES DE DOMFER POUDRES MÉTALLIQUES LTÉE. / THIS DOCUMENT OWNED BY DOMFER METAL POWDERS LTD. USE AS PER DOMFER METAL POWDERS LTD REQUIREMENTS. REPRODUCING IN TOTALITY OR PARTIALLY IS FORBIDDEN WITHOUT DIRECT AUTHORIZATION FROM DOMFER METAL POWDERS LTD.						
DOMFER DOMFER POUDRES MÉTALLIQUES LTÉE DOMFER METAL POWDERS LTD 6990, BOUL. NEWMAN, MONTRÉAL (QUÉBEC) H3N 2S3 DEPT.ING@DOMFER.COM TEL: 514.345.8254 FAX: 514.345.0644		TITRE / TITLE SLEEVE AUTOMATIC SAMPLER MODEL BASED CONTROL				
CRÉÉ PAR / CREATED BY P.TANGUAY DATE 2004/02/25		DISCIPLINE CODE MACHINE CODE DWG NO. DE DESSIN REV. M M408 P122-02004 A				
ÉCHELLE / SCALE 1" = 2"		PAGE 5/7				

D

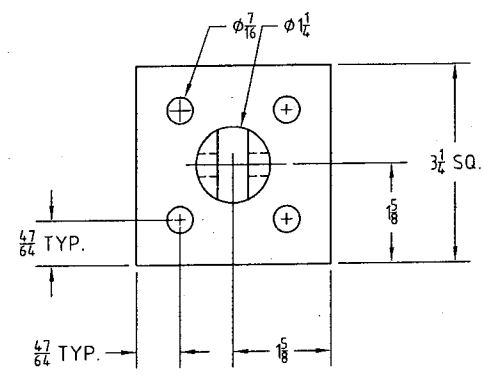
C

B

A



NO.	QTE/DTY	DESCRIPTION	PART NO. PIÉCE	COUPLE / TORQUE	PODS / WEIGHT
-----	---------	-------------	----------------	-----------------	---------------



A. Lail
8/18/2005

A		FOR CONSTRUCTION		P. TANGUAY	A. RAIL	04/03/18
ZONE	NO.	DESCRIPTION		RÉVISÉ PAR	APPROUVÉ PAR	DATE
CE DOCUMENT EST LA PROPRIÉTÉ DE DOMFER POUDRES MÉTALLIQUES LTÉE. UTILISER TEL QUE PRESCRIT PAR DOMFER POUDRES LTÉE. TOUTE REPRODUCTION, EN TOTALITÉ, OU EN PARTIE EST INTERDITE SANS LE CONSENTEMENT EXPRES DE DOMFER POUDRES MÉTALLIQUES LTÉE. / THIS DOCUMENT OWNED BY DOMFER METAL POWDERS LTD. USE AS PER DOMFER METAL POWDERS LTD REQUIREMENTS. REPRODUCING IN TOTALITY OR PARTIALLY IS FORBIDDEN WITHOUT DIRECT AUTHORIZATION FROM DOMFER METAL POWDERS LTD.						
DOMFER DOMFER POUDRES MÉTALLIQUES LTÉE DOMFER METAL POWDERS LTD 6999, BOUL. NEWMAN, MONTRÉAL (QUÉBEC) H3N 2S3 DEPT. ENG@DOMFER.COM TEL: 514.365.8254 FAX: 514.365.8666				TITRE / TITLE CLEVIS BASE AUTOMATIC SAMPLER MODEL BASED CONTROL		
CRÉÉ PAR / CREATED BY P. TANGUAY		DATE 2004/02/25		DISCIPLINE CODE MACHINE CODE M M408		
RÉFÉRENCE / REFERENCE ---		ÉCHELLE / SCALE 1 = 2		DWG NO. DE Dessin P122-02004		REV. A

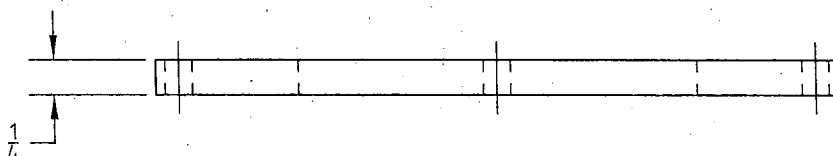
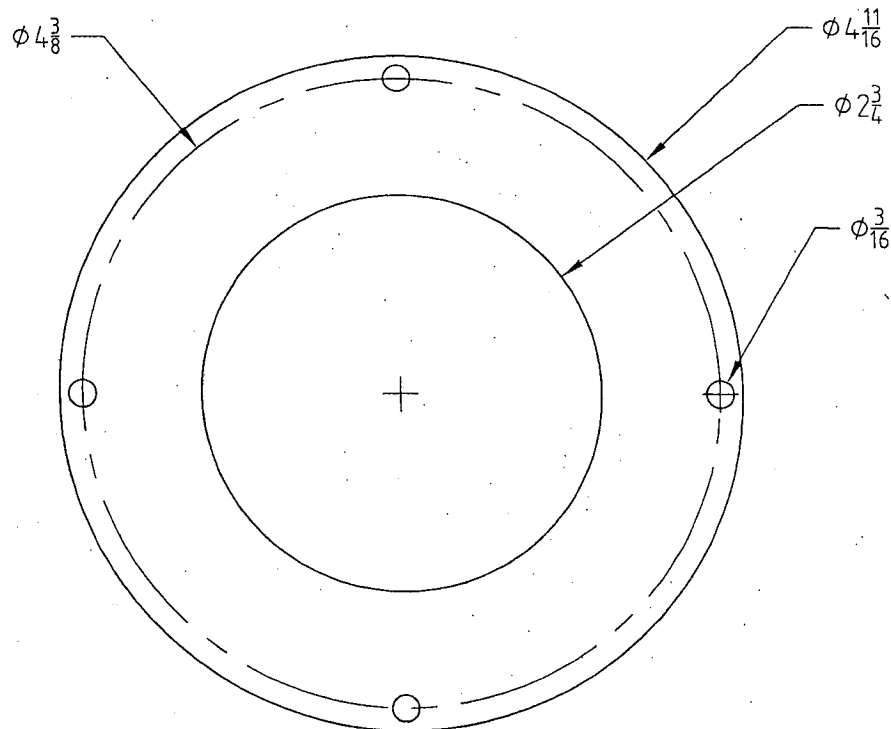
D

C

B

A

NO.	QTE/QTY	DESCRIPTION	PART NO. PIÈCE	COUPLE / TORQUE	POIDS / WEIGHT
-----	---------	-------------	----------------	-----------------	----------------



A. Rail
8/8/2005

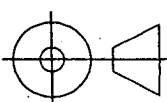
	A	FOR CONSTRUCTION	P.TANGUAY	A.RAIL	04/03/18
ZONE	NO.	DESCRIPTION	RÉVISÉ PAR	APPROUVÉ PAR	DATE

CE DOCUMENT EST LA PROPRIÉTÉ DE DOMFER POUDRES MÉTALLIQUES LTÉE. UTILISER TEL QUE PRESCRIT PAR DOMFER POUDRES LTÉE. TOUTE REPRODUCTION, EN TOTALITÉ, OU EN PARTIE EST INTERDITE SANS LE CONSENTEMENT EXPRES DE DOMFER POUDRES MÉTALLIQUES LTÉE. / THIS DOCUMENT OWNED BY DOMFER METAL POWDERS LTD. USE AS PER DOMFER METAL POWDERS LTD REQUIREMENTS. REPRODUCING IN TOTALITY OR PARTIALY IS FORBIDEN WITHOUT DIRECT AUTHORIZATION FROM DOMFER METAL POWDERS LTD.

DOMFER

DOMFER POUDRES MÉTALLIQUES LTÉE
DOMFER METAL POWDERS LTD

6090, BOUL. NEWMAN, MONTRÉAL (QUÉBEC) H8N 2S3
DEPT.ING@DOMFER.COM TEL.: 514.365.8254 FAC.: 514.365.0664



CRÉÉ PAR / CREATED BY
P.TANGUAY

DATE
2004/02/25

RÉFÉRENCE / REFERENCE

ÉCHELLE / SCALE
3/4" = 1"

PAGE
7/7

TITRE / TITLE

RETAINING RING
SAMPLER VALVE
PROCESS CONTROL

DISCIPLINE

CODE MACHINE CODE

DWG NO. DE DESSIN

REV.

M

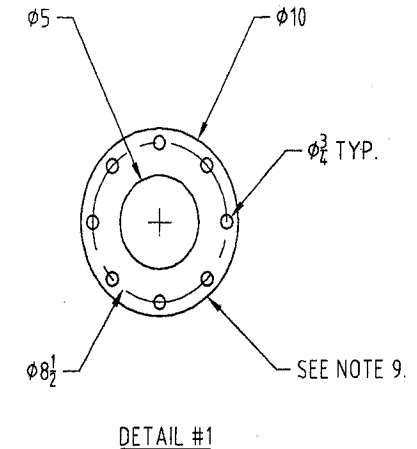
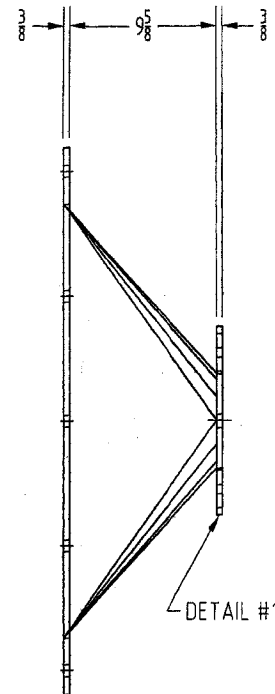
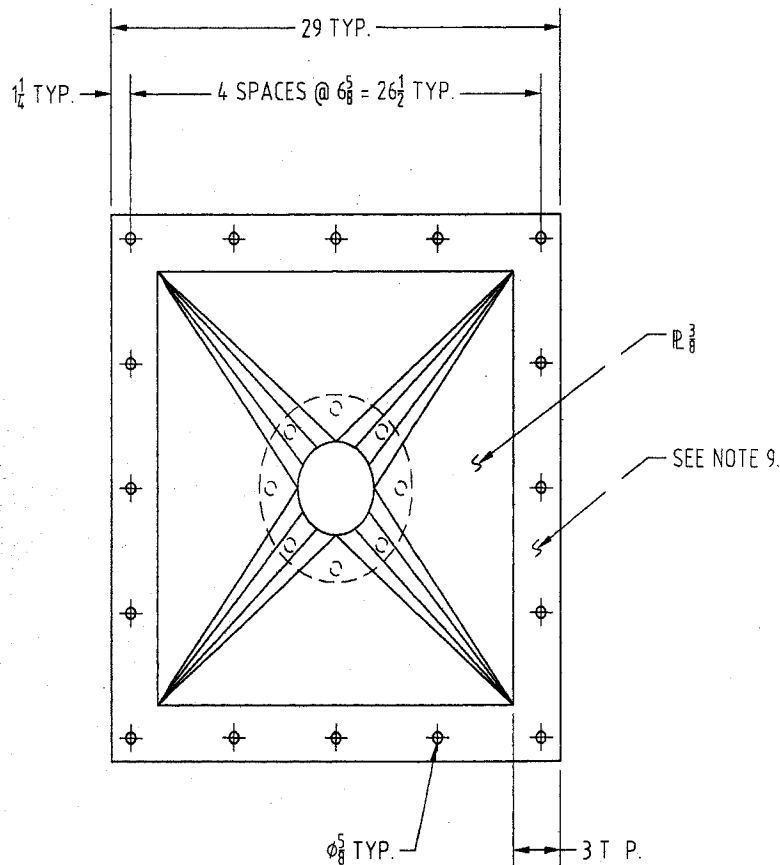
M408

P122-02004

A

B

A



NOTES:

1. MTL: ASTM-A36
2. QTE: 1
3. FINIS: N/A
4. POIDS TOTAL ESTIMÉ: --- lbs
5. ENLEVER TOUTES BAVURES
6. ARRONDIR TOUT CÔTÉ TRANCHANT
7. TOLÉRANCE LINÉAIRE GÉNÉRALE $\pm 1/32$
8. DIMENSIONNEMENT IMPÉRIAL (POUCHES) SAUF NOTÉ(S)

NOTE 9:

A 2ND FREE FLANGE MUST BE BUILT

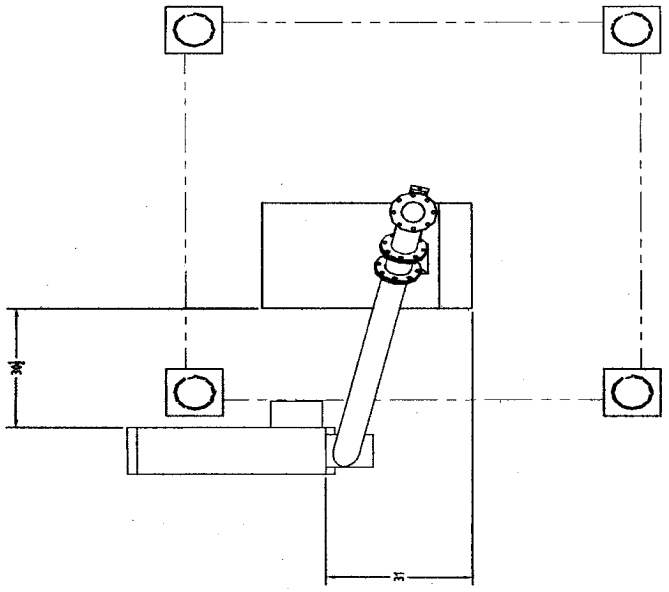
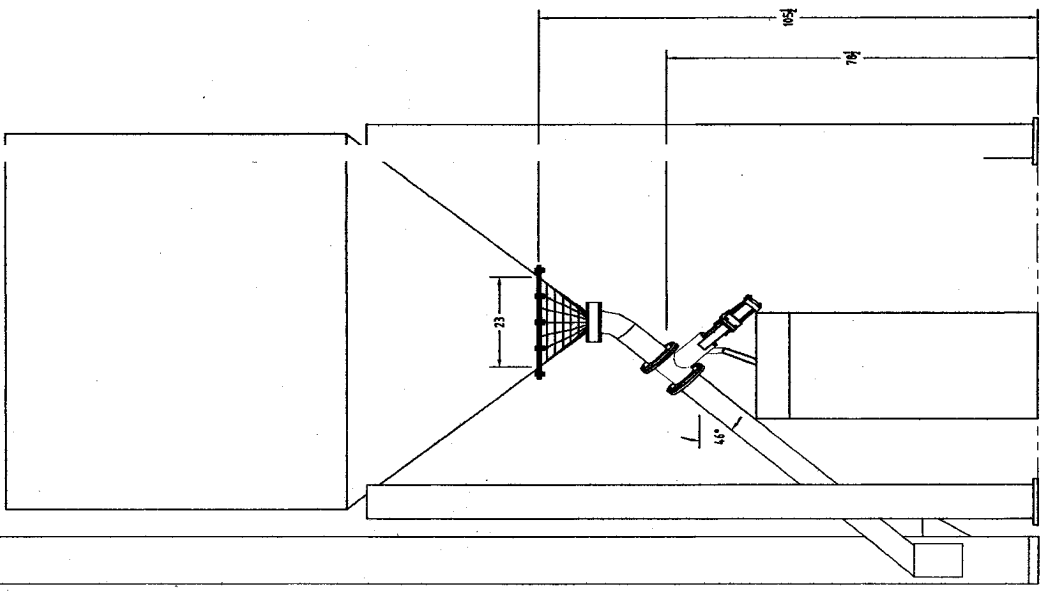
1 FIRST DRAFT		P. TANGUAY	A. RAIL	04/03/09
ZONE	NO.	DESCRIPTION		DATE
		RÉVISÉ PAR		APPROUVÉ PAR
CE DOCUMENT EST LA PROPRIÉTÉ DE DOMFER POUDES MÉTALLIQUES LTÉE. UTILISER TEL QUE PRESCRIT PAR DOMFER POUDES MÉTALLIQUES LTÉE. TOUTE REPRODUCTION, EN TOTALITÉ, OU EN PARTIE EST INTERDITE SANS LE CONSENTEMENT EXPRES DE DOMFER POUDES MÉTALLIQUES LTÉE. / THIS DOCUMENT OWNED BY DOMFER METAL POWDERS LTD. USE AS PER DOMFER METAL POWDERS LTD REQUIREMENTS. REPRODUCING IN TOTALITY OR PARTIALLY IS FORBIDDEN WITHOUT DIRECT AUTHORIZATION FROM DOMFER METAL POWDERS LTD.				
DOMFER DOMFER POUDES MÉTALLIQUES LTÉE DOMFER METAL POWDERS LTD 6999 BOUL. NEWMAN, MONTRÉAL (QUÉBEC) H1N 2S3 DEPT. ENG@DOMFER.COM TEL: 514.365.8254 FAX: 514.365.0664		TITRE / TITLE ROUND TO SQ. TRANSITION TANK R413 MODEL BASED CONTROL		
CRÉÉ PAR / CREATED BY P. TANGUAY		DATE 2004/03/09		
RÉFÉRENCE / REFERENCE ---		DISCIPLINE M		
ÉCHELLE / SCALE 1" = 8"		CODE MACHINE CODE R413, P122-02007-1, 1		
PAGE 1/1		DWG NO. DE DESSIN REV.		

D

C

B

A



A. G. 1000
8/1/2000

INSTALLATION SAMPLER & ANALYSER MODEL BASED CONTROL	
DATE 10/1/2000	BY A. G. 1000
PROJECT G. M408, PPSPPNNN, 0	REVISION 1

Liste des éléments a acheter
projet d'échantillonneur automatique

Item	Quantité	Description	Fournisseur	Prix
1	1	Fabrication d'un échantillonneur automatique	Abco	3500.00 \$
2	1	Fabrication d'une transition carrée a rond	R. Liard	945.00\$
3	1	Cylindre pneumatique Numatics	Teckno-Valve RS	889.00\$
4	2	Reed switch #SR6-004	Teckno-Valve RS	32.40\$/ch = 64.80\$
5	1	Valve solenoïd 1/4 npt 3 positions #082 SS 63 AK	Teckno-Valve RS	242.40\$
6	2	Valves Flow control #IN135C-308-022	Teckno-Valve RS	30.64\$/ch = 61.28\$
7	2	Dowel pin ϕ 1/8" #98381A473	Mc Master	7.79\$US/100 = 10.45\$
8	1	Clevis pin ϕ 3/8" #98306A273	Mc Master	11.32\$US/25 = 15.18\$
9	1	Cotter pin ϕ 5/32" #98338A220	Mc Master	3.87\$US/100 = 5.19\$
10	4	Vis Truss #8-32 X 1" long #90271A199	Mc Master	3.14\$US/100 = 4.21\$
11	21'	Tuyau ϕ 5" sch 40	Crane	8.30\$/pi = 174.30\$
12	8	Bride ϕ 5" 125 LBS "slip-on"	Crane	18.50\$/ch = 148.00\$
13	21	Tuyau ϕ 1" sch 40	Crane	1.05\$/pi = 22.05\$
14	1	Coude 90° ϕ 5" sch 40	Crane	24.06\$
15	1	Coupling ϕ 1"	Crane	0.48\$
Total=				6106.40\$

ATELIER D'USINAGE

ABCO INC.
MACHINE SHOP



Date : 12 Mars 2004

Nom du client : DOM FERN

No. Tél. : 365-8254
258

No. Fax : 365-0664

À l'attention de : ALEXANDRE BAIL Nombre de pages : 1

Bonjour, par la présente, je vous confirme l'évaluation du travail à faire que vous nous avez demandée.

Voici le prix pour fabriquer un système de contrôle pour la poudre, soit :

1 Hair Body, 1 Clevis Base, une sleeve en bronze, 2 Holding Part, 1 Sampling part- "Piston", 1 Retaining Ring, tout le reste sera fourni par le client. Le prix du projet :

Délai de livraison : 2 semaines

Proci
Total Matériaux et M.O. : 3,000\$ à 3,500\$
T.P.S. & T.V.Q (En plus)

Préparé par : Manuel

Si vous acceptez, veuillez signer : _____

S.V.P. inscrire votre bon de commande (P.O.) : _____

MERCI !

Réserver pour ABCO:

BT # : _____

Si modification : _____

Par : _____

Date : _____ Par : _____

SOUMI - 98.01

R A N E

DISTRIBUTION CRANE
CRANE SUPPLYDivision de Crane Canada Co. / Division of Crane Canada Co.
4805 AVENUE DUNN MONTREAL, QUEBEC
H4E 1B9SOUSSION
QUOTATIONTEL: 514-766-8541
FAX: 514-766-7138NO SOUSSION
QUOTATION NO.

786963-01

CUMIS À / QUOTED TO

LIVRÉ À / SHIP TO

PAGE 1 de 1

FER POUDRES METALLIQUES LTD

DOMFER POUDRES METALLIQUES LTD

0 BOUL. NEWMAN

6090 BOUL. NEWMAN

ALLE (QUEBEC)
283LASALLE (QUEBEC)
H8N 2S3

Customer Fax 514-365-0664

DE LA SOUSSION QUOTATION DATE	DATE D'ÉCHEANCE DE LA SOUSSION QUOTATION EXPIRATION DATE	REPRÉSENTANT WRITER	REPRÉSENTANT SALES REP	BUREAU BRANCH	POIDS WEIGHT
/18/2004	03/23/2004	JS	JL	0014	447.74

QTE COMM. QTY ORDERED	UNIT	DESCRIPTION	PRICE PRICE	ESCOMpte DISCOUNT	NET	MULTIPLICATION EXTENDED AMOUNT
21	PI	5 TUYAU/AC NR STD A53B SOUD/RES EL/B.B. ES C LCS	830.33	NET	830.33	174.37
6	CH	5 BRIDE COULISSANTE EN ACIER FORGE 150# SURF. ELEVEE	18.50	NET	18.50	111.00
21	PI	1 TUYAU/AC NR STD A53B SOUDE/RES EL/B B/LONG COUR	105.21	NET	105.21	22.09
1	CH	5 COUDE 90 A LONG RAYON EN ACIER SOUDE STANDARD WPB	24.07	NET	24.07	24.07
1	CH	1 MANCHON DROIT EN FONTE MALLEABLE NOIR STD	0.48	NET	0.48	0.48
		1MICPLG				

CONDITIONS DE PAIEMENT / TERMS OF PAYMENT

30 JOURS

SOUSSION EST SOUMISE AUX TERMES ET CONDITIONS TEL QUE STIPULÉES SUR L'ENTENTE DE CRÉDIT.
QUOTATION IS SUBJECT TO THE TERMS AND CONDITIONS STATED IN THE CUSTOMER CREDIT AGREEMENT.

SOUS TOTAL / SUB TOTAL

332.01

T.P.S. / G.S.T.

23.24

T.V.P. / P.S.T.

26.64

TOTAL

\$381.89

41:30 P. 2004-05-18

(514) 766-7138

CRANE MONTREAL

514 766 7138

Mar. 19. 2004 12:18AM



FAXÉ

2131, de la Province
Longueuil, Québec J4G 1Y6
Tel (450) 646-3201
Fax (450) 463-1440
Ligne sans frais 1-877-646-3201
www.tecknovalve.com

SOUMISSION / QUOTATION

# SOUMISSION :	AL210104
DATE :	21 JANVIER 2004

CLIENT	DOMFER	Tel :	
		Fax :	514.365.0664
		VOTRE/YOUR REFERENCE :	NUMATICS ACTUATEUR
CONTACT	ALEXANDRE RAIL		

Il nous fait plaisir de vous transmettre prix et livraison pour l'(les) article(s) suivant(s) :
We are pleased to submit price and delivery for the following :

QUANTITÉ QUANTITY	CODE	DESCRIPTION	PRIX UNITAIRE UNIT PRICE	LIVRAISON DELIVERY
1		MODEL FIFP-03A1D-AKA2	889.00	2 SEM
		WITH STROKE AJUSTER		
		VOIR LITTERATURE		
		MERCI		

Taxes : Non inclues
FAB : Longueuil
Termes : Net 30 jours
Prix fermes : 30 jours
Livraison : Sujet aux ventes prioritaires

Taxes : Not included
FOB : Longueuil
Terms : Net 30 days
Price firm : 30 days
Delivery : Subject to prior sales

Lavoie

Armand Lavoie
Président

a.lavoie@tecknovalve.com



2101, de la Province
Longueuil, Québec J4G 1Y6
Tel (450) 646-3201
Fax (450) 463-1440
Ligne sans frais 1-877-646-3201
www.tecknovalve.com

SOUSSION / QUOTATION

SOUSSION : AL 220404

DATE : 22 JANVIER 2004

CLIENT	DOMFER	Tel	
		Fax	514 365 0664
		VOTRE/YOUR REFERENCE :	
CONTACT	ALEXANDRE RAIL		

Il nous fait plaisir de vous transmettre prix et livraison pour l'(les) article(s) suivant(s) :

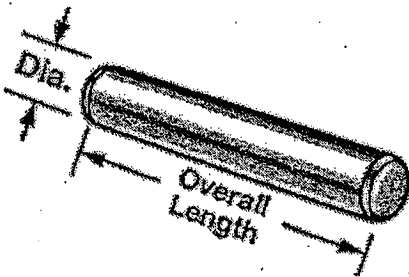
We are pleased to submit price and delivery for the following :

QUANTITÉ QUANTITY	CODE	DESCRIPTION	PRIX UNITAIRE UNIT PRICE	LIVRAISON DELIVERY
2		REED SWITCH NO SR6 -004	32.40	
1		082 SS 63 AK VALVE 1/4 NPT 3 POSITIONS		
		CENTRE FERME 2 SOLENOID	242.40	
		*****LIVRAISON***** 2 SEMAINES		

Taxes : Non incluses
 FAB : Longueuil
 Termes : Net 30 jours
 Prix fermes : 30 jours
 Livraison : Sujet aux ventes prioritaires

Taxes : Not included
 FOB : Longueuil
 Terms : Net 30 days
 Price firm : 30 days
 Delivery : Subject to prior sales

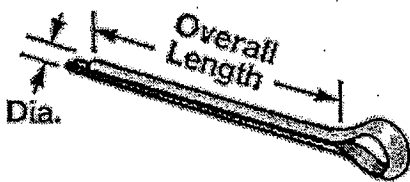
Richard Rousseau pour ARMAND LAIBIE
 Richard Rousseau Ventes Internes
 rrousseau@tecknovalve.com



Part Number 98381A473

\$7.79 per Pack of 100

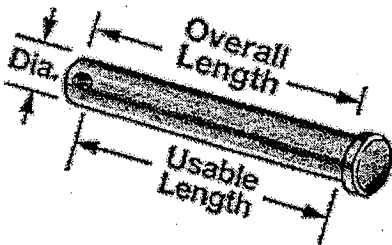
Pin Type	Dowel Pins
Dowel Pin Type	Standard
Material	Steel
Steel Type	Hardened Steel
System of Measurement	Inch
Diameter	1/8"
Actual Diameter (Min.-Max.)	.1251"-.1253"
Overall Length	3/4"
Length Tolerance	±.01"
Specifications Met	Not Rated
Single Shear Strength	130,000 PSI



Part Number 98338A220

\$3.87 per Pack of 100

Pin Type	Cotter Pins and Rings
Cotter Pin and Retaining Ring Type	Standard Cotter Pin
Material	Steel
Steel Type	Zinc-Plated Steel
System of Measurement	Inch
Diameter	5/32"
Overall Length	1"
Specifications Met	Not Rated



Part Number 98306A273

\$11.32 per Pack of 25

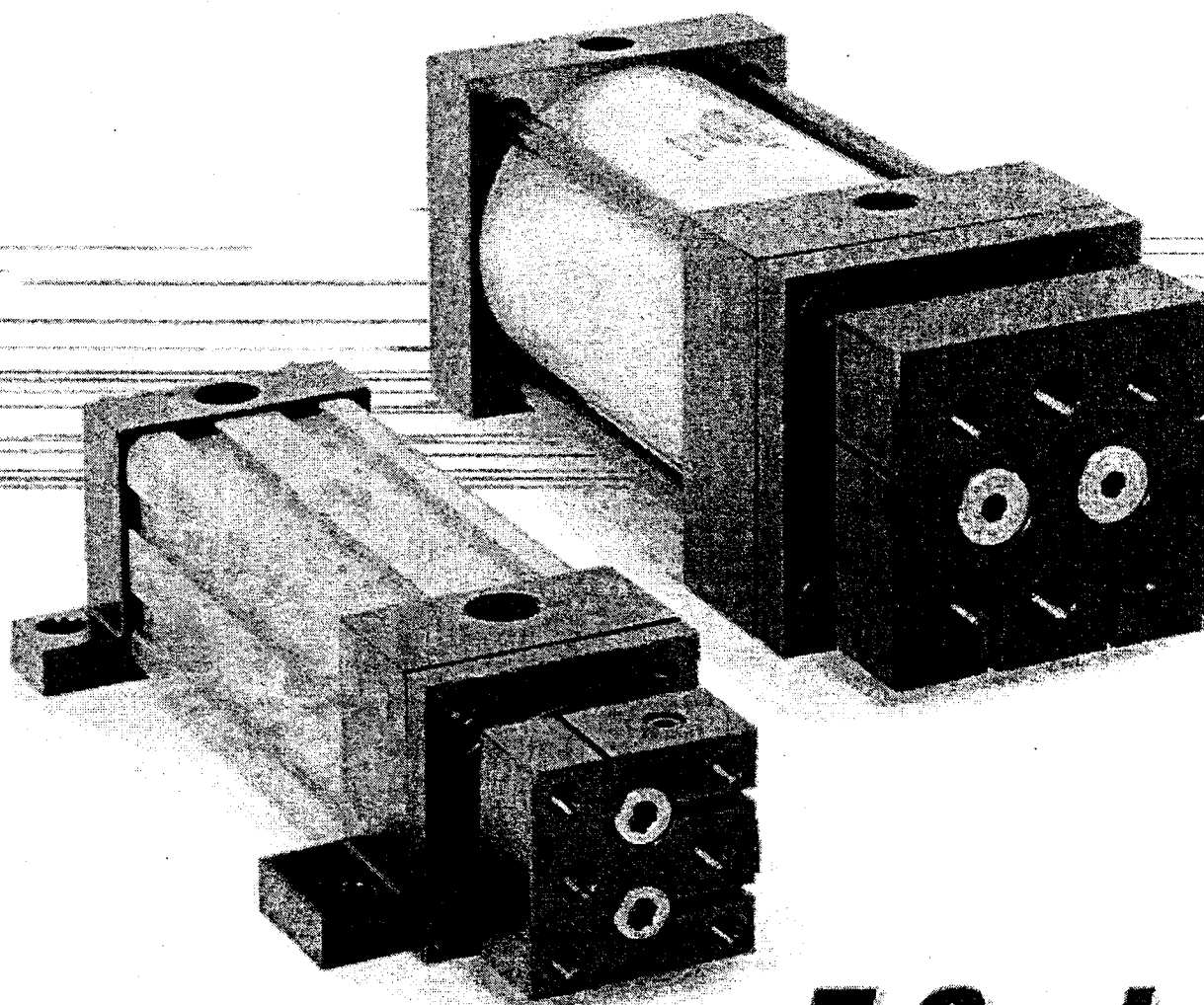
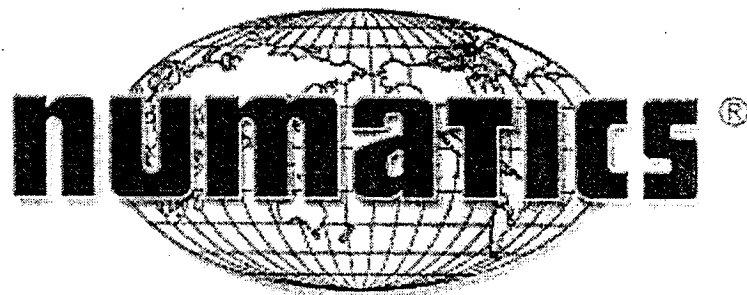
Pin Type	Clevis Pins
Clevis Pin Type	Standard
Recommended Cotter Pin Diameter	5/32"
Material	Steel
Steel Type	Plain Steel
System of Measurement	Inch
Diameter	3/8"
Actual Head Diameter (Min.-Max.)	.490"-.510"
Actual Diameter (Min.-Max.)	.368"-.373"
Usable Length	1-17/64"
Overall Length	1-1/2"
Actual Head Height (Min.-Max)	.120"-.130"
Specifications Met	Not Rated
Single Shear Strength	5,400 lbs.



Part Number 90271A199

\$3.14 per Pack of 100

Material	Zinc-Plated Steel
Head Style	Truss
Drive Style	Slotted
System of Measurement	Inch
Thread Size	#8-32
Length	1"
Thread Point Style	Standard Machine
Specifications Met	Not Rated



F Series

Non-Rotating NFPA Interchangeable Cylinder Line

We're everywhere you need us to be!



F Series Non-Rotating NFPA Interchangeable



The **F Series** is a Non-Rotating NFPA Interchangeable pneumatic cylinder line that provides the solution to specific applications where piston rotation is not acceptable. Our innovative dual rod design provides precision positioning and linear movement. This makes the F Series ideal for a multitude of high-tech applications.

Tube

The **tube** is hard coat anodized. The hard coating is an electro-chemical process which produces a very dense surface of aluminum oxide. This surface has extreme hardness (60 RC.), excellent wear and corrosion resistance, and a low coefficient of friction. Additionally, profile tubing is standard on 1-1/2" through 2-1/2" bore sizes (3-1/4" and 4" bores are the tie rod construction).

End Caps

The **end caps** are accurately machined from (6061-T6) solid aluminum bar stock. They are anodized for corrosion resistance. Additionally, a recess on the piston-mating surface (at both ends) enables the air to work on a larger piston area for effortless breakaway.

Rod Bushing

The F Series includes a graphite filled, cast iron **rod bushing** that is extra long in length. Graphite filling offers the best bearing surface when using a hard chrome plated piston rod. Cast iron provides maximum resistance against wear. The added length adds superior alignment and support of the piston rod as well as provides maximum load bearing support.

Rod Seal and Wiper

The unique **rod seal and wiper** combination is made with carboxylated nitrile with Teflon® compound and is self-lubricating and durable. The rounded lip design ensures proper sealing and long life.

Piston Rod

High strength steel (100,000 psi minimum yield) **piston rod** has a ground, polished, and chrome plated surface. This surface provides maximum life for both the rod bushing and the seals.

Retaining Plate

The steel **retaining plate** has dual functions. It retains the bushing as well as inhibits rod rotation. Precise tolerances on both the bushing and the retaining plate allows for a exact fit which prevents rod rotation. By simply removing the four countersunk screws that maintain exact alignment, the orientation of the piston rod and tooling plate can be rotated 90° without cylinder disassembly.

Tooling Plate

The **tooling plate** is machined from solid steel. The tooling plate is reversible, offering both a flush or concentric mount.

Piston Seal

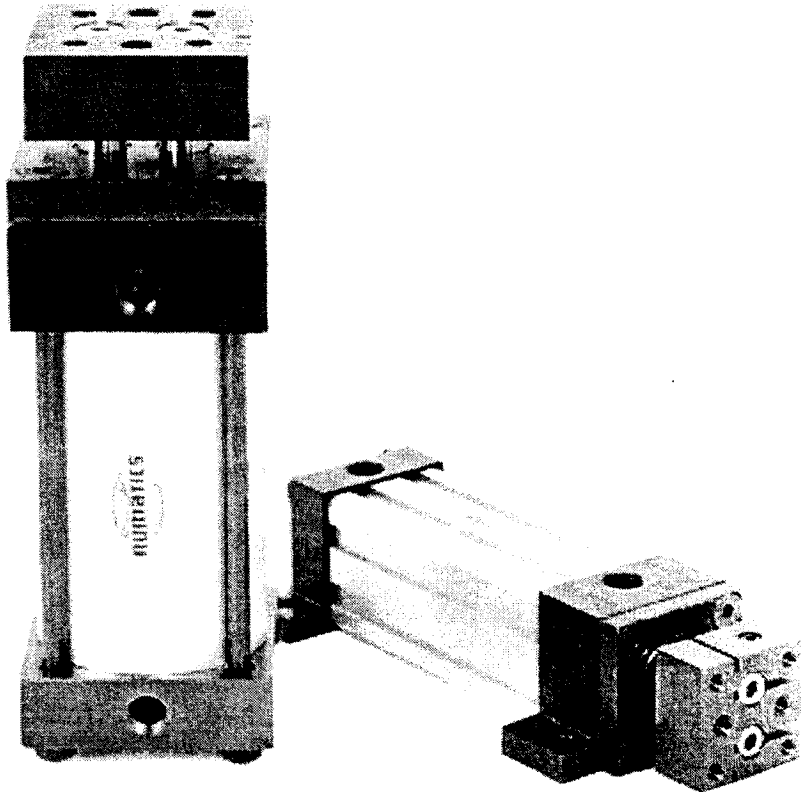
The **piston seal** is a carboxylated nitrile with Teflon® compound for self-lubricating. The "T" seal with back-up ring construction prevents rolling and seals at all pressures.

Wear Band

The **wear band** is a stable, lubricating strip located on the piston. We separated the load bearing points by locating the wear band at the rear of the piston. This maximizes column strength at full extension.

Piston

The solid aluminum alloy **piston** is strong and durable.



Cushion Seal

The floating **cushion seal** design enables rapid stroke reversal by providing instantaneous full flow to the piston. Each cushion has a flush, retained adjustment needle.

Tube End Seal

The **tube end seals** are compression type and reusable.

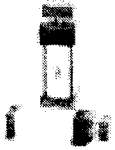
Ports

Our enhanced **port** design enables the cylinder to work more efficiently. Through the use of precise machining depths and tool shape, we are able to smooth the flow path into and out of the cylinder.

Teflon® is a registered trademark of DuPont™. For detailed information regarding the properties of Teflon®, please call 1-800-441-0573.

Standard Specifications:

- Meets NFPA specifications
- Bore sizes from 1-1/2" through 4"
- Piston rod diameters from 5/16" to 3/4"
- Nominal pressure rating is 250 psi air
- Standard temperature -10°F to 165°F (-23°C to 74°C)
- All aluminum construction, except retaining plate and tooling plate (steel)
- NPTF ports
- Flexible port and cushion locations



F Series
Non-Rotating NFPA Interchangeable



Standard F Series Mounts

Centerline Mounts

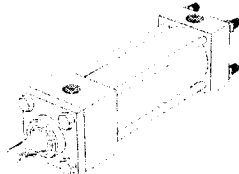
X0 Mount

Basic No Mount



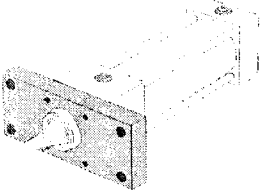
X2 Mount

Extended Tie Rods – Cap End



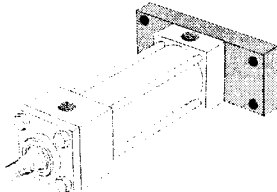
F1 Mount

Head Rectangular Flange



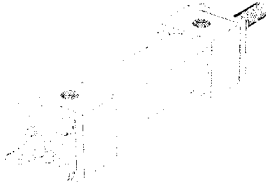
F2 Mount

Cap Rectangular Flange



DA Mount

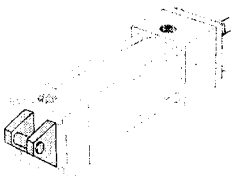
Double Rod End



Pivot Mounts

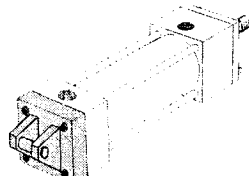
P1 Mount

Fixed Clevis



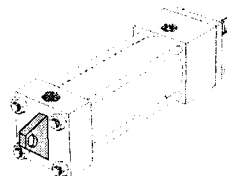
P2 Mount

Detachable Clevis



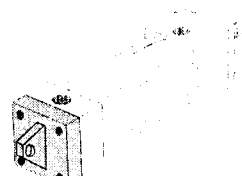
P3 Mount

Fixed Eye



P4 Mount

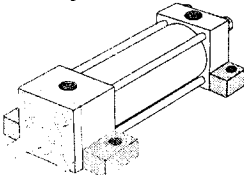
Detachable Eye



Foot Mounts

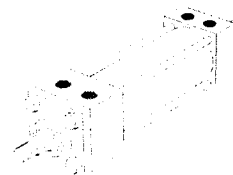
S2 Mount

Side Lugs



S4 Mount

Bottom Tapped





F Series Non-Rotating NFPA Interchangeable



How to Order

Order Code Example: F1 F K - 00 A 1 P - C AA 0

Mounting
 F1 = Front Flange
 F2 = Rear Flange
 P1 = Fixed Clevis
 P2 = Detachable Clevis
 P3 = Fixed Eye
 P4 = Detachable Eye
 S2 = Side Lug Mount
 S4 = Bottom Tapped
 X0 = Basic No Mount
 X2 = Cap Extended Tie Rods

Type
 F = F Series Non-Rotating NFPA Interchangeable

Bore
 K = 1-1/2"
 L = 2"
 M = 2 1/2"
 P = 3 1/4"
 R = 4"

Full Inch of Stroke
 00 = 0" Stroke
 01 = 1" Stroke
 02 = 2" Stroke
 03 = 3" Stroke
 20 = 20" Stroke

Fractional Inches of Stroke
 A = 0" I = 1/2"
 B = 1/16" J = 9/16"
 C = 1/8" K = 5/8"
 D = 3/16" L = 11/16"
 E = 1/4" M = 3/4"
 F = 5/16" N = 13/16"
 G = 3/8" O = 7/8"
 H = 7/16" P = 15/16"

Magnet
 0 = No Magnet
 2 = Magnet

Options
 AA = No Options
 BA** = Bumpers Both Ends (3-1/4" and 4" only)
 BH** = Bumper Head only (3-1/4" and 4" only)
 BC** = Bumper Cap only
 KA* = Stroke Adjuster
 DA = Double Rod End
 NA = Nickel Plated Cylinder
 Stainless Steel Rod and Tie rods
 RA* = Save Air Stroke Adjuster
 SA = Stainless Steel Piston Rod
 SS = Stainless Piston Rod and Tie Rod
 ST = Stainless Tie Rods
 1A* = Rod Extension
 4A* = Stop Tube
 * Specify length.
 **Bumpers add 0.062" to OAL (per bumper).

Cushions

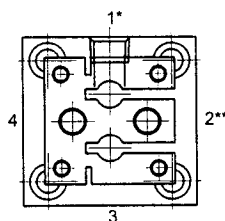
Position	1	2	3	4
No Cushion	A	A	A	A
Head and Cap	B	C	D	E
Head Only	F	G	H	J
Cap Only	K	L	M	N

Ports

Position	1/8"	1/4"	3/8"	1/2"	3/4"
1	B	C	D	E	F
2	H	I	J	K	L
3	N	O	P	Q	R
4	T	U	V	W	X

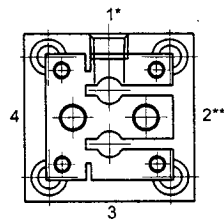
Rod End Codes
 1 = Vertical rod Style # 1
 2 = Vertical Rod Style # 2
 3 = Vertical Rod Style # 3
 4 = Special Rod Ends
 6 = Horizontal Rod Style # 1
 7 = Horizontal Rod Style # 2
 8 = Horizontal Rod Style # 3

Port and Cushion Orientation

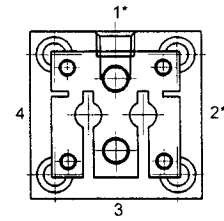


* Ports Normally In Position 1
 ** Cushions Normally In Position 2

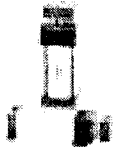
Cylinder Rod Orientation



Standard Rod
Orientation Vertical

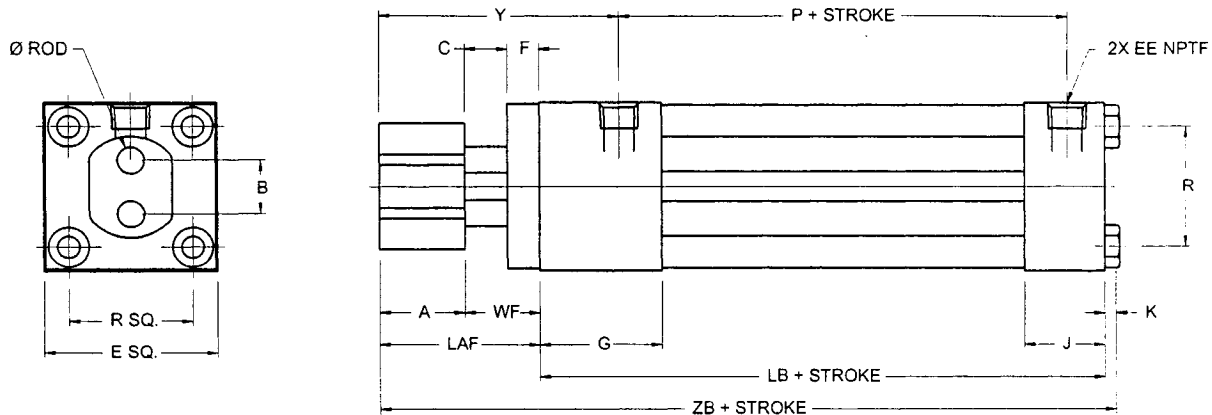


Optional Rod
Orientation Horizontal



F Series Non-Rotating NFPA Interchangeable

Basic-No Mount Cylinder



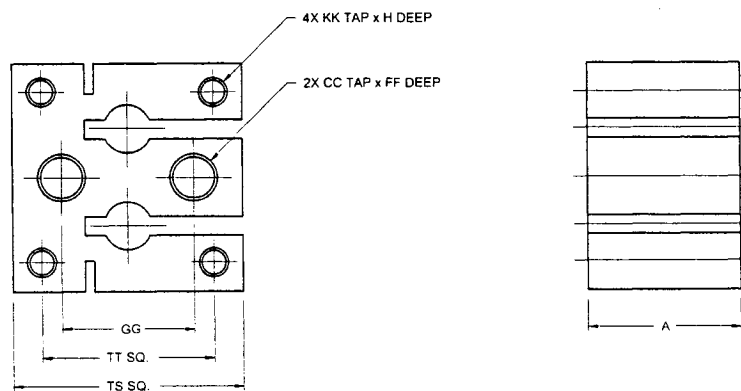
NOTE: Tooling plate removed for clarity.

NFPA Mount Code MX0

Dimensions

BORE	ROD	A	B	C	E	F	G	J	K	P	R	V	Y	EE	LB	WF	ZB	LAF
1-1/2"	0.313	1.000	3.640	0.500	2.000	0.375	1.500	1.000	0.250	2.250	1.430	0.160	2.813	3/8	3.625	0.875	5.750	1.875
2"	0.500	1.000	0.844	0.500	2.500	0.375	1.500	1.000	0.313	2.250	1.840	0.200	2.813	3/8	3.625	0.875	5.813	1.875
2-1/2"	0.625	1.250	1.219	0.500	3.000	0.375	1.500	1.000	0.313	2.375	2.190	0.200	3.063	3/8	3.750	.875	6.188	2.125
3 1/4"	0.750	1.250	1.219	0.500	3.750	0.625	1.750	1.250	0.375	2.625	2.760	0.200	3.438	3/8	4.250	1.125	7.000	2.375
4"	0.750	1.250	1.907	0.500	4.500	0.625	1.750	1.250	0.375	2.625	3.320	0.200	3.438	1/2	4.250	1.125	7.000	2.375

Tooling Plate



Dimensions

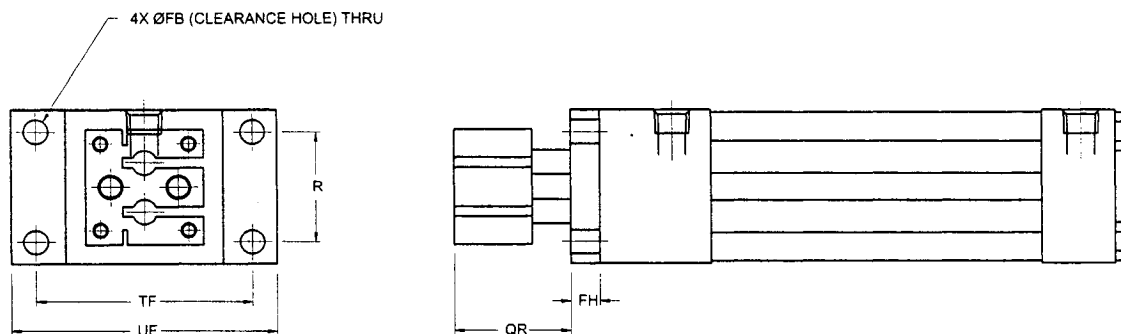
BORE	D	CC	FF	GG	KK	H	TS	TT
1-1/2"	1.575	5/16-18	0.375	0.860	#10-32	0.625	1.500	1.120
2"	1.970	5/16-18	0.375	1.180	1/4-28	0.750	2.000	1.430
2-1/2"	2.480	3/8-16	0.625	1.500	5/16-24	0.875	2.500	1.840
3 1/4"	3.150	1/2-13	0.625	1.970	3/8-24	0.875	3.250	1.790
4"	3.937	1/2-13	0.625	2.760	3/8-24	0.875	4.000	3.440



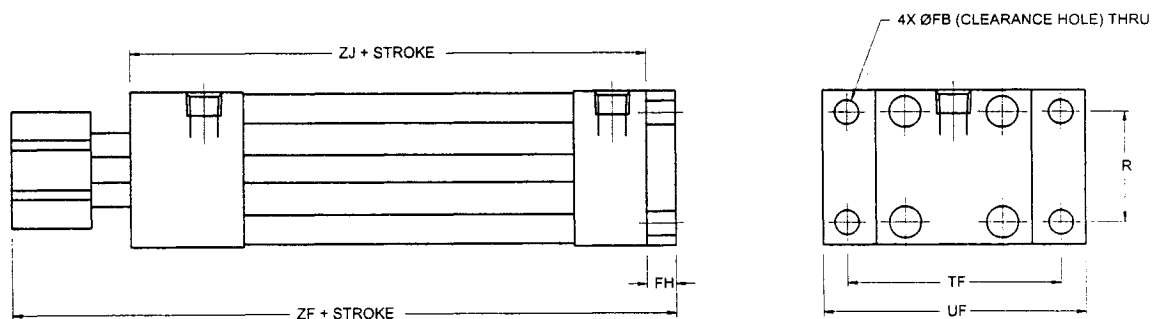
F Series
Non-Rotating NFPA Interchangeable



Flange Mounts



Mount Code NFPA MF1



Mount Code NFPA MF2

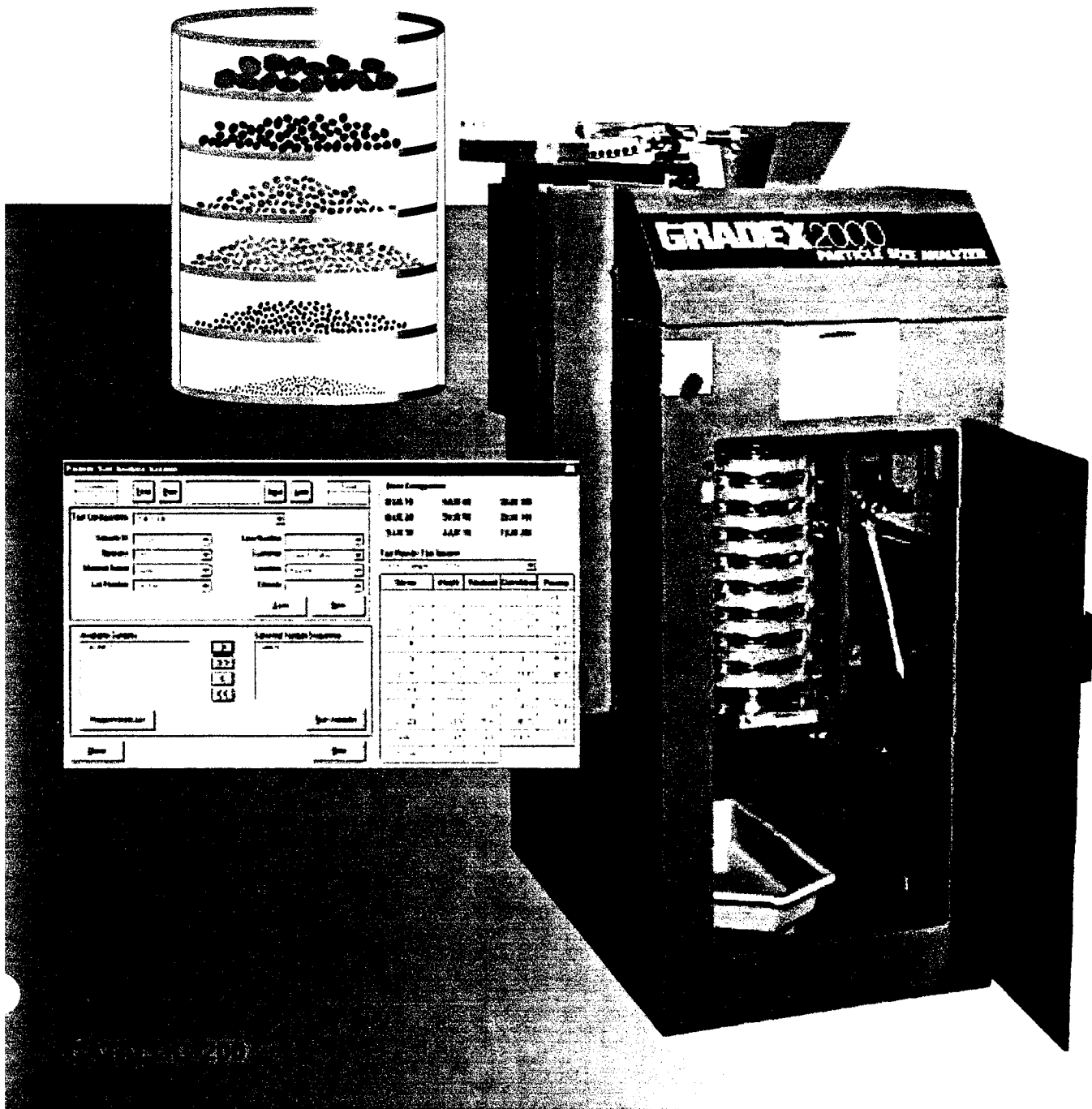
Dimensions

BORE	FB	FH	QR	R	TF	UF	ZF	ZJ
1-1/2"	1/4	0.375	1.500	1.430	2.750	3.375	5.875	5.500
2"	5/16	0.375	1.500	1.840	3.375	4.125	5.875	5.500
2-1/2"	5/16	0.375	1.750	2.190	3.875	4.625	6.250	5.875
3-1/4"	3/8	0.625	1.750	2.760	4.688	5.500	7.250	6.625
4"	3/8	0.625	1.750	3.320	5.438	6.250	7.250	6.625

RODEX INC.

GRADEXTM PARTICLE SIZE ANALYZER

Fully automated sieve analyzer.

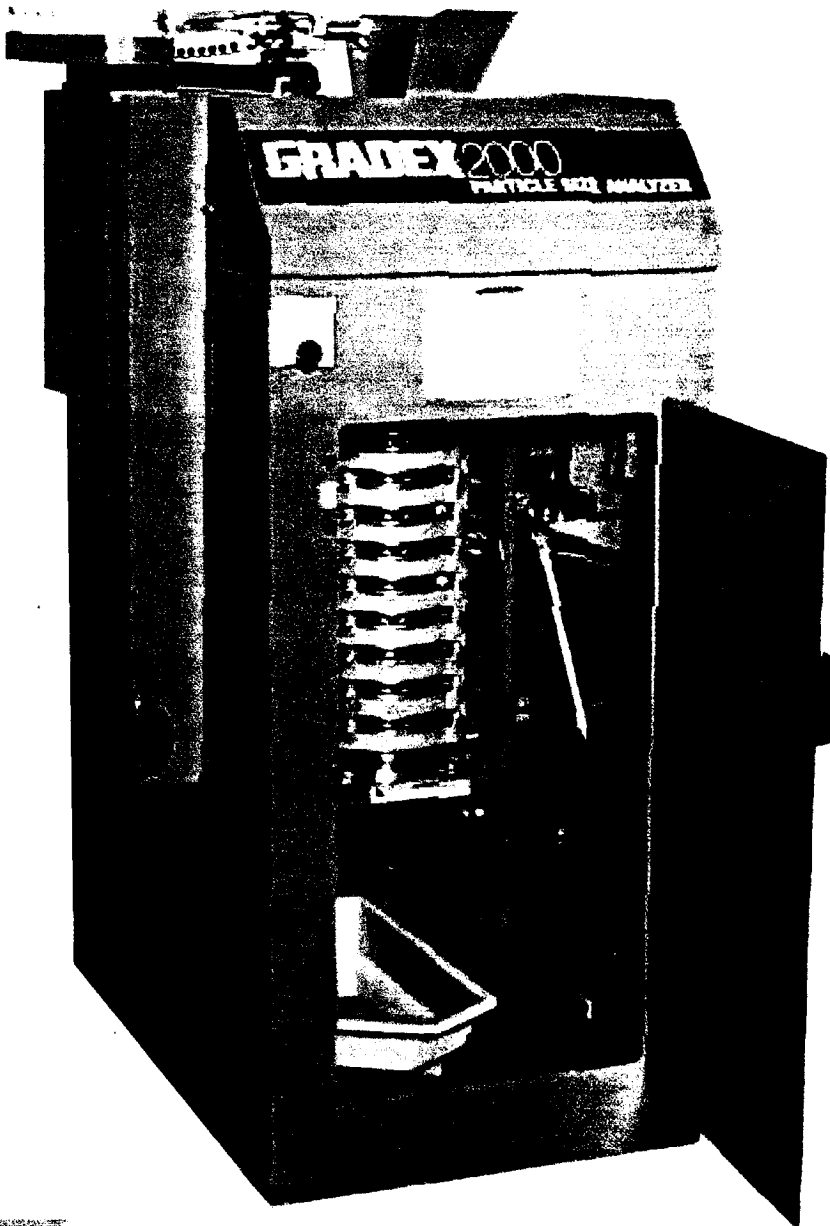


GRADEXTM automated sieve analyzer ...assures consistent product quality

The GRADEX is a patented PC-controlled device which fully automates the sieve analysis process. Available in two models, the GRADEX 1000 and GRADEX 2000 provide analysis and complete data printout automatically – in the lab or on the plant floor – making SPC a reality for today's quality-conscious processor.

- The GRADEX is designed to utilize a stack of standard 8" (or 200mm) round test sieves, either full or half-height size. These test sieves can be easily changed to suit specific test requirements.
- Sieving action is provided by the same rotary shaking/tapping motion used on typical manual sieve shakers.
- The samples to be tested are loaded individually by the operator — or multiple samples may be loaded for continuous testing, or on-line testing can be conducted in conjunction with your automatic sampling devices.
- The GRADEX automatically classifies and weighs each sieve fraction, calculates and stores weight values and reports the data to a PC or controller. The data is stored in a format compatible with most QC/SPC software.

By fully automating the entire sieve analysis process, GRADEX enables the user to analyze product on a more frequent and timely basis — permitting closer control of raw material receipts, materials in process and finished product. Further, it frees technicians to perform other work, while at the same time it improves test accuracy and repeatability over manual methods by eliminating operator error and bias.

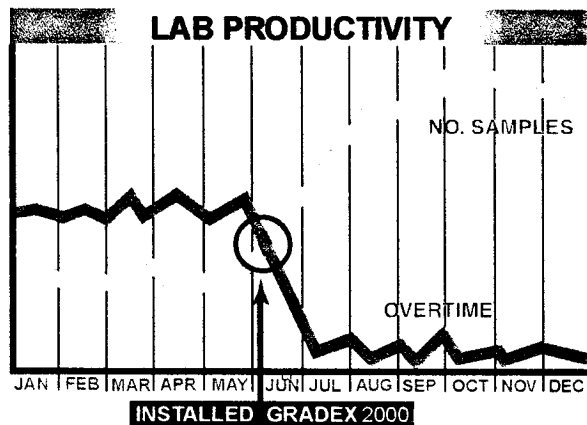


Automatic Sample Feeder.

The GRADEX "AutoFeed" enables staging up to seven samples for uninterrupted testing. Additional samples may easily be added or the sequence changed during operation.

GRADEX reduces costs and frees manpower through automatic, frequent and timely analysis

- Frees technicians to perform other work
- Increases testing capacity without additional manpower
- Enables testing to move to point of sample, so line operators can conduct the testing



Elevates test quality by eliminating operator error

- Eliminates manual steps where errors often occur
- Improves repeatability by avoiding sieve damage due to overbrushing, because Gradex brushes the sieves evenly and consistently
- Electronic data transfer eliminates transposition and calculation errors



Operation of GRADEX is so automatic that it can be used at the point of the sample, enabling operators to perform the analysis right on the plant floor, and use the results immediately without waiting for laboratory test response.

Typical Gradex Applications

Chemical Processing

Chlorine
Detergent
Fertilizer
Pharmaceutical
Super Absorbents

Plastics

Pellets
Resins

Stone, Clay, Glass

Refractory Ceramics
Roofing Granules

Mineral/Mining Processing

Sand
Limestone
Soda Ash

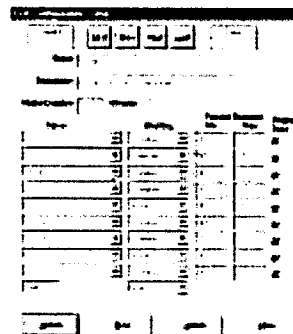
Food Processing

Citric Acid
Coffee
Sugar
Salt
Tobacco

Sequence of Operation

1. Standard test sieves.

GRADEX uses standard 8" (or 200mm) round test sieves, either full or half-height size, which can be easily inserted and changed to suit specific test requirements.

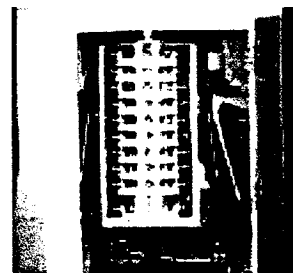


2. Preset test config files.

Operator simply selects from his list, the test to be run.

3. Easy loading of material.

Operator pours sample into machine onto the sieve stack, and initiates test with a single keystroke.

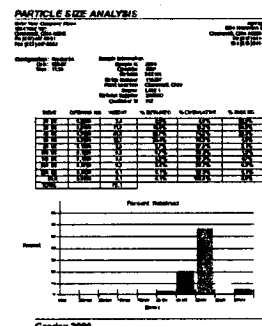


4. Duplicates common, accepted manual sieving process. GRADEX shakes and taps for a preset time, using the same stroke and frequency as typical manual shakers.

5. Automates dumping, weighing, brushing. Each fraction is dumped into a collection tray which rests on a digital electronic balance. Each sieve is brushed prior to the material being weighed. Data is recorded for all fractions and electronically transferred to the PC.



6. Customized data presentations (available with GRADEX 2000 only). Operator can view data one test at a time, or create custom reports to view groups of results, data vs. time, lot summaries, etc.



Control Options

GRADEX Control Options provide the flexibility to locate the Gradex where its operation has the greatest benefit.

PC-CONTROL

The Gradex software is Windows® based and provides the greatest operational flexibility. It can be set up in the test lab or any other environment where a standard PC can be used.

ON-BOARD CONTROL

The On-Board Control Option enables Gradex to be used in environments where PC operation is not



practical ... on the plant floor, in shipping docks, for hazardous materials, etc. ... wherever there is air and electrical service. Gradex results can be transmitted to a remote PC via an RS-485 interface.

ON-LINE CONTROL

For maximum testing automation, the On-Line Gradex 2000 can accept feed directly from the processing line, analyze the sample automatically, and transfer the results to a process control computer. The GRADEX control software is self-contained, and a PC is connected for remote data collection and software maintenance.

COMPUTER CONTROL CABINET.

The GRADEX control system can be housed in this free-standing console, complete with cooling air supplied by dual fans. This console serves as an operator work station, housing the PC keyboard, monitor and printer.

AGGREGATE GRADATION WITH THE GRADEX™ 3000

The GRADEX 3000 Particle Size Analyzer improves or expands quality control programs by providing reliable, fully automatic sieve analysis for the gradation of aggregate material.

The GRADEX 3000 offers the same benefits as the GRADEX 1000 and 2000, but is designed to classify larger samples and particle sizes for materials such as gravel and crushed stone.

The GRADEX 3000 analyzes up to 13 fractions utilizing a stack of standard, 12" diameter, half-height, round test sieves that can be easily changed to meet specific test requirements.

For more information on the GRADEX 3000, contact Rotex today.

Two Models Available

Rotex now offers two models of particle size analyzers – the new low cost GRADEX 1000 and the GRADEX 2000. Customers can choose between two models depending on the number of tests being run at a time, the size of the samples being tested and the level of data analysis required. Each model offers unique operating benefits.

GRADEX 1000

- O'Haus Navigator Balance with capacity of 2,100 grams
- Accepts standard sieves
- 5–10 Samples can be loaded before tray must be emptied
- Standard GRADEX software

GRADEX 2000

- Mettler Balance with capacity of 5,100 grams
- Accepts any manufacturer's sieves
- 30–50 Samples can be loaded before tray must be emptied
- Enhanced GRADEX software with customized reports, flexible reporting and more

Over 10 years GRADEX experience

GRADEX is now being used to automate sieve analysis and augment quality control programs in scores of applications worldwide. More than ten years' in-use experience has demonstrated that GRADEX provides consistent, reliable performance with extremely low maintenance. Every aspect of design is engineered to provide dependability and low maintenance operation typical of the screening equipment manufactured by ROTEX INC. for over 80 years. When maintenance is required, all components are easily accessed and serviced.

GRADEX TECHNICAL DATA

General Specifications, All Models

Dimensions - Manual.....	27" wide, 52" deep, 60" ht.
- AutoFeed	32" wide, 52" deep, 65" ht.
Weight	810 lbs. (368 kg.)
Power - Electrical	110 v, 60 hz, 1ø-10 amp.
Air	90 psi, 1 cfm
Balance Capacity - GRADEX 1000	2100 gm
- GRADEX 2000	5100 gm
Balance Resolution	0.1 gm

ROTEX INC.

1230 Knowlton St.
Cincinnati, OH 45223 USA
(513) 541-1236
Fax (513) 541-4888
info@rotex.com
www.rotex.com

©2002 ROTEX INC. Information herein subject to change without notice.

® Windows is a registered trademark of Microsoft Corp.

Catalog 200 Printed in U.S.A.

PROPOSAL ROTEX INC.

PROPOSAL # «Proposal_no»

PAGE 1

TO: Domfer Poudres Métalliques
Ltée
6090, boulevard Newman
LaSalle, QC
H8N 2S3

FAX: 514-365-0664

ATTN: Alexandre Rail

DATE: October 31, 2003

REFERENCE: GRADEX™ 2000 Particle
Size Analyzer

PROPOSAL #:

SHIPMENT: 8 weeks

Thank you for your inquiry. We are pleased to quote for acceptance within 20 days.

GRADEX® 2000 PARTICLE SIZE ANALYZER

GRADEX® 2000 Particle Size Analyzer,

- Provides/Includes:
- Fully automatic sieve analysis; with enclosed shaking, tapping and brushing mechanisms
- I/O devices to control all machine functions
- Mettler/Toledo digital electronic balance, 5000 gm capacity, 0.1 gm resolution. Allows for 30 to 50 tests before the balance tray needs to be emptied.
- Enhanced Gradex Windows Software for machine control and data collection.
- Manufactured for use with customer specified 8" round test sieves.
- Set of sieves.
- Data leads for the control of the machine

Power requirement 110 VAC, 60 Hz

Air requirement 1 CFM at 90 PSI

GRADEX 2000 Six-Sieve:

Model G203-SM1 with 6 full-height 8" diameter sieves (See Note #1)

Price for manually fed six sieve unit **\$25,000**

GRADEX 2000 Nine-Sieve:

Model G203-NM1 with 9 half-height 8" diameter sieves (See Note #1)

Price for manually fed nine sieve unit..... **\$27,300**

PROPOSAL

ROTEX INC.

PROPOSAL # «Proposal_no»

PAGE 2

CONTROL OPTION:

GRADEX requires PC to control the operation of the unit.

PC: Dell L Series **\$2,355**

- 1.80 GHz Processor
- 128 Mb Memory: 30 GB Hard Drive
- 3.5" Floppy Drive, 48 x Max CD Rom
- Windows® versions of GRADEX Software
- Keyboard/Mouse/15" Monitor
- HP Deskjet 970Cxi Printer
- Microsoft® Office XP

Computer Integration: Customer supplied computer can be sent to ROTEX to integrate into the GRADEX 2000 system. This includes software loading, expansion card installation and run off performed by an electronics technician .

..... **No Charge**

Cables: Standard length of ribbon and scale cable is 10 feet for PC operation of the GRADEX 2000. This is sufficient to install the computer adjacent to the GRADEX. Cables are also available in sets in the following lengths:

25 feet..... **\$126**

50 feet..... **\$339**

PROPOSAL ROTEX INC.

PROPOSAL # «Proposal_no»
PAGE 3

MISCELLANEOUS:

Control Cabinet: Equipped with dual fan system to house and cool computer system components.

..... \$3,131

Scale Display: Digital display unit for Mettler/Toledo electronic balance.

..... \$1,961

Sonic Cleaner: Unit complete with heater and timer for cleaning of test sieves.

..... \$2,153

Auxiliary Tapper: Assists in passing material through the finer mesh sieves.
(Not required on all applications -- consult your ROTEX representative regarding your specific application)

..... \$ 258

Modified Inlet Chute: Inlet designed for large volume material.

..... \$ 450

START UP & TRAINING (North America)

Startup and training by a factory serviceman is available at a rate of \$1,200 per eight hour day plus all travel and living expenses.

PROPOSAL ROTEX INC.

PROPOSAL # «Proposal_no»

PAGE 4

NOTE #1:

Test Sieves: The GRADEX includes a set of U.S. Standard Sieves, all stainless steel construction, 8" diameter (203mm) to fit in the GRADEX sieve holders. If customer supplied sieves are to be used, they must be sent to ROTEX to be fitted into the unit. This ensures proper operation of the GRADEX.

Additional test sieves may be purchased at the following prices:

US SIEVE NO.	STAINLESS STEEL FRAME STAINLESS STEEL WIRE
Blank	\$ 37
4-120	\$ 63
140-200	\$100
230	\$124
270	\$133
325	\$175

NOTE #2:

Gross Shipping Weight:

GRADEX without computer cabinet - 1350 pounds (613 kgs)

Computer cabinet including computer - 200 pounds (91 kgs)

Gross Shipping Dimensions: 48" wide x 97.5" long x 72.5" high

NOTE #3:

Machine Dimensions:

Machine Only - 27" wide x 50" long x 61" high

With AutoFeed - 27" wide x 55" long x 73" high

Computer Cabinet - 35" wide x 30" long x 71" high

Recommended Installation Space:

Length* - 99"

Width - 36"

Height - 80"

- This dimension includes space required for operation (22") with recommended space in the rear of the machine for maintenance 32").

NOTE #4:

Sale Terms: Please see ROTEX Conditions of Sale included with this proposal.

NOTE #5:

Computer system price is valid for 30 days from the date of this quotation.

Pricing for computer systems ordered outside of this time frame will be revised to reflect the current pricing.

NOTE #6:

Warranties:

Computer: 1 Year / Parts & Labor / On-Site

2nd & 3rd Year / Carry-In

Printer & Scale: 1 Year / Parts & Labor / At Authorized Center

NOTE #7:

Price includes two installation, operation and maintenance manuals. Additional manuals are available for a price of \$20 each.

PROPOSAL ROTEX INC.

PROPOSAL # «Proposal_no»

PAGE 5

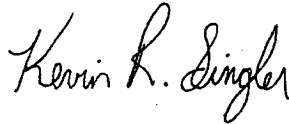
NOTE #8: Minimum computer requirements:

- WINDOWS 95 or higher operating system
- 1 serial port
- 1 PCI slot (free)
- Microsoft® Excel 97 or higher

NOTE #9: Export Terms: See attached Letter of Credit Conditions.

NOTE #11: Pricing is in U.S. funds, F.O.B. Cincinnati, Ohio.

ROTEX INC.



Kevin Singler
Gradex Coordinator

KRS:daf

GRADEX® 2000 Particle Size Analyzer

Cost Justification

(Yellow blocks are inputs that can be adjusted to reflect your situation)

TIME SAVINGS WITH GRADEX					
	Manual (Rotap)	Gradex Manually Fed	Gradex Autofeed	Time Savings	
				Gradex Manual Feed	Gradex Autofeed
- Shake time required by the machine.	Equal	Equal	Equal	0	0
- Preparation - Technician time to perform the steps of stacking the sieves into the shaking device, loading the sample into the stack and turning on the device.	4	1.5	0.4	2.5	3.6
- Sample Analysis - Technician time to remove the stack, dump each fraction, brush each sieve, weigh and record the data and either manually calculate percent retained or enter data into a PC for this calculation.	13	0	0	13	13
				15.5	16.6

SAVINGS CALCULATION		
	GRADEX Manual Feed	GRADEX Autofeed
Tests per Day	15	15
Savings per Test (Minutes)	15.5	16.6
Technician Rate (Inc. benefits)	\$35.00	\$35.00
Operation Days	250	250
TOTAL YEARLY SAVINGS	\$33,906	\$36,250

EFFECT OF TEST FREQUENCY ON SAVINGS					
GRADEX MANUAL FEED SAVINGS PER YEAR		GRADEX Price \$26,200	GRADEX AUTOFEED SAVINGS PER YEAR		GRADEX Price \$32,300
Tests Per Day	Yearly Savings	Payback	Tests Per Day	Yearly Savings	Payback
5	\$11,302	2.3	5	\$12,083	2.7
10	\$22,604	1.2	10	\$24,167	1.3
15	\$33,906	0.8	15	\$36,250	0.9
20	\$45,208	0.6	20	\$48,333	0.7
25	\$56,510	0.5	25	\$60,417	0.5
30	\$67,813	0.4	30	\$72,500	0.4
35	\$79,115	0.3	35	\$84,583	0.4
40	\$90,417	0.3	40	\$96,667	0.3
45	\$101,719	0.3	45	\$108,750	0.3
50	\$113,021	0.2	50	\$120,833	0.3

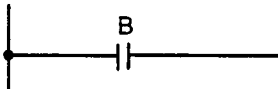
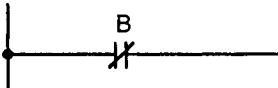
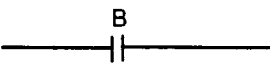
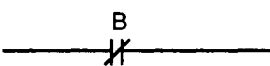
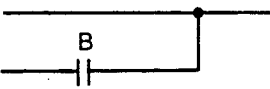

Appendix 5

Ladder diagram instructions

5-8 Ladder Diagram Instructions

Ladder Diagram instructions include Ladder instructions and Logic Block instructions and correspond to the conditions on the ladder diagram. Logic block instructions are used to relate more complex parts.

5-8-1 LOAD, LOAD NOT, AND, AND NOT, OR, and OR NOT

	Ladder Symbols	Operand Data Areas		
LOAD – LD		<table><tr><td>B: Bit</td></tr><tr><td>IR, SR, AR, HR, TC, LR, TR</td></tr></table>	B: Bit	IR, SR, AR, HR, TC, LR, TR
B: Bit				
IR, SR, AR, HR, TC, LR, TR				
LOAD NOT – LD NOT		<table><tr><td>B: Bit</td></tr><tr><td>IR, SR, AR, HR, TC, LR</td></tr></table>	B: Bit	IR, SR, AR, HR, TC, LR
B: Bit				
IR, SR, AR, HR, TC, LR				
AND – AND		<table><tr><td>B: Bit</td></tr><tr><td>IR, SR, AR, HR, TC, LR</td></tr></table>	B: Bit	IR, SR, AR, HR, TC, LR
B: Bit				
IR, SR, AR, HR, TC, LR				
AND NOT – AND NOT		<table><tr><td>B: Bit</td></tr><tr><td>IR, SR, AR, HR, TC, LR</td></tr></table>	B: Bit	IR, SR, AR, HR, TC, LR
B: Bit				
IR, SR, AR, HR, TC, LR				
OR – OR		<table><tr><td>B: Bit</td></tr><tr><td>IR, SR, AR, HR, TC, LR</td></tr></table>	B: Bit	IR, SR, AR, HR, TC, LR
B: Bit				
IR, SR, AR, HR, TC, LR				
OR NOT – OR NOT		<table><tr><td>B: Bit</td></tr><tr><td>IR, SR, AR, HR, TC, LR</td></tr></table>	B: Bit	IR, SR, AR, HR, TC, LR
B: Bit				
IR, SR, AR, HR, TC, LR				

Limitations

There is no limit to the number of any of these instructions, or restrictions in the order in which they must be used, as long as the memory capacity of the PC is not exceeded.

Description

These six basic instructions correspond to the conditions on a ladder diagram. As described in *Section 4 Writing and Inputting the Program*, the status of the bits assigned to each instruction determines the execution conditions for all other instructions. Each of these instructions and each bit address can be used as many times as required. Each can be used in as many of these instructions as required.

The status of the bit operand (B) assigned to LD or LD NOT determines the first execution condition. AND takes the logical AND between the execution condition and the status of its bit operand; AND NOT, the logical AND between the execution condition and the inverse of the status of its bit operand. OR takes the logical OR between the execution condition and the status of its bit operand; OR NOT, the logical OR between the execution condition and the inverse of the status of its bit operand. The ladder symbol for loading TR bits is different from that shown above. Refer to *4-4-3 Ladder Instructions* for details.

Flags

There are no flags affected by these instructions.

5-7 Instruction Set Lists

This section provides tables of the instructions available in the C200HS. The first table can be used to find instructions by function code. The second table can be used to find instruction by mnemonic. In both tables, the @ symbol indicates instructions with differentiated variations.

Note Refer to 5-5 *Expansion Instructions* for a list of the expansion instructions.

5-7-1 Function Codes

The following table lists the instructions that have fixed function codes. Each instruction is listed by mnemonic and by instruction name. Use the numbers in the leftmost column as the left digit and the number in the column heading as the right digit of the function code.

Left digit	Right digit									
	0	1	2	3	4	5	6	7	8	9
0	NOP NO OPERATION	END END	IL INTERLOCK	ILC INTERLOCK CLEAR	JMP JUMP	JME JUMP END	(@) FAL FAILURE ALARM AND RESET	FALS SEVERE FAILURE ALARM	STEP STEP DEFINE	SNXT STEP START
1	SFT SHIFT REGISTER	KEEP KEEP	CNTR REVERSIBLE COUNTER	DIFU DIFFERENTIATE UP	DIFD DIFFERENTIATE DOWN	TIMH HIGH-SPEED TIMER	(@) WSFT WORD SHIFT	(@) ASFT ASYNCHRONOUS SHIFT REGISTER	(@) SCAN CYCLE TIME	(@) MCMP MULTI-WORD COMPARE
2	CMP COMPARE	(@) MOV MOVE	(@) MVN MOVE NOT	(@) BIN BCD TO BINARY	(@) BCD BINARY TO BCD	(@) ASL SHIFT LEFT	(@) ASR SHIFT RIGHT	(@) ROL ROTATE LEFT	(@) ROR ROTATE RIGHT	(@) COM COMPLEMENT
3	(@) ADD BCD ADD	(@) SUB BCD SUBTRACT	(@) MUL BCD MULTIPLY	(@) DIV BCD DIVIDE	(@) ANDW LOGICAL AND	(@) ORW LOGICAL OR	(@) XORW EXCLUSIVE OR	(@) XNRW EXCLUSIVE NOR	(@) INC INCREMENT	(@) DEC DECREMENT
4	(@) STC SET CARRY	(@) CLC CLEAR CARRY	---	---	---	TRSM TRACE MEMORY SAMPLE	(@) MSG MESSAGE DISPLAY	(@) LMSG LONG MESSAGE	(@) TERM TERMINAL MODE	---
5	(@) ADB BINARY ADD	(@) SBB BINARY SUBTRACT	(@) MLB BINARY MULTIPLY	(@) DVB BINARY DIVIDE	(@) ADDL DOUBLE BCD ADD	(@) SUBL DOUBLE BCD SUBTRACT	(@) MULL DOUBLE BCD MULTIPLY	(@) DIVL DOUBLE BCD DIVIDE	(@) BINL DOUBLE BCD-TO-DOUBLE BINARY	(@) BCDL DOUBLE BINARY-TO-DOUBLE BCD
6	CMPL DOUBLE COMPARE	(@) MPRF TRANSFER BITS	(@) XFRB TRANSFER BITS	(@) LINE COLUMN TO LINE	(@) COLM LINE TO COLUMN	(@) SEC HOURS-TO-SECONDS	(@) HMS SECONDS-TO-HOURS	(@) BCNT BIT COUNTER	(@) BCMP BLOCK COMPARE	(@) APR ARITHMETIC PROCESS
7	(@) XFER BLOCK TRANSFER	(@) BSET BLOCK SET	(@) ROOT SQUARE ROOT	(@) XCHG DATA EXCHANGE	(@) SLD ONE DIGIT SHIFT LEFT	(@) SRD ONE DIGIT SHIFT RIGHT	(@) MLPX 4-TO-16 DECODER	(@) DMPX 16-TO-4 ENCODER	(@) SDEC 7-SEGMENT DECODER	(@) FDIV FLOATING POINT DIVIDE
8	(@) DIST SINGLE WORD DISTRIBUTE	(@) COLL DATA COLLECT	(@) MOVb MOVE BIT	(@) MOVd MOVE DIGIT	(@) SFTR REVERSIBLE SHIFT REGISTER	(@) TCMP TABLE COMPARE	(@) ASC ASCII CONVERT	TTIM TOTALIZING COUNTER	ZCP AREA RANGE COMPARE	(@) INT INTERRUPT CONTROL
9	(@) SEND NETWORK SEND	(@) SBS SUBROUTINE ENTRY	SBN SUBROUTINE DEFINE	RET SUBROUTINE RETURN	(@) WDT WATCHDOG TIMER REFRESH	---	---	(@) IORF I/O REFRESH	(@) RECV NETWORK RECEIVE	(@) MCRO MACRO

5-7-2 Alphabetic List by Mnemonic

Mnemonic	Code	Words	Name	Page
7SEG	—	4	7-SEGMENT DISPLAY OUTPUT	302
ADB (@)	50	4	BINARY ADD	220
ADBL (@)	—	4	DOUBLE BINARY ADD	226
ADD (@)	30	4	BCD ADD	206
ADDL (@)	54	4	DOUBLE BCD ADD	207
AND	None	1	AND	129
AND LD	None	1	AND LOAD	130
AND NOT	None	1	AND NOT	129
ANDW (@)	34	4	LOGICAL AND	251
APR (@)	69	4	ARITHMETIC PROCESS	240
ASC (@)	86	4	ASCII CONVERT	195
ASFT (@)	17	4	ASYNCHRONOUS SHIFT REGISTER	157

Mnemonic	Code	Words	Name	Page
ASL (@)	25	2	ARITHMETIC SHIFT LEFT	154
ASR (@)	26	2	ARITHMETIC SHIFT RIGHT	154
AVG (@)	—	4	AVERAGE VALUE	236
BCD (@)	24	3	BINARY TO BCD	182
BCDL (@)	59	3	DOUBLE BINARY-TO-DOUBLE BCD	183
BCMP (@)	68	4	BLOCK COMPARE	174
BCNT (@)	67	4	BIT COUNTER	284
BIN (@)	23	3	BCD-TO-BINARY	181
BINL (@)	58	3	DOUBLE BCD-TO-DOUBLE BINARY	182
BSET (@)	71	4	BLOCK SET	160
CLC (@)	41	1	CLEAR CARRY	206
CMP	20	3	COMPARE	170
CMPL	60	4	DOUBLE COMPARE	173
CNT	None	2	COUNTER	145
CNTR	12	3	REVERSIBLE COUNTER	148
COLL (@)	81	4	DATA COLLECT	164
COLM (@)	64	4	LINE TO COLUMN	202
COM (@)	29	2	COMPLEMENT	250
CPS	—	4	SIGNED BINARY COMPARE	179
CPSL	—	4	DOUBLE SIGNED BINARY COMPARE	180
DBS (@)	—	4	SIGNED BINARY DIVIDE	232
DBSL (@)	—	4	DOUBLE SIGNED BINARY DIVIDE	233
DEC (@)	39	2	BCD DECREMENT	205
DIFD	14	2	DIFFERENTIATE DOWN	131
DIFU	13	2	DIFFERENTIATE UP	131
DIST (@)	80	4	SINGLE WORD DISTRIBUTE	162
DIV (@)	33	4	BCD DIVIDE	213
DIVL (@)	57	4	DOUBLE BCD DIVIDE	214
DMPX (@)	77	4	16-TO-4 ENCODER	189
DSW	—	4	DIGITAL SWITCH	305
DVB (@)	53	4	BINARY DIVIDE	225
END	01	1	END	138
FAL (@)	06	2	FAILURE ALARM AND RESET	276
FALS	07	2	SEVERE FAILURE ALARM	276
FCS (@)	—	4	FCS CALCULATE	284
FDIV (@)	79	4	FLOATING POINT DIVIDE	215
FPD	—	4	FAILURE POINT DETECT	286
HEX (@)	—	4	ASCII-TO-HEXADECIMAL	196
HKY	—	4	HEXADECIMAL KEY INPUT	309
HMS (@)	66	4	SECONDS TO HOURS	185
IL	02	1	INTERLOCK	135
ILC	03	1	INTERLOCK CLEAR	135
INC (@)	38	2	INCREMENT	205
INT (@)	89	4	INTERRUPT CONTROL	263
IORF (@)	97	3	I/O REFRESH	282
JME	05	2	JUMP END	137
JMP	04	2	JUMP	137
KEEP	11	2	KEEP	133
LD	None	1	LOAD	129

Mnemonic	Code	Words	Name	Page
LD NOT	None	1	LOAD NOT	129
LINE (@)	63	4	COLUMN TO LINE	201
LMSG (@)	47	4	32-CHARACTER MESSAGE	280
MAX (@)	—	4	FIND MAXIMUM	234
MBS (@)	—	4	SIGNED BINARY MULTIPLY	230
MBSL (@)	—	4	DOUBLE SIGNED BINARY MULTIPLY	231
MCMP (@)	19	4	MULTI-WORD COMPARE	169
MCRO (@)	99	4	MACRO	261
MIN (@)	—	4	FIND MINIMUM	235
MLB (@)	52	4	BINARY MULTIPLY	225
MLPX (@)	76	4	4-TO-16 DECODER	186
MOV (@)	21	3	MOVE	159
MOVB (@)	82	4	MOVE BIT	166
MOVD (@)	83	4	MOVE DIGIT	167
MPRF (@)	61	4	GROUP-2 HIGH-DENSITY I/O REFRESH	283
MSG (@)	46	2	MESSAGE	279
MTR	—	4	MATRIX INPUT	314
MUL (@)	32	4	BCD MULTIPLY	212
MULL (@)	56	4	DOUBLE BCD MULTIPLY	213
MVN (@)	22	3	MOVE NOT	159
NEG (@)	—	4	2'S COMPLEMENT	203
NEGL (@)	—	4	DOUBLE 2'S COMPLEMENT	204
NOP	00	1	NO OPERATION	138
OR	None	1	OR	129
OR LD	None	1	OR LOAD	130
OR NOT	None	1	OR NOT	129
ORW (@)	35	4	LOGICAL OR	252
OUT	None	2	OUTPUT	130
OUT NOT	None	2	OUTPUT NOT	130
PID (@)	—	4	PID CONTROL	243
RECV (@)	98	4	NETWORK RECEIVE (CPU31-E/33-E only)	294
RET	93	1	SUBROUTINE RETURN	260
ROL (@)	27	2	ROTATE LEFT	155
ROOT (@)	72	3	SQUARE ROOT	218
ROR (@)	28	2	ROTATE RIGHT	155
RSET	None	2	RESET	133
RXD (@)	—	4	RECEIVE	298
SBB (@)	51	4	BINARY SUBTRACT	222
SBBL (@)	—	4	DOUBLE BINARY SUBTRACT	228
SBN	92	2	SUBROUTINE DEFINE	260
SBS (@)	91	2	SUBROUTINE ENTRY	258
SCAN (@)	18	4	CYCLE TIME	277
SCL (@)	—	4	SCALING	199
SDEC (@)	78	4	7-SEGMENT DECODER	192
SEC (@)	65	4	HOURS TO SECONDS	184
SEND (@)	90	4	NETWORK SEND (CPU31-E/33-E only)	292
SET	None	2	SET	133
SFT	10	3	SHIFT REGISTER	150
SFTR (@)	84	4	REVERSIBLE SHIFT REGISTER	152

Mnemonic	Code	Words	Name	Page
SLD (@)	74	3	ONE DIGIT SHIFT LEFT	156
SNXT	09	2	STEP START	267
SRCH (@)	—	4	DATA SEARCH	290
SRD (@)	75	3	ONE DIGIT SHIFT RIGHT	156
STC (@)	40	1	SET CARRY	206
STEP	08	2	STEP DEFINE	267
SUB (@)	31	4	BCD SUBTRACT	208
SUBL (@)	55	4	DOUBLE BCD SUBTRACT	210
SUM (@)	—	4	SUM CALCULATION	238
TCMP (@)	85	4	TABLE COMPARE	176
TERM (@)	48	4	TERMINAL MODE	281
TIM	None	2	TIMER	139
TIMH	15	3	HIGH-SPEED TIMER	143
TKY (@)	—	4	TEN KEY INPUT	312
TRSM	45	1	TRACE MEMORY SAMPLE	278
TTIM	87	4	TOTALIZING TIMER	144
TXD (@)	—	4	TRANSMIT	300
WDT (@)	94	2	WATCHDOG TIMER REFRESH	282
WSFT (@)	16	3	WORD SHIFT	157
XCHG (@)	73	3	DATA EXCHANGE	162
XDMR (@)	—	4	EXPANSION DM READ	291
XFER (@)	70	4	BLOCK TRANSFER	161
XFRB (@)	62	4	TRANSFER BITS	168
XNRW (@)	37	4	EXCLUSIVE NOR	254
XORW (@)	36	4	EXCLUSIVE OR	253
ZCP	88	4	AREA RANGE COMPARE	177
ZCPL	—	4	DOUBLE AREA RANGE COMPARE	178

Appendix 6

Controller hardware specifications

Build Networks Easily with the Alpha's Built-in Features.

Using built-in Host Link function of the C200H Alpha, connect directly to operator interface terminals using a cable as an interface, or use a One-to-One data links between alpha PLCs are just as easy to make.

When networking with a PC, the TXD and RXD instructions can be used to carry out RS-232C communications from the PLC, and the STUP instruction can be used to switch between Host Link and RS-232C, communications.

Open up Your Communications Possibilities in All Three Automation Network Levels

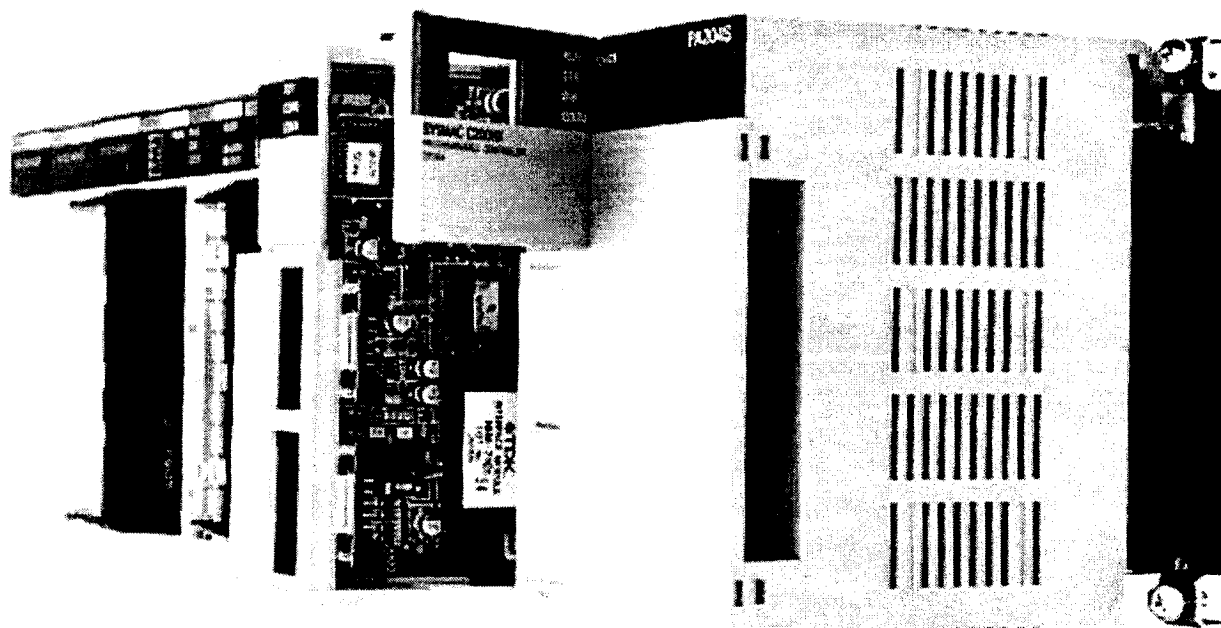
DEVICE LEVEL NETWORKS: The new C200HW-DRM21 Module supports DeviceNet open multi-vendor network communications. DeviceNet makes it possible to connect devices that have a wide variety of parameters or data, such as inverters or analog devices. It also allows other DeviceNet products to be connected as well.

CONTROL LEVEL NETWORKS: Omron's SYSMAC Link and SYSMAC Net networks provide high-speed real-time data transfer. SYSMAC Link's data link capacity has been increased from 918 words to 2,966 words.

INFORMATION LEVEL NETWORKS: The C200HW-PCS01 PCMCIA Module allows data exchange with CV Ethernet units, PCs and workstations using Omron's FINS protocol via Ethernet UDP/IP.

Connect to a Variety of Serial Devices

The C200H α CPU's can be equipped with one of six communication boards. By installing the appropriate communication board, the CPU can communicate with SYSMAC Link / SYSMAC Net modules, a PC Card module or serial devices. Using the Protocol Macro Function built into the C200HW-COM04-E, C200HW-COM05-E or C200HW-COM06-E communications boards, communications sequences for one of seven types of installed Omron protocols may be used or customized for a modem, operator interface, bar code reader, temperature controller, or any kind of RS-232C, RS-422 or RS-485 device.



BUILD YOUR OWN CONTROL AND DATA PROCESSING SYSTEM

CPU

- Choose from 11 CPU models
- Separate CPU and power supply

CPU and Expansion Backplanes

- CPU and power supply mount on a dedicated CPU backplane
- Local expansion may be done with the new space-saving C200H α expansion backplanes or current C200H backplanes
- Connect up to 5 remote I/O backplanes

Special I/O

- Take full advantage of the C200H α 's power with any combination of 20 Special I/O Modules

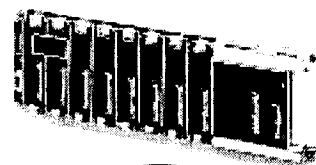
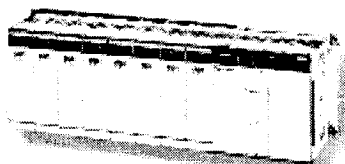
Communications

- All CPUs include a multifunctional peripheral port to communicate to programming peripherals
- Standard Host Link port is built into selected CPUs
- One of six communications boards can also be installed in the CPU. When used with the protocol macro function, these boards provide a simple way to connect with a SYSMAC Link or SYSMAC Net Link module, to communicate with a Modem, operator interface, bar code reader, Process Controller or any kind of RS-232C, RS-422 or RS-485 device.

Software Support

- Supported by both SYSMAC Support Software Version 1.2 or greater and SYSWIN version 3.0 or greater

CPU RACK



CPU BACKPLANE
C200HW-BC031 C200HW-BC051
C200HW-BC081 C200HW-BC101



EEPROM MEMORY CASSETTES
4K words C200HW-ME04K
8K words C200HW-ME08K
16K words C200HW-ME16K
32K words C200HW-ME32K

EPROM MEMORY CASSETTES
16/32K words C200HS-MP16K

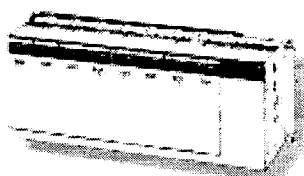


CPU
C200HE-CPU11-E C200HE-CPU32-E
C200HE-CPU33-E C200HE-CPU42-E
C200HG-CPU43-E C200HX-CPU34-E
C200HG-CPU44-E C200HX-CPU44-E
C200HG-CPU53-E C200HX-CPU54-E
C200HG-CPU63-E C200HX-CPU64-E



POWER SUPPLY MODULE
C200HW-PA204
C200HW-PA204S
C200HW-PD024

EXPANSION I/O RACK



I/O CONNECTING CABLE
C200H-CN001
(30cm, 70cm, 2m, 5m, 10m)

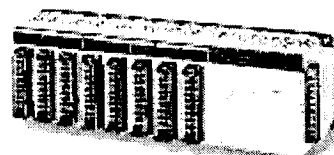


POWER SUPPLY MODULE
C200HW-PA204
C200HW-PA204S
C200HW-PD024



EXPANSION I/O BACKPLANE
C200HW-BI031
C200HW-BI051
C200HW-BI081
C200HW-BI101

SLAVE RACKS



REMOTE I/O SLAVE MODULE
Fiber-optic, 100/200 VAC C200H-RT001-P
Fiber-optic, 24 VDC C200H-RT002-P
Wired, 100/200 VAC C200H-RT201
Wired, 24 VDC C200H-RT202



SLAVE I/O BACKPLANE
C200H-BC031-V2
C200H-BC051-V2
C200H-BC081-V2
C200H-BC101-V2

COMMUNICATIONS BOARDS (cannot be mounted to the CPUHE-CPU11-E)



C200HW-COM01



C200HW-COM02



C200HW-COM03



C200HW-COM04-E



C200HW-COM05-E

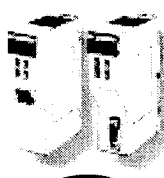


C200HW-COM06-E

COMMUNICATIONS MODULES



**DEVICENET
SCANNER**
C200HW-DRM21



HOST LINK
RS422 C200H-LK202-V1
Fiber-optic C200H-LK101-PV1
RS232 C200H-RM201-V1



PC LINK
C200H-LK401



PC CARD*
C200HW-PCU01
Ethernet Set*
C200HW-PCS01-E



REMOTE I/O MASTER
Fiber-optic C200H-RM001-V1
Wired C200H-RM201-V1



SYSMAC LINK*
Coaxial C200HW-SLK23/24
Fiber-optic C200HW-SLK13/14



SYSMAC NET LINK*
C200HS-SNT32

*Use these modules together with communications boards (C200H-COM01/04-E) in the CPU Rack.

SPECIAL I/O MODULES



ANALOG INPUT
C200H-AD001
C200H-AD002



ANALOG OUTPUT
C200H-DA001
C200H-DA002



ASCII/BASIC
C200H-ASC02



CAM POSITIONER
C200H-CP114



FUZZY LOGIC
C200H-FZ001



**HIGH-SPEED
COUNTER**
C200H-CT000



RFID SENSOR
C200H-IDS01



**DUAL-AXIS
MOTION CONTROL**
C200H-MC221



PID CONTROL
C200H-PID00



**POSITION
CONTROL**
C200H-NC211
C200H-NC112



**TEMPERATURE
SENSOR**
C200H-TS000



**TEMPERATURE
CONTROL**
C200H-TC000
C200H-TV000



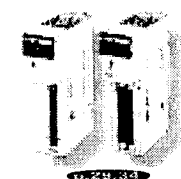
VOICE
C200H-OV001



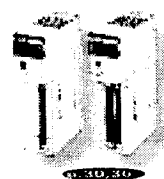
B7A INTERFACE
16 points
C200H-B7A01



B7A INTERFACE
32 points/64 points
C200H-B7A00
(cannot be used on Slave rack)



HIGH DENSITY INPUT
C200H-ID000
Group 2 C200H-ID210



HIGH DENSITY OUTPUT
C200H-OD000
Group 2 C200H-OD210



ANALOG TIMER
C200H-TM001

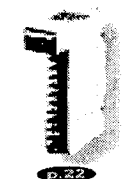


MIXED I/O
16 inputs/16 outputs
C200H-MD000

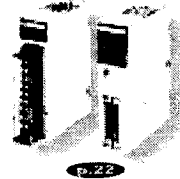


INTERRUPT INPUT
C200HS-INT01
(CPU Backplane ONLY)

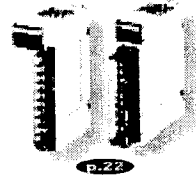
DISCRETE I/O MODULES



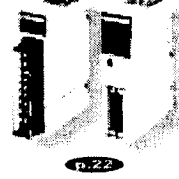
8 POINT INPUT
C200H-ID000



16/32 POINT INPUT
C200H-ID000



5/8/16 POINT OUTPUT
C200H-OD000



12/32 POINT OUTPUT
C200H-OD000

SYSTEM OVERVIEW

C200HX/HG/HE SPECIFICATIONS

C200Hα PLC – System Specifications

ITEM	SPECIFICATIONS
Supply voltage	AC power supply: 100 to 120/200 to 240 VAC selectable 50/60 Hz DC power supply: 24 VDC
Operating voltage range	AC power supply: 85 to 132/170 to 264 VAC DC power supply: 19.2 to 28.8 VDC
Power consumption	AC power supply: 120 VA max. DC power supply: 50 W max.
Surge current	30 A max.
Output capacity	4.6 A, 5 VDC; 0.6 A, 26 VDC; 0.8 A, 24 VDC ^{+10%/−20%} (C200HW-PA204S only)
Insulation resistance	20 MΩ between AC terminals and the GR terminal at 500 VDC (see note 1)
Dielectric strength	2,300 VAC at 50/60 Hz for 1 minute between AC terminals and housing; 1,000 VAC at 50/60 Hz for 1 minute between DC terminals and housing. Leakage current: 10 mA max. (see note 1)
Noise immunity	1,500 Vp-p, pulse width: 100 ns to 1 μs, rise time: 1 ns pulse (by noise simulator)
Vibration	10 to 57 Hz; 0.075 mm amplitude, 57 to 150 Hz; acceleration: 1 G, in X, Y, and Z directions, for 80 minutes each (sweep time 8 min x 10 sweeps = 80 min); (When mounted on DIN track, 2 to 55 Hz, 0.3 G, in X, Y, and Z directions for 20 minutes each)
Shock	15G (147 m/s ²) in X, Y, and Z directions, 3 times each
Ambient temperature	Operating: 0 to 55°C (32° to 131.0°F) Storage: −20 to 75°C (−4.0 to 167.0°F) without battery
Humidity	10% to 90% (without condensation)
Atmosphere	Must be free of corrosive gases
Grounding	Less than 100 Ω
Enclosure rating	IEC IP30 (mounted in a panel)
Weight	6 kg max. (CPU: 315 g max., Power Supply Module: 510 g max., Backplane: 445 g to 1040 g)

Note: Be sure to disconnect the LG and GR terminals when conducting insulation resistance tests or dielectric strength tests. Internal components might be damaged if insulation resistance tests are repeated many times with the LG and GR terminals connected.

CPU

YOUR INTRODUCTION TO THE C200HX/HG/HE CPU

Features

Select from Eleven C200Hα CPUs within Alpha's Three Basic Model Types

Each model has different program capacities, processing speeds, I/O capabilities, communications connections and features. (The *C200Hα CPU Selection Table* is provided later in this section.)

Optional Back-up Memory Cassettes

For program back-up or rewrite option, each CPU has a special Memory Cassette compartment.

Multifunctional Peripheral Port

Directly connect to programming peripherals or communicate to Omron's Operator Interface Terminals and other third party devices using an optional CIF Convertor Cable.

Built-in RS-232C Port

Direct Host Link communications to the CPU or interface with other devices through serial communications. Available on selected models only.

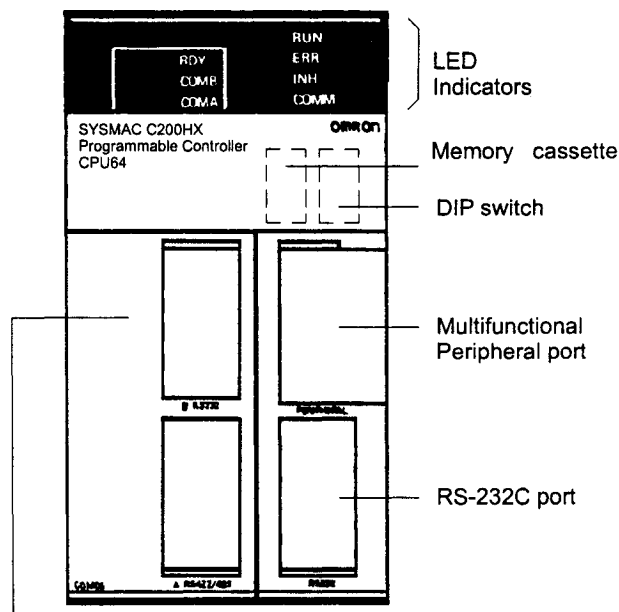
Versatile Communications

Install one of six C200Hα Communications Boards to have additional communications ports. The boards fit into the communications slot in the CPU and enable communication with SYSMAC LINK or SYSMAC NET modules, a PC card module or a variety of serial devices – including Operator Interfaces. Order the Communications Board and Memory Cassette separately (not provided with the CPU).

Protocol Macro

Three C200Hα Communications Boards offer the Protocol Macro Instruction that controls data transfer with various communications devices and components equipped with RS-232C or RS-422/485 ports. With the Protocol Macro Function built into the C200HW-COM04, C200HW-COM05-E and C200HW-COM06-E Communications Boards, communications sequences (data transfer procedures) may be modified with Omron's Protocol Support Software.

Although seven Omron Communications sequences are built-in, you can use the Protocol Support Software to create other communications sequences. For more details, refer to the *Communication Board* section that follows.



Communications Board (C200HW-COM06-E shown here)

Indicators

INDICATOR ON THE CPU	FUNCTION
RUN (green)	Lit when the PLC is operating normally.
ERR (red)	Flashes if the PLC in operation detects any non-fatal error. (The PLC will continue operating.) Lit if the PLC in operation detects any fatal error. (The PLC will stop operating.) After the PLC stops operating, the RUN indicator will be off, and all output signals of the Output Modules will be interrupted.
INH (orange)	Lit when the Load OFF flag (AR bit) is ON. (All output signals of the Output Modules will be interrupted.)
COMM (orange)	Flashes when the CPU is communicating with the device connected to the peripheral port or RS-232C port.

C200Hα CPU Characteristics

ITEM	SPECIFICATIONS
Control method	Stored program
I/O control method	Cyclic scan with direct output and immediate interrupt processing are both possible.
Programming method	Ladder diagram
Instruction length	1 address/instruction, 1 to 4 words/instruction
Number of instructions	14 basic instructions, 231 special instructions
Execution time	<p>Basic instructions: e.g., LD C200HE-CPU□□-E:0.3 μs C200HG-CPU□□-E:0.15 μs C200HX-CPU□□-E:0.1 μs</p> <p>Special instructions: e.g., MOV(21) C200HE-CPU□□-E:1.2 μs C200HG-CPU□□-E:0.6 μs C200HX-CPU□□-E:0.4 μs</p>
Program capacity	C200HE-CPU11-E: 3.2K words max. C200HE-CPU32-E/CPU42-E: 7.2K words max. C200HG-CPU□□-E: 15.2K words max. C200HX-CPU□□-E: 31.2K words max.
I/O bits	640 (00000 to 02915, 30000 to 30915)
IR bits	6,464 (03000 to 23115, 31000 to 51115)
SR bits	1,080 (23200 to 25507, 25600 to 29915)
TR bits	8 (TR 0 to 7)
HR bits	1,600 (HR 0000 to 9915)
AR bits	448 (AR 0000 to 2715)
LR bits	1,024 (LR 0000 to 6315)
Timers/Counters	512 (TIM/CNT 000 to 511)
DM words	Read/Write: 6,144 (DM 0000 to 6143) Read-only: 512 (DM 6144 to 6655) Expansion: Up to 3,000 words max. (DM 7000 to 9999)
EM words	Read/Write: C200HE-CPU□□-E: None C200HG-CPU□□-E: 6,144 (EM 0000 to EM 6143) C200HX-CPU□□-E: 6,144 × 3 banks (EM 0000 to EM 6143)
Power failure backup function	Holds HR, AR, CNT, DM, and EM and clock (RTC) contents.
Memory backup time	The battery service life is five years at 25°C (77°F). The service life will be shortened if the battery is used at higher temperatures. Replace the battery within one week after the battery alarm indicator starts flashing. When replacing the battery, install the new battery within five minutes after removing the old one.
Self-diagnostic function	CPU errors (watchdog timer), I/O verification errors, host link errors, memory errors, battery errors, I/O bus errors, remote I/O errors, etc.
Program check function	Checks the program from the time the program starts running and checks the omission of the END instruction or any other improper instruction. This function allows three-level checking of programs through the Programming Console.

CPU

SPECIFICATIONS, CHARACTERISTICS

Comparing C200Hα CPU Specifications

Use the following table to compare the functions of the C200HX, C200HG, and C200HE with those of the C200HS and C200H.

FUNCTION		C200HX/HG/HE	C200HS	C200H
Memory	User Memory (UM)	3.2K words (C200HE-CPU11-E) 7.2K words (C200HE-CPU□2-E) 15.2K words (C200HG-CPU□3-E) 31.2K words (C200HX-CPU□4-E)	15.2K words	3.2K words/7.2K words
	Normal Data Memory (DM)	C200HX/G: 6,144 words (DM 0000 to DM 6143) (DM 4000 to DM 5999 do not exist in the C200HE-CPU11-E) C200HE-CPU16: 4000 words (DM0000-3999)	6,144 words (DM 0000 to DM 6143)	1,000 words (DM 0000 to DM 0999)
	Fixed Data Memory	512 words (DM 6144 to DM 6655)	512 words (DM 6144 to DM 6655)	1,000 words (DM 1000 to DM 1999)
	Fixed Expansion Data Memory	0 to 3,000 words (DM 7000 to DM 9999)	0 to 3,000 words (DM 7000 to DM 9999)	None
	Extended Data Memory (EM)	C200HE: No EM C200HG: 6,144 words x 1 bank C200HX: 6,144 words x 3 banks	None	None
I/O	Expansion Racks	3 max. (2 max. for C200HE-CPU□□-E and C200HG/HX-CPU-3□-E/4□-E)	2 max.	2 max.
	Group-2 High-density I/O Modules	0 to 9 and A to F Modules per PLC C200HE-CPU11-E: No Group-2 Modules connected C200HE-CPU□2-E, C200HG/HX-CPU-3□-E/CPU4□-E: 0 to 9 Units per PLC	0 to 9 Modules per PLC	0 to 9 Modules per PLC
	Special I/O Modules	0 to 9 and A to F Modules per PLC C200HE-CPU□□-E, C200HG/HX-CPU-3□-E/CPU4□-E: 0 to 9 Modules per PLC	0 to 9 Modules per PLC	0 to 9 Modules per PLC
Execution time	Basic instructions (LD)	0.1 μs (C200HX) 0.15 μs (C200HG) 0.3 μs (C200HE)	0.375 μs	0.75 μs
	Special instructions (MOV)	0.4 μs (C200HX) 0.6 μs (C200HG) 1.2 μs (C200HE)	19 μs	88 μs
	Other special instructions	C200HX and C200HG: Approx. 1/3 to 2/3 of the time required by the C200HS. C200HE: Approx. 3/4 to 4/5 of the time required by the C200HS.	---	---
	END processing time	0.7 ms (C200HX/HE-CPU□2-E) 2.1 ms (C200HE-CPU11-E)	0.7 ms	2.8 to 3.5 ms
CPU	RS-232C port	C200HX/HG/HE-CPU2□-E/4□-E/6□-E	C200HS-CPU2□-E/3□-E	None
	Clock function	All models except the C200HE-CPU11-E.	All models	Incorporated by the Memory Module
	SYSMAC LINK Module and SYSMAC NET Link Module connection	C200HW-COM01 and C200HW-COM04-E Communications Boards available for connection except the C200HE-CPU11-E.	C200HS-CPU3□-E	C200H-CPU11-E/31-E
Communications Board		The Communications Board can be mounted to all CPUs except the C200HE-CPU11-E. The following are possible with the Communications Board: Use of the SYSMAC LINK Module and SYSMAC NET Link Module expansion of up to 2 communications ports, and use of a protocol macro function	None	None
Interrupts	Interrupt Input Modules	2 (16 points)	1 (8 points)	None
	Interruption with Communications Board	Possible	---	---
	Response time	Same as the C200HS. 1 ms if the C200HW-SLK□□ is used.	C200H-compatible mode: 10 ms C200H mode: 1 ms The C200HS in any mode connected to the SYSMAC LINK Module or SYSMAC NET Link Module 10 ms	---
SYSMAC LINK	Service time	3.5 ms max. (1 system)	10.8 ms max. (1 system)	11.5 ms max. (1 system)
	Remote programming	Via the peripheral port, RS-232C port, and Communications Board	Via the peripheral port only	---
	Influence on interrupt response performance	None	10 ms is required by the C200HS in any mode.	---

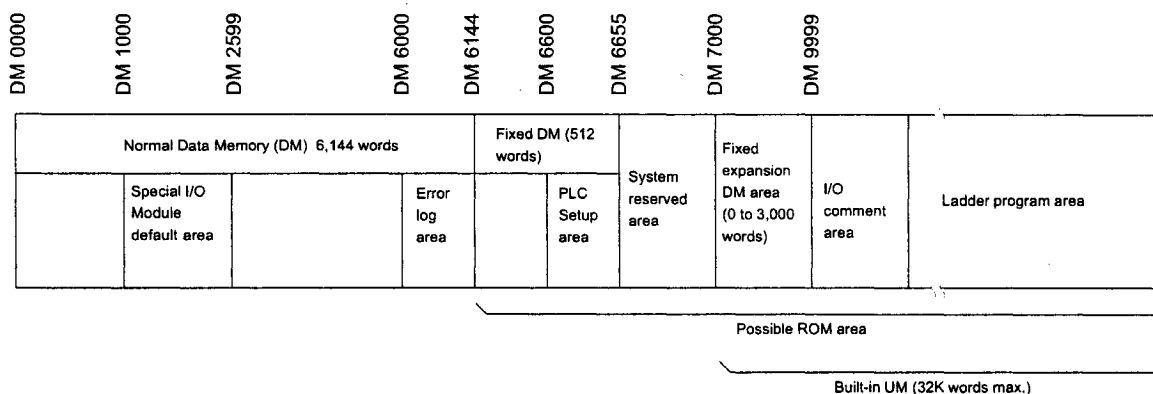
CPU

SPECIFICATIONS, CHARACTERISTICS

User Memory Area

The C200HX, C200HG, and C200HE have a User Memory (UM) area allocation function. This function allows the use of the ladder program area of the UM as a fixed expansion DM area and I/O comment area. The function is enabled with the SYSMAC Support Software (SSS), SYSWIN, or the Programming Console. Only SSS can be used to designate any part of the ladder program area as an I/O comment area (i.e., the Programming Console cannot be used to designate any part of the ladder program area as an I/O comment area).

C200HX/HG/HE Memory Area Structure

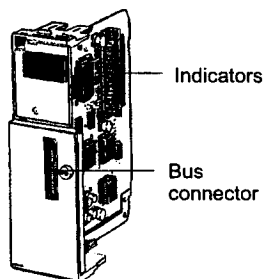


Ladder program area	A user program is stored in the ladder program area. If part of the UM is used as a fixed expansion DM area or I/O comment area, the capacity of the ladder program area storing the user program will be reduced accordingly.
I/O comment area	I/O comments are stored in the I/O comment area. The I/O comments can be stored with a program. The I/O comments can be monitored <i>without</i> loading the comment, just as with conventional comments.
Fixed expansion DM area	The default values of the Special I/O Module, Programmable Terminal, the character string of the Programmable Terminal, and operation data are stored in the fixed expansion DM area. By changing the I/O monitor present value of the Programming Console or using the DM edit transfer operation of the Ladder Support Software, the default values can be written to DM 7000 to DM 9999.
System reserved area	The system reserved area is used by the system only.
PLC Setup area	The settings required for the operation of the PLC are stored in the PLC Setup area.
Normal DM area	The user can freely use the normal DM as a data area for arithmetic operations. If the Special I/O Module is used, DM 1000 to DM 2599 will be a Special I/O Module default area.

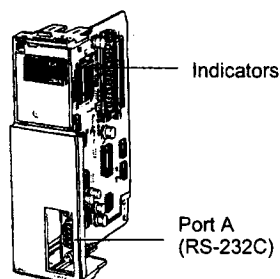
- DM 1000 to DM 2599 can be used as a normal DM if DM 7000 to DM 8599 are set as a Special I/O Module default area with the PLC Setup. DM 6000 to DM 6030 are used exclusively as an error log area.
- Unlike the normal DM area, nothing can be written to the fixed expansion DM area using ladder programming.
- The capacity of a ladder program will decrease if the size of the fixed expansion DM area and the total capacity of the I/O comments increase.
- The C200HX, C200HG, and C200HE do not have a fixed expansion DM area or I/O comment area before shipping. The user must allocate these areas in the UM according to the application.

COMMUNICATIONS BOARDS

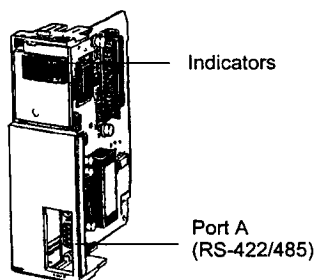
SPECIFICATIONS, SELECTION GUIDE



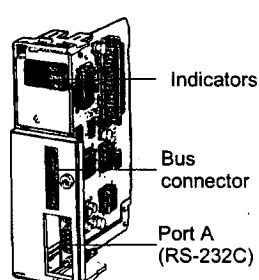
C200HW-COM01



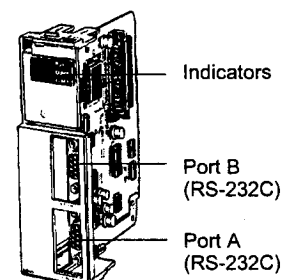
C200HW-COM02



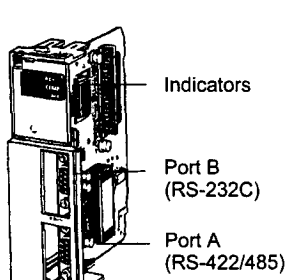
C200HW-COM03



C200HW-COM04-E



C200HW-COM05-E



C200HW-COM06-E

The C200Hα offers the industry's most versatile PLC communications options. With six Communications Board options, you can select just the right communications for your application. The boards fit into the communications slot in the CPU and let you expand the PLC functionality by connecting to other PLCs or computers with Omron's SYSMAC LINK, SYSMAC NET or, a PC Card Module. A variety of serial ports let you connect to Operator Interfaces, PCs, or other serial communication devices.

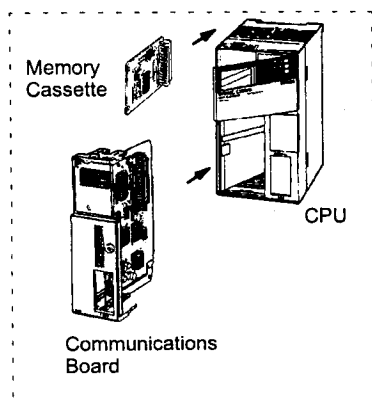
Specifications

PART NUMBER	DESCRIPTION
C200HW-COM01	CPU connection when using SYSMAC LINK or SYSMAC NET Link Communications Modules
C200HW-COM02	One RS-232C port
C200HW-COM03	One RS-422/485 port
C200HW-COM04-E	CPU connection for the SYSMAC LINK Module or SYSMAC NET Link Module, and an RS-232C port, with a protocol macro function
C200HW-COM05-E	Two RS-232C ports with a protocol macro function
C200HW-COM06-E	One RS-422/485 port, and one RS-232C port, with a protocol macro function

Communications Board Indicators

INDICATOR	COLOR	STATUS	MEANING	FUNCTION
RDY	Green	Not lit	Board not ready for use	Hardware error
		Flashes	Setting error	System setting or protocol data error
		Lit	Board ready for use	Normal operation
COMB	Orange	Flashes	Communicating	Port B is in use for communication
COMA				Port A is in use for communication

Note: Order the Communications Board and Memory Cassette separately (not provided with the CPU).



BACKPLANES

SPECIFICATIONS

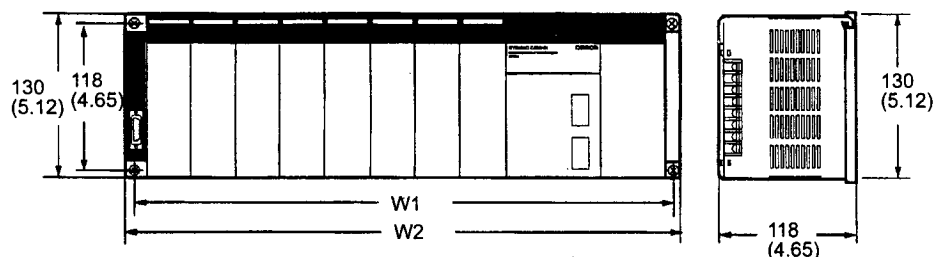
Select the Appropriate Backplane for the CPU with its I/O Modules

When selecting Backplanes for the CPU, the Expansion I/O, and the Slave Rack(s), each type of Backplane is a different model number. To order, refer to the specific information provided separately in the *Standard Parts* section of this catalog.

Dimensions

CPU I/O Backplane C200HW-BC□□□

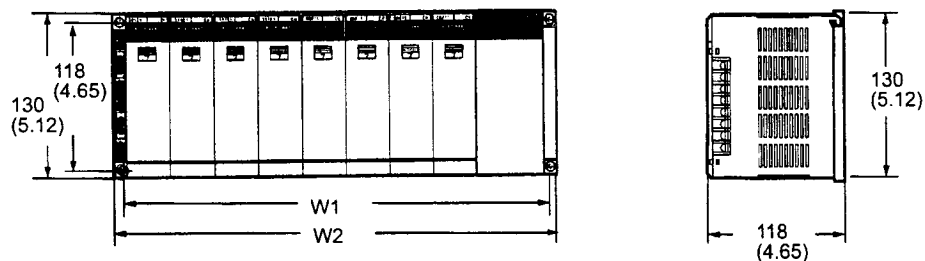
Unit: mm (inch)



NO. OF SLOTS	W1	W2	PART NUMBER
3 slots	246 (9.69)	260 (10.24)	C200HW-BC031
5 slots	316 (12.44)	330 (12.99)	C200HW-BC051
8 slots	421 (16.57)	435 (17.13)	C200HW-BC081
10 slots	491 (19.33)	505 (19.88)	C200HW-BC101

Expansion I/O Backplane C200HW-BI□□□

Unit: mm (inch)



NO. OF SLOTS	W1	W2	PART NUMBER
3 slots	175 (6.89)	189 (7.44)	C200HW-BI031
5 slots	245 (9.65)	259 (10.20)	C200HW-BI051
8 slots	350 (13.78)	364 (14.33)	C200HW-BI081
10 slots	420 (16.54)	434 (17.09)	C200HW-BI101

DISCRETE I/O MODULES

INPUT MODULE SPECIFICATIONS

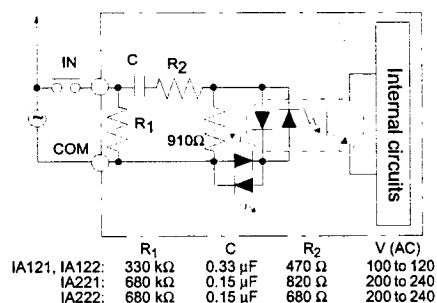
Input Module Specifications

TYPE	NO. OF INPUTS	INPUTS PER COMMON	INPUT VOLTAGE	INPUT CURRENT	OPERATING VOLTAGE		INPUT RESPONSE TIME		MODULE-STYLE	PART NUMBER
					ON	OFF	ON	OFF		
AC Input	8 pts.	8 pts.	100 to 120 VAC +10%/-15%	10 mA, 100 VAC	60 VAC min.	20 VAC max.	35 ms max.	55 ms max.	A	C200H-IA121
	16 pts.	16 pts.							B	C200H-IA122
	8 pts.	8 pts.	200 to 240 VAC +10%/-15%	10 mA, 200 VAC	120 VAC min.	40 VAC max.			A	C200H-IA221
	16 pts.	16 pts.							B	C200H-IA222
DC Input	8 pts.	8 pts.	12 to 24 VDC +10%/-15%	10 mA, 24 VDC	10.2 VDC min.	3.0 VDC max.	1.5 ms max.	1.5 ms max.	A	C200H-ID211
	16 pts.	16 pts.	24 VDC +10%/-15%	7 mA, 24 VDC	14.4 VDC min.	5.0 VDC max.			B	C200H-ID212
AC/DC Input	8 pts.	8 pts.	12 to 24 VAC/DC +10%/-15%	10 mA, 24 VDC	10.2 VDC min.	3.0 VDC max.	15 ms max.	15 ms max.	A	C200H-IM211
	16 pts.	16 pts.	24 VAC/DC +10%/-15%	7 mA, 24 VAC/ DC	14.4 VDC min.	5.0 VDC max.			B	C200H-IM212

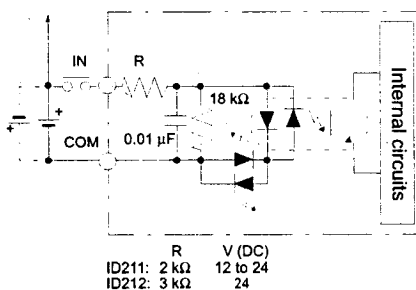
- Note:**
1. All models feature photocoupler isolation and LED indicator.
 2. Each Discrete I/O Module has a removable terminal block. See the above *STYLE* column for a reference to the module style/connector type and refer to the accompanying drawing and chart for specific connector details.

Input Module Circuit Configuration

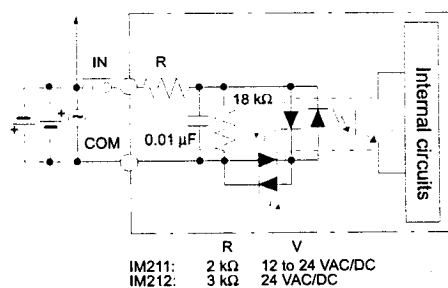
AC Input: IA121, IA122, IA221, IA222



DC Input: ID211, ID212



AC/DC Input: IM211, IM212



DISCRETE I/O MODULES

OUTPUT MODULE SPECIFICATIONS

Output Module Specifications

No. of outputs	Rated load voltage	Max. load current	Min. switching capacity	Output response times		Leakage current	Outputs/ per common	Fuse	External power supply	Internal power consumption (VDC)	Part number	
				ON	OFF							
Relay Output											Relay Output	
8 pts.	250 VAC (cos ϕ = 1)/ 250 VAC (cos ϕ = 0.4)/ 24 VDC max.	2 A/pt. 8 A/8 pts.	10 mA, 5 VDC	10 ms max.	10 ms max.	---	8 pts.	---	---	10 mA max.	C200H-OC221	
12 pts.		2 A/pt. 8 A/ 12 pts.					12 pts.				C200H-OC222 (see note)	
16 pts.		2 A/pt. 8 A/ 16 pts.					16 pts.				50 mA max.	C200H-OC225 (see note)
5 pts.		2 A/pt. 10 A/5 pts.					1 pt.				10 mA max.	C200H-OC223
8 pts.		2 A pts. 16 A/8 pts.									C200H-OC224	
Triac Output											Triac Output	
8 pts.	120 VAC	1 A/pt. 4 A/8 pts.	Resistive load: 10 mA; inductive load: 40 mA (10 VAC)	1 ms max.	1/2 of load fre- quen- cy max.	3 mA max., 100 VAC; 6 mA max., 200 VAC	8 pts.	5 A		140 mA max.	C200H-OA121-E	
12 pts.	250 VAC, 50/60 Hz	0.3 A/pt. 2 A/12 pts.		1/2 of load fre- quen- cy max.			12 pts.	3 A		200 mA max.	C200H-OA222V	
8 pts.		1.2 A/pt. 4 A/8 pts.	Resistive load: 100 mA; inductive load: 50 mA (10 VAC)	1 ms max.	8 pts.	5 A	180 mA max.	C200H-OA223				
12 pts.		0.5 A/pt. 2 A/12 pts.	100 mA, 10 VAC; 50 mA, 24 VAC; 100 mA, 100 VAC	1/2 + 1 ms of load fre- quen- cy max.	1.5 mA max., 120 VAC; 3 mA max., 240 VAC	12 pts.	3.15 A	270 mA max.	C200H-OA224			
Transistor Output											Transistor Output	
8 pts.	12 to 48 VDC +10%/–15%	1 A/pt. 3 A/8 pts.	Residual voltage: 1.4 V max.	0.2 ms max.	0.3 ms max.	0.1 mA max.	8 pts.	5 A	30 mA, 12 to 48 VDC min.	140 mA max.	C200H-OD411	
	24 VDC +10%/–15%	2.1 A/pt. 5.2 A/8 pts.						8 A	30 mA, 24 VDC min.		C200H-OD213	
		0.8 A/pt. 2.4 A/8 pts.	Residual voltage: 1.5 V max.	1 ms max.	1 ms max.	1 mA max.		None	150 mA, 24 VDC min.		C200H-OD214	
		5 to 24 VDC	0.3 A/pt.	10 mA, 5 VDC	1.5 ms max.	2 ms max.		0.1 mA max.		5 to 24 VDC	10 mA max.	C200H-OD216
12 pts.	24 VDC +10%/–15%	0.3 A/pt. 2A/12 pts.	Residual voltage: 1.4 V max.	0.2 ms max.	0.3 ms max.		12 pts.	5 A	25 mA, 24 VDC min.	160 mA max.	C200H-OD211	
16 pts.		0.3 A/pt. 4.8 A/12 pts					16 pts.	8 A	35 mA, 24 VDC min.	180 mA max.	C200H-OD212	
12 pts.	5 to 24 VDC	0.3 A/pt.	10 mA, 5 VDC	1.5 ms max.	2 ms max.		12 pts.	None	5 to 24 VDC	10 mA max.	C200H-OD217	
16 pts.	24 VDC +10%/–15%	1 A/pt. 4 A/16 pts.	Residual voltage: 0.8 V max.	0.1 ms max.	0.3 ms max.		16 pts.		35 mA, 24 VDC min.	160 mA max.	C200H-OD21A	

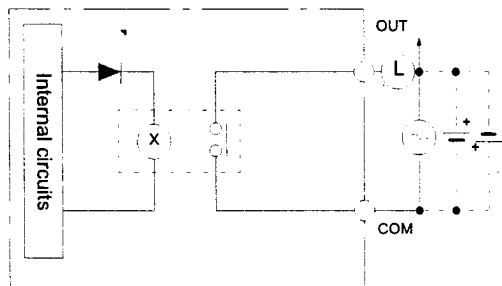
Note: Do not exceed the load current of 8 A per common. No more than 8 outputs can be turned ON simultaneously.

DISCRETE I/O MODULES

OUTPUT MODULE SPECIFICATIONS

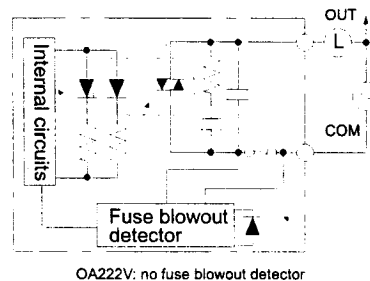
Output Module Circuit Configuration

Relay Output: OC221, OC222, OC223, OC224, OC225



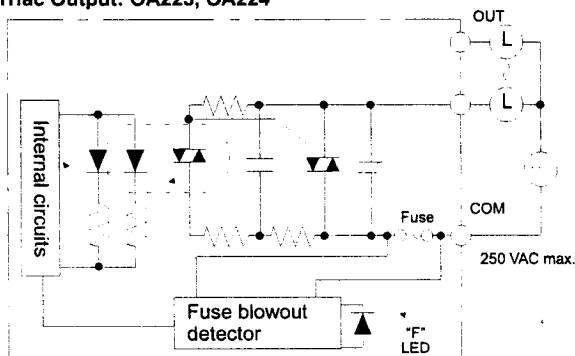
Use either + or - VDC

Triac Output: OA222V, OA121-E



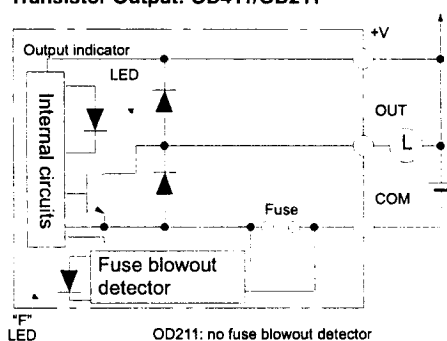
OA222V: no fuse blowout detector

Triac Output: OA223, OA224



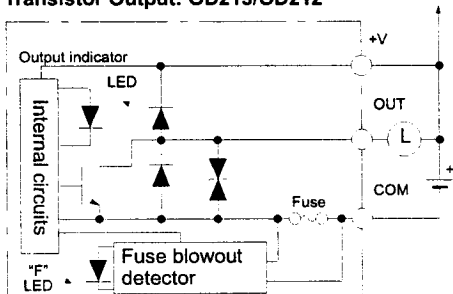
OA224: no fuse blowout detector

Transistor Output: OD411/OD211



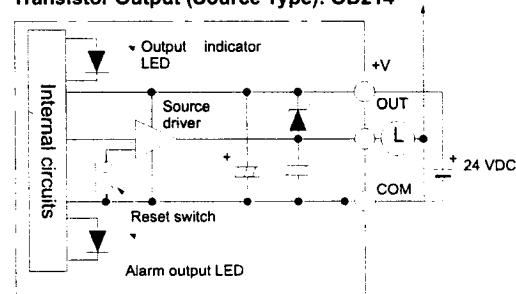
OD211: no fuse blowout detector

Transistor Output: OD213/OD212

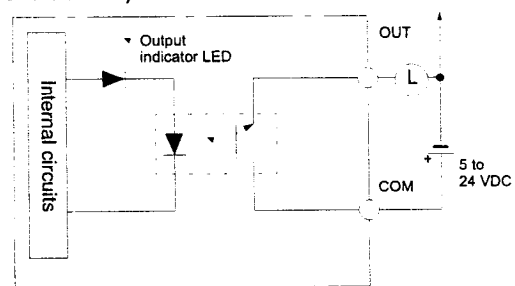


OD212: No fuse blowout detector

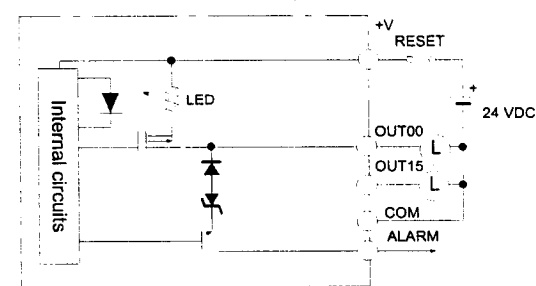
Transistor Output (Source Type): OD214



Transistor Output (Protective Circuit for Load Short-circuit): OD216/OD217



Transistor Output (Source Type with Protective Circuit for Load Short-circuit): OD21A



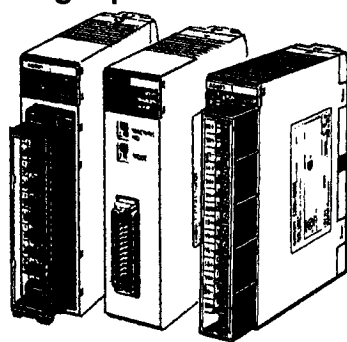
Note: Fuse blowout detection circuit: The F indicator is lit and the 08 bit turns ON. The 08 to 15 bits cannot be used as ordinary IR bits.

Special I/O Units

Analog I/O Units

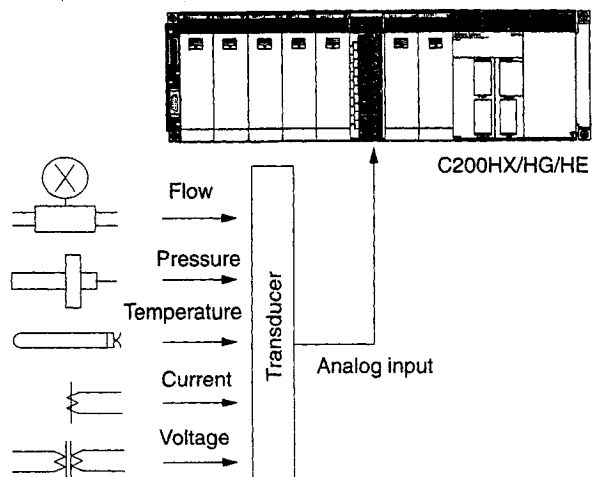
The C200H-AD001/AD002/AD003 Analog Input Unit is used to convert analog signals, such as voltages or currents, to binary data for input into the PLC, and the C200H-DA001/DA002/DA003/DA004 Analog Output Unit is used to convert digital signals to analog signals for output to external devices.

Analog Input Units



C200H-AD001
C200H-AD002
C200H-AD003

System Configuration



Features of C200H-AD003

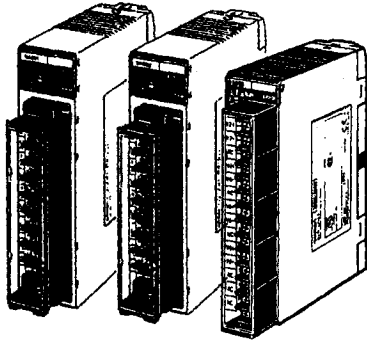
- ∞ A conversion speed of 1 ms max./pt
- ∞ Analog signals such as voltages and currents are received from various sensors through a maximum of eight inputs and converts them into 16-bit binary data.
- ∞ External input signal range can be freely set to satisfy diverse needs.
- ∞ Other built-in functions, such as the scaling function, mean function, peak-hold function, and wire burnout function, are available.

Specifications

Item		Specifications		
		C200H-AD001	C200H-AD002	C200H-AD003
Input points		4	8	8
Voltage input		1 to 5V or 0 to 10 V	1 to 5 V, 0 to 10 V, or -10 to 10 V	
	Current input	4 to 20 mA		
External input impedance	Voltage input	1 MΩ min.		
	Current input	250 Ω		
Resolution	Voltage	1/4,000 FS		
	Current			
Accuracy	25℃	±0.5% FS	Voltage: ±0.25% FS Current: ±0.4% FS	Voltage: ±0.2% FS Current: ±0.4% FS
	0℃to 55℃	±1.0% FS	Voltage: ±0.6% FS Current: ±0.8% FS	Voltage: ±0.4% FS Current: ±0.6% FS
Conversion speed		2.5 ms max./pt		1 ms max./pt
Converted data		12-bit binary	12-bit binary or 4-digit BCD code (selectable)	16-bit binary
Maximum input signals	Voltage input	±15 V max.		±15 V
	Current input	±30 mA max.		±30 mA
I/O words required		10 (Special I/O area)		
External connections		Terminal block	Connector	28-point removable terminal block (M3-screw size)
Current consumption		550 mA max., 5 VDC	450 mA max., 5 VDC	100 mA max., 5 VDC/ 100 mA max. 26 VDC
Weight		450 g max.	290 g max.	450 g max.

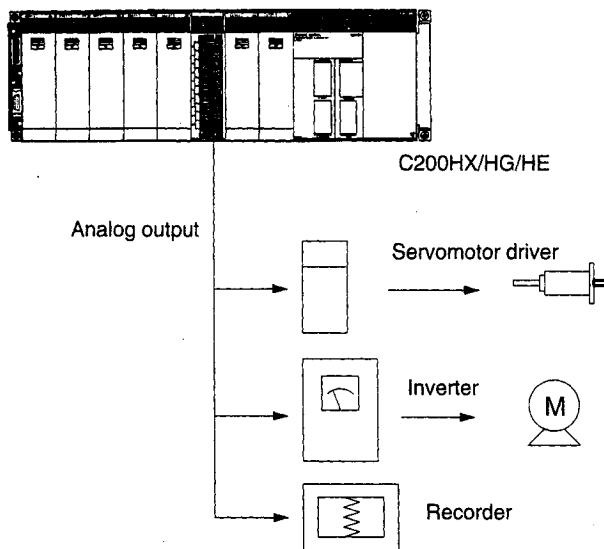
Special I/O Units continued.

Analog Output Units



C200H-DA001
C200H-DA002
C200H-DA003
C200H-DA004

System Configuration



Features of C200H-DA003/DA004

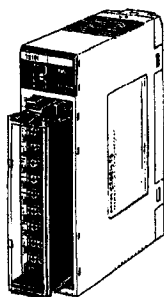
- ∞ A conversion speed of 1 ms max./pt
- ∞ 16-bit binary data is converted into analog output (voltage/current) and is output externally.
- ∞ Output signal range can be freely set to satisfy diverse needs.
- ∞ Other built-in functions, such as the peak-hold function, and scaling function, are available.

Specifications

Item		Specifications			
		C200H-DA001	C200H-DA002	C200H-DA003	C200H-DA004
Output points		2	4	8	
Voltage output		1 to 5V or 0 to 10 V	-10 to 10 V	1 to 5V or 10 to 10 V or -10 to 10 V	---
	Current output	4 to 20 mA		---	4 to 20 mA
Resolution	Voltage	1/4,095 FS	1/8,190 FS	1/4,000	
	Current	1/4,095 FS			
Accuracy	25°C	±0.5% FS	Voltage: ±0.3% FS Current: ±0.5% FS	±0.3% FS	±0.5% FS
	0°C to 55°C	±1.0% FS	Voltage: ±0.5% FS Current: ±1.0% FS	±0.5% FS	±0.8% FS
Conversion speed		2.5 ms max./pt		1 ms max./pt	
External output impedance		0.5 Ω min.			
Maximum external output current	Voltage output	15 mA	10 mA	12 mA	---
	Current output	---		---	---
Allowable load resistance of external output	Voltage output	---		1 kΩ	---
	Current output	400 Ω	350 Ω	---	600 Ω
Converted data		12-bit binary	Voltage code bit + 12-bit binary Current code bit + 12-bit binary	16-bit binary	
I/O words required		10 (Special I/O area)			
External connections		Terminal block	Connector	Terminal block	Terminal block
Current consumption		650 mA max., 5 VDC	600 mA max., 5 VDC	100 mA max., 5 VDC 200 mA max., 26 VDC	100 mA max., 5 VDC 250 mA max., 26 VDC
Weight		450 g max.	320 g max.	450 g max.	

SPECIAL I/O MODULES

TEMPERATURE SENSOR MODULES



C200H-TS001

C200H-TS101

Monitor up to 4 temperature sensor inputs directly from the PLC rack. Choose thermocouple inputs (types J and K), or platinum RTD inputs. Each module offers multiple ranges and a choice of Fahrenheit or Celsius scaling.

Features

- Available for thermocouple types J and K, or platinum RTD temperature sensors
- Selectable number of inputs
- Wide range of temperature settings

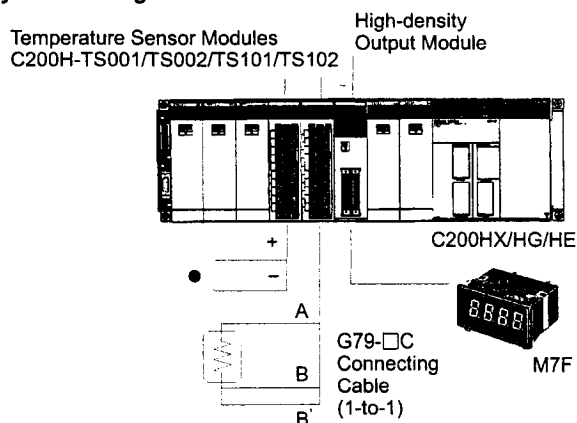
Specifications

PART NUMBER	C200H-TS001	C200H-TS101
TYPE	THERMOCOUPLE	PLATINUM RESISTANCE THERMOMETER
Temperature sensor	Thermocouples: K (CA), J (IC) (selectable)	RTD (JPt 100 Ω)
Input points	4 points/Unit max. (1, 2, or 4 points can be selected)	
Converted data	±(1% FS + 1°C) max.	
Total precision	4.8 s max. when 4 points/Unit is set 2.4 s max. when 2 points/Unit is set 1.2 s max. when 1 points/Unit is set	
PLC fetch time	Conversion cycle + PLC1 cycle time (5 s max.)	
Insulation	Between points: Uninsulated Between input terminal and PLC signal: Insulated with a photocoupler	
I/O words required	10 (Special I/O area)	
Current consumption	450 mA max., 5 VDC	
Weight	400 g max.	
Manual	W124	

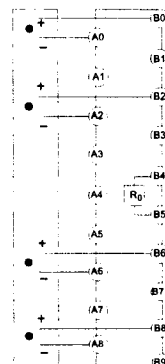
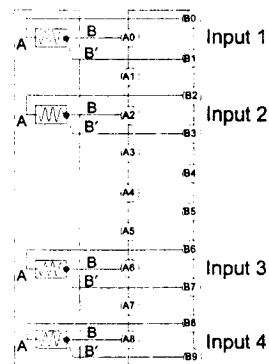
SPECIAL I/O MODULES

TEMPERATURE SENSOR MODULES

System Configuration



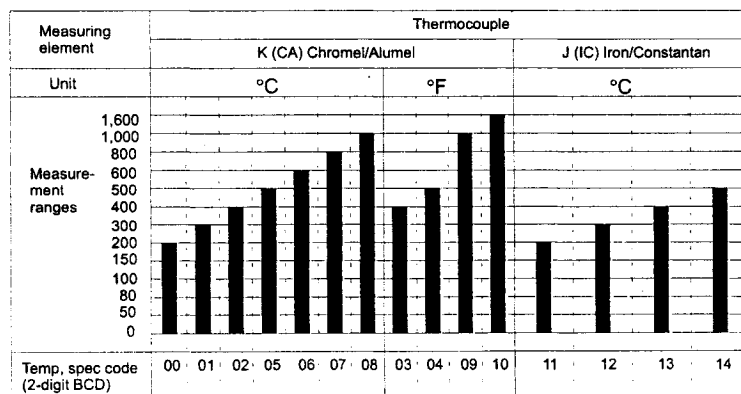
External Connections

C200H-TS001/TS002
Thermocouple InputC200H-TS101/TS102
Platinum Resistance
Thermometer Input

Note: A cold junction compensating circuit, whose precision is adjusted together with the Module, is provided between the B4 and B5 terminals of the C200H-TS001 (for thermocouple).

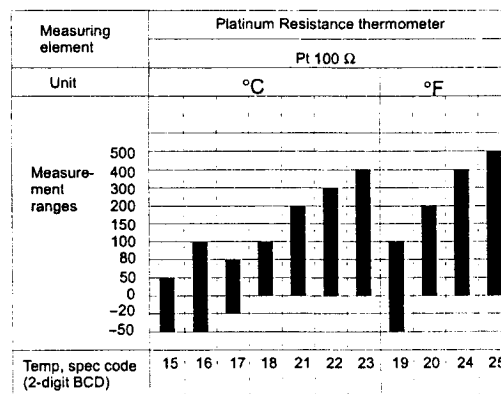
Temperature Ranges

C200H-TS001



Note: Use the IR bit for setting the temperature range. (Common settings for 4 inputs.)

C200H-TS101



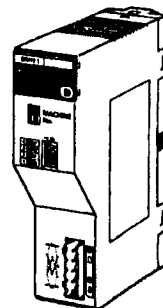
COMMUNICATIONS MODULES

DEVICENET SCANNER MODULE

The DeviceNet Scanner Module for the C200Hα allows open communication over DeviceNet networks with Omron and other vendors' I/O products. DeviceNet's open communications protocol allows the greatest flexibility in design of distributed I/O, while at the same time reducing installation costs.

Features

- Dedicated cable saves wiring effort – two nodes are connected through a single dedicated cable, greatly reducing installation costs
- Allows T-type bifurcation, branching, and multi-drop wiring.
- Connects to 50 slaves max. for 1,600-point I/O control possible with the C200HX-, C200HG-, and C200HE-series Master
- Network length of 500 meters max. – possible with a speed of 125K bps
- Communication at 500K bps max. – possible with a network length of 100 m max.
- Conforms to DeviceNet specifications



C200HW-DRM21

DeviceNet Communications Specifications

The communications specifications of the DeviceNet Master Module conform to the DeviceNet communications protocol.

ITEM	SPECIFICATIONS			
Baud rate	500K, 250K, or 125K bps (selectable)			
Communications distance	Communications speed (K bps)	Max. network length (m)	Branch length (m)	Total branch length (m)
	500	100 max.	6 max.	39 max.
	250	250 max.		78 max.
	125	500 max.		156 max.
Error control	CRC, node address multiple check, and scan list collation			
Cable	Dedicated cable			

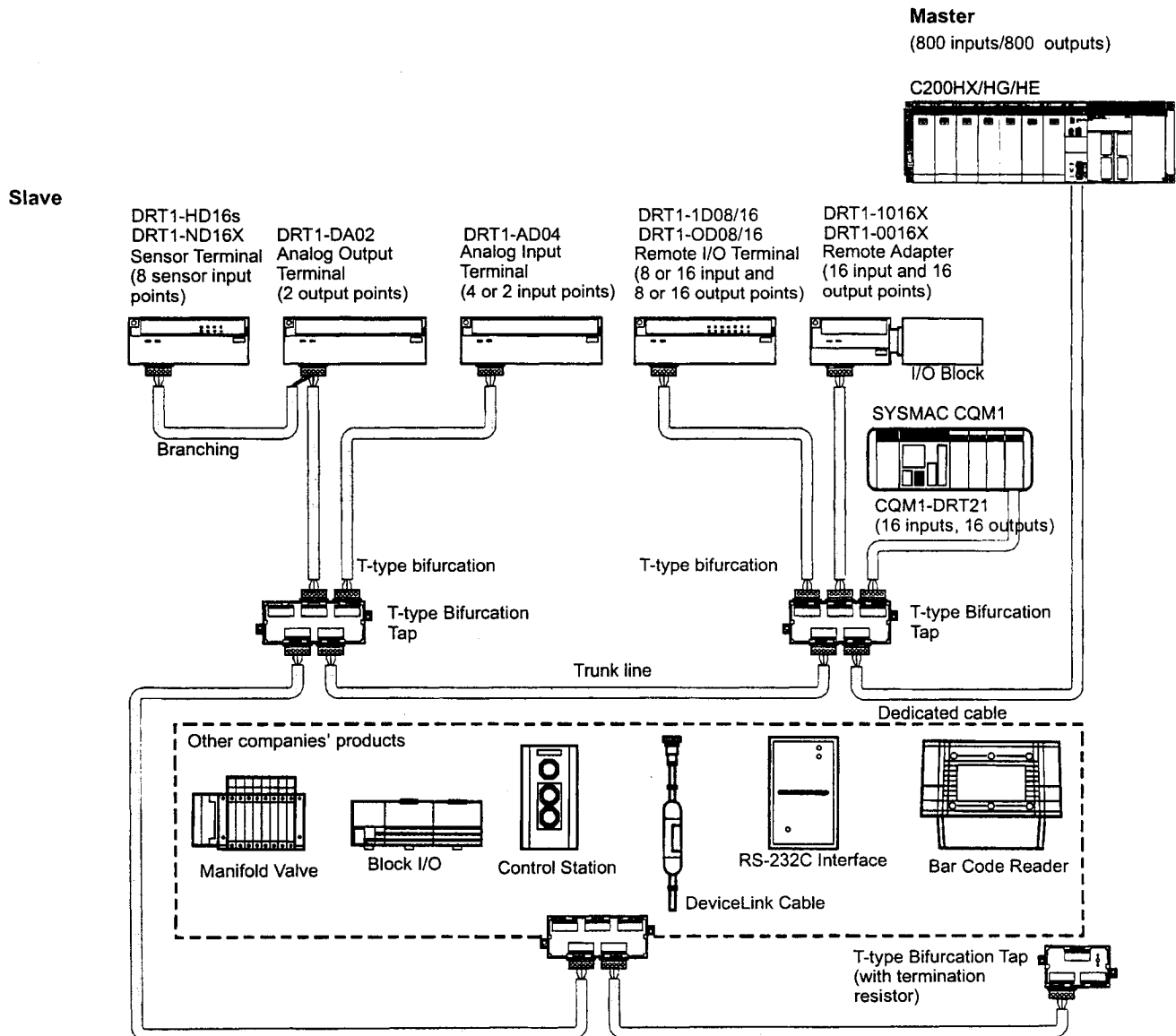
Specifications

PART NUMBER	C200HW-DRM21
Available PLC	C200HX/HG/HE
Max. No. of connecting PLCs	1
Mounting position	Mounted to the CPU or Expansion I/O Rack. (Cannot be mounted to the Slave Rack)
Max. no. of I/O points	1,600
Max. no. of connecting slaves	50
Manual	W267

COMMUNICATIONS MODULES

DEVICENET SCANNER MODULE

System Configuration Example

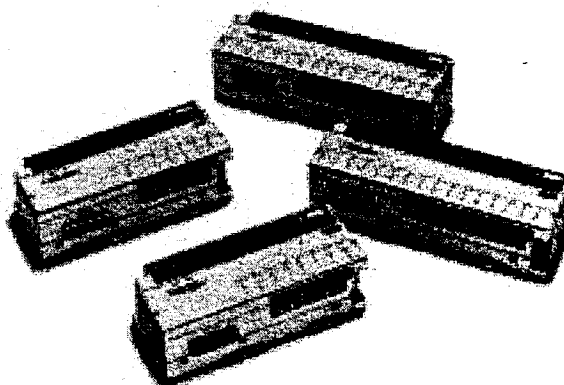


Transistor Remote Modules

DRT1-ID/OD

Compact 8-point and 16-point Transistorized Modules

- Compact
(8-point models: 125 x 40 x 50 mm (W x H x D);
16-point models: 150 x 40 x 50 mm (W x H x D))
- Two independent power supplies can be used because the I/O terminals are insulated from the internal circuits.
- DIN track mounting and screw mounting are available.
- Approved by UL and CSA.



Ordering Information

I/O classification	Internal I/O circuit common	I/O points	Terminal	Rated voltage	I/O rated voltage	Model
Input	NPN (+ common)	8	Screw terminal	24 VDC	24 VDC	DRT1-ID08
	PNP (– common)					DRT1-ID08-1
Output	NPN (– common)					DRT1-OD08
	PNP (+ common)					DRT1-OD08-1
Input	NPN (+ common)	16				DRT1-ID16
	PNP (– common)					DRT1-ID16-1
Output	NPN (– common)					DRT1-OD16
	PNP (+ common)					DRT1-OD16-1

Note: A communications cable, GCN1–004, is included with each module.

Specifications

■ Ratings

Input

Item		DRT1-ID□□(-1)
Input current		10 mA max./point
ON delay time		1.5 ms max.
OFF delay time		1.5 ms max.
ON voltage	NPN	15 VDC min. between each input terminal and V
	PNP	15 VDC max. between each input terminal and G
OFF voltage	NPN	5 VDC max. between each input terminal and V
	PNP	5 VDC max. between each input terminal and G
OFF current		1 mA max.
Insulation method		Photocoupler
Input indicators		LED (yellow)

Output

Item	DRT1-OD□□(-1)
Rated output current	0.3 A/point (see note)
Residual voltage	1.2 V max.
Leakage current	0.1 mA max.
Insulation method	Photocoupler
Output indicators	LED (yellow)

Note: Do not connect the DRT1-OD16 (-1) to loads consuming a total current exceeding 2.4 A.

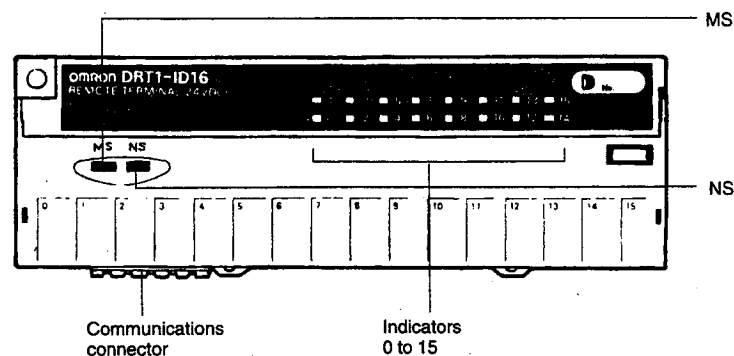
■ Characteristics

Communications power supply voltage	11 to 25 VDC (supplied from the communications connector)
Internal power supply voltage	24 VDC +10%/–15%
I/O power supply voltage	24 VDC +10%/–15%
Current consumption (see note)	Communications: 30 mA max. at 24 VDC Internal circuit: 60 mA max. at 24 VDC for DRT1-ID08-1, DRT1-ID16-1, DRT1-OD08-1, DRT1-OD16-1 70 mA max. at 24 VDC for DRT1-ID08 and DRT1-ID16 80 mA max. at 24 VDC for DRT1-OD08 90 mA max. at 24 VDC for DRT1-OD16
Dielectric strength	500 VAC for 1 min (1-mA sensing current between insulated circuits)
Noise immunity	Power supply normal: ±600 V for 10 minutes with a pulse width of 100 ns to 1 μs Power supply common: ±1,500 V for 10 minutes with a pulse width of 100 ns to 1 μs
Vibration resistance	10 to 55 Hz, 1.5-mm double amplitude
Shock resistance	Malfunction: 200 m/s ² (approx. 20G) Destruction: 300 m/s ² (approx. 30G)
Mounting strength	No damage when 50 N (approx. 5 kgf) pull load was applied for 10 s in all directions (10 N min. (approx. 1 kgf) in the DIN Track direction)
Terminal strength	No damage when 50 N (approx. 5 kgf) pull load was applied for 10 s
Screw tightening torque	0.6 to 1.18 N • m (6 to 12 kgf • cm)
Ambient temperature	Operating: 0°C to 55°C (with no icing or condensation) Storage: –20°C to 65°C (with no icing or condensation)
Ambient humidity	Operating: 35% to 85%
Weight	8-point model: Approx. 135 g max. 16-point model: Approx. 170 g max.

Note: The above current consumption is a value with all 8 and 16 points turned ON excluding the current consumption of the external sensor connected to the input Remote Module and the current consumption of the load connected to the output Remote Module.

Nomenclature

DRT1-□D08 (-1)
DRT1-□D16 (-1)



Specifications

■ Ratings

Input

Item	DRT1-AD04		DRT1-AD04H	
	Voltage input	Current Input	Voltage Input	Current Input
Input points	4 points			
Input type	0 to 5 V 1 to 5 V 0 to 10 V -10 to 10 V	0 to 20 mA 4 to 20 mA	0 to 5 V 1 to 5 V 0 to 10 V	0 to 20 mA 4 to 20 mA
Max. signal input	±15 V	±30 mA	±15 V	±30 mA
Input impedance	1 MΩ min.	Approx. 250 Ω	1 MΩ min.	Approx. 250 Ω
Resolution	1/6,000 (full scale)		1/30,000 (full scale)	
Overall accuracy	25°C : ±0.3% FS 0°C to 55°C: ±0.6% FS	25°C : ±0.4% FS 0°C to 55°C: ±0.8% FS	25°C : ±0.3% FS 0°C to 55°C: ±0.6% FS	25°C : ±0.4% FS 0°C to 55°C: ±0.8% FS
Conversion time	2 ms/point (8 ms/4 points, 4 ms/2 points)		250 ms/4 points	
Converted output data	Binary data -10- to 10-V range: 8BB8 to 0BB8 full scale Other signal ranges:0000 to 1770 full scale		Binary data 0000 to 7530 full scale	
Insulation resistance	20 MΩ min. at 250 VDC (between insulated circuits)			
Insulation method	Photocoupler insulation between inputs and communications lines (There is no insulation between input signals.)		Photocoupler insulation (between input and communications lines and each analog input signal)	

■ Characteristics

Communications power supply voltage	11 to 25 VDC (supplied from the communications connector)
Internal power supply voltage	20.4 to 26.4 VDC (24 VDC +10%/-15%)
Current consumption	Communications: 30 mA max. at 24 VDC Internal circuit: 80 mA max. (DRT1-AD04) at 24 VDC 130 mA max. (DRT1-AD04H) at 24 VDC
Dielectric strength	500 VAC for 1 min (1-mA sensing current between insulated circuits)
Noise immunity	Power supply normal: ±600 V for 10 minutes with a pulse width of 100 ns, 1 μs Power supply common: ±1,500 V for 10 minutes with a pulse width of 100 ns, 1 μs
Vibration resistance	10 to 55 Hz, 1.5-mm double amplitude
Shock resistance	Malfunction: 200 m/s ² (approx. 20G) Destruction: 300 m/s ² (approx. 30G)
Mounting method	M4 screw mounting or 35-mm DIN track mounting
Mounting strength	No damage when 50 N (approx. 5 kgf) pull load was applied for 10 s in all directions (10 N min. (approx. 1 kgf) in the DIN track direction)
Terminal strength	No damage when 50 N (approx. 5 kgf) pull load was applied for 10 s in all directions
Ambient temperature	Operating: 0°C to 55°C (with no icing or condensation) Storage: -25°C to 65°C (with no icing or condensation)
Ambient humidity	Operating: 35% to 85% (with no condensation)
Weight	160 g max.

Nomenclature

DRT1-AD04□

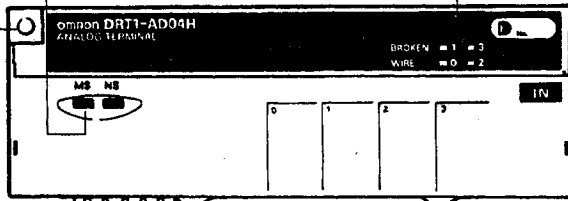
Mounting Hole
Used for panel mounting.

Indicators

Indicates the status of the Slave and the network.

Broken Wire Indicator (DRT1-AD04H)

If an input wire is disconnected or broken, the corresponding indicator is lit.



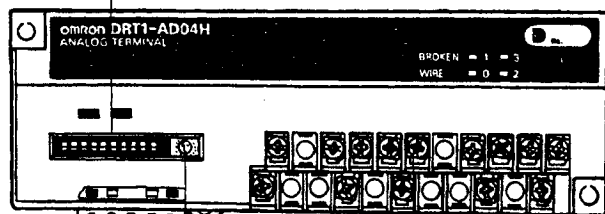
The DIP switch pins are used for node address and baud rate settings.

Pins 1 to 6: Node number

Pins 7 and 8: Baud rate

Pin 9: Number of inputs setting (4 points or 2 points)

Pin 10: Averaging function setting



Rotary Switch

Sets the input ranges.

Terminal Block

Connects the input power supply and analog inputs.

Communications Connector

Connects the network communications cable. The communications power is also supplied through this connector.

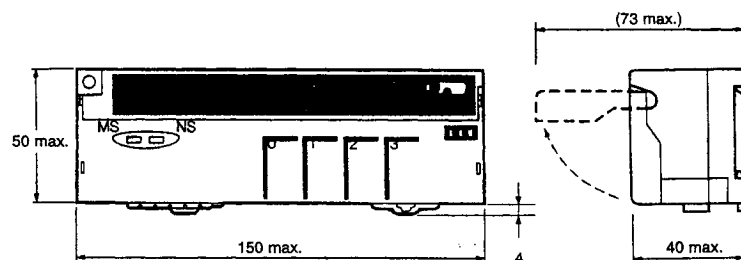
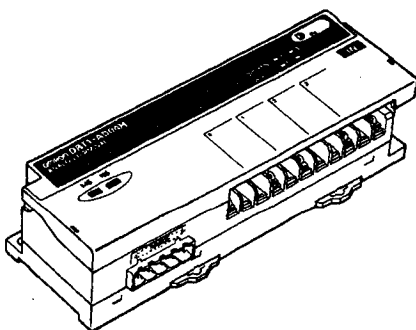
DIN-track Mounting Hook

Used for DIN-track mounting.

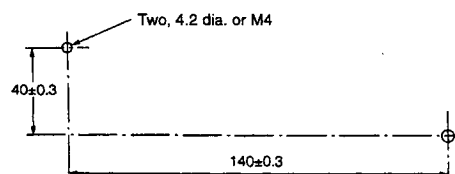
Dimensions

Note: All units are in millimeters unless otherwise indicated.

DRT1-AD04□



Mounting Holes

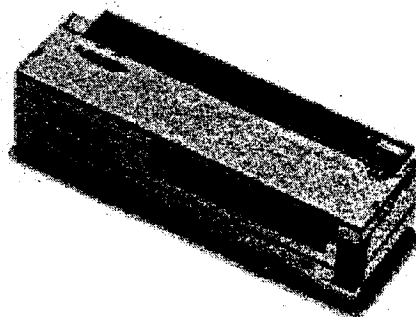


Analog Output Module

DRT1-DA02

I/O Interface Converts Binary Data into Analog Output Data

- Two outputs available.
- High resolution of 1/6000.
- Conversion is possible within a range of -5% to 150% full scale.
- High conversion speed of 4 ms/two points.
- Handles a wide range of outputs including 1 to 5 V, 0 to 10 V, -10 to 10 V, 4 to 20 mA, and 0 to 20 mA.
- Bears the CE marking.



Ordering Information

Classification	I/O points	Model
Analog output Module	2 outputs (Occupies 2 output words of the Master.)	DRT1-DA02

Specifications

■ Ratings

Output

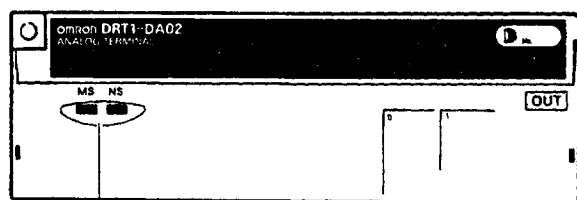
Item	Type	
	Voltage output	Current output
Output points	2 points	
Output type	1 to 5 V 0 to 10 V -10 to 10 V	0 to 20 mA 4 to 20 mA
Allowable external output load resistance	1 K Ω min.	600 Ω max.
External output impedance	0.5 Ω max.	---
Resolution	1/6000 full scale	
Overall accuracy	25°C : $\pm 0.4\%$ full scale 0°C to 55°C: $\pm 0.8\%$ full scale	
Conversion time	4 ms/2 points	
Converted output data	Binary data -10- to 10-V range: 8BB8 to 0BB8 full scale Other signal ranges: 0000 to 1770 full scale	
Insulation resistance	20 M Ω min. at 250 VDC (between insulated circuits)	
Insulation method	Photocoupler insulation between outputs and communications lines (There is no insulation between output signals.)	

■ Characteristics

Communications power supply voltage	11 to 25 VDC (supplied from the communications connector)
Internal power supply voltage	20.4 to 26.4 VDC (24 VDC +10%/−15%)
Current consumption	Communications: 30 mA max. at 24 VDC Internal circuit: 150 mA max. at 24 VDC
Noise immunity	Power supply normal: ±600 V for 10 minutes with a pulse width of 100 ns to 1 μs Power supply common: ±1,500 V for 10 minutes with a pulse width of 100 ns to 1 μs
Vibration resistance	10 to 55 Hz, 1.5-mm double amplitude
Shock resistance	Malfunction: 200 m/s ² (approx. 20G) Destruction: 300 m/s ² (approx. 30G)
Dielectric strength	500 VAC for 1 min (1-mA sensing current between insulated circuits)
Mounting method	M4 screw mounting or 35-mm DIN track mounting
Mounting strength	No damage when 50 N (approx. 5 kgf) pull load was applied for 10 s in all directions (10 N min. (approx. 1 kgf) in the DIN track direction)
Terminal strength	No damage when 50 N (approx. 5 kgf) pull load was applied for 10 s in all directions
Ambient temperature	Operating: 0°C to 55°C (with no icing or condensation) Storage: −25°C to 65°C (with no icing or condensation)
Ambient humidity	Operating: 35% to 85% (no condensation)
Weight	200 g max.

Nomenclature

DRT1-DA02



Indicators

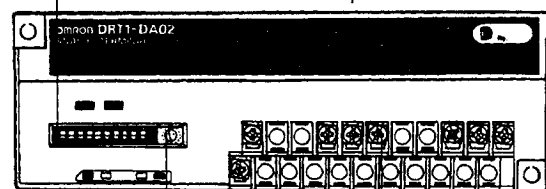
Indicates the status of the Slave and network

The DIP switch pins have the following functions:

Pins 1 to 6: Node number

Pins 7 and 8: Baud rate

Pin 9 and 10: Output status after communications error



Communications Connector

Connects the network communications cable. The communications power is also supplied through this connector.

Rotary Switch

Sets the output ranges.

Terminal Block

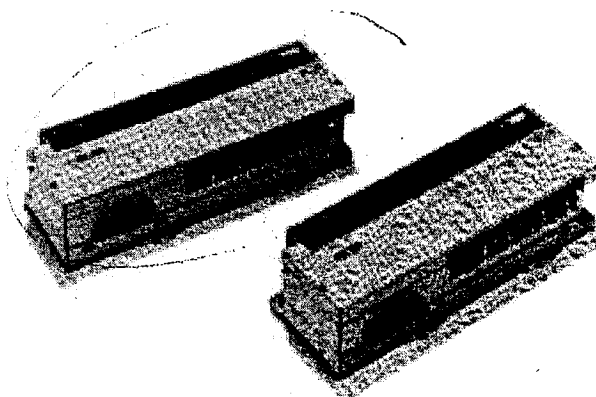
Connects the output power supply and analog outputs.

Temperature Input Module

DRT1-TS04□

Converting Temperature Inputs into Binary Data

- Four inputs
- Models for platinum resistance thermometers or thermocouples are available.
- Incorporating wire burnout detecting function.
- All inputs are insulated to one another.



Ordering Information

Classification	I/O points	Model
Temperature Input Module	4 inputs (Occupies 4 input words of the Master)	DRT1-TS04T
		DRT1-TS04P

Specifications

■ Ratings

Input

Item	DRT1-TS04T	DRT1-TS04P
Input type	R, S, K1, K2, J1, J2, T, E, B, N, L1, L2, U, W, and PLII	Pt100, JPt100
Indicator accuracy	($\pm 0.5\%$ of indication value or $\pm 2^\circ\text{C}$, whichever is larger) ± 1 digit max.	($\pm 0.5\%$ of indication value or $\pm 1^\circ\text{C}$, whichever is larger) ± 1 digit max.
Conversion time	250 ms/4 points	
Insulation system	Between the input and communications lines: Photocoupler insulation Between temperature input signals: Photocoupler insulation	

Note: The following are exceptions.

K1, T, and N at -100°C max., U, L1, and L2 at $\pm 4^\circ\text{C} \pm 1$ digit max. and R and S at 200°C max.: $\pm 6^\circ\text{C} \pm 1$ digit max.

B at 400°C max.: Not specified.

W: ($\pm 0.5\%$ of indication value or 6°C , whichever is larger) ± 1 digit max.

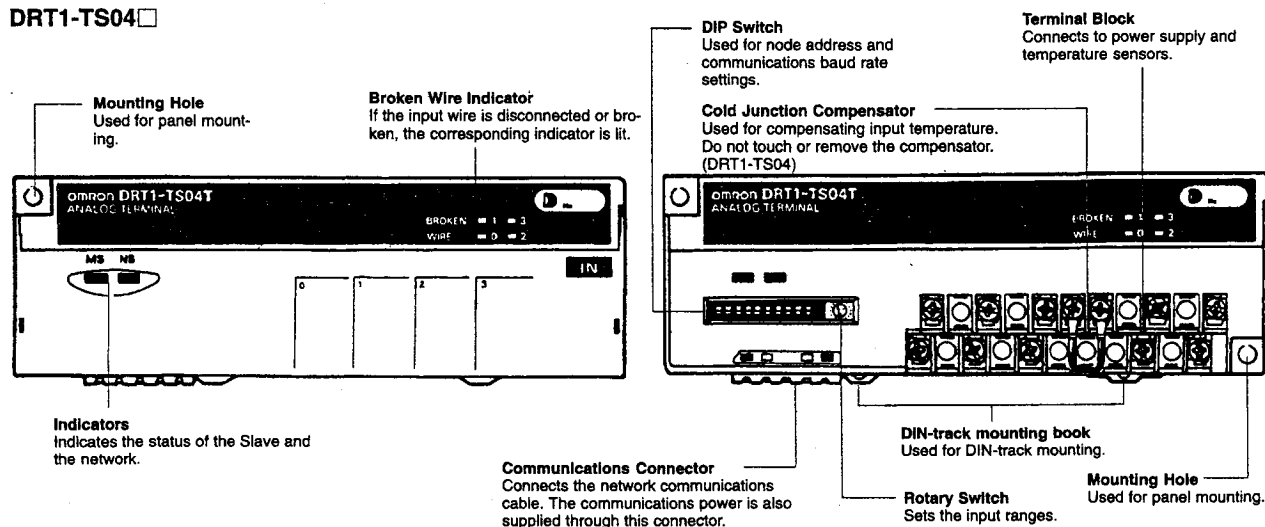
PL2: ($\pm 0.5\%$ of indication value or 4°C , whichever is larger) ± 1 digit max.

■ Characteristics

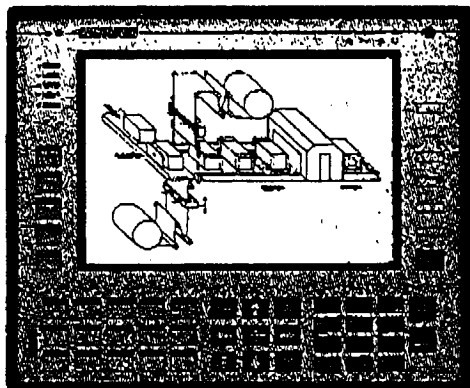
Item	DRT1-TS04T	DRT1-TS04P
Communications power supply voltage	11 to 25 VDC (supplied through communications connector)	
Internal power supply voltage	20.4 to 26.4 VDC (24 VDC +10%/–15%)	
Current consumption	Communications: 30 mA max. at 24 VDC Internal circuit: 130 mA max. at 24 VDC	
Noise immunity	Power supply normal: ±600 V Power supply (common): ±1.5 kV	
Vibration resistance	10 to 55 Hz, 1.5-mm double amplitude	
Shock resistance	Malfunction: 200 m/s ² (approx. 20G) Destruction: 300 m/s ² (approx. 30G)	
Dielectric strength	500 VAC for 1 min between insulated circuits	
Mounting method	M4 screw mounting or 35-mm DIN track mounting	
Mounting strength	50 N (approx. 5 kgf) for 10 s In the DIN track direction: 10 N (approx. 1 kgf) for 10 s	
Terminal strength	Pulling: 50 N (approx. 5 kgf) for 10 s	
Ambient temperature	Operating: 0°C to 55°C (with no icing or condensation) Storage: –25°C to 65°C (with no icing or condensation)	
Ambient humidity	Operating: 35% to 85% (no condensation)	
Weight	230 g max.	160 g max.

Nomenclature

DRT1-TS04



UniPlus - Industrial PLC Workstation UniOP™ - Universal Operator Panel Family



- 25 Line x 80 Character LCD or ELD
- Full-Graphic 640x400 Pixels
- 50 Programmable Keys
- Keyboard Macro Editor
- Recipe Capabilities
- UniNET Networking Capabilities
- Links Directly to PLC Programming Port
- NEMA 4/12 Compliant Enclosure

MKDL-25 and MKDR-25 models fulfill the need for a full yet cost effective operator interface system. Displays available with 25 lines and your choice of a pixel based LCD or ELD display. Each line can contain up to 80 characters. Each screen can contain up to 32 lines which can be accessed by scrolling with the arrow keys. Brightness control is provided to adjust the display for easy viewing under nearly any condition.

Display Variables

Internal variables can be shown on any of the many display screens. The number of variables that can be viewed at one time is limited only by the screen size. UniOP also provides scaling and conversion of the displayed data. The final value can then be shown in several useful formats including bargraph, date, time, integer, bit, hexadecimal, floating point, and string. Data entry and range verification is also available for each data type.

Key Entry

The integral keypad offers 50 programmable keys (21 with LED or lamps). Slide-in legends make it easy to customize and identify the operation of each key which has an LED indicator. Numeric and alphabetic keypads are conveniently located to make data entry easier than you ever imagined.

UniOP also features an internal battery-backed real time clock. Time and date information from the clock are periodically updated to the PLC to enable processing based on time-of-day, day-of-week, or any other period.

Alarms

UniOP can monitor and display up to 1024 alarms. Attributes and messages for each alarm can be defined. Operator acknowledgment can also be required. The last 256 alarm events triggered by the PLC are retained in an internal event list. This list

can be viewed on screen or printed on a serial printer to obtain a permanent record.

Security

An eight-level password protection scheme protects critical system features from undesired access.

Adaptability

Custom display screens are developed using the UniOP Designer™ for Windows™ programming software. Your completed program can be downloaded to any UniOP display through the serial line and permanently stored in a Flash EPROM.

Graphic Capabilities

The MKDL-25 and MKDR-25 allow you to display bitmap graphics. These bitmaps can be created with any Windows™ based software package capable of BMP format.

Keyboard Macro Editor

A feature that allows you to configure your UniOP keys to do a variety of functions locally in the UniOP. For example: turning pages, setting attributes, setting LEDs, writing to the PLC, going to the alarm list, uploading or downloading a recipe set and many more. This can save many hours of ladder logic programming.

Recipes

This feature allows you to create a recipe with up to 255 parameter sets for each page of the project file. UniOP has a total of 16K reserved for recipe storage. You can upload or download a parameter set from or to the PLC. Once a parameter set has been downloaded to the PLC, the data contained within the parameter set can be modified.



UNET Network

UniNET network allows the user to design a network in many different ways for use of several UniOP panels with several PLCs. Any data can be written to or retrieved from the PLCs in

many different locations at one time. The UniNET network creates a bridge between UniOP panels which allows data to be shared by all PLCs in the network, regardless of their type or manufacturer.

Important Features

• IEC 4/12 compliant enclosure
• CE approved
• UniNET network capabilities
• Keyboard macro editor
• Recipe configuration
• One RS-232 / RS-422 / RS-485 / 20mA current loop serial port, speeds up to 38,400 baud for direct PLC connection
• One RS-232 port for PC or printer communications
• One auxiliary port for high speed bus network connection

- 512 KB internal memory standard Flash EPROM
- Optional 512 KB memory upgrade (1 MB total memory)
- Unlimited number of variables per page
- Real time clock with battery back-up
- 1024 prioritized alarms
- Historical event list (last 256 events)
- Eight-level password protection
- Prints reports, alarm list, and event list to serial printer
- Displays ASCII standard character set

Specifications

Physical Dimensions

Unit Width and Height See drawing below right
Unit Depth 82 mm (3.23")
Panel Thickness (max.) 5 mm (0.20")
Panel Height 277 mm (10.90")
Panel Width 309 mm (12.17")
Weight 3.0 kg (6.6 lb)

Environment

Operating Temperature 0 to 50°C (32 to 122°F)
Humidity 0 to 95% RH (non-condensing)
• Requirements MKDL-25 24 VDC, 1.3A maximum
• Requirements MKDR-25 24 VDC, 600 mA maximum

Display

..... Liquid Crystal (55k hrs. MTBF \pm 1 Sigma)
..... 16 lines x 40 characters/line
Panel Size 9.1 in
Character height 5.15 mm (13/64 inch)
..... Electroluminescent (125k hrs. MTBF \pm 1 Sigma)
..... 16 lines x 40 characters/line
Panel Size 9.2 in
Character height 4.4 mm (approx. 23/128 inch)

Input

Technology Tactile feedback (tested 5M times)

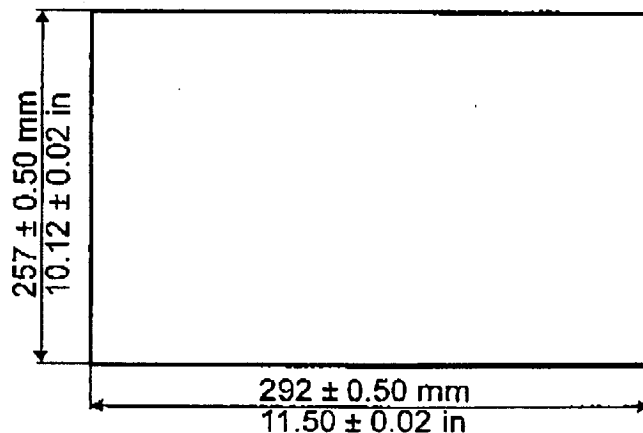
Warranty

All products are warranted for one year against defects in material and workmanship.

Ordering Information

Description	Part No.
EL, 25 x 80	MKDL-25
LCD, 25 x 80	MKDR-25

Panel Cutout Dimensions



Specifications subject to change without notice

EXOR®
ELECTRONIC R&D

3420 Fairlane Farms
Wellington, FL 33
TEL: (561) 753-2250
FAX: (561) 753-2291
BBS: (561) 753-8253

E-mail: info@exor-rd.com
WWW: <http://www.exor-rd.com>